EVALUATION OF LOCAL SITE CHARACTERISTICS OF SEDIMENTARY DEPOSITS FROM SEISMIC OBSERVATIONS

Kiyotaka SATO

EVALUATION OF LOCAL SITE CHARACTERISTICS OF SEDIMENTARY DEPOSITS FROM SEISMIC OBSERVATIONS

December 2001

Kiyotaka SATO

SUMMARY

In this dissertation local site effects are analyzed and evaluated considering incident wave fields based on seismic observation records and flowchart of strong motion evaluation scheme.

At the beginning, the feasibility of various analytical methods, the importance of proper delineation of geological structure and the use of seismic observation records are examined. Numerical and analytical methods for assessing seismic ground motion of layered ground models are investigated and evaluated using observation records. Various analytical methods are used for assessing wave propagations and geological structure for seismic ground response of horizontally and irregularly layered grounds.

In the next place, characteristics of nonlinear seismic ground response based on strong motion records are investigated. The nonlinear behavior is an important factor for seismic ground response of sedimentary deposits. During the 1995 Hyogoken-Nanbu Earthquake (M_{JMA}=7.2), strong ground motions were recorded at several sites in and around the city of Kobe. These records indicate peculiar nonlinear local site effects in reclaimed sand fill and Holocene and Pleistocene deposits.

Weak motion records at several sites, where vertical arrays of strong motion seismographs have been installed in laterally layered ground, are analyzed to propose assessment methods of vertical distribution of seismic ground motions. Those soil deposits are various grounds ranging from hard rock to relative soft ground. The assessment method is developed to evaluate vertical distribution of seismic coefficients taking into account dynamic behavior of multiple horizontally layered grounds and irregularly layered grounds including slopes. Moreover, the assessment methods are confirmed to be able to apply strong motion of sedimentary deposits except strong liquefied site.

Lastly, the effects of surface geology on seismic ground motion of sediment-filled valleys are investigated. Understanding these effects is important for earthquake resistant design of long and large-scaled civil structures such as buried lifelines, duct structures, tunnels, and pipelines. Earthquake records obtained at two types of filled-valleys fronting the Sagami bay are analyzed. One is located at Kuno in the Ashigara plane, where the sediments consist of diluvial and alluvial gravel deposits of sediment-filled valley. The second is located at Takeyama in Miura peninsula, where the sediments consist of soft clay of alluvial buried valley. Records of these two sites are extensively analyzed to evaluate the influences of incident wave field related to the source and path effects on local site effects of horizontally irregularly layered grounds.

These total evaluations make it possible to synthesize strong motion of sedimentary deposits. The remaining problem is to quantitatively evaluate the spatial variation of local site effects and the incident wave fields during strong motion on the basis of available information on deep and shallow geological structures.

ACKNOWLEDGEMENTS

This dissertation presents the results of fifteen years of study after graduating the master's course at the Graduate School of Engrg., Kyoto University. I here wish to acknowledge the supervision, guidance, support, encouragement, and assistance received from professors, colleagues, and friends.

I am deeply grateful to Professor Kenzo Toki of the Graduate School of Engrg., Kyoto University for his expert supervision of my research, scholarly education, wholehearted guidance, and continuous encouragement. Professor Toki taught me how to extract concluding remark of study from analyses and observations and how to make logical explanation based on reasonable composition of research approach. He has provided not only a research goal of earthquake engineering but also a moral of human being, such as what the earthquake engineers are about.

I also owe the particular thanks to Professor Tadanobu Sato of the Disaster Prevention Research Institute, Kyoto University who taught me how to make report of study in English. Professor Sato has provided useful advice, and stimulating discussions on all subjects covered in this dissertation as well as encouragement with no stint.

I am particularly indebted to Professor Fumio Oka of the Graduate School of Engrg., Kyoto University, for his suggestions and critical reading of the manuscript. I wish also to thank Professor Fusanori Miura of the Graduate School of Engrg., Yamaguchi University and Dr. Junji Kiyono of the Graduate School of Engrg., Kyoto University, for his support and encouragement of my dissertation research.

I am deeply indebted to Dr. Satoshi Shiomi of the Head Office, Dr. Koichi Nishi of the Geotech. and Earthq. Engrg. Department, Central Research Institute of Electric Power Industry, Professor Yoshihiro Sawada of the Graduate School of Engrg., Nagoya University, Professor Takeji Kokusho of the Graduate School of Science and Engrg., Chuo University, Professor Kazuyoshi Kudo of the Earthquake Research Institute, the University of Tokyo, Professor Tsutomu Sasatani of the Graduate School of Science, Hokkaido University, Dr. Hiroshi Itoh, Dr. Katuhiko Ishida, Dr. Shunji Sasaki, Dr. Junichi Tohma, Dr. Chizuko Kurihara and Dr. Sadanori Higashi of the Geotech. and Earthq. Engrg. Department, Central Research Institute of Electric Power Industry for their many discussions of my work and constructive suggestions.

I also wish to express my appreciation to Professor Koji Nakagawa of the Graduate School of Engrg., Yamaguchi University, Professor Takahiro Iwadate of the Faculty of Engrg., Tokyo Metropolitan University, Professor Hirokazu Takemiya of the Graduate School of Engrg., Okayama

University, Professor Takanori Harada of the Faculty of Engrg., Miyazaki University, Professor Hiromichi Higashihara of the Earthquake Research Institute, the University of Tokyo, Professor Makoto Kamiyama of the Faculty of Engrg., Tohoku Institute of Technology, Professor Takanobu Suzuki of the Faculty of Engrg., Toyo University, Dr. Sumio Sawada of the Disaster Prevention Research Institute, Kyoto University, Dr. Shunichi Kataoka of the Faculty of Science and Engrg., Hirosaki University, Dr. Takumi Toshinawa of the Faculty of Science and Engrg., Meisei University and Dr. Hitoshi Morikawa of the Graduate School of Engrg., Tokyo Institute of Technology, for their informative suggestions and advice.

I also owe thank to Mr. Yasunaga Tatsumi of Takenaka Corporation, Mr. Joji Ejiri of Ohbayashi Corporation, Dr. Yoshio Sunasaka of Kajima Corporation, Dr, Takeyasu Suzuki of Chuo Fukken Consultants Co. Ltd., Dr. Shinji Akiyama, Dr. Iwao Suetomi of Sato Kogyo Co. Ltd., and Hisakazu Sakai of Wakachiku Co. Ltd. for their frequent, stimulating and helpful suggestions of my dissertation. Mr. Shimada, Mr. Hiroshi Ishikawa, Mr. Tomiichi Uetake of Tokyo Electric Power Co., Inc., and Mr. Mamoru Matsumoto of Kansai Electric Power Co., Inc. are also greatly appreciated for provided many important ideas and information about earthquake observation.

The very significant contributions made by my many colleagues in Central Research Institute of Electric Power Industry are appreciated. In particular, Dr. Teruyuki Ueshima, Dr. Keizo Ohtomo, Mr. Hiroshi Yajima, Mr. Yoshiaki Shiba, Mr. Hiroaki Sato, Dr. Mamoru Kanatani of Geotech. and Earthq. Engrg. Department and Dr. Koji Shirai of Materials Sci. and Structural Department are acknowledged, as well as many collegues of Eathquake Research Devision, Ministry of Education, Sport, Culture and Technology. I also owe special thank to Mr. Yoshihiro Tazawa of GA Technology Co. Ltd. and Mr. Eiji Yamada of Yoshizawa Technology Co. Ltd. for their computer management, programming and many support.

I also thank many colleagues in Central Research Institute of Electric Power Industry. I owe thank to Mr. Shigeru Himori of Katsushima Corporation for helpful and important support about earthquake observation. Ms. Yumi Iizumi is also appreciated for provided research environment support. Ms. Taeko Sato and Ms. Junko Iida are also acknowledged for typing the manuscript, as well as the other assistance. I am also deeply indebted to Ms. Mitsuko Kitagawa and Ms. Yoko Tatsumi for greatly and helpful support about paper works and native checking of my dissertation. Dr. Roger Ghanem of my friend of the Johns Hopkins University is so acknowledged for his greatly support.

Lastly, I appreciate my wife, Sayuri, her father and mother, Kensuke and Yoshiko Kuwahara for their abiding understanding and support during my life of study. I dedicate this dissertation to them in token of my gratitude for their belief and support. I also thank my late father, Jun and to my mother, Harumi for their support during my years of study.

TABLE OF CONTENTS

CHAPTER 1

INTRODUCTION

1.1 Historical Disastrous Earthquakes

To begin with, examples of local site effects observed in overseas disastrous earthquakes are summarized. In the 1963 Scopjie earthquake in Yugoslavia the largest damage to houses and manmade structures was concentrated in an area where the alluvial deposit was laterally irregular[1]. In China, during the 1976 Tangshang earthquake, the damage was especially concentrated at the old riverside area along the banks of the Koga river where the ground consisted of local alluvial deposits. As for the 1976 north Italy earthquake, it was reported[1), 2)] that damage was distributed in an area of sedimentary deposits close to the mountain ridge in close proximity to the seismic fault. This site did not exactly have the thickest sedimentary deposits, but it is on a transitional zone where the alluvial layer gradually thickens in the direction towards the mountain region.

A well known earthquake disaster with strong local site effects is the 1985 Michoacan earthquake in Mexico City which though located at an epicentral distance of about 400 Km from the seismic source had the largest damage and more than 10 thousand people were killed. The damage was distributed in areas of thin alluvial deposits close to the surrounding hills at outcrops of rock. Mexico City is built on land reclaimed from an old lake area and the strong motion records during this earthquake had long periods from 2 to 4 seconds for about one minute. The interpretation of these records is far from over and is still being debated[3), 4), 5)].

In the 1989 Loma Prieta earthquake, the area with the most severe damage was the portion of the city of San Francisco reclaimed from the bay. A two-level highway in Embacadero sustained major damage and in the Marina district many buildings were severely damaged. Both locations are close to a transitional zone between the reclaimed soft and stiff alluvial deposits. In the area outside the transitional zone, little damage was found even at sites with soft sedimentary deposits[6)]. In the 1994 Northridge earthquake, damage to houses and structures were concentrated on regions with

alluvial deposits along the sides of the Santa Monica Mountains.

As in the case of overseas earthquakes many examples of strong local site effects can be found in historical earthquakes in Japan. At Noubi plane during the 1891 Noubi earthquake and Fukui plane during the 1948 Fukui earthquake, severe damage was found in areas close to the mountain side[7] on transitional zones where alluvial gravel deposits were overlain. The major damage at Fukui city was apparently caused by its geological structure. When the effects of different types of geological structure on the ground motion during the earthquake were investigated, rock sites were found to be more stable and safe than sites with unconsolidated sedimentary deposits[8].

In the 1854 Ansei-Tokai earthquake Kozai-cho located at the edge of the Kofu basin sustained severe damage even though the city of Kofu located at the central part of the basin reported no damage. Some sedimentary deposit zones at Ueno, Ikenohata, Soto-Kanda, Ginbo-cho and Iidabashi had damages and the downtown in Tokyo district built on soft ground had severe damages. A similar concentration of damage to houses on alluvial deposits was observed in the 1923 Kanto earthquake.[9]

In the 1944 Tou-Nankai earthquake, significant damage was observed in the alluvial plane along the banks of the Ohta and Kiku rivers in Shizuoka prefecture. In particular, the largest damage was found in the area south of Ohta River near a diluvial hill where the sedimentary deposits are laterally irregular. At other sites, the sedimentary deposits are horizontally layered and reported little damage.[10]

In the 1968 Off-shore Tokachi earthquake the collapse of the tower of Hachinohe, the City library, and City hall built on the edge of cliffs were surely caused by the local irregular topography and geology. In the 1978 off-shore Miyagi earthquake embankments for residential houses sustained large damages resulting from differential settlement.[11] The damage in the last two earthquakes were a little different than in the other earthquakes but in both instances it can be concluded that local site characteristics of the irregularly layered ground significantly contributed to their damages.

In the Great Hanshin-Awaji disaster during the 1995 Hyogoken-Nanbu earthquake the areas with heavily damaged buildings and collapsed residential houses were concentrated in a narrow zone in a damage belt oriented WSW-ENE across the city of Kobe. The damage belt was defined by the area of JMA intensity scale Ⅶ where more than 30 % of residential houses collapsed. In this area, the granite bedrock of Mt. Rokko drops steeply to a depth greater than 1 Km within a horizontal distance of a few kilometers extending from the mountain edge to the central part of downtown Kobe. This bedrock underlies the thick Osaka Group formation, which consists mostly of early Pleistocene sand and gravel.

Sato et al.[12), 13)] reported that the primary mechanism responsible for this damage belt is site amplification resulting from the deep irregularly layered ground and the nature of the incident wave

field. Kawase et al.[14), 15)] named this effect as "basin-edge effect" to describe the site amplification caused by a constructive interference of the direct S-wave with the basin-induced and diffracted surface waves. Another report[16)] has similarly concluded that the damage can be attributed to the incident wave field and geological structure

1.2 Structural Damage in Irregularly Layered Ground

In previous research on historical disastrous earthquakes, it has been pointed out that damage in these earthquakes was strongly correlated to the geological and geotechnical structure of the ground[1)]. It has been noted from reconnaissance reports of past disastrous earthquakes that damage to buildings and other structures was locally concentrated on filled lands, unconsolidated sedimentary deposits, transitional zones between soft and hard grounds, edges of topography like a cliff[17), 18), 19)] and irregularly layered ground at the interface of sedimentary deposits and base layers.[20), 21)] The primary cause of damage in the above-mentioned sites is the permanent deformations in the soils on account of their physically weak geotechnical properties. The other reason for the high damage could, also, be the effect of seismic wave propagation from the source to the site by which seismic waves are locally focused by repeated reflections and refractions at the irregular interface between sedimentary deposits and bedrock.[22), 23), 24)] The first is a one- or at best a two-dimensional problem possibly including nonlinear dynamic characteristics and the latter is a two-[25), 26), 27), 28), 29)] or three-dimensional[30), 31)] problem. These two issues need to be investigated using numerical simulations and recorded motions from strong motion seismograph arrays.

Imaoka[8)] has devised a scheme for classifying geological and geotechnical conditions where severe structural damages were concentrated in past disastrous earthquakes. His classification scheme is as follows:

(1) Sedimentary deposit with irregular topography at surface
a. Topographical discontinuities, e.g. cliff
b. Steep hill sites

(2) Irregularly layered ground at the interface between surface and base layers
a. Transitional zones between soft and hard grounds
b. Zones of horizontal sudden change of sedimentary deposits thickness
c. Soft alluvial buried valleys with high contrast in seismic wave velocities

(3) Irregularly layered ground at surface and interface between surface and base layers

a. Filled ground on alluvial valleys

b. Embanked grounds on a hill slope

Among the many sites that were investigated, Kuno at Ashigara plane and Takeyama at Miura peninsula, facing Sagami bay belong to category (2)a and (2)c, respectively. Both sites are test fileds of Effect of Surface Geology on Seismic Motion[33]. Kuno is on a transitional zone between soft alluvial and hard diluvial deposits overlying Hakone volcanic andesite[32]. The geology at this site is really complex. The irregularity in the layering of the soil and the interface between the sedimentary deposits and bedrock is not exactly clear up to a depth of a few hundred meters[33), 34), 35)]. The Takeyama site[36] is a typical, soft alluvial buried valley reclaimed from the sea in historical times and consists of irregularly layered ground.

Seismic wave velocity structures at both sites were identified analytically using observed seismic records. These identification results of seismic wave velocity structure make it possible to interpret the incident wave field and clarify its effect on the site response of irregularly layered ground. These two observation sites are found to be very useful for investigating local site effects.

1.3 Evaluation of Local Site Effects on Strong Motion

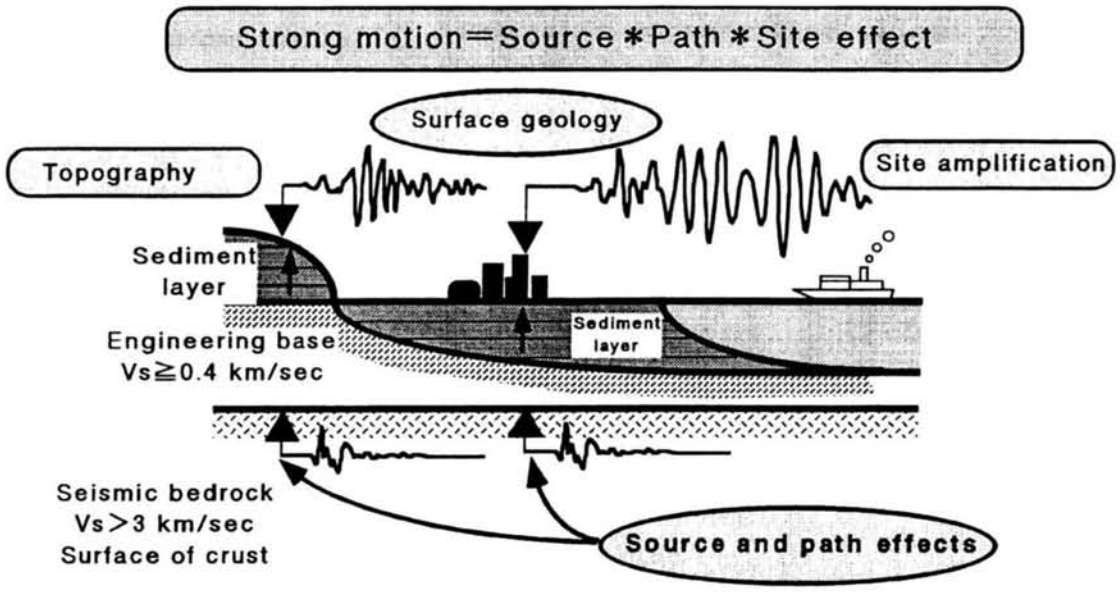

Fig. 1.1 Schematic graph of evaluation of strong motion

The basic flowchart for determining the design ground motion for earthquake resistant design of important buildings and structures is shown in Fig. 1.1. The ground motion at a site is

obtained from considerations of seismic waves propagating from a source through the earth's crust and amplified by the surface layer at the site. Ground motion at a site is expressed as the convolution of three factors[37] which are source effect, path effect and local site effect. This can be expressed in the frequency domain by the following equation:

$$o(\omega) = S(\omega) \cdot P(\omega) \cdot G(\omega), \tag{1.1}$$

where $G(\omega)=2.0$ on outcropped rock and $G(\omega)=1.0$ at the interface on the wave propagation process.

Wave propagation in a layered ground is computed using elasticity theory on a soil model composed of vertical and lateral distributions of wave velocity, density and damping factor. It is easy to evaluate path and site effects quantitatively if the geological and geotechnical parameters for layered ground is simple. In the case of homogeneous elastic half-space, the solution in the space and time domain for a dislocation point source is known analytically. Complicated focal processes can also be determined by inverting recorded seismograms to the dislocation of the source fault except path and site effects of horizontally layered ground[38]. In order to properly do this it is necessary to evaluate, as accurately as possible, the seismic wave velocity structure used in the numerical analysis. However, surface layered grounds in alluvial planes are not exactly simple, even if they are simply approximated as a horizontally layered ground[39]. Thus, observation points on outcrop of rock are needed to investigate the incident wave field related to the seismic source and path effects. Ground motions are influenced by various factors, but generally a deep geological structure contributes to long- period motions and shallow geological structures to short-period motions. Therefore geological and geotechnical information of the soil structure at a site are required to assess the design input ground motion for important structures.

As for the prediction of strong motion, the goal is to evaluate seismic waves with a relatively broadband frequency that contain waves of frequencies of less than 1 Hz to about 10 Hz. For the reason of the effects of irregular surface geology in the short period, a horizontally layered ground model is not adequate to evaluate amplification effects in case of sedimentary basins, buried valleys, dipping layers and fault zones. Therefore, it is necessary to evaluate the seismic ground response for laterally irregularly layered ground using seismic wave propagation theory. In the literature there are quite a few examples of seismic ground response calculations in alluvial planes. However, in real world cases this kind of analysis is constrained because of the lack of good quality geological and geotechnical data from surveys of seismic wave velocity structure. With time PS loggings and other techniques for conducting physical exploration surveys will undoubtedly increase. Physical exploration surveys were carried out to evaluate seismic wave velocity structure inverted from seismic observation. Thus, a proper evaluation of seismic wave velocity structure is necessary for

numerical simulations of seismic motions on layered ground[40), 41), 42), 43), 44)].

Seismic ground response of irregularly layered ground was used not only to evaluate site effects but also to investigate seismic path and source process. A quantitative evaluation of local site effects during strong motion can be done properly only if the incident wave field is based on an analysis of seismic source and path effects. Only if all three components, source, path and site effects, are known, it is possible to synthesize strong motion[37)] as indicated in Fig. 1.2 for the earthquake resistant design of important structures. As numerical simulations, modeling of underground seismic wave velocity structures and seismic observations become more reliable and available, it is possible to quantitatively evaluate strong motions. A thorough investigation of the three items is required to build a greater confidence in the design input motions simulated using the approach shown schematically in Fig. 1.2.

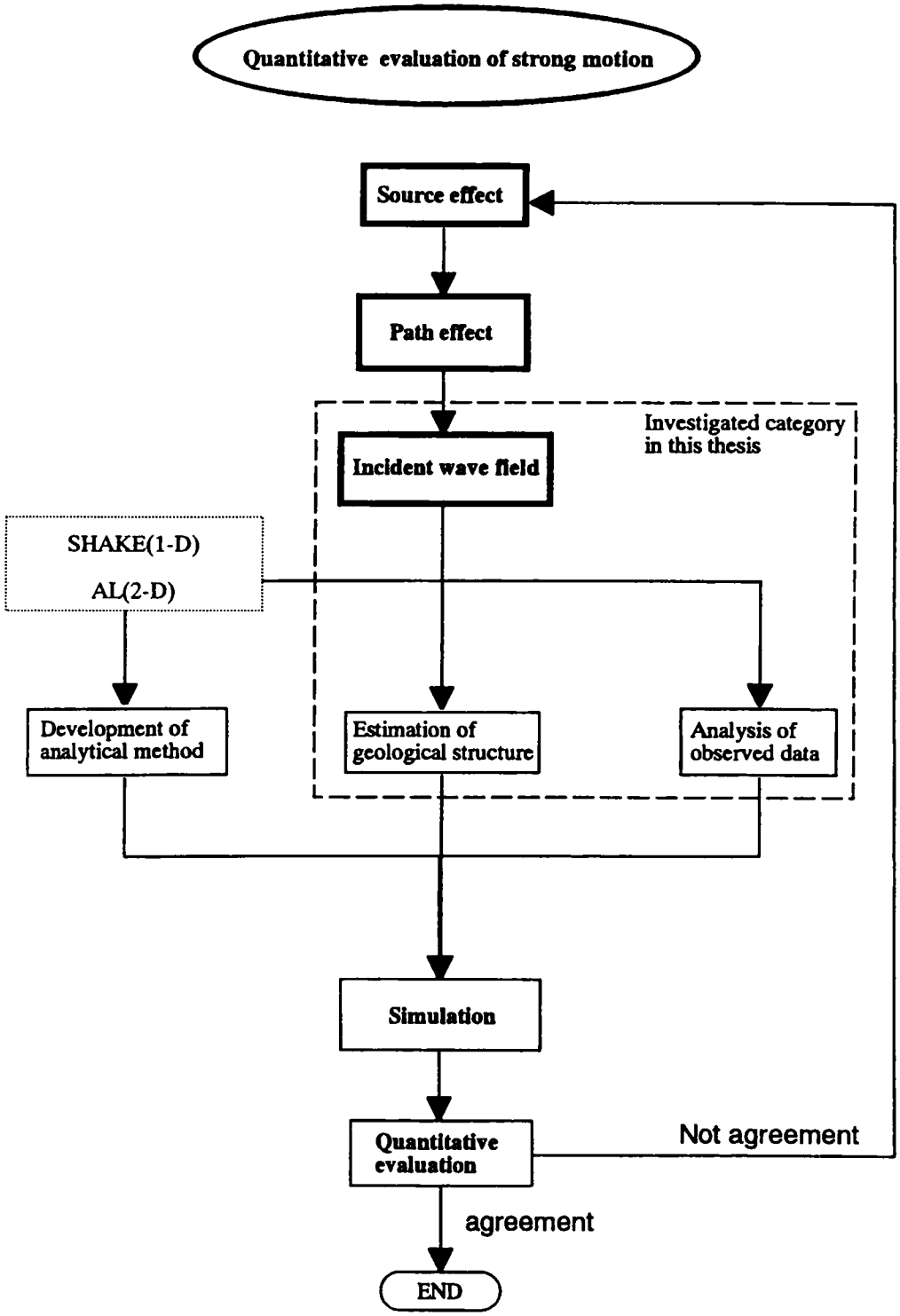

Fig.1.2 Flow chart of quantitative evaluation for strong motion[37)]

1.4 Outline of the Dissertation

In the dissertation the characteristics of local site effects are analyzed and evaluated considering incident wave fields based on seismic observation records. Fig. 1.2 shows a flowchart of the evaluation scheme.

In chapter 2, numerical and analytical methods for assessing seismic ground motion of layered ground models are investigated and evaluated using observed earthquake records. Various analytical methods are used for assessing seismic ground response of horizontally and irregularly layered grounds. The feasibility of various analytical methods, the importance of a proper delineation of geological structure and the use of seismic observation records are examined in this chapter.

In chapter 3, characteristics of nonlinear seismic ground response based on earthquake observations are investigated. The nonlinear behavior is an important factor for seismic ground response of horizontal and irregularly layered grounds. During the 1995 Hyogoken-Nanbu Earthquake (M_{JMA}=7.2), strong ground motions were recorded at several sites in and around the city of Kobe. At some of these recording sites, multi-depth vertical arrays of accelerographs had been installed. These records indicate peculiar nonlinear local site effects in reclaimed sand fill and Holocene and Pleistocene deposits.

In chapter 4, weak motion records at eleven sites where vertical arrays of strong motion seismographs have been installed in laterally layered ground with soil ranging from hard rock to relative soft ground are analyzed. The purpose is to develop a method for evaluating underground seismic coefficients taking into account dynamic behavior in multiple horizontally layered grounds and irregularly layered grounds including sloped layers.

In chapter 5, the effects of surface geology on seismic ground motion of laterally irregularly layered grounds are investigated. Understanding these effects is important in earthquake resistant design of long and large-scaled civil structures such as buried lifelines, duct structures, tunnels, and pipelines. Records obtained from vertical arrays of strong motion seismographs at two sites fronting the Sagami bay are analyzed. One observation site is located at Kuno on the Ashigara plane and the ground at the site consists of diluvial and alluvial gravel deposit of sediment-filled valley. The second site is located at Takeyama in Miura peninsula on soft clay of alluvial buried valley. Records from these two sites are extensively analyzed to evaluate the influences of incident wave field related to the source and path effects on local site effects.

In chapter 6, the results of the analyses described in this dissertation are summarized and suggestions for future research are noted.

REFERENCES

1) Irikura, K., S. Kasuga and M. Yoshikawa; Relationship between Irregularity of Geological Structure and Damage due to Seismic Motion, Special research report on natural disaster No. A-57-5, Science research report of Natural Disaster, 1980.
2) Taga, N.; Ground motion in irregular subsurface structure in "Decade history on ground motion symposium - seismic motion and ground –", 164-178, Architectural Institute of Japan.
3) The Association for the Development of Earthquake Prediction; Mexico earthquake survey team in Japan Society of Civil Engineers; The report of Mexico earthquake disaster and the repair, December, 1986.
4) Architectural Institute of Japan; Survey report on 1985 Mexico earthquake, 1986.
5) Fukushima, Y. and H. Kawase; The Irregular Ground Analyses of Mexico City Focused on the Time-Varying Characteristics of the Strong Ground Motion Records for Michoacan Earthquake 1985, The 7th Japan Earthquake Engineering Symposium (1986)
6) Watabe Research Team in Tokyo Metropolitan University; Prompt report of Loma Prieta earthquake disaster survey, October 1989.
7) Moriya, K.; Earthquake and ground disaster , Kajima publishing company.
8) Imaoka, K.; A study on dynamic properties of irregular ground, Doctoral Dissertation, Nagoya University, 1937.
9) Conference on disaster prevention in Tokyo metropolitan; Research on estimation of earthquake disaster in the district of Tokyo metropolitan
10) Nakado promotion center in Shizuoka prefecture; Tou-Nankai earthquake record, 1944
11) The center on fire service science; The all issued data of disaster prevention, a volume of earthquake and volcano disaster prevention.
12) Sato, K., S. Higashi, S. Abe, Y. Oda, H. Ishikawa and T. Takeda; Three-dimensional simulation based on underground structure in Kobe city, Proceedings of 24-th JSCE earthquake engineering symposium, July 1997.
13) Sato, K. and S. Higashi; The development of analytical method on seismic wave propagation considering three-dimensional underground structure included seismic source, Research report of the CRIEPI, U96043, March 1997.
14) Kawase, H.; The cause of the damage belt in Kobe: "The basin-edge effect", constructive interference of the direct S-wave with the basin-induced diffracted/ Rayleigh waves, Seismological Research Letters, Vol.67, No.5, pp25-34, September/October 1996.
15) Kawase, H. and S. Matsushima; Three-dimensional wave propagation analysis of simple two-dimensional basin structures with special reference to "the basin-edge effect" -The cause of

the damage belt during the Hyogo-ken nanbu earthquake, Zishin, the second series, Vol.50, pp431-449, 1998.

16) Satoh, T. and H. Kawase; Simulation of site amplification factors obtained from borehole records considering both two-dimensional effect and nonlinear behavior of soil sediments - Analysis of weak motion and strong motion observed at a vertical array at Kuno district in the Ashigara valley, J. Struct. Constr. Eng., AIJ, No.468,39-49,Feb., 1995.

17) H.L. Wong.; Effect of Surface Topography on the Diffraction of P, SV and Rayleigh Waves, Bulletin of the Seismological Society of America, Vol.72, No.4, pp.1167-1183. August 1982.

18) Michel Bouchon; Effect of Topography on Surface Motion, Bulletin of the Seismological Society of America,. Vol.63, No.3, pp. 615-632. April 1973.

19) M. D. Trifunac.; Surface Motion of a Semi-Cylindrical Alluvial Valley for Incident Plane SH Waves, Bulletin of the Seismological Society of America, Vol.61, pp1755-1770. December,1971.

20) Toki, K., T. Sato and K. Fujita; Seismic Response Analysis of surface layered media with irregular interface, 17th Symposium on the study of natural disaster (in Japanese) 1980.

21) Ohtsuki, A., T. Tazoh and K. Shimizu; Effect of Lateral Inhomogeneity on Seismic Waves and Ground Strains, Journal of Japan Society of Civil Engineering, No.350 /I-2 1984.

22) Higashi, S. and K. Kudo; Polarization and Frequency-Wavenumber Spectrum Analysis for the Strong-Motion Array Data in Ashigara Valley, Japan, J. Phys. Earth, 40, 5-25, 1992.

23) Koketsu, K. and S. Higashi; Three-Dimensional Topography of the Sediment/Basement Interface in the TOKYO Metropolitan Area, Central Japan, Bulletin of the Seismological Society of America,Vol.82, No.6, pp.2328-2349, December 1992.

24) Kawase, H., T. Sato, T. Watanabe, H. Yokota and S. Kataoka; Synthetics of strong ground motion considering diffracted waves generated at the edge of the basin, Proceedings of the National Symposium on Effects of Surface Geology on Seismic Motion, December 6-7, 1989, Tokyo Japan.

25) Ohori, Michihiro. and T. Minami; Seismic response of sedimentary basin using 2 dimensional Aki Larner Method, Bull. Earthq, Res. Inst. Univ.Tokyo, vol.65 , pp.809-850, 1990.

26) Pierre-Yves Bard and M. Bouchon; The Seismic Response of Sediment-filled Valleys. Part1. The Case of incident SH Waves, Bulletin of the Seismological Society of America, Vol.70, No.4, pp.1263-1286, August 1980.

27) Pierre-Yves Bard and M. Bouchon; The Seismic Response of Sediment-filled Valleys Part2 The Case of incident SH Waves, Bulletin of the Seismological Society of America, Vol.70, No.5, pp.1921-1941, October 1980.

28) Michel Bouchon and K. Aki; Discrete Wave-Number Representation of Seismic-Source Wave

Fields, Bulletin of the Seismological Society of America. Vol.67, No.2, pp.259-277. April 1977.

29) Ohori, Michihiro. H. Takenaka, K. Koketsu, and T. Minami; Reduction of the Memory Consumption in the AKi-Larner Method Journal of the seismological society of Japan, Vol.45, Second series, 1993.

30) Uebayashi, H., M. Horike, and Y. Takeuchi; Seismic Motion in a Three-Dimensional Arbitrarily-Shaped Sedimentary Basin, due to a Rectangular Dislocation Source, J. Phys. Earth,40.223-240,1992.

31) Ohori, M., K. Koketsu, and T. Minami; Sesmic Responses of Three-Dimensionally Sediment-Filled Valleys due to Incident Plane Waves , J. Phys.Earth, 40, 209-222, 1992.

32) Sato, K., S. Higashi, Y. Shiba and S. Abe; Seismic amplification on irregular subsurface ground -Various geological surveys , modeling for subsurface layer and seismic amplification based on earthquake observation-, Research report of CRIEPI, U95061, March 1996.

33) IASPEI/IAEE Joint WG and Japanese National WG; Proceedings of the International Symposium on the Effect of Surface Geology on Seismic Motion, ESG 1992 Vol II , March 1992.

34) Takeuchi, Y. (The representative researcher, Osaka Institute of Technology University); Synthetic research for the effect of surface geology on seismic motion, Synthetic research (A) on support foundation of science research in the Ministry of Education ministry, March 1993.

35) Kawase, H. and T. Sato; Simulation Analysis of Strong Motion in the Ashigara Valley Considering One- and Two-Dimensional Geological Structures, J. Phys. Earth ,40, 27-56, 1992.

36) Sato, K., H. Yajima, S. Higashi, Y. Shiba and S. Sasaki; Site amplification and incident wave field in irregularly layered ground - A case study for Kuno site in Ashigara valley during Eastern Yamanashi earthquake in 1996-, Research report of CRIEPI, U98007, October 1998.

37) Kawase, H.; A brief review of studies on the effects of surface geology on seismic motion and their perspective, 18 th Symposium on ground motion, Architectural Insititute of Japan, 7.1990.

38) Satoh, T., H. Kawase and T. Sato; Engineering Bedrock Waves Obtained Through the Identification Analysis Based on Borehole Records and Their Statistical Envelope Characteristics, J. Struct. Constr. Eng., AIJ, No.461, 19-28, Jul,1994.

39) M. Campillo., F.J. Sanchez-Sesma and K. Aki; Influence of small Lateral variations of a soft surficial Layer on seismic ground motion, Soil Dynamics and Earthquake Engineering, 1990, Volume 9, Number 6, November

40) John C. Wilson and Paul C. Jennings; Spatial Variation of Ground Motion Determined from Accelerograms Recorded on a Highway Bridge, Bulletion of the Seismological of America, Vol.75, No.6, pp.1515-1533, December 1985.

41) Toki, K., T. Sato, J. Kiyono, T. Nishioka and H. Mizutani; Modeling of Spatial Variation of Seismic Ground Notion on Layered Media Having an Irregular Interface, Annuals, Disas. Prev.

Res. Inst., Kyoto Univ,. No.33 B-2, 1990.

42) Kawase, H. and Y. Hayashi; Strong Motion Simulation in Chuo Ward, KOBE, During the Hyogo-Ken Nambu Earthquake of 1995 Based on the inverted Bedrock Motion, J. Struct. Constr. Eng., AIJ, No.480,67-76, Feb,1996.

43) Toki, K., T. Sato and K. Sato; Identification and dynamic behavior of an irregular ground thorough the array observations of earthquake motions, Vol.27, B-2, 1984.

44) Toki, K., T. Sato, J. Kiyono and T. Nishioka; A Method to Detect Intersection Phase Velocity From Short Period Seismic Motions, Annuals. Disas. Prev. Inst, Kyoto Univ., No.30 B-2, 1987.

CHAPTER 2

INVESTIGATION OF ANALYTICAL METHODS FOR AMPLIFICATION AND PROPAGATION OF SEISMIC WAVES

2.1 General Remarks

In this chapter, various analytical methods for seismic response of horizontally and irregularly layered grounds are examined. Such an examination is needed to assess the efficacy of analytical methods in modeling geological structure and their ability to make use of recorded motions in analyzing the effect of surface geology[1] on ground motion. Methods such as inversion techniques for geotechnical parameters of soil profile, seismic wave analytical methods and complex polarization analysis of recorded motions are employed to investigate the characteristics of seismic ground response.

Seismic ground response of a horizontally layered ground is typically computed by wave propagation matrix methods based on Haskel model[2] of multiple reflection in a layered medium. In the case of nonlinear ground response, the SHAKE computer code[3] is commonly used and strain dependency of soils is taken into account by performing an equivalent linear analysis. These methods require as input a geotechnical model of the soil profile for evaluating the seismic ground response. This chapter discusses a system parameter identification based on Newton's steepest gradient Method [4], SPIN[5] for short, to identify geotechnical parameters of soil profiles using records from down-hole observation sites. As described in more detail later, the identification method is performed using the average of spectral ratios at the down-hall sites.

Numerical methods for analyzing the seismic response of irregularly layered ground utilize one of the following four approaches:

1) Element type methods (include FEM and FDM)

2) Boundary integral equation methods (include BEM and AL method)

3) Ray theory methods

4) Hybrid methods

In this dissertation, the AL method is used to analyze irregularly layered ground and results of the analyses are discussed in section 2.3.

Recorded seismic ground motions are not stationary, as the motion is a composite of various kinds of waves such as body waves, surface waves, coda waves, converted, reflected, refracted and scattered waves generated in the process of wave propagation from the seismic source to the observation sites. Techniques for detecting these wave types such as evolutionary power spectra[6] and complex polarization analysis[7] of three-component seismograms are discussed.

These representative analytical methods are useful in understanding the seismic response of horizontally layered and irregularly layered grounds. In this chapter attention is focused on these analytical methods so as to determine their efficacy in determining the site response.

2.2 Local Site Characteristics of Horizontally Layered Ground

2.2.1 Estimation of Underground Soil Profiles using System Identification

One of the methods for estimating geotechnical parameters of soil profiles is based on the study of site amplification using spectral ratios of recorded seismograms between surface and base layers. Spectral ratios were strongly dependent on the type of seismic waves such as P-waves, S-waves, Love waves and Rayleigh waves as well as on the incident and the propagation azimuth angles of incident wave on the base layer. It is therefore important to compile a data set of recorded seismograms at sites with down-hole arrays.

In the analytical model developed to identify the underground soil profile, two assumptions made regarding the layering of the ground and the incidence angle were:

1) soil profile is horizontally layered in which each layer is isotropic and homogeneous, and

2) the incidence of SH-wave on the base layer is vertical.

The soil amplification is therefore considered to be the result of multiple reflection and refraction of the SH-wave propagating vertically in a horizontally layered ground.

In general, it is difficult to identify different wave types from observation records on soft ground. A data set was selected from observed records at various sites for testing the feasibility of identification of wave types using the following procedure. First the transfer function is calculated as the ratio of the fourier spectrum of the record at the surface to the fourier spectrum of the record at the base layer. First the transfer function is calculated as the ratio of the fourier spectra of records at the surface to the base layer. The fourier spectra are actually calculated using the same time window of running fourier spectra as shown in Fig. 2.1. The signals of records with high amplitudes on the

surface and base layers are used for their transfer function. From this set of records only those with phase characteristics of the transfer function that were in good agreement with the approximate values from preliminary models based on soil profiles from PS-logging, as shown in Fig. 2.2, were selected as the final data set. Table 2.1 lists the records in the earthquake data set.

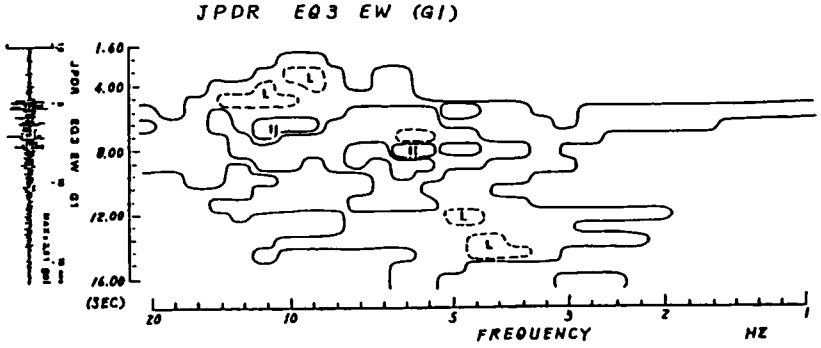

(a) Base layer

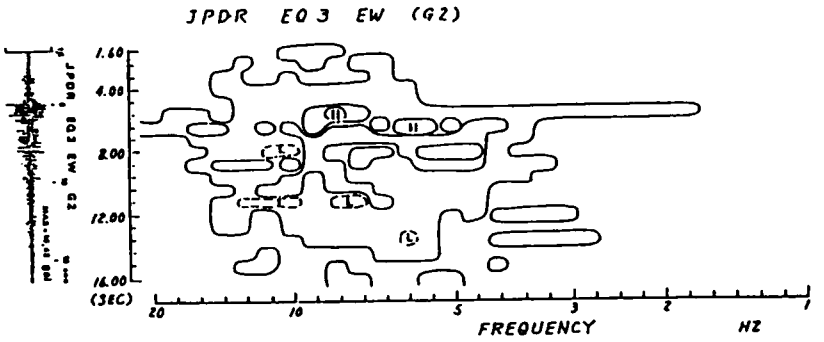

(b) Surface layer

Fig. 2.1 Running fourier spectrum (H: higher amplitude, L: lower amplitude)

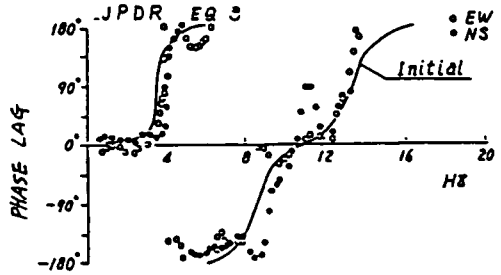

Fig. 2.2 Phase characteristics of transfer function of layered ground

Table 2.1(a) Earthquake Data

EQ.No.	Origin Time	Epicenter Long.	Lat	Depth (km)	M	Acc.max (gals)GL	Epicentral Dist. (km)
		TADOTSU					
1	Jan. 22, 1981	133°55'	34°57'	10	4.2	3.63	76.9
2	Mar. 6, 1981	135°23'	33°49'	50	4.5	1.08	158.5
		TEGANUMA					
1	Nov. 4, 1979	120°04'	35°31'	60	3.7	1.23	36.1
2	Nov. 16, 1979	141°00'	35°36'	40	4.2	2.02	83.6
3	Nov. 19, 1979	141°24'	37°31'	60	4.5	2.05	218.4
4	Nov. 22, 1979	140°08'	35°35'	70		0.74	28.3
5	Nov. 23, 1979	139°52'	36°07'	60	3.5	1.98	38.6
6	Nov. 23, 1979	141°06'	36°17'	50	3.8	1.15	100.9
7	Nov. 25, 1979	141°00'	36°47'	90	5.4	21.56	131.1
8	Dec. 7, 1979	140°15'	35°54'	60	3.6	0.79	13.3
9	Dec. 12, 1979	141°28'	29°02'	160	6.7	5.68	765.1
10	Dec. 12, 1979	*	*	*	*	0.43	*
11	Dec. 13, 1979	140°06'	35°38'	80	*	0.57	22.8
12	Dec. 13, 1979	140°55'	36°36'	50	3.6	1.04	110.6
		SENDAI (SDI)					
1	Jan. 18, 1981	143°14'	38°25'	5	6.1	5.08	205.1
2	Jan. 19, 1981	143°09'	38°38'	5	6.1	5.36	200.2
3	Jan. 19, 1981	142°58'	38°36'	11	7.0	34.07	183.9
4	Jan. 19, 1981	143°05'	38°36'	5	6.0	4.63	193.9
5	Jan. 23, 1981	143°03'	36°14'	8	6.6	21.25	189.2
6	Jan. 23, 1981	143°04'	38°10'	6	6.2	9.08	191.3
7	Feb. 25, 1981	143°14'	36°27'	4	5.7	3.88	205.2
8	Apr. 15, 1981	142°21'	37°16'	30	5.7	12.20	173.8
		SHIN-FUKUSHIMA					
1	Nov. 25, 1979	141°00'	36°41'	90	5.4	3.72	74.7
2	Dec. 19, 1979	141°11'	36°26'	50	4.9	3.24	104.2
3	Feb. 4, 1980	141°38'	37°18'	50	4.6	33.43	59.7
4	Feb. 13, 1980	141°47'	36°34'	50	4.2	8.55	114.0
5	Mar. 30, 1980	141°33'	37°04'	50	4.3	5.02	61.1
6	Mar. 30, 1980	141°34'	37°55'	90	3.8	4.68	81.9
7	Apr. 15, 1980	141°42'	37°55'	60	4.0	8.56	90
8	June. 30, 1980	141°47'	37°48'	50	5.1	17.68	87.6
9	July. 13, 1980	141°56'	37°18'	40	4.6	9.19	86.1
10	Oct. 9, 1980	141°00'	36°20'	40	5.1	7.38	113.5
11	Apr. 13, 1981	142°21'	37°16'	30	5.7	13.05	123.3
12	Nov. 6, 1981	141°43'	37°53'	70	4.9	22.38	88.6

Table 2.1(b) Earthquake Data

EQ.No.	Origin Time	Epicenter Long.	Lat	Depth (km)	M	Acc.max (gals)GL	Epicentral Dist. (km)
		KINOKAWA					
1	Dec. 18, 1980	135°14'	34°18'	0	2.8	5.36	14.3
2	Dec. 18, 1980	135°13'	34°14'	10	2.5	4.25	11.7
3	Dec. 18, 1980	135°13'	34°16'	0	3.1	6.12	13.2
4	Dec. 20, 1980	135°12'	34°13'	10	3.1	3.54	12.8
5	Sep. 29, 1981	135°13'	34°13'	0	3.7	10.92	11.8
6	Nov. 12, 1981	135°20'	34°19'	0	2.6	3.88	12.4
7	Dec. 16, 1981	135°08'	34°11'	0	2.9	3.10	19.1
8	Dec. 19, 1981	135°13'	34°08'	0	3.5	12.41	13.8
		TOKAI (TKI)					
1	May. 29, 1983	141°53'	36°57'	40	5.5	4.76	125.8
2	June. 29, 1983	141°06'	36°44'	40	4.7	13.91	53.0
3	July. 2, 1983	141°07'	36°54'	50	5.8	89.74	66.2
		JPDR					
1	July. 23, 1982	141°55'	36°15'	10	7.0	104.09	119.8
2	July. 25, 1982	141°52'	36°21'	10	5.9	8.19	113.6
3	Aug. 12, 1982	140°49'	36°21'	50	4.0	16.42	22.2
4	Aug. 14, 1982	141°29'	36°22'	30	5.8	18.03	79.2
5	Aug. 29, 1982	141°108'	37°04'	60	4.9	20.12	82.5
6	Sep. 15, 1982	140°11'	36°36'	110	4.5	28.1	41.2
		ST-1 (HMY)					
1	June. 22, 1979	139°09'	35°47'	0	3.9	4.82	32.0
2	July. 2, 1979	139°58'	36°01'	60	4.1	10.5	52.6
3	Aug. 12, 1979	140°23'	34°35'	50	5.7	1.35	181.6
4	Oct. 9, 1979	139°50'	36°09'	50	4.1	6.97	43.8
5	Oct. 29, 1979	140°45'	35°07'	90	5.5	2.11	158.0
6	Nov. 25, 1979	141°00'	36°41'	90	5.4	13.16	93.9
7	Feb. 2, 1980	139°51'	36°06'	50	4.2	20.69	43.5
8	Mar. 12, 1980	140°31'	34°57'	80	5.6	2.97	155.4
9	Apr. 22, 1980	137°55'	32°09'	400	6.6	4.67	448.0
10	May. 8, 1980	140°27'	34°31'	60	5.7	2.78	191.1
11	June. 10, 1980	139°32'	35°56'	50	4.3	13.42	15.4
12	June. 18, 1980	140°01'	35°38'	80	4.6	3.12	70.2
13	June. 6, 1980	139°14'	34°55'	10	6.7	8.57	121.0
14	Aug. 15, 1980	139°46'	34°51'	90	5.0	1.40	132.3
15	Aug. 31, 1980	139°50'	36°04'	50	3.5	5.44	41.2
16	Sep. 25, 1980	140°10'	35°34'	70	4.8	2.84	85.6
17	Sep. 25, 1980	140°06'	35°33'	80	4.7	2.40	81.8
18	Oct. 6, 1980	140°07'	36°08'	70	4.6	10..44	67.7
19	Oct. 9, 1980	141°00'	36°20'	40	5.1	3.83	150.1

The incidence angles at the base layers at sites for earthquakes in the above earthquake data set estimated from the traveling time table developed by Dr. Ichikawa and Mochizuki[8] were highly variable but were less than 15° at all sites and occasionally close to 30° as shown by their distribution in Fig. 2.3. Fig. 2.4 shows the effect of incidence angle on the spectral ratio and this figure indicates that spectral ratios are not relatively variable for incidence angle.

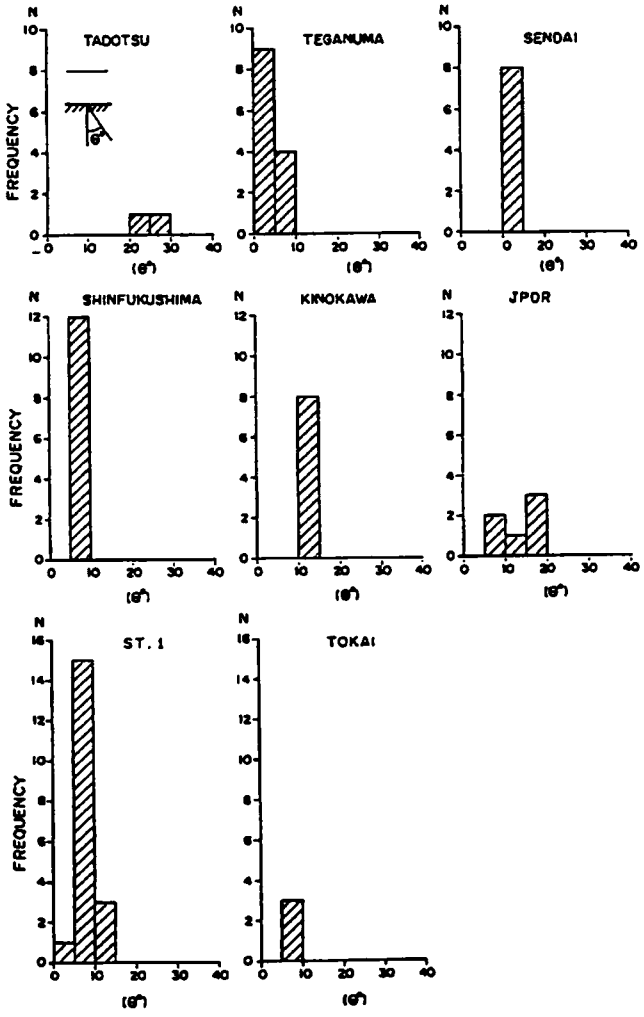

Fig. 2.3 Distribution of incident angles of earthquake records

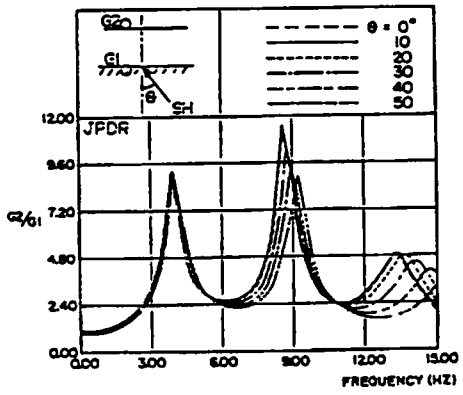

Fig. 2.4 Variation of spectral ratios for different angles

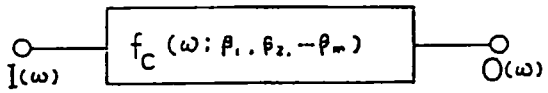

Fig. 2.5 Schematic concept of system identification

(I(ω) indicate input, O(ω) indicate output,fc($\omega, \beta_1, \beta_2, \cdots \beta_m$) is system function)

A system identification method is used to estimate geotechnical parameters of underground soil profile using spectral ratios of down-hall records. The unknown system parameters were identified using spectra of the input to and output of the system as shown conceptually in Fig. 2.5. The inversion technique uses least squares and parameters of the soil profile were estimated by minimizing the sum of square of the errors between the recorded and estimated transfer functions.

If the recorded function is fo(ω) and the computed one is fc(ω ; $\beta_1, \beta_2, \ldots \beta_m$), the parameters $\beta_1, \beta_2, \beta_3, \cdots \beta_m$, which in this case are the geotechnical parameters of soil profile were estimated by minimizing the objective function S as shown in the equation below.

$$S = \sum_{i=1}^{n} \left[f_0(\omega_i) - f_c(\omega_i; \beta_1, \beta_2, \beta_3 \cdots \beta_m) \right]^2 \cdot W(\omega_i) \rightarrow \min(n >> m) \tag{2.1}$$

where W(ω_i) is a weighting function. The parameters $\beta_1, \beta_2, \beta_3, \cdots \beta_m$ are estimated by solving the following equations:

$$\frac{\partial S}{\partial \beta_j} = 0 \quad (j = 1,2,\cdots m) \tag{2.2}$$

Simple as equation (2.2) appears, it is not a trivial task to solve the equation for the case when it is nonlinear with respect to the parameters β_j. In the literature several methods have been proposed for solving equation (2.2) in nonlinear system identification. In this dissertation the optimal gradient method belonging to the family of steepest descent methods as proposed by Ohta[9] is used.

The fundamental issue in steepest descent methods is to determine the gradient direction (P(h)) to search for parameters $\beta_1, \beta_2, \beta_3, \cdots \beta_m$ using gradient vectors of the objective function S. The searching direction for the k-th parameter is given by the gradient direction as indicated in the equation:

$$P^{(k)} = -\nabla S\left(x^{(k)}\right) \tag{2.3}$$

This direction corresponds to the best direction along which the objective function S reduces in the vicinity of $x^{(k)}$. In the optimal gradient method the decision to move to a new point $x^{(k+1)}$ in order to reduce the objective function S is made on the basis of the following three equations:

$$\begin{aligned} &x^{(k+1)} = x^{(k)} + \alpha^{(k)} p^{(k)} \\ &S(x^{(k)} + \alpha^{(k)} p^{(k)}) = \min S(x^{(k)} + \alpha^{(k)} p^{(k)}) \\ &p^{(k)} = -\nabla S\left(x^{(k)}\right) \end{aligned} \tag{2.4}$$

In order for this method to work an analytical expression for the transfer function of a soil profile is needed. For this purpose, the transfer function between the surface and base layers is expressed using S-wave multiple reflection for vertical incidence at the base layer. The relationship between the spectral amplitudes at the surface and at a depth of Z is given by,

$$Uz(\omega) = B_{11} \; U_0(\omega) \tag{2.5}$$

where $Uz(\omega)$ is the displacement spectral amplitude at depth Z and $U_0(\omega)$ is the displacement spectral amplitude at the ground surface. The B_{11} is the (1,1) element of matrix B. The matrix B is given by the following equation:

$$B = a_l \cdot a_{l-1} \cdot a_{l-2} \cdots a_2 \cdot a_1 . \tag{2.6}$$

The term a_l in the above equation is called the layer matrix and is related to the structural parameters of the l-th soil layer as follows:

$$a_l = \begin{bmatrix} \cos k_l d_l (k_l \mu_l)^{-1} & \sin k_l d_l \\ -k_l \mu_l \sin k_l d_l & \cos k_l d_l \end{bmatrix} \tag{2.7}$$

where $k_l = \omega / Vs_l$, μ_l, Vs_l, and dl are the wave number, rigidity, shear wave velocity and thickness of the l-th layer, respectively.

The damping of the soil is included by making the rigidity term complex-valued ($\mu_l \rightarrow \mu_l + i\omega \mu'_l$, μ'_l: coefficient of viscosity) on the assumption that the soil is a Voigt-type elastic material. In such a material the cyclic dissipated energy Q is given by $\Delta E / 2\pi E$, in which E represents the strain energy of one cycle. Q is related to μ_l and μ'_l through the equation $Q_l^{-1} = \omega \mu'_l / \mu_l$, and can be expressed in terms of the damping factor h as $Q = 1/2h$.

When estimating damping factors for soils, attention needs to given to the damping mechanism of soil deposits. Typically, Q-values of soil deposits were taken to be constant in the frequency domain which means that the damping factor is not dependent on frequency. Although damping factor of soil is taken to be constant over a wide range of frequency based on in-house soil tri-axial tests, recent studies[4] of seismic coda waves have shown that Q is dependent on frequency. The frequency dependency of damping of soil deposits has, also, been recognized from analyses of spectral ratios between the records at the surface and base layers[4]. However, damping is taken to be independent of frequency because of the difficulty in interpreting the physical meaning of frequency dependent damping from considerations of the source and site characteristics.

In the system identification method the parameters of soil deposits such as thickness and density were taken directly from PS logging tests and only Vs and Q were identified from observed records. First Vs is identified using $U_0(\omega)/U_z(\omega)$ and then Q is identified using $U_z(\omega)/U_0(\omega)$ following Ohta's method[9].

2.2.2 Numerical Investigation of System Identification Method

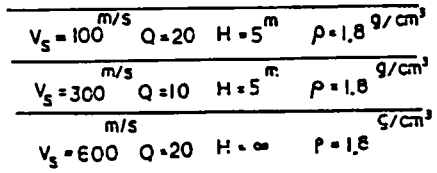

Fig. 2.6 Layered model for system identification

In system identification parameters of the system are identified by minimizing an objective function which is expressed by the sum of squares of the differences between the observed and estimated values. A big issue in the solution to this problem is the convergence of the solution when the objective function S is nonlinear. The optimal gradient method is known to be globally convergent, i.e. it converges to the exact solution, if there is no local minimum in the objective function S but in real world problems it is almost impossible to guarantee global convergence. An experiment was performed to evaluate the convergence of soil parameters using a simple layered ground model as shown in Fig. 2.6. The mean S-wave velocities of the first and second layers were 100 m/s and 300 m/s, respectively and the mean Q values for the two layers were 20 and 10, respectively. A degree of uncertainty was introduced in the model by assigning random values generated from a normal distribution with a coefficient of variation (σ / μ) of 0.2. The variation introduced in the soil parameters can be interpreted to represent the uncertainty of PS logging results and is in conformity with measured errors of about 10 % and 20 - 30 % for S-wave velocity and Q,

respectively, as reported by Ohta[9].

Identified values of Vs are shown in Fig. 2.7 by using solid lines for the first layer and chained lines for the second layer. As an example, the initial values of Vs for the second layer were 200, 313, 360 and 310 m/s in the first to fourth tests, respectively. The number next to a graph in Fig 2.7 refers to the number of the test. The results shown here indicated that the number of iterations increased depending on how far the initial value was from the target value.

Fig. 2.8 shows results of identification of Q in the two layers from tests conducted by varying Q and keeping S-wave velocities in the layers the same as their target values. As an example the initial values of Q for the second layer were 6.5, 10.5,12, 10.3 in the first to fourth tests, respectively. Unlike in the case of Vs, the number of iterations for convergence did not always increasie with distance of the initial value from the target. Starting with an initial value of 6.5 the target of 10.0 was reached in the second iteration itself.

Fig. 2.9 shows the target spectral ratio and the initial and final spectral ratios. The results of the tests indicate that the optimal gradient method can be effectively used to estimate S-wave velocity and Q of soil deposits within the region of their measurement errors. Moreover, as shown in Fig.2.7 and Fig. 2.8, the sum of the square of the residuals decreases to a value less than 50 % in just the second iteration.

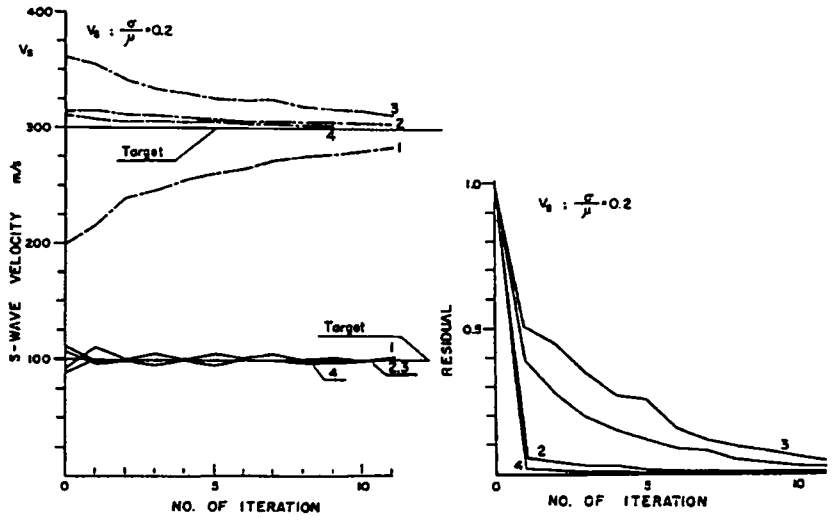

Fig. 2.7 Results of sensitivity of identified S-wave velocities

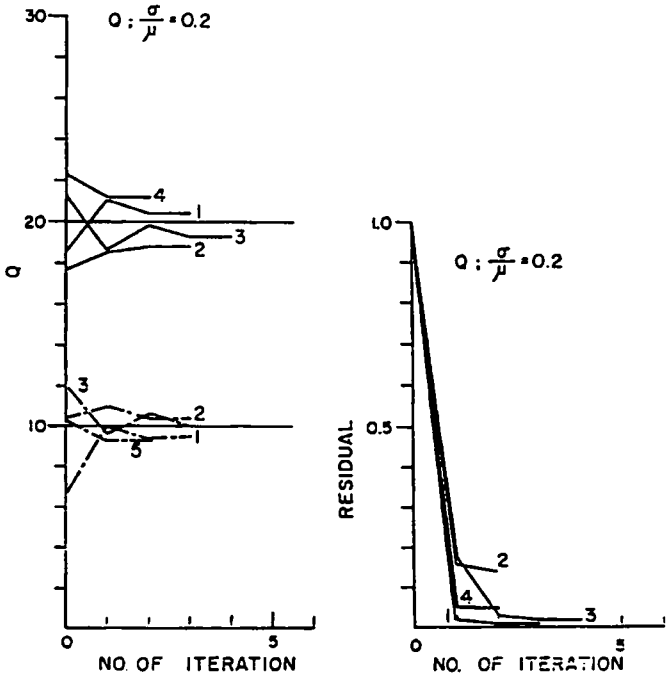

Fig. 2.8 Results of sensitivity of identified Q-values

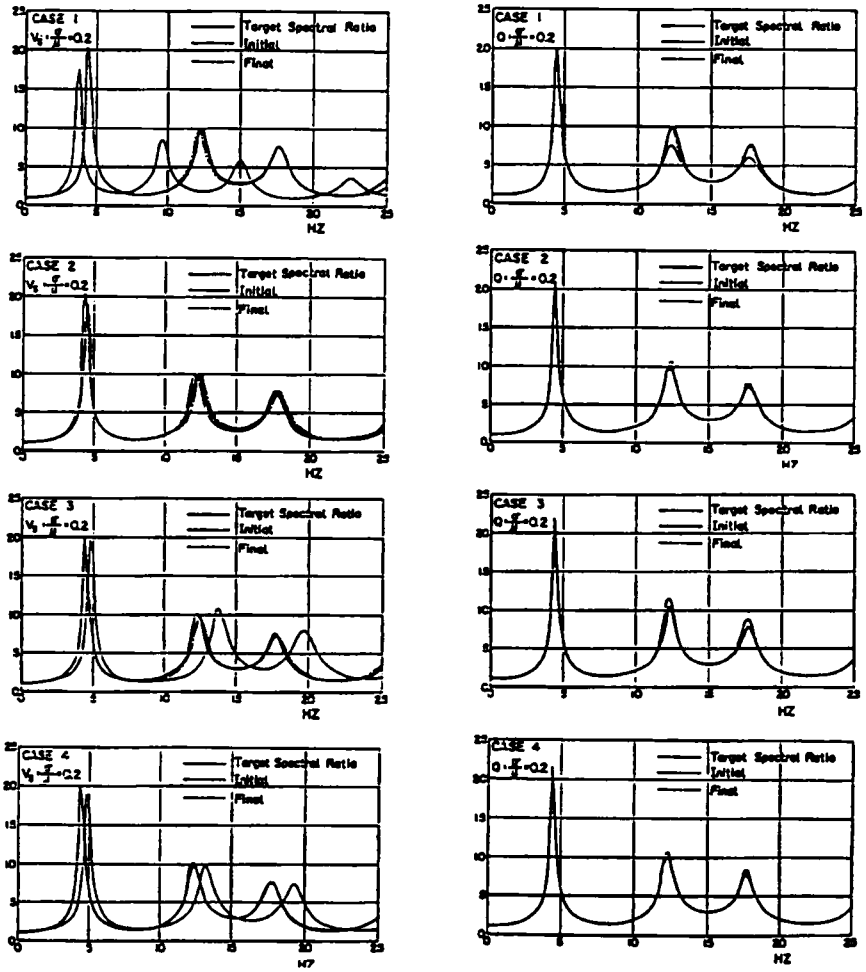

Fig. 2.9 Comparison of the transfer function characteristics related to system identification

(Left: S-wave velocity, Right: Q-value)

2.3 Local Site Characteristics of Irregularly Layered Ground

2.3.1 Discrete-wave-number Method (Aki-Larner Method)

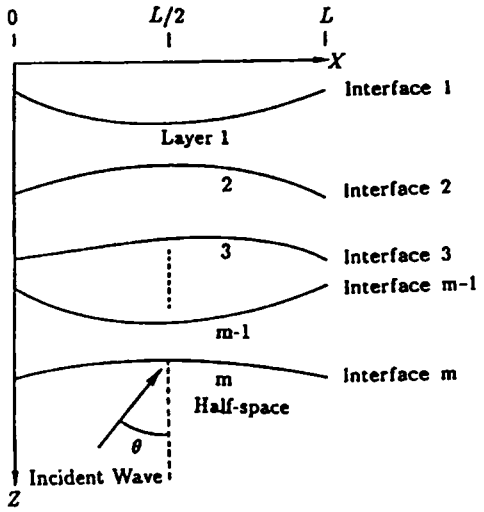

Fig. 2.10 Irregularly multi-layered model[7]

Fig. 2.10[10] shows a irregularly multi-layered model with shear wave velocity $\beta_1, \beta_2, \cdots$ and density $\rho_1, \rho_2, \cdots$. The problem here is to determine the motion at the free surface z = 0, when plane SH waves polarized in the y-direction with frequency ω are incident in the x-z plane at an angle θ^0 measured clockwise from the z-direction. This is a two-dimensional problem in the x-z plane and the solution is independent of y. Numerical computational method for this two-dimensional problem was developed by Keiichi A. and K. L. Larner[11]. The method is discussed in some detail below.

Let the displacements in the upper and lower layers of the medium be $u_1(x, z)$ and $u_2(x, z)$, respectively. For a sinusoidal time dependence represented by e-i ω t, the amplitudes of the displacements can be expressed as a superposition of plane waves as follows:

$$u_1(X,Z) = \int_{-\infty}^{\infty}\left[A_1(k)e^{ikX+i\nu_1 Z} + B_1(k)e^{ikX\ i\nu_1 Z}\right]dk \tag{2.7}$$

$$u_2(X,Z) = e^{ik_0 X\ i\nu_0 Z} + \int_{-\infty}^{\infty} A_2(k)e^{ikX+i\nu_2 Z}dk \tag{2.8}$$

where the time term e-i ω t is omitted hereafter to simplify the equations, and k_0 and ν_0 are wavenumbers of the input waves at the base layer in the x and z components, respectively. In equations (2.7) and (2.8), Ai(k) and Bi(k) are scattering coefficients. The first of these coefficients expresses the waves coming from z=+∞ and the second expresses the waves scattered back toward

$z=+\infty$. The first term on the right hand side of equation (2.8) expresses the incident wave. ν_i indicates the vertical wavenumber in each layer. Subscript (0) for k_0, ν_0 indicates wavenumber in the base layer. θ_0 means incident angle. The following relationships can be obtained from considerations of

$$\begin{aligned} k_0 &= \omega/\beta_2 \sin\theta_0 \\ \nu_0 &= \sqrt{\omega^2/\beta_2{}^2 - k_0^2} = \omega/\beta_2 \cos\theta_0 \\ \nu_1 &= \sqrt{\omega^2/\beta_1{}^2 - k^2} \\ \nu_2 &= \sqrt{\omega^2/\beta_2{}^2 - k^2} \end{aligned} \tag{2.9}$$

The boundary conditions for this idealized problem (see Fig.2.10) are as follows:

1) stress equals to zero on the ground surface, and

2) displacement and stress satisfy continuity at the interface between the surface and base layers.

Applying the first boundary condition, the relation $B_1(k) = A_1(k)$ is obtained and substituting for $B_1(k)$ in equation (2.7), $u_1(x, z)$ can be expressed as,

$$u_1(x,z) = 2 \int_{-\infty}^{\infty} A_1(k) e^{ikx} \cos \nu_1 z dk \tag{2.10}$$

Applying the second boundary condition, the following relationships are satisfied at z = H:

$$u_1[x,H] = u_2[x,H] \tag{2.11}$$

$$\mu_1(\partial u_1/\partial z) = \mu_2(\partial u_2/\partial z) \tag{2.12}$$

where μ_1 and μ_2 are the rigidity of the surface and base layers, respectively.

Substituting into equations (2.11) and (2.12) the expressions for u_1 and u_2 from equations (2.10) and (2.8), respectively, the following equations are obtained:

$$\begin{aligned} \int_{-\infty}^{\infty} [A_1(k) g_{11}(k,x) + A_2(k) g_{12}(k,x)] e^{ikx} dk &= h_1(x) e^{ik_0 x} \\ \int_{-\infty}^{\infty} [A_1(k) g_{21}(k,x) + A_2(k) g_{22}(k,x)] e^{ikx} dk &= h_2(x) e^{ik_0 x} \end{aligned} \tag{2.13}$$

where

$$
\begin{aligned}
g_{11}(k,x) &= 2\cos\nu_1 H \\
g_{12}(k,x) &= -e^{i\nu_2 H} \\
g_{21}(k,x) &= -2\mu_1\nu_1 \sin\nu_1 H \\
g_{22}(k,x) &= -i\mu_2\nu_2 e^{i\nu_2 H} \\
h_1(x) &= e^{-i\nu_0 H} \\
h_2(x) &= i\mu_2\nu_0 e^{-i\nu_0 H}
\end{aligned}
\tag{2.14}
$$

$A_1(k)$ and $A_2(k)$ are obtained by solving the integral equations (2.13). In order to solve these equations, they are converted into infinite-sum equations by assuming a periodicity in the surface or subsurface irregularity along the horizontal direction. This requires that the wavenumber k be expressed as,

$$
k = k_0 + \frac{2\pi n}{L} \quad (n = 0,\pm 1,\pm 2,\cdots) \tag{2.15}
$$

where L is the length in the x direction of the layered model. If the irregularity of the layer expresses by the function f(x) is periodic, then the following hold:

$$
f(x+mL) = f(x) \quad (m = \pm 1,\pm 2,\cdots). \tag{2.16}
$$

Making use of equations (2.15) and (2.16) in equation (2.13) the later equation is converted into the next equation.

$$
\sum_{n=-\infty}^{\infty}\left[A_n^{(1)} g_n^{(j1)}(x) + A_n^{(2)} gn^{(j2)}(x)\right]\cdot e^{2\pi i n x/L} = h_j(x) \qquad (j = 1,2) \tag{2.17}
$$

where,

$$
\begin{aligned}
A_n^{(i)} &= A_i(k_n)\Delta k_n \\
g_n^{(ij)} &= g_{ij}(k_n, x) \\
kn &= k_0 + \frac{2\pi n}{L} \\
\Delta k_n &= \frac{2\pi}{L}
\end{aligned}
\tag{2.18}
$$

The infinite-sum equation can now be approximated by a finite- sum equations n = N, where N is the limit number of horizontal discrete wave numbers. The finite-sum displacement u_{1N} in the surface layer, is given by

$$u_{1N}(x,z) = 2\sum_{n=-N}^{N} A_n^{(1)} \cos \nu_n^{(1)} z e^{ik_n x} \tag{2.19}$$

Similarly, the finite-sum displacement u_{2N} in the base layer is given by,

$$u_{2N}(x,z) = e^{ik_0 x - i\nu_0 z} + \sum_{n=-N}^{N} A_n^{(2)}(k) e^{ik_n x + i\nu_n^{(2)} z} \tag{2.20}$$

where

$$\nu_n^{(j)} = \left(\omega^2 / V_j^2 - k^2\right)^{1/2} \tag{2.21}$$

The value of N corresponding to the limit number of horizontal discrete wave numbers is decided on the basis of the fundamental mode of Love and Rayleigh waves as:

$$N \geq 1.1L / \beta_{min} T \tag{2.22}$$

where T is the period of seismic wave and β_{min} means minimum shear wave velocity of the softer layer.

2.3.2 Two Dimensional Response Analysis for Plane SH and SV Waves Incidence

(1) Description of site

The site called TKY is located in a buried valley and it has a sedimentary layer of soil profile along a east to west section. The sedimentary layer is non-symmetric as shown in Fig. 2.11. The site amplification characteristics at this site were analyzed using records from vertical and horizontal strong motion seismograph arrays that are described in more detail in chapter 5. The AL-method[12] is used to compute the seismic ground response of this buried valley site. The parameters used in the 2-D analysis were:

Length of 2-D model: L = 0.9 Km

Maximum wave-number: K = 32

Incident wave angle: $\theta = 0°$

Maximum frequency: $f_{max} = 5.0$ Hz

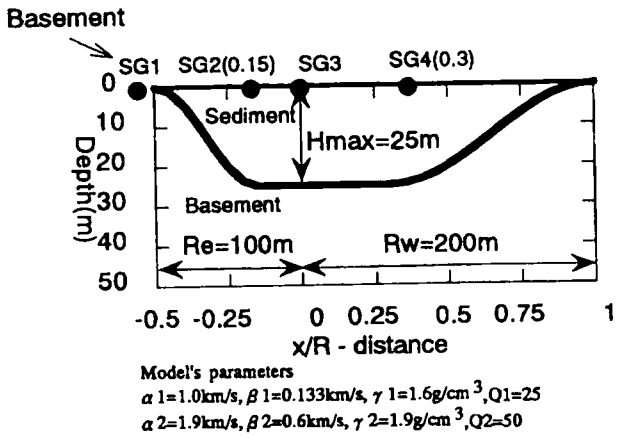

Fig. 2.11 Buried valley model at TKY site

(2) Seismic ground response

Acceleration time histories at the surface of the buried valley were computed using the 2-D AL method and for the sake of comparison the 1-D SHAKE program was, also, used for plane SH and SV waves incidence. The Ricker wavelet with a natural frequency ω_0 is typically assumed to represent the seismic wave. At the TKY site, the natural frequency of the Ricker wavelet was taken as 1.3 Hz which corresponded to the fundamental natural frequency of the sedimentary layer.

Seismic ground responses were plotted for different frequencies and locations on the surface. In subsequent plots of seismic ground response the frequencies were normalized by the fundamental natural frequency of the sedimentary layer (=f_1) and distances measured from the center of the buried valley to points on the surface were normalized by a distance R from the edge to the center hereafter called "sloped interface length".

The 2-D model at TKY shown in Fig. 2.11 is non-symmetric and the distance to the western edge of the valley is 100 m while that to the eastern edge is 200 m. The distances measured from the center were normalized by the slope interface length on the east side of 200 m. Therefore points on the surface of the valley located at distances x from the center have normalized distances x/R ranging from -0.5 to +1.0.

The ground responses to SH-wave incidence obtained from 1-D and 2-D models are shown in Fig. 2.12. In the 2-D response, secondary surface waves generated at the edge of the buried valley after the arrival of the first SH-wave were clearly seen but were totally absent in the 1-D ground response. The horizontal and vertical ground responses to SV-wave incidence obtained from the 2-D model are shown in Fig. 2.13. The horizontal ground responses at various locations were amplified in almost perfect synchronicity indicating an absence of surface waves. However, in the vertical

response secondary surface waves generated at the edge of the valley can be found. The results shown in Figs. 2.12 and 2.13 are typical examples of secondary surface waves in a buried valley. The secondary surface wave for SH- and SV-wave incidences are predominantly Love and Rayleigh waves, respectively.

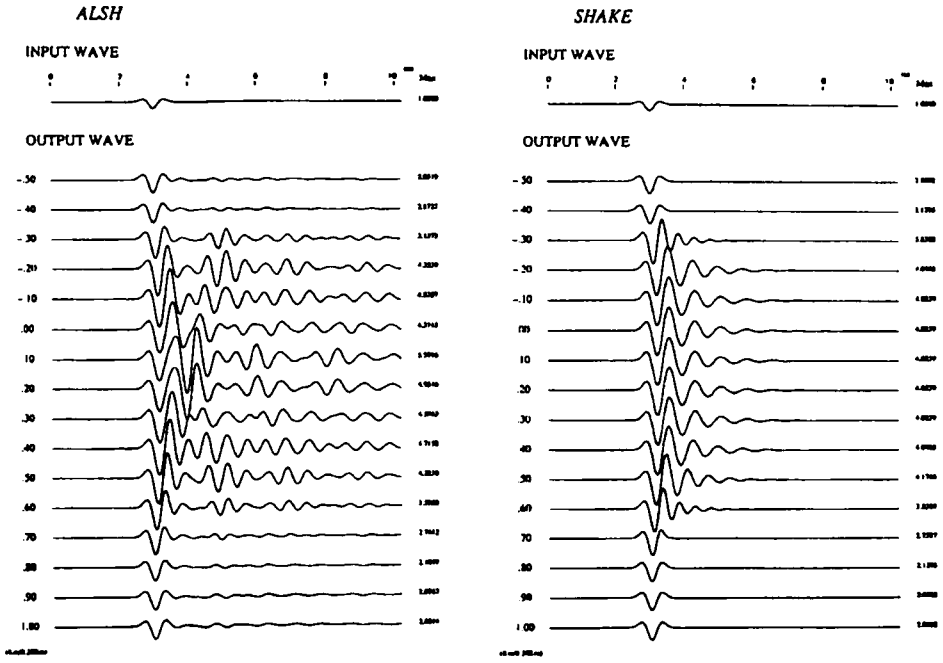

Fig. 2.12 Horizontal ground response for SH wave analyzed from 1-D and 2-D models at TKY

(Ricker wave input of fp=1.3Hz)

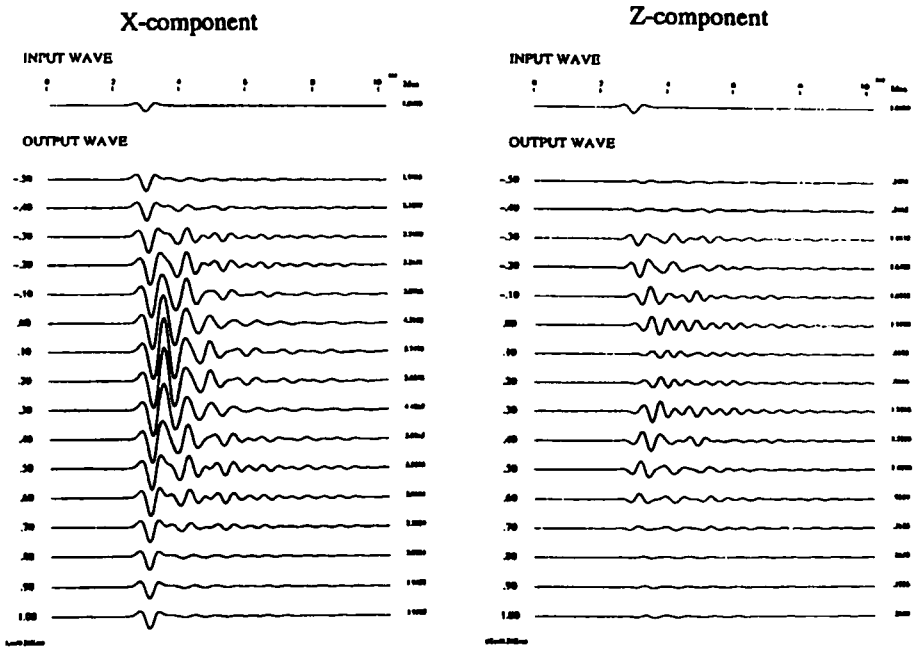

Fig. 2.13 Horizontal and vertical ground response for SV wave analyzed from 2-D model at TKY

(Ricker wave input of fp=1.3Hz)

The transfer functions of 1-D and 2-D horizontal and vertical ground responses for SH and SV-wave incidences are plotted in Figs. 2.14 to 2.17 against normalized frequency and normalized lateral distance. The 1-D transfer function represents the frequency response of a horizontally layered medium while the 2-D transfer function is more representative of the frequency response characteristic of irregularly layered ground and this lead to the apparent difference in the responses to SH- and SV-wave incidences seen in these figures.

From past observations of seismic response characteristics of irregular layered ground, it is well known that peaks of amplitude of 2-D analyses are concentrated at the central parts of the sediment layer and the intermediate area between the flat and sloped layers. The response to SH-wave incidence along the anti-plane of the 2-D model typically has many peaks at regularly increasing frequency because of the interference generated by dispersion of the secondary surface waves. The horizontal and vertical responses of the 2-D model to in-plane SV-wave incidence have peaks resulting from dispersion of secondary surface waves that were more than twice as large as the peaks at the natural frequency of 1.3 Hz for the 1-D model at the central part of the valley. An examination of these secondary surface waves shows that the phase velocity of Rayleigh waves for SV-wave incidence is larger than that of Love waves for SH-wave incidence for frequencies less than twice the natural frequency.

Fig 2.18 shows the 1-D and 2-D transfer functions at frequencies of 0.98 times, 1.2 times and 1.7 times the natural frequency of 1.3 Hz. At frequencies of 1.2 times the natural frequency (=1.6Hz) and 1.7 times (2.2Hz), secondary peaks of the seismic response in the horizontal and vertical directions for SH- and SV-wave incidences appear at x/R= -0.25 and 0.5, respectively. The locations at which the peaks occur correspond to points along the interface of the flat and sloped layers. These observations support the hypothesis of secondary waves generated by Love and Rayleigh waves.

Amplification factors at the central part for 2-D analyses were about 1.3 to 1.5 and 2 to 4 times larger than amplification factors for 1-D analysis at 1.3 Hz and 2.2 Hz, respectively. The 2-D amplification factors at locations along the interface of the flat and sloped layers were about 2 to 4 times larger than those obtained from 1-D analysis for frequencies close to 2.2 Hz. On the average the 2-D seismic response of irregularly layered ground was seen to be amplified by about 2 to 3 times as compared to the response computed from a 1-D model of a horizontally layered ground.

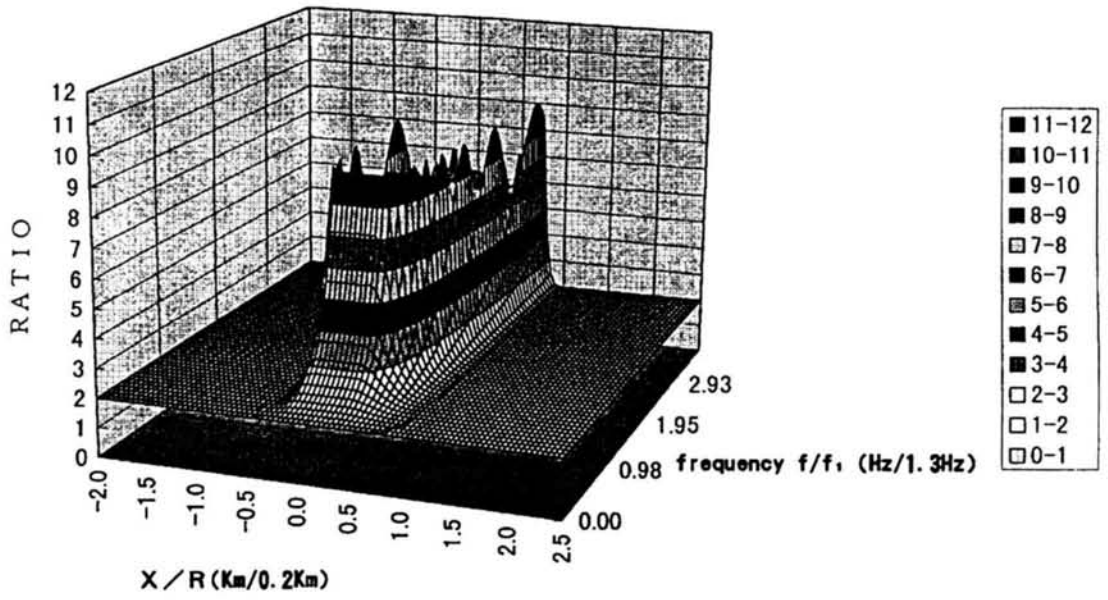

(a) 3-D view

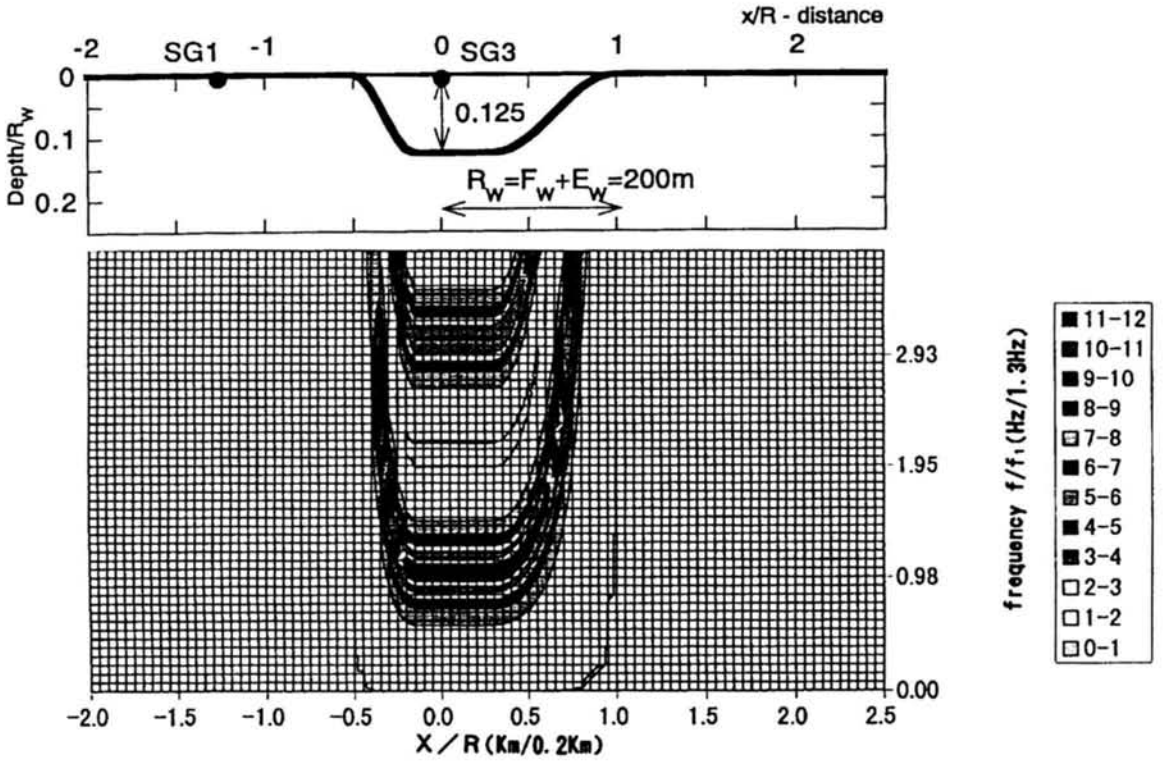

(b) 3-D contour map

Fig. 2.14 Transfer function of horizontal ground response for SH wave analyzed from 1-D model at TKY

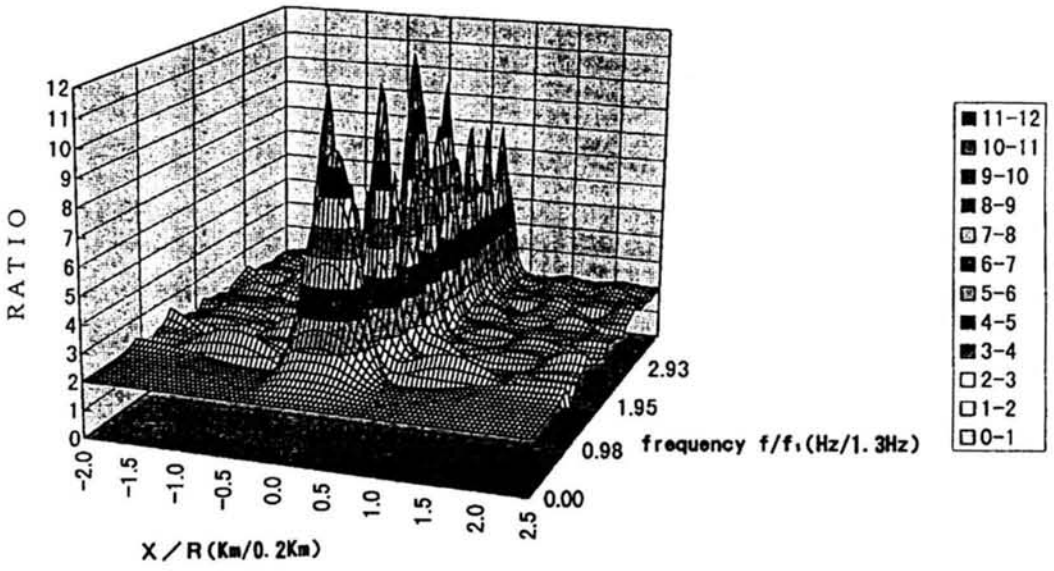

(a) 3-D view

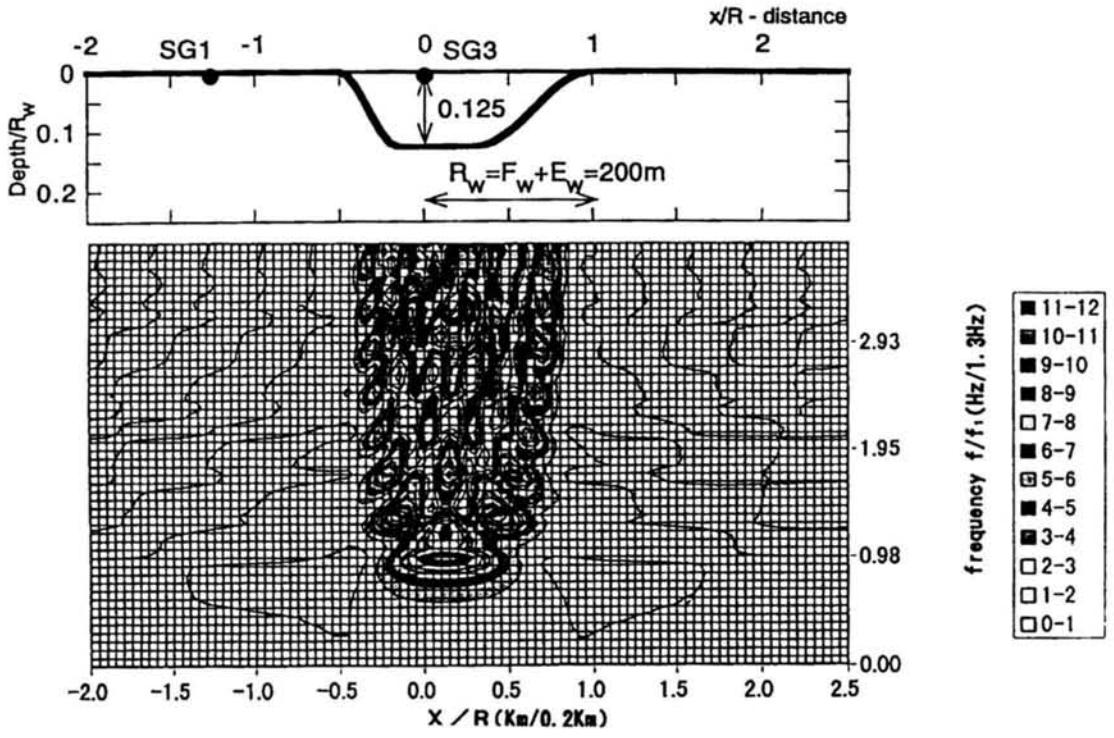

(b) 3-D contour map

Fig. 2.15 Transfer function of horizontal ground response for SH wave analyzed from 2-D model at TKY

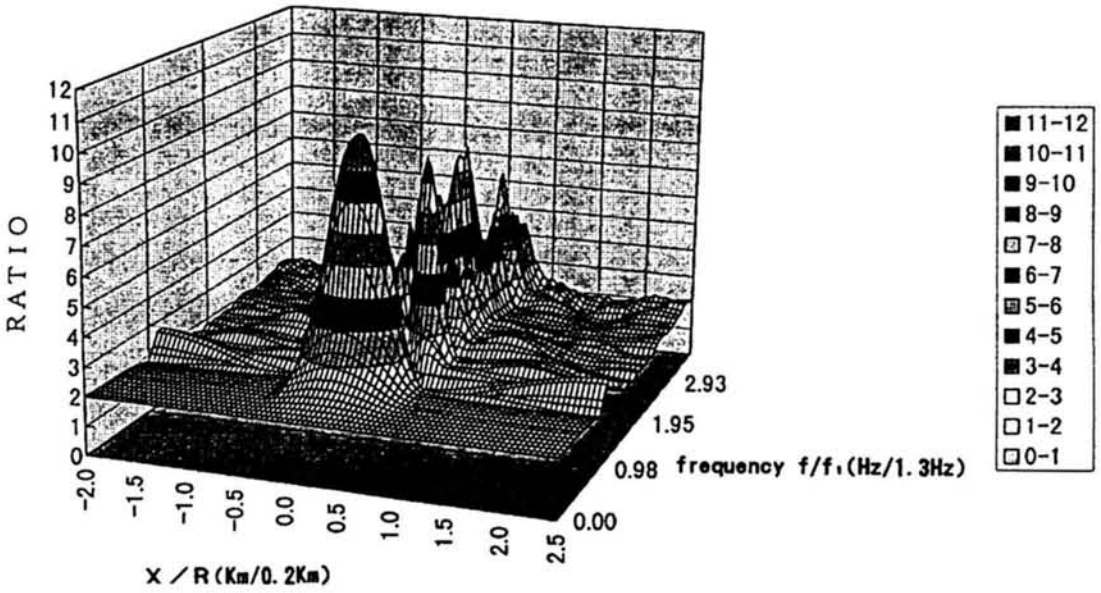

(a) 3-D view

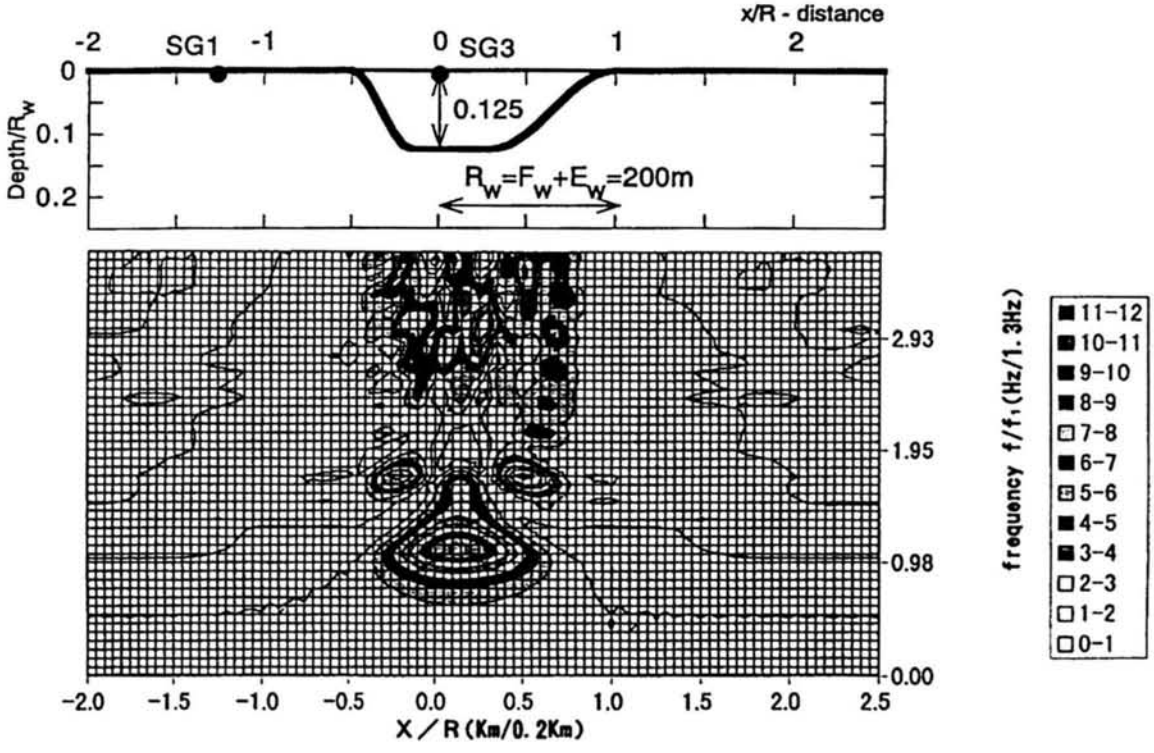

(b) 3-D contour map

Fig. 2.16 Transfer function of horizontal ground response for SV wave analyzed from 2-D model at TKY

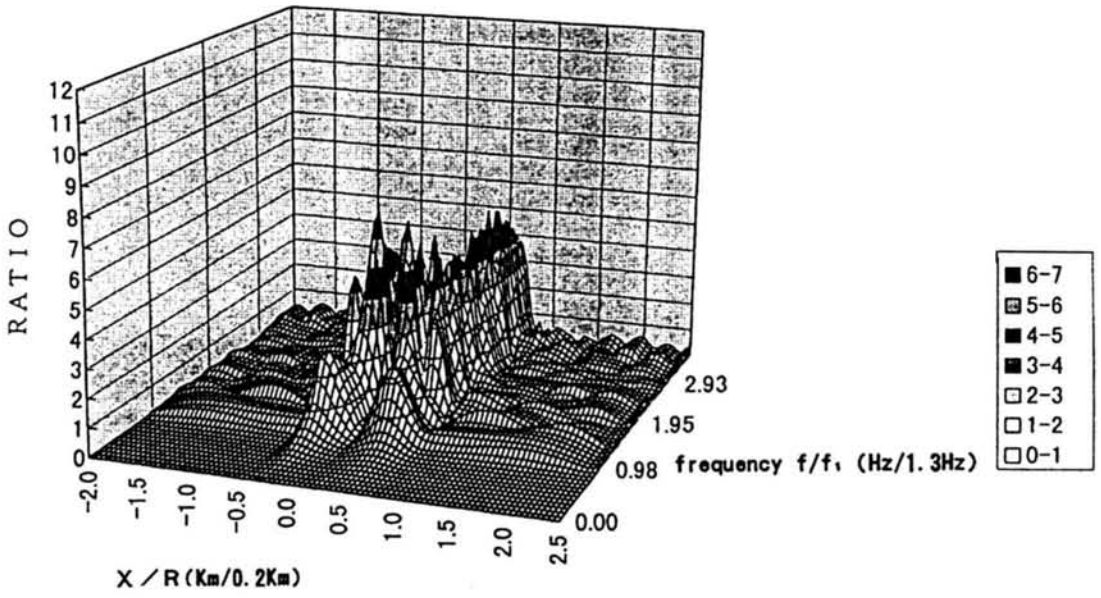

(a) 3-D view

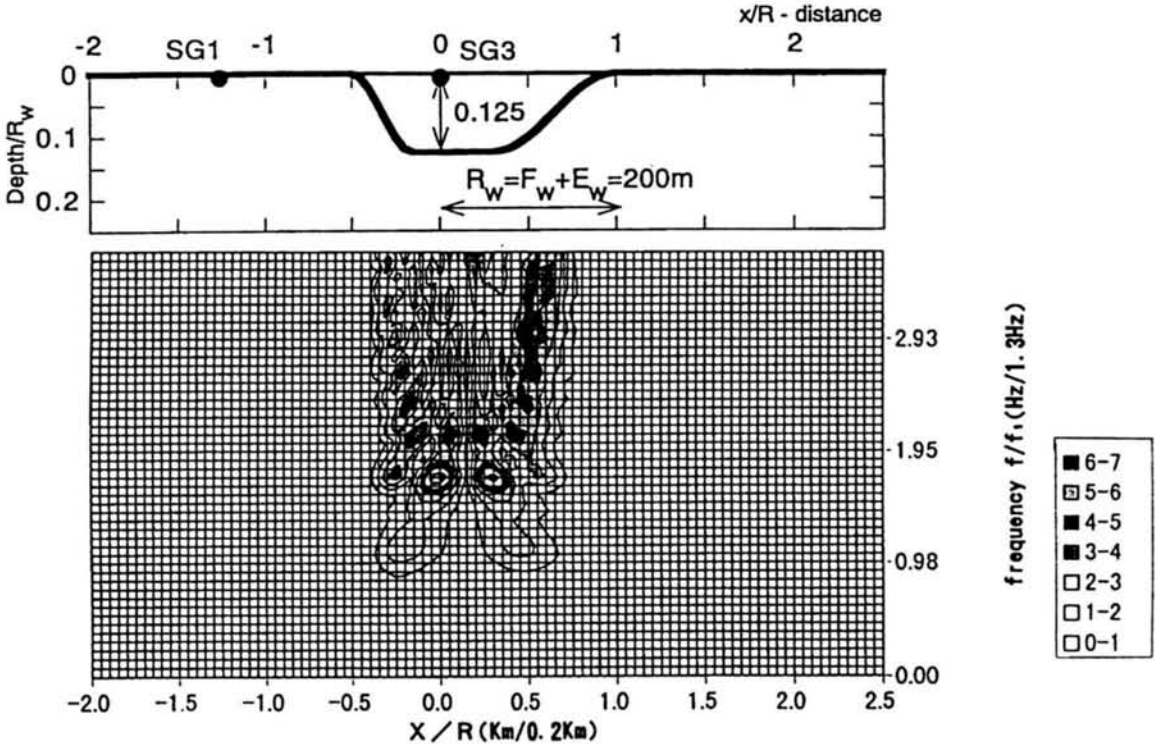

(b) 3-D contour map

Fig. 2.17 Transfer function of vertical ground response for SV wave analyzed from 2-D model at TKY

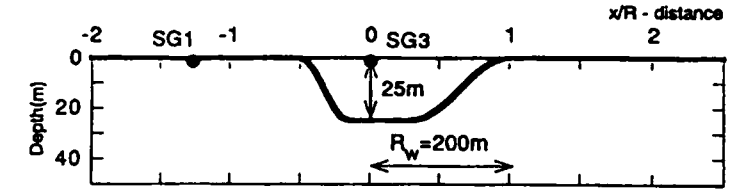

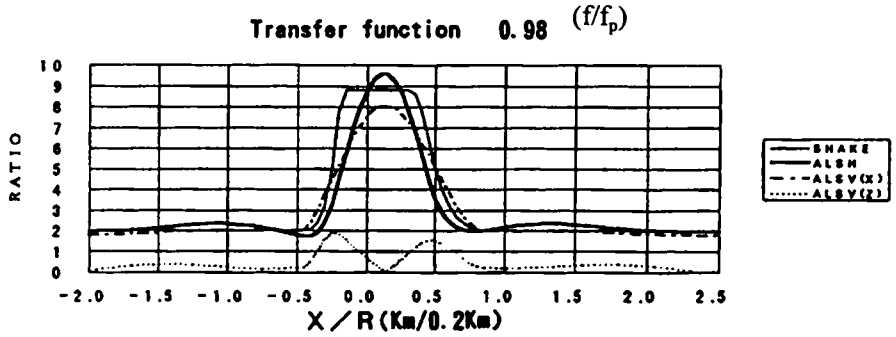

(a) 1.0 times to fp(1.3Hz)

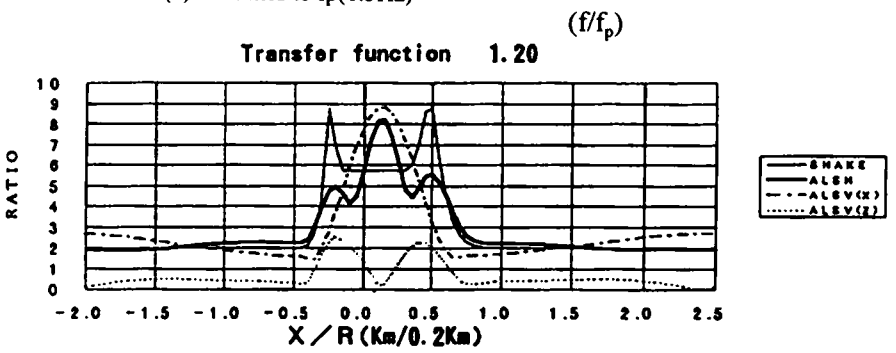

(b) 1.2 times to fp(1.3Hz)

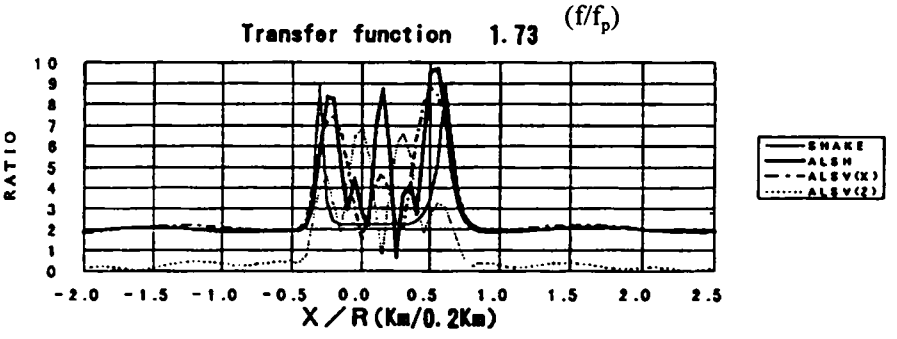

(a) 1.7 times to fp(1.3Hz)

Fig. 2.18 Transfer functions for specific normalized frequency analyzed from 1-D and 2-D models

2.4 Analysis of Propagation of Seismic Waves

In order to fully investigate the effect of soil deposits on seismic ground motion it is necessary to detect wave types and wave propagating directions. The following computational methods are used for analysis of the seismic wave propagation in this thesis. Those methods are so much useful to analyze non-stationary observed seismograms.

2.4.1 Evolutionary Power Spectra

Priestley[13] developed the concept of an evolutionary power spectrum to describe the dependence of the conventional power spectrum on the time domain. The evolutionary power spectrum of a signal is computed by repeated applications of the Fourier transform of the signal after filtering it through a data window moving along the time and frequency domains. Unfortunately, the computation time becomes too large for repeated applications of the Fourier transform that are necessary to investigate the time variation of spectrum in the high frequency domain..

As an alternative, Trifunac[14] proposed the concept of response envelope spectrum (RES) which envelopes the peaks of the output of a linear single degree of freedom dynamical system which can be considered to function as a narrow band pass filter. RES is handy because it eliminates the necessity of repeated applications of the Fourier transform using a moving time and frequency window. RES has been found to be quite adequate in picking up sudden time variations of spectral characteristics even in the high frequency domain because the width of window is proportional to the inverse of the predominant frequency in the signal[14]. Kameda[6] computed evolutionary power spectra for strong motion records obtained in the United States and Japan using RES and examined the issue of optimal damping coefficients for use in calculating RES.

Priestley[13] expressed the evolutionary power spectrum $G(t,\omega)$ and variance $\sigma_{X^2}(t)$ of a stochastic process X(t) as:

$$X(t) = \int_0^\infty e^{i\omega t} dF(t,\omega) \tag{2.23}$$

$$G(t,\omega)d\omega = \frac{1}{2} E\left[|dF(t,\omega)|^2\right] \tag{2.24}$$

$$\sigma_{x^2}(t) = E[X^2(t)] = \int_0^\infty G(t,\omega)d\omega \tag{2.25}$$

where $dF(t,\omega)$ is the differential term with respect to ω of the random complex amplitude $F(t,\omega)$.

$G(t,\omega)$ as expressed here is a function of ω and t and can be taken to be the non-stationary power spectrum of X(t). On the other hand, if $G(t,\omega)$ is independent of t it becomes equal to the stationary power spectral density.

The equation of motion for a linear single degree of freedom vibration system is given by,

$$\ddot{Y}(t)+2h_0\omega_0\dot{Y}(t)+\omega_0^2Y(t)=-X(t), \tag{2.26}$$

where Y(t) is the relative displacement, h_0 is damping coefficient and ω_0 is natural circular frequency. A function R(t) is defined as the output of the system and it is expressed in terms of Y(t) and $\dot{Y}(t)$ as,

$$R^2(t)=\frac{Q(t)}{k/2}=Y^2(t)+\frac{\dot{Y}^2}{\omega_0^2}, \tag{2.27}$$

In the above equation, Q(t) is the total energy of the vibrating system and k is the spring coefficient. If ho is small in value, R(t) becomes a smooth curve representing the envelope of the response Y(t).

If $G(t,\omega)$ is slowly varying such that R(t) doesn't change much, the variance $\sigma_Y^2(t)$ and $\sigma_{\dot{Y}}^2(t)$ of Y(t) and $\dot{Y}(t)$ can be approximated by the following equations:

$$\left.\begin{aligned}\sigma_Y^2(t)&\cong\frac{\pi}{4h_0\omega_0^3}G(t,\omega_0)\\ \sigma_{\dot{Y}}^2(t)&\cong\frac{\pi}{4h_0\omega_0}G(t,\omega_0)\end{aligned}\right\}. \tag{2.28}$$

Taking expectation of both sides of equation (2.27) and substituting for $\sigma_Y^2(t)$ and $\sigma_{\dot{Y}}^2(t)$ from equation (2.28), $G(t,\omega_0)$

$$G(t,\omega_0)\cong\frac{2h_0\omega_0^3}{\pi}E[R^2(t)]. \tag{2.29}$$

Therefore the power spectrum $G(t,\omega)$ of X(t) can be computed if the ensemble mean of $R^2(t)$ is known.

For the case of a linear single degree of freedom system its frequency response function $A(\omega)$ for an acceleration input is given by the following equation:

$$|A(\omega)|^2 = \frac{1/\omega_0^4}{\{1-(\omega/\omega_0)^2\}^2 + 4h_0^2(\omega/\omega_0)^2}. \tag{2.30}$$

With $A(\omega)$ given as above the following equations can be obtained:

$$\left.\begin{aligned} |A(\omega_0)|^2 &= \frac{1}{4h_0^2\omega^3} \\ \int_0^\infty |A(\omega)|^2 d\omega &= \frac{\pi}{4h_0\omega^3} \end{aligned}\right\} \tag{2.31}$$

If the response variance is assumed to be equal to variance of the response of an ideal band-pass filter, the equivalent filter bandwidth, $\Delta\omega$, is given by,

$$\Delta\omega = \int_0^\infty |A(\omega)|^2 d\omega / |A(\omega_0)|^2 = \pi h_0 \omega_0 . \tag{2.32}$$

So far the input motion was assumed to be a stochastic process but if it is a deterministic function x(t), the following equations are obtained by replacing the stochastic processes X(t), Y(t), R(t) in equations (2.26) and (2.29) by deterministic functions x(t), y(t), r(t):

$$\left.\begin{aligned} G(t,\omega_0) &\cong \frac{2h_0\omega_0^3 r^2(t)}{\pi} \\ r^2(t) &= y^2(t) + \frac{\dot{y}^2(t)}{\omega_0^2} \end{aligned}\right\}, \tag{2.33}$$

where y(t) is the relative displacement of a linear single degree of freedom vibration system excited by an acceleration input x(t).

Equation (2.33) can be also be derived following another interpretation. In the case that the filter responds to only one frequency, ω_0 of x(t), the incident amplitude is equal to $\sqrt{2G(t,\omega_0)\Delta\omega}$ and the amplification factor is $|A(\omega_0)|$, then r(t) is given as,

$$r(t) = |A(\omega_0)|\sqrt{2G(t,\omega_0)\Delta\omega} . \tag{2.34}$$

Equation (2.33) is obtained by substituting equations (2.31) and (2.32) into equation (2.34).

Fig. 2.19 shows an example of an evolutionary power spectrum with damping coefficient of 5 % for the radial and transverse velocity seismograms recorded at Kuno located on a sedimentary layer of Ashigara valley during the 1996 Eastern Yamanashi earthquake. The arrival times of the first S-wave motion indicated by line A were about 9 sec for all frequencies and the latter waves indicated by line B have different arrival times ranging from 14 to 18 seconds for frequencies less than 1.0 Hz. From this spectrum it can be surmised that A corresponds to S-wave arrivals and B to the arrival of secondary surface waves that characterize the dispersion in the irregularly layered underground soil structure of the valley.

Radial Transverse

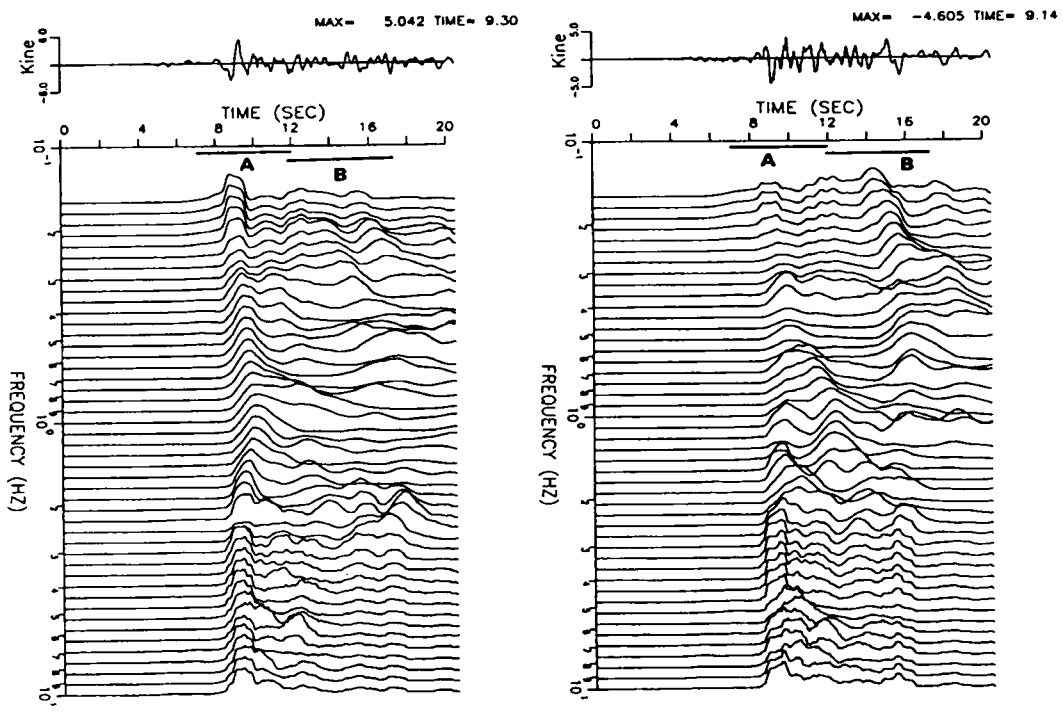

Fig.2.19 Evolutionary power spectrum(h=5%) on OA related to 1996 E.Yamanashi earthquake(M5.3)

Fig. 2.19 Evolutionary power spectra (h=5%) at OA (the 1996 E.Yamanashi earthquake M5.3)

2.4.2 Complex Polarization Analysis

To detect wave types from recorded seismograms, the trace of particle motion can be used to get qualitative properties of wave types. SH-wave shows an anti-plane motion recorded along the transverse component of a three-component seismogram while P- and SV-waves show in-plane motion recorded along the radial and vertical components. The complex polarization filter is an

analytical method suggested by Vidale[7] in order to quantitatively describe particle motion. This method is an improvement of a scheme developed by Montalbetti and Kanasewich[15].

Using the complex polarization filter the azimuth and dip corresponding to the direction of maximum polarization and the degree of elliptical polarization as functions of time were obtained. Records from a three-component seismogram are required for the polarization analysis, that is, three time series: $u_r(t)$ for the radial (x) component of motion, which is positive outward, $v_r(t)$ for the tangential y(t) component which is positive in the clockwise direction, and $w_r(t)$ for the vertical (z) component, which is positive upward. Each component is converted to an analytic signal as shown below.

$$u(t) = u_r(t) + iH(u_r(t)) \tag{2.35}$$

$$v(t) = v_r(t) + iH(v_r(t)) \tag{2.36}$$

$$W(t) = W_r(t) + iH(W_r(t)) \tag{2.37}$$

where H represents the Hilbert transform and i is $\sqrt{-1}$.

The analytic signal may be used to compute the covariance matrix c(t) which is given by,

$$c(t) = \begin{bmatrix} uu^* & uv^* & uw^* \\ vu^* & vv^* & vw^* \\ wu^* & wv^* & ww^* \end{bmatrix} \tag{2.38}$$

where the asterisks represent complex conjugation. The three eigenvalues λ_i and eigenvectors (x_i, y_i, z_i) of the 3 by 3 covariance matrix can be computed analytically[16] for each time step. The eigenvector X=(x_0, y_0, z_0) associated with the largest eigenvalue λ_0 corresponds to the direction of the largest amount of polarization. The components of the eigenvector are complex and by rotating the eigenvector in the complex plane by α from 0° to 180°, a value for α can be found which maximizes the length of the real component, X.

$$X = \sqrt{\left((R_e(x_0 cis\alpha))^2 + (R_e(y_0 cis\alpha))^2 + (R_e(z_0 cis\alpha))^2\right)} \tag{2.39}$$

where cis α is $\cos\alpha + i.\sin\alpha$ and Re(x) is the real part of x.

The elliptical component of polarization, called angular polarization, is estimated by

$$P_E = \sqrt{\frac{1-X^2}{X}} = \frac{|\mathrm{Im}(X)|}{|\mathrm{Re}(X)|}. \quad 0 \le P_E \le 1 \tag{2.40}$$

P_E is 1 for circularly polarized motion and 0 for linearly polarized motion.

The strike of the direction of maximum polarization is

$$\phi = \tan^{-1}\left(\frac{\mathrm{Re}(y_0)}{\mathrm{Re}(x_0)}\right), \; 90^0 \le \phi \le 90^0. \tag{2.41}$$

and the dip of the direction of maximum polarization is

$$\delta = \tan^{-1}\left(\frac{\mathrm{Re}(z_0)}{\sqrt{\mathrm{Re}(x_0)^2 + \mathrm{Re}(y_0)^2}}\right) \quad -90^0 \le \delta \le 90^0. \tag{2.42}$$

When the strike of the direction is 0° , the recorded motion is predominant in the radial component relative to the seismic source. SH-wave is predominant when the strike angle is +/-90° along the transverse component.

A measure of the strength of polarization P_s in the signal is

$$P_s = \frac{\lambda_0}{\lambda_{max}}\left(1 - \frac{\lambda_1 + \lambda_2}{\lambda_0}\right), \; 0 \le P_s \le 1. \tag{2.43}$$

where λ_{max} is the largest eigenvalue. Hereafter, the threshold value of 0.05 is set for P_s above which the data is classified as signal and below which it is taken to be noise.

An example of polarization analysis[17] is shown in Figure 2.20. This is one of many analyses conducted using band-pass filtered seismograms in the frequency range from 1.0 to 2.5 Hz. Velocity time histories in radial, transverse, and vertical components, the strength of polarization, the angular polarization of particle motion, the strike and dip angles of polarization direction are shown in the figure. From this figure, three types of waves can be detected in the recorded ground motion. Time interval (1) shown in Fig.2.20 is the arrival of P-waves. The P-waves were coming from the vertical direction below the ground with a dip angle of 0°. Time interval (2) is the arrival of SV-waves which are polarized in the radial direction indicated by the strike angle of 0°. Time interval (3) shows SH- or Love waves, which differ from the wave type of time interval (2) as their predominant polarization is in the transverse component as indicated by the strike angle of ±90°.

The above example illustrates the effectiveness of the complex polarization filter in detecting wave types in a three-component seismogram.

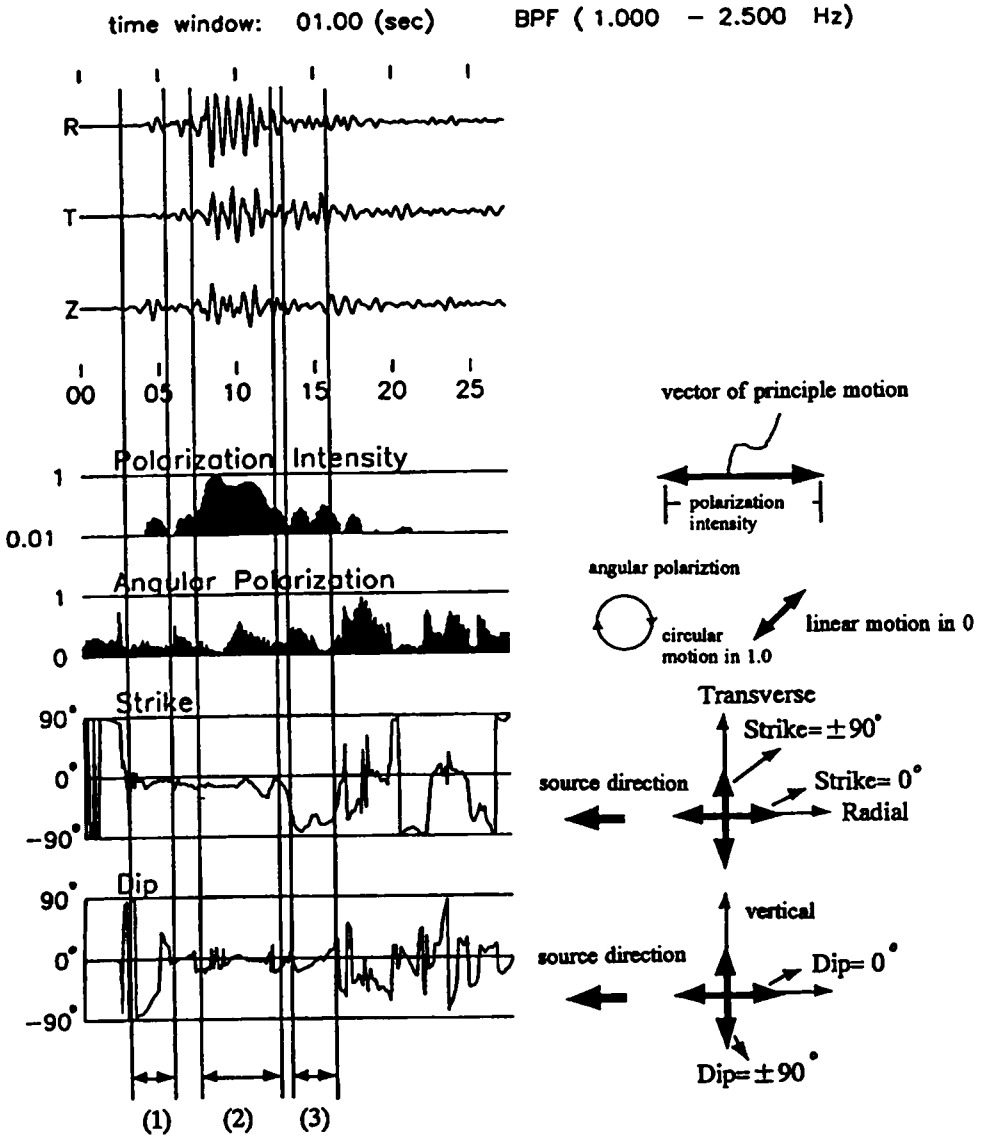

Fig. 2.20 Example of polarization analysis for B.P.F velocity records in the frequency from 1.0 to 2.5Hz at KZR

2.5 Conclusions

(1) Using the proposed system identification technique it was possible to evaluate S-wave velocity and Q-value of a layered soil profile within measurement errors that are typically in the range of 20 %.

(2) Using the AL-method the seismic response at the surface of buried valley was shown to be effectively computed using a 2-D model of SH- and SV-wave incidences. The 2-D amplification factors at the central part were about 1.3 to1.5 and about 2 to 4 times larger than 1-D amplification factors at 1.3 Hz and 2.2 Hz, respectively. The 2-D amplification factors at the interface of the surface and sloped layers at 2.2 Hz were about 2 to 4 times larger 1-D amplification factors. As a result, it can be concluded that the seismic response of an irregularly layered ground can be amplified about 2 to 3 times larger than the response of a 1-D model for a horizontally layered ground.

(3) The example of an evolutionary power spectrum with damping coefficient of 5 % using radial, transverse and vertical components of velocity time histories recorded at the surface of a buried valley illustrated the usefulness of this method in detecting P-waves, S-waves and secondary surface waves.

(4) The method of complex polarization filter was shown to be effective in detecting wave types and their propagating directions. Using this method it was possible to detect the principal axis and the polarization intensity of P-waves, S-waves and secondary surface and converted waves.

(5) All analytical methods presented in this chapter were found to be useful in elucidating the incident wave field and its effect on site amplification.

REFERENCES

1) Kawase, Hiroshi; Review: Amplification of seismic waves by sedimentary layers and its simulation, Zisin vol2, No.46, pp111-130, 1993.

2) Haskell, N.; Crustal reflection of plane SH waves, J. Geophys. Res., 65, pp4147-4450, 1960.

3) Schnable, P.B., J.Lysmer and H.B.Seed; SHAKE-a computer program for earthquake response analysis of horizontally layered sites', Report EERC 72-12, Earthquake Engineering Research Center, University of California, Berkeley, 1972.

4) Ishida, K., K. Sato, H. Yajima and Y. Sawada; Estimation of soil property and characteristics of response spectra based on earthquake observations' CRIEPI Report 385005, pp55-62, August 1985.

5) Hanada, K.; Data Reduction Method for Forced Vibration Tests (No.2)-System Parameter Identification Method-, CRIEPI Report 383045, January 1984.

6) Kameda, H.; On a method of computing evolutionary power spectra of strong motion seismograms, JSCE Journal, No.235, March 1975.

7) Vidale, J. E.; Complex polarization analysis of particle motion, Bulletin of the Sesmological Society of America, Vol.76, No.5, pp1393-1405, October 1986.

8) Ichikawa M. and H. Mochizuki; Time travel table for near-by earthquake, Institute of Meteorology report, vol.22,No.3-4,pp.229-290, Nobember 1971.

9) Ohta, Y.; Application of inverse method to earthquake engineering-1 Estimation of underground structural parameters on SMAC observatory at Hachinohe harbor port, AIJ Journal, Vol.229, pp3-41, 1975.

10) Horike, M.; Extension of the Aki and Larner method to absorbing media with plural curved interfaces and several characteristics of a seismic response on a sedimentary basin, Zishin, No.2, Vol.40, pp247-259.

11) Aki, K. and K.L.Larner; Surface motion of a layered medium having an irregular interface due to incident plane SH waves, J. Geophs. Res., 75, pp933-954, 1970.

12) Ohori, Michihiro. and T. Minami; Seismic response of sedimentary basin using 2 dimensional Aki Larner Method, Bull. Earthq. Res. Inst. Univ.Tokyo vol.65 (1990) pp.809-850.

13) Priestley, M.B.; Evolutionary spectra and nonstationary processes, Journal of Royal Statist. Soc., Ser. B, Vol.27, pp204-237, 1965.

14) Trifunac, M.D.; Response envelope spectrum and interpretation of strong ground motion, Bull. Seism. Soc. Amer., Vol. 62, Oct., 1972, pp343-356, 1972.

15) Montalbetti, J. R. and E.R.Kanasewich; Enhancement of teleseismic body phases with a polarization filter, Geophys. J. R. Astr.Soc. 21, pp119-129, 1970.

16) Malvern, L.E.; Introduction to the mechanics of a continuous medium, Prentice-Hall, Inc., Englewood Cliffs, New Jersey, 1969.

17) Higasi, S., K. Sato, H. Yajima and S. Sasaki; Analaysis of incident wave field on Kuno site, Ashigara Valley, Japan, The 10th Japan Earthquake Enigineering Symposium, pp971-976, November 1998.

CHAPTER 3

NONLINEAR SITE EFFECTS ON STRONG GROUND MOTION DURING THE HYOGOKEN-NANBU EARTHQUAKE

3.1 General Remarks

In this chapter the characteristics of nonlinear seismic amplification effects are investigated on the basis of recorded earthquake motions at several sites in and around the city of Kobe during the 1995 Hyogoken-Nanbu earthquake (M_{JMA}=7.2). Some of these recording sites had multi-level vertical arrays of seismograms, which demonstrated very peculiar nonlinear features of seismic amplification in reclaimed land areas and on Holocene and Pleistocene deposits. Acceleration records from a down-hole site at Port Island were analyzed using the inversion technique to estimate Vs and damping ratio h from the main shock as well as a smaller aftershock. Records[1, 2] at three other down-hole sites at different distances from the epicenter were, also, analyzed using the same inversion technique. The analyses of these records disclosed peculiar seismic amplification mechanisms at these sites related to soil liquefaction and nonlinear soil properties.

Also, down-hole distributions of peak acceleration were examined to investigate non-linear amplification effects caused by varying levels of input acceleration at the bottom of the vertical arrays. The nonlinear soil properties at Port Island were identified using recorded earthquake motions during the main shock at different ground depths[3), 4)]. The change in Vs and h for the main shock is discussed from the viewpoint of liquefaction and strain-dependency of soil characteristics. The same identification technique was applied at three other down-hole sites where smaller accelerations were observed during the main shock so as to compare results with those from the much stronger records at Port Island.

3.2 Nonlinear Seismic Response and Change of Dynamic Soil Properties During Main Shock

3.2.1 Vertical Acceleration Distributions at Four Down-hole Sites

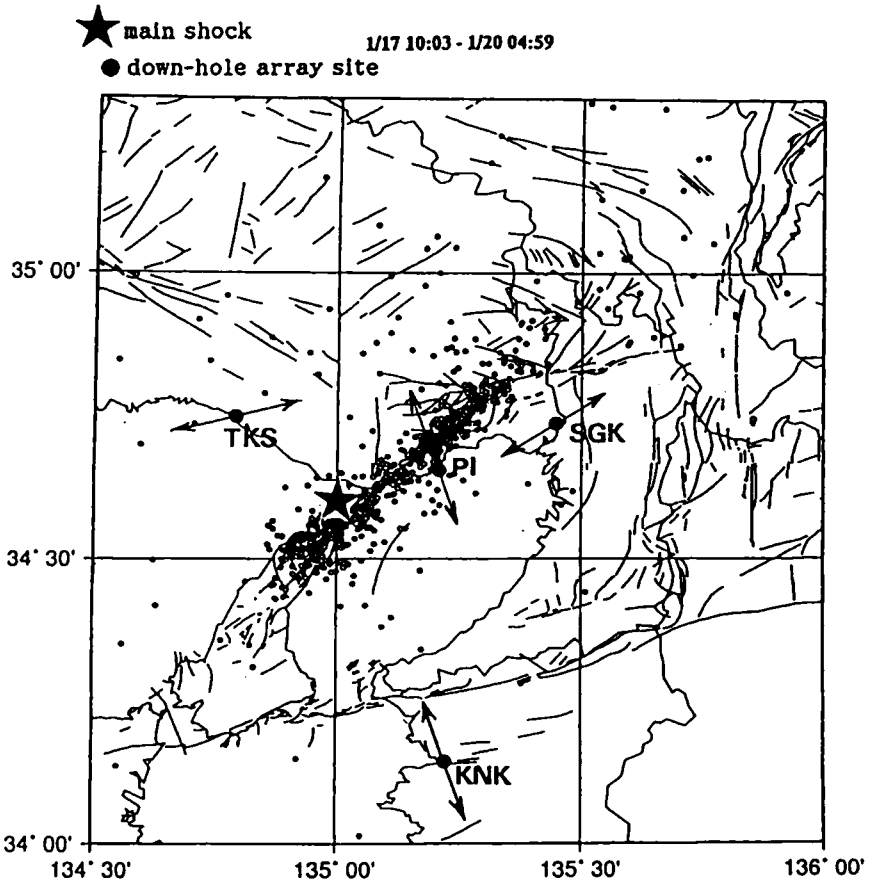

Fig.3.1 S wave principle direction at the downhole recording sites
and epicenters of the 1995 Hyogoken-Nanbu Earthquake (summarized by Disas. Prev. Res. Inst.)

Fig. 3.1 shows the locations of four vertical array observation sites (designated PI, SGK, TKS and KNK) and the epicenters of the main shock and the accompanying aftershocks. The epicenters were evaluated by the Disaster Prevention Research Institute, Kyoto University and their distribution coincides almost perfectly with the area of the earthquake fault, which was activated during the main shock[5].

The deepest depths of the seismopraphs in the arrays at the four sites ranged from GL-80 to GL-100 m. The soils at the deepest depth of the four arrays are Pleistocene gravelly soils except at KNK, which has hard rock. The upper layers consist of alternating Pleistocene gravel/clay layers and Holocene sand/clay layers which are

overlain by fill.

Fig. 3.2 indicates the horizontal orbits of the long-period particle motions at different ground depths of the four observation sites, which were filtered using a low-pass filter with a cutoff frequency of 0.2 Hz. The principal axis of ground motion at each site is shown by using a dashed line with arrow symbols at the two ends in the figure. The directions of the principal axes corresponded to the source mechanism of a right-lateral slip fault. The principal axis of the motion was N30W at PI, N55E at SGK, N110E at TKS, and N95E at KNK and at all sites the directions of the principal axes was pretty much unchanged with depth.

Based on analyses of the original down-hole array records[1)], the directional drift of buried seismometers detected by these orbits was as follows:

a. 15° rotation at GL-83.4 m at PI,
b. Reversal of NS component at GL-0 m and 34° rotation at GL-97 m at SGK,
c. 30° rotation at GL-25 m at TKS, and
d. Reversal of EW component at GL-0 m and 60° rotation at GL-100 m at KNK.

The measured data was adjusted for the above directional drifts except at PI where the 15° rotation was neglected because of small errors in the peak acceleration of about 4 %.

Fig. 3.3 shows the pseudo velocity response spectra with a 5 % damping ratio for three components of the recorded motions at the deepest depth of the four sites. The predominant periods of the motions in the horizontal directions were about 1.0 to 2.0 sec at PI, 0.6 to 0.7 sec at SGK, 1.0 sec at TKS, and 1.0 to 2.0 sec at KNK. The maximum values of the amplitude were about 100 to 150 kine at PI, 80 kine at SGK, 40 kine at TKS, and 8 kine at KNK. The values of the amplitude in the vertical direction were about 30 to 60 kine at PI, 40 kine at SGK, 20 kine at TKS, and 6 kine at KNK at more or less the same period as in the horizontal direction. The values of the spectral amplitude in the vertical direction therefore were nearly one-half or less than one-half of the respective maximum values in the horizontal direction except at KNK.

Fig. 3.4 shows the vertical distribution of peak acceleration in two horizontal directions (NS, EW) and vertical direction (UD) at all four sites. The epicentral distances of the four sites vary quite a bit and accordingly the peak accelerations at the deepest depth range from 21 gal at KNK to 679 gal at PI. For motions in the horizontal direction, the amplification of the ground surface with respect to the motion at the deepest level

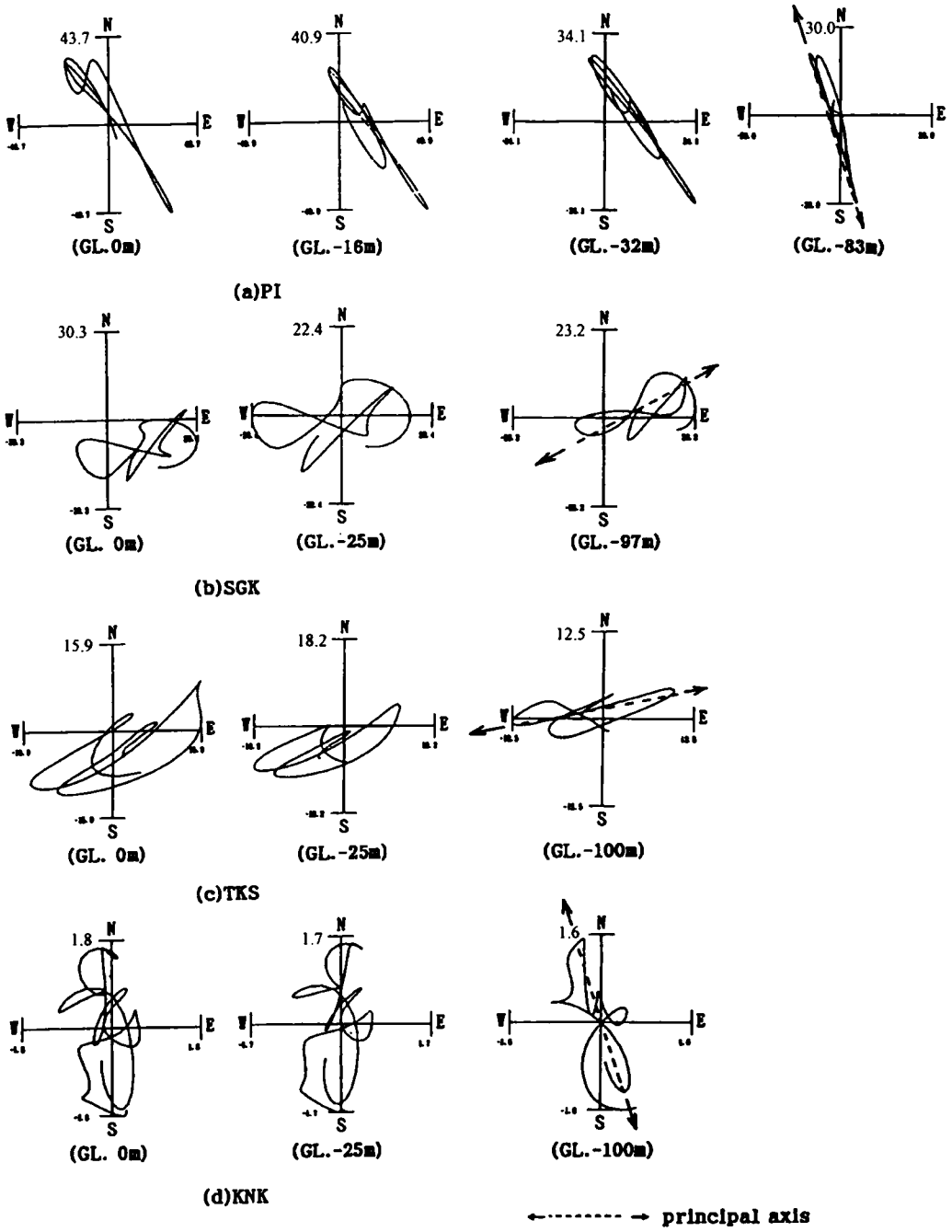

Fig.3.2 Orbits of particle motion at the downhole recording sites

(Low pass filter 5.0sec≦T)

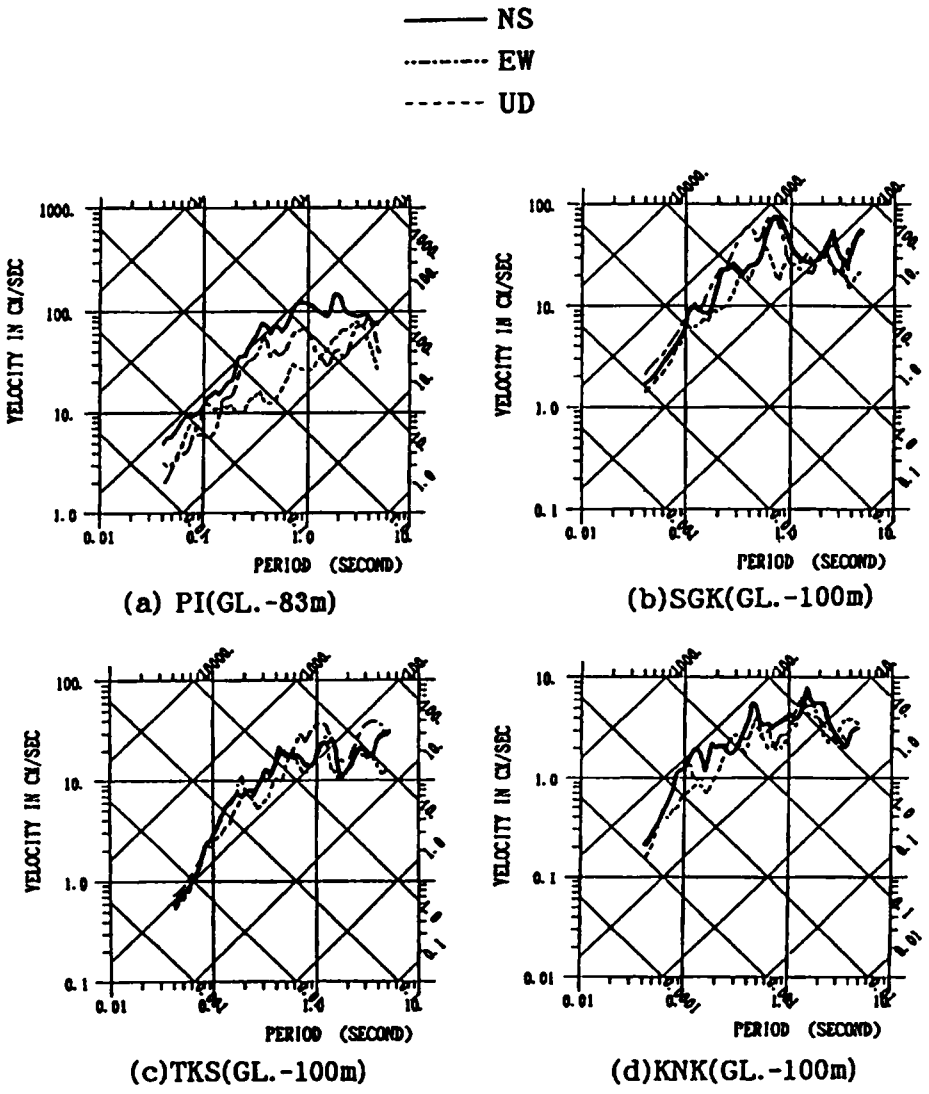

Fig.3.3 Pseudo velocity response spectra with damping ratio h=5%

was about 4 to 5 times at KNK and about 2 times at TKS which had a peak acceleration of 100 gal at the engineering bedrock. It was between 1 to 2 times at SGK with a peak acceleration of about 300 gal and about one-half at PI which recorded a peak acceleration of 680 gal at the deepest layer. The surface sandy fill layer area around PI experienced very extensive liquefaction during the main shock which obviously led to the de-amplification of horizontal acceleration between the top and bottom of the liquefied layer.

With regard to vertical acceleration, the amplification between the top and the bottom was 4.5 at KNK, 2 at TKS and 1 at SKG. Therefore, there was an apparent downward trend of amplification with increasing input acceleration at the bottom. However at PI amplification was as large as 3 times, implying that the amplification may not be dependent on only the intensity of acceleration at the base layer. Only at PI, the peak vertical acceleration at the surface was much higher than the peak horizontal acceleration because of the de-amplification in the horizontal motions and the amplification of 3 times in the vertical motion.

Peak vertical accelerations are plotted against peak horizontal accelerations in Fig. 3.5 for some other sites where peak horizontal accelerations above 300 gal were recorded. Two straight lines drawn in the figure correspond to 1 to 1 and 1 to 2 slopes. Comparison of the plotted data with the above two lines reveals that the ratios of peak vertical acceleration to peak horizontal acceleration (V/H) tended to be larger at liquefied sites. On the other hand at non-liquefied sites the ratio of V/H was around one-half, which is well known relationship in seismic design for non-liquefied sites.

3.2.2 System Identification Analysis for Down-hole Records at Port Island

The down-hole array site Port Island (called PI) is located in the northwestern part of the artificial island of Port Island. The surface soil at the site is sandy fill (17.5 m thick) called "Masa" (decomposed granite transported from the nearby Rokko Mountains), underlain by Holocene soft clay and sand. Alternating layers of Pleistocene gravel and clay lie below the Holocene soft clay and sand. Strong motion accelerographs in three components were installed at four levels of a borehole at PI. The deepest one was located in a dense gravel layer with a SPT blow count of more than 60. P- and S-wave velocities measured by down-hole seismic wave logging indicated that Vs was about 200 m/s at the top and 400 m/s at the bottom while Vp showed a big increase between the top (300 m/s) and the bottom (2000 m/s).

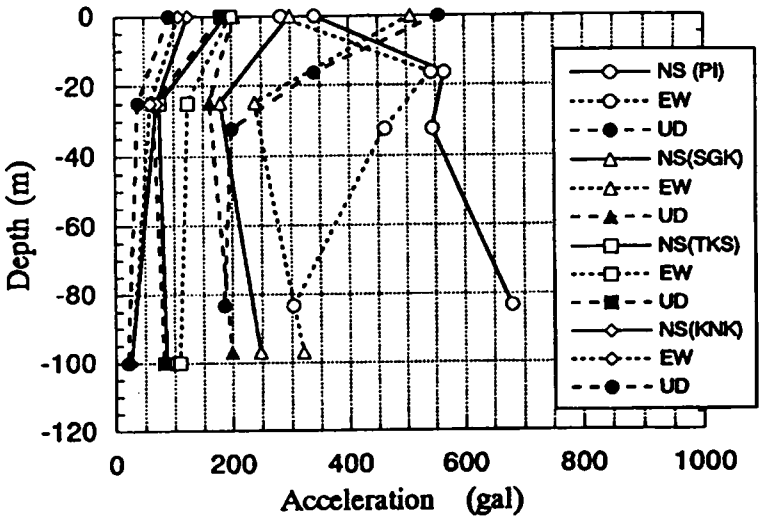

Fig.3.4 Distribution of maximum acceleration along the depth at the downhole recording sites

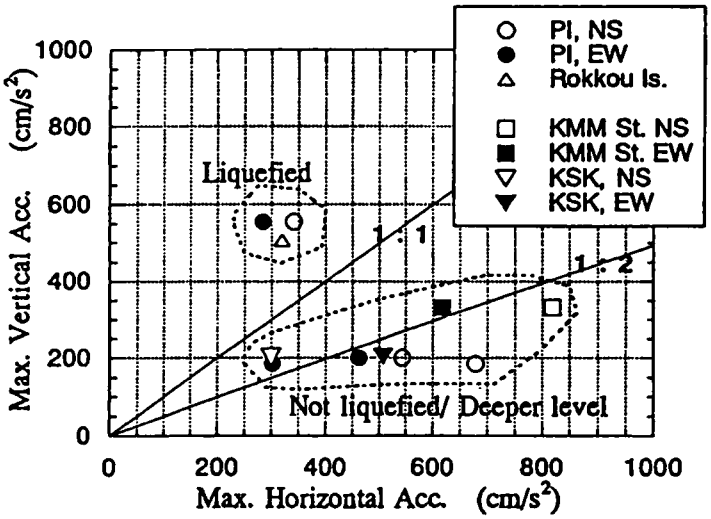

Fig.3.5 Relation of peak ground acceleration between vertical and horizontal motions

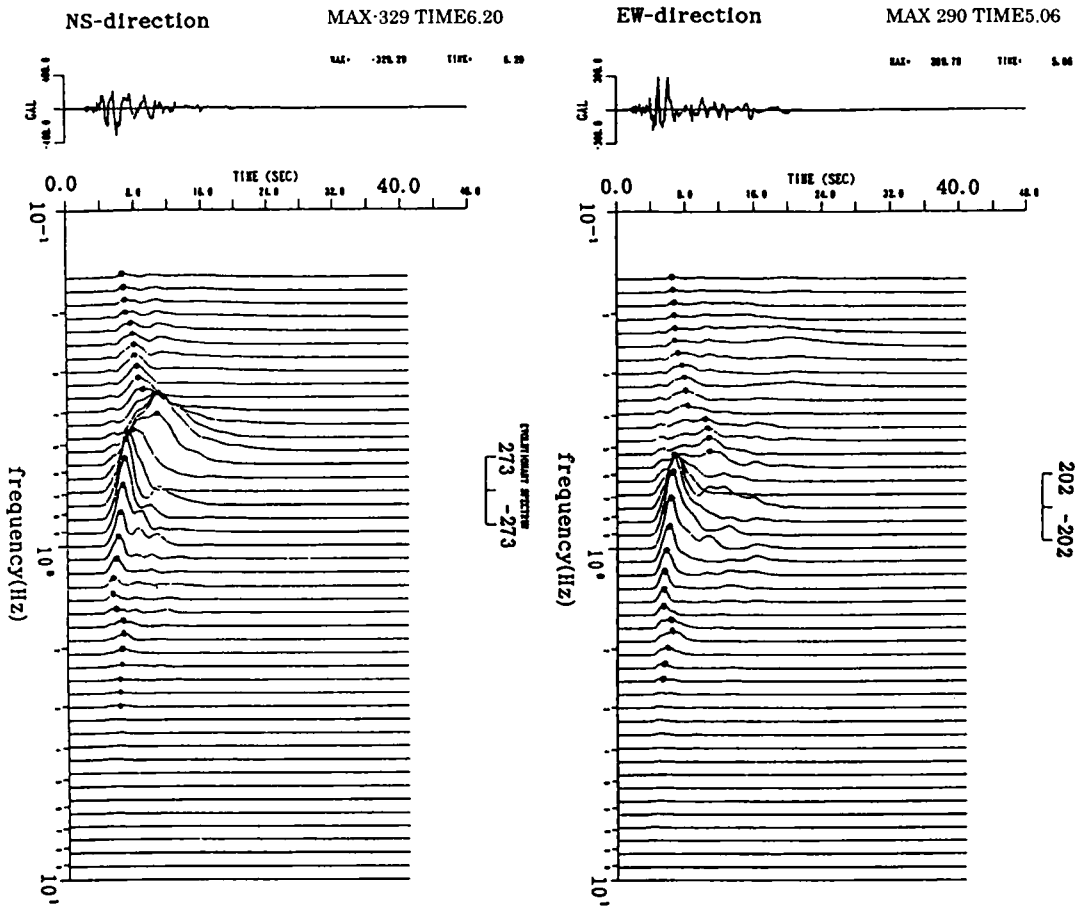

Fig.3.6 Evolutionary spectra (damping ratio h=5%) at PI (GL.0m) (see [Kameda 1975] [6])

Fig. 3.6 shows the evolutionary spectra[6] with a constant damping ratio of 5 % of the acceleration timehistories in the NS and EW components at the ground surface level (GL-0 m) at PI. As seen in the figure, S-wave motions in both horizontal components showed a wave with several cycles of predominant period of 1.2 sec. Peaks of both spectra for the S-wave motion appeared in frequency range from 0.7 Hz to 0.9 Hz and were concentrated in the time interval from 5.0 to 6.0 sec. The other peak in the NS component was found after the S-wave motion for frequencies lower than 0.5 Hz. As for lower frequency waves, the times of their peaks shifted with increasing frequency, as shown by the dashed lines in Fig. 3.6. This result was interpreted to be a clear indication of the dispersion characteristics of the strong motion.

Fig. 3.7 shows the vertical distribution of the identified Vs and Vp in the NS direction using a computer program for inversion analysis developed by Ohta[7] and Ishida[8]. The identified Vs values using the total duration of the main shock (T=20 seconds) were approximately 20 % and 40 % smaller than the PS-logging values for the

Pleistocene and Holocene layers, respectively. For the fill layer, reductions of 80 % and 50 % were obtained in the identified Vs for the saturated and unsaturated layers, respectively, presumably because of the extensive liquefaction in the fill.

In Fig. 3.7, also, shown is the distribution of Vs identified using only a portion of the record from T = 4.10 to 9.22 seconds in which SH-wave was expected to be dominant. No meaningful difference could be seen between the results for the total time and the partial time except for the fill layer where the partial time analysis gives a smaller reduction of Vs implying that liquefaction was still developing during this time period.

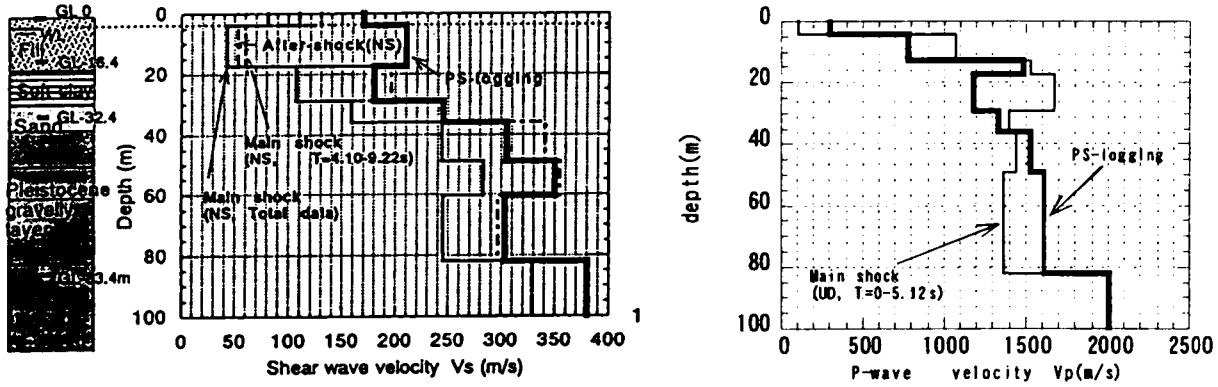

Fig.3.7 Identified soil profile of S-wave and P-wave velocities at PI

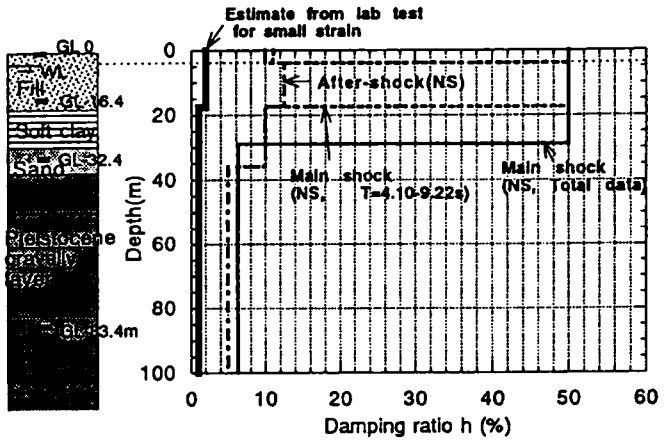

Fig.3.8 Identified soil profile of damping factor (h) at PI

Another interesting result was obtained from the analysis of a record with a peak ground acceleration of about 10 gal during one of the aftershocks, which occurred within about two minutes after the main shock. As shown in the figure, Vs for Pleistocene and Holocene layers could be interpreted to have recovered to the PS-logging value as the strains in these layers were within the elastic domain during the main shock and aftershock. However, Vs of the fill layer is still as much reduced as the identified Vs for the main shock. This is an indication that the fill was still under a liquefied condition.

A similar inversion analysis was carried using the vertical motion record. At the time of the analysis, it was assumed that vertical motion could be computed by the multi-reflection theory of P-wave propagating vertically in layered media. The identified Vp using the partial record for the time interval T = 0 to 5.12 seconds in which P-wave motion was expected to be dominant is shown in Fig. 3.7. Since P-wave is dominant in the time domain prior to S-wave arrival, it may be concluded that the identified P-wave velocity profile should be close to that obtained from PS-logging. This is shown to be more or less the case except for the unsaturated fill layer where the identified Vp was reduced by 50 %.

Fig. 3.8 shows damping ratio (h) identified using the NS horizontal motion for the main shock and aftershock. These values are compared with the values estimated from previous laboratory test data measured at small strains[9]. The h identified using the aftershock record was much larger than the h from the laboratory tests. Values of 5 % for the Pleistocene soils and about 10 to 12 % for the Holocene and fill layers were estimated. The identified h from the main shock was 6 % for the Pleistocene soils and Holocene sand layer and 50 % for the upper layer. The damping ratios identified using records during the main shock were high everywhere and especially so in the liquefied layers. A similar dependency on the intensity of the input acceleration has been observed in past investigations[10].

3.2.3 Comparison of Recorded and Simulated Motions

As a further test of the identified model, motions were simulated at various depths based on a linear 1-D model and compared with the recorded motions. The soil parameters for the 1-D model were taken from the soil parameters identified using records from the main shock. The motion at the deepest layer was taken as the input excitation to the 1-D model and motions at the upper three levels were computed. Fig. 3.9 shows the recorded and simulated motions. The simulated horizontal motions agreed

with the recorded motions quite satisfactorily at the middle two levels but at the ground surface there were some difference in phase in the motions following the principal S-wave motion. In general, simulated motions appeared smoother than recorded motions as a linear 1-D analysis cannot model the saturated high frequency motion after the occurrence of strong liquefaction in the ground. As for the vertical motion, the recorded and simulated motions were in good agreement and showed no effect of liquefaction.

One thing to note about the peak value of 340 gal in the recorded vertical

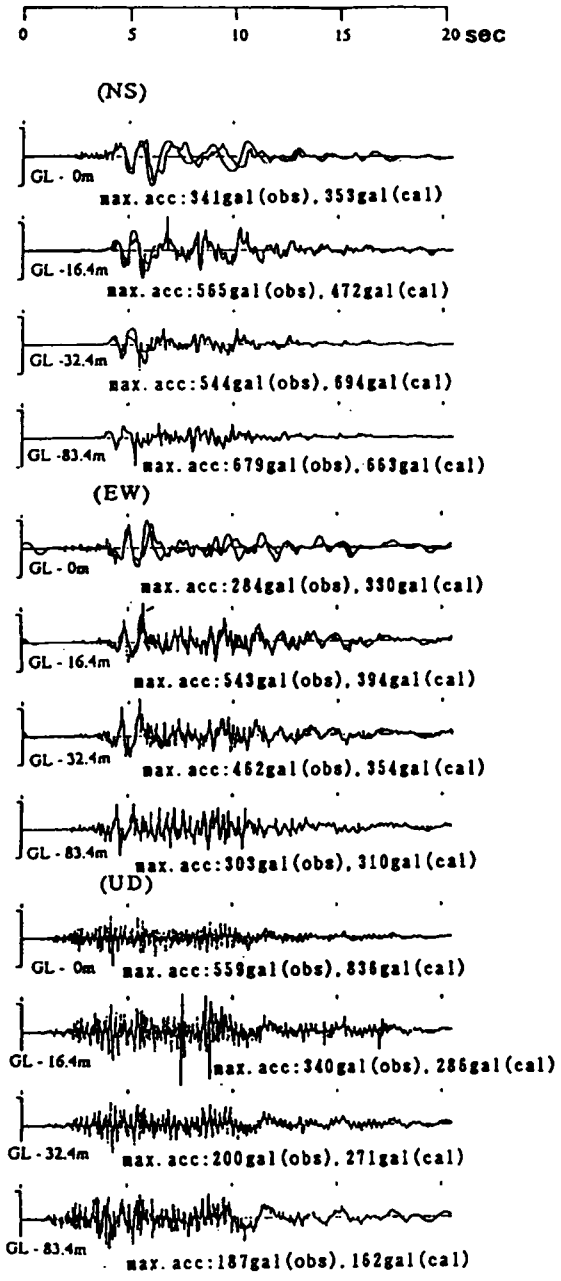

Fig.3.9 The acceleration time history of main shock at PI

(bold line: observed, broken line: analyzed)

motion at GL-16.4 m is that this was a spike caused by noise in the recorder.

Fig. 3.10 shows the vertical distribution of simulated and recorded peak ground accelerations in all three components. The maximum errors between the simulated and recorded values were within 30 %. This figure clearly revealed the large amplification of the vertical acceleration in the surface layer above the water table.

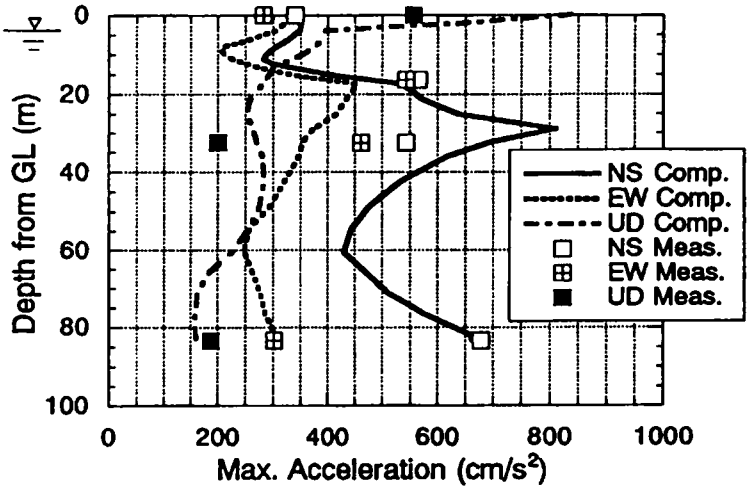

Fig.3.10 Distribution of peak ground acceleration along the depth at PI

3.2.4 Identification Analysis for the Other Three Down-hole Sites in Kobe

Results of soil profile identifications and comparisons of simulated and recorded motions at sites SGK, TKS, and KNK are shown in Figs. 3.11 through 3.19. As shown in Fig. 3.11, Vs identified at SGK using the total duration of the main shock (T=20 seconds) in the NS and EW components were approximately 25 % and 45 % smaller than PS-logging values for the Pleistocene and Holocene layers, respectively. The occurrence of weak liquefaction in the fill layer seemed to have had little, if any, influence at this site, since no sand boils at the ground surface and no soil subsidence were found after the quake. The identified Vp in the Holocene layer was larger than the PS-logging value. Fig. 3.12 shows the EW and UD components of the recorded and simulated at SGK. SGK is located close to the front of the ruptured faults but it is twice as far away from the epicenter as PI. The duration of the S-wave motion at SGK was about 5 seconds the same as at PI. Fig. 3.13 shows the vertical distribution of peak ground acceleration. The amplification of the horizontal motion was most remarkable in the Holocene and fill layers with sand and silt. On the contrary, the vertical motion was not amplified to the same degree as the horizontal motion. This could be explained in

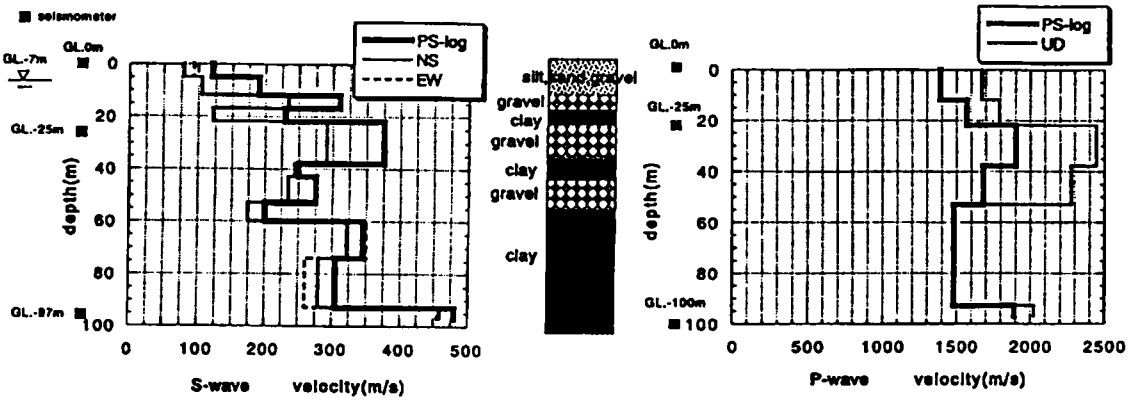

Fig.3.11 Identified soil profile of S-wave and P-wave velocities at SGK

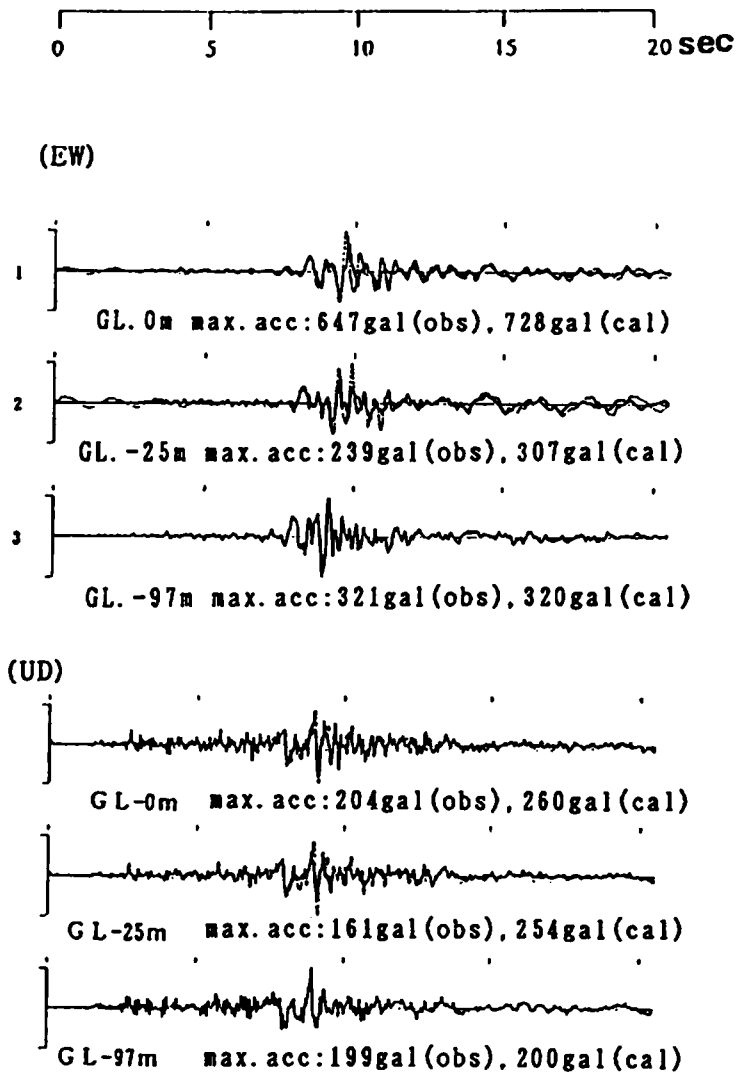

Fig.3.12 The acceleration time history at SGK

(bold line: observed, broken line: analyzed from 1-D identified model)

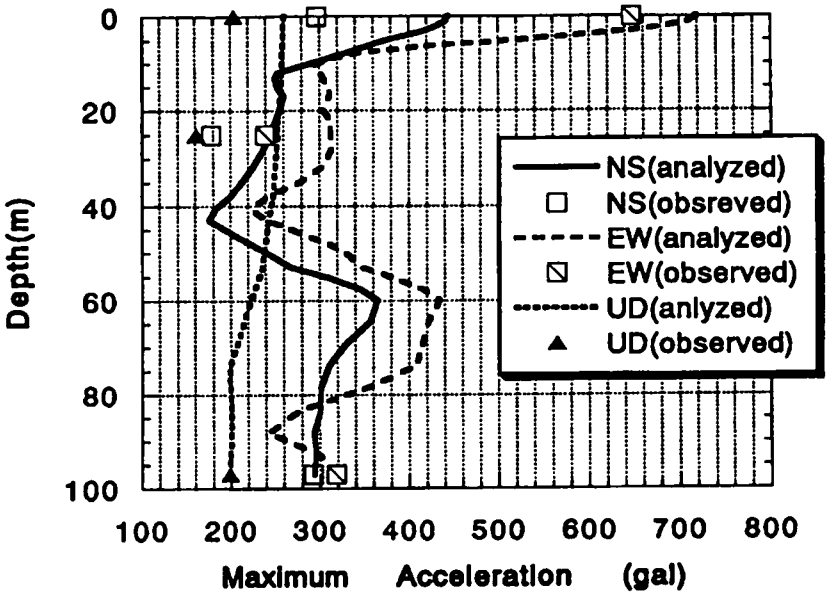

Fig.3.13 Distribution of peak ground acceleration along the depth at SGK

terms of the small impedance ratio between the identified Vp of surface and bedrock layers.

Fig. 3.14 shows the identified Vs and Vp at TKS using the entire duration of the record. The identified values of Vs were approximately 10 % and 30 % smaller than the PS-logging values for the Pleistocene and Holocene layers, respectively. However, the identified Vs of the sand layer at a depth of about GL-10 m was reduced by as high as 80 % as compared to the PS-logging value as was observed for the sand fill at PI. This result was interpreted to be an indication of occurrence of liquefaction in this layer. Fig. 3.14 shows that the identified Vp was, also, much smaller than Vp from PS-logging. The vertical motion at this site was very complicated and it was recognized that various types of waves, such as P-, SP-, and SV-waves may be included. Fig. 3.15 shows the recorded and simulated strong motions of the main shock at TKS, which is located at the northwest blind side of the strike-slip ruptured fault. The total duration of the record of the main shock was about 40 seconds, which is longer than the durations at PI and SGK which are located at the front of ruptured region of the source. Sand boils were observed at TKS after the quake. The vertical distribution of peak ground acceleration shown in Fig. 3.16 indicated that the horizontal motion was de-amplified in the Holocene layer with sand and silt at the depth of 10 m. This layer was most likely liquefied. The simulated peak accelerations for all three components were greatly overestimated with respect to the observed peak values at the level of GL-25 m.

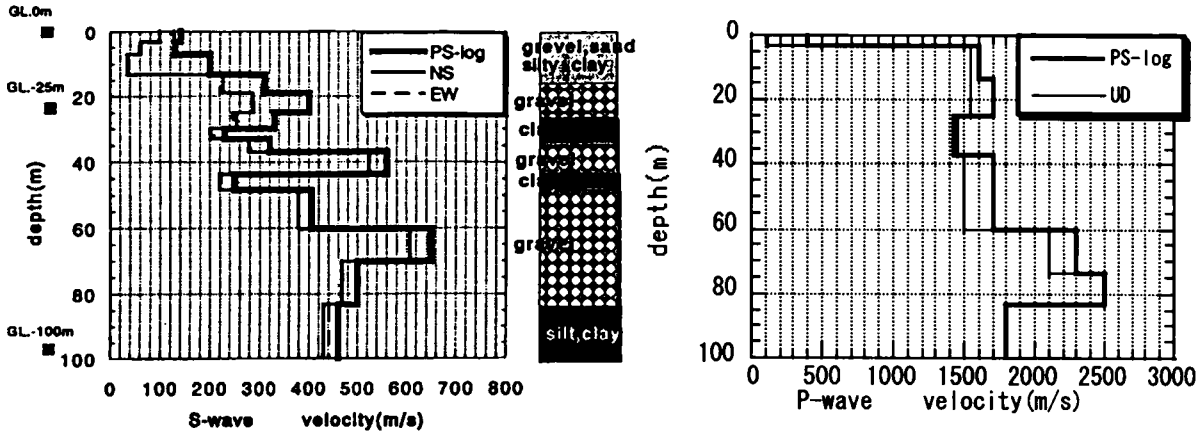

Fig.3.14 Identified soil profile of S-wave and P-wave velocities at TKS

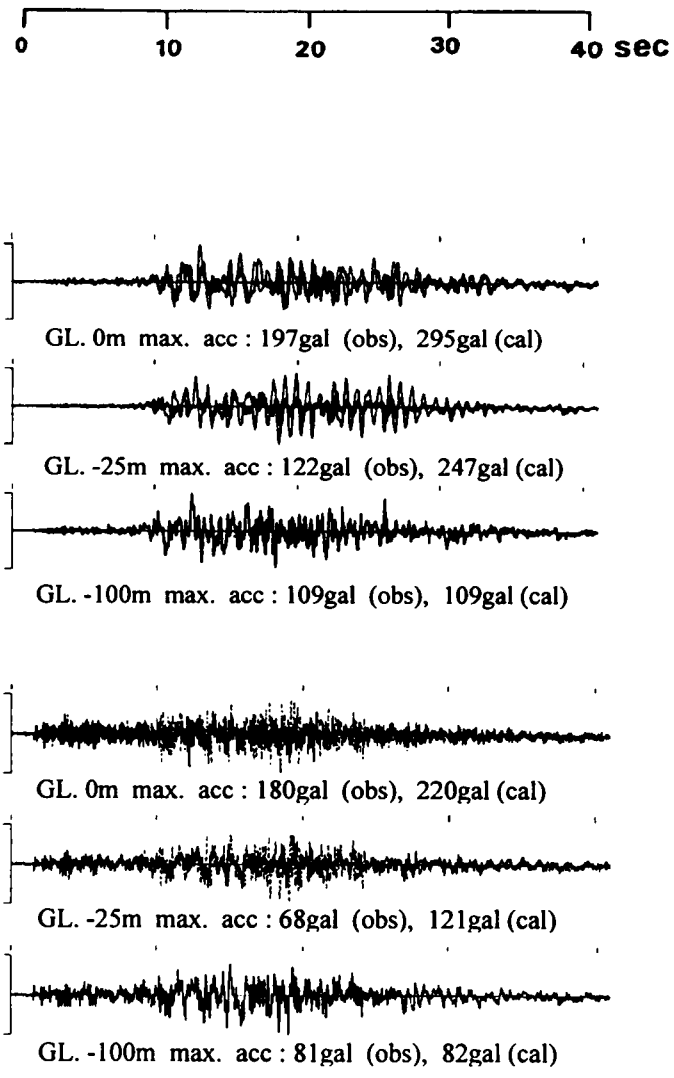

Fig.3.15 The acceleration time history at TKS

(bold line: observed motion, broken line: analyzed from 1-D identified model)

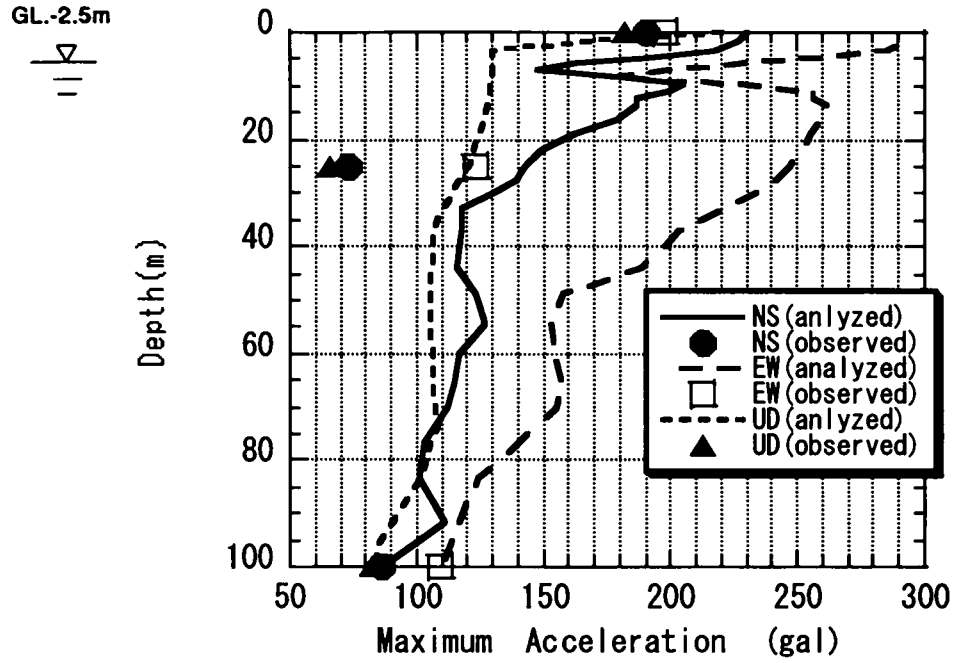

Fig.3.16 Distribution of peak ground acceleration along the depth at TKS

Fig. 3.17 compares the Vs and Vp identified using the strong motions recorded during the main shock at KNK with their PS-logging values. The identified Vs was approximately 20 % smaller than the PS-logging value for the Holocene layers but was nearly the same as the PS-logging value for the Pleistocene layer. This result was taken to imply that motion of the deeper Pleistocene layer was in all probability linear for the relatively small earthquake input intensity of 25 gal experienced at KNK during the main shock. The identified Vp was, also, 20 % smaller than the PS-logging value. The EW and UW components of the recorded and simulated motions are plotted in Fig.3.18, which indicated that simulated motions were in good agreement with the recorded motion. Fig. 3.19 shows the vertical distribution of recorded and simulated peak ground acceleration. The recorded and simulated values were in very good agreement. Based on the analyses of the ground motions at this site it appeared that the ground motions were almost linearly amplified on account of the relatively weak input motion at the base as this site was quite far form the source.

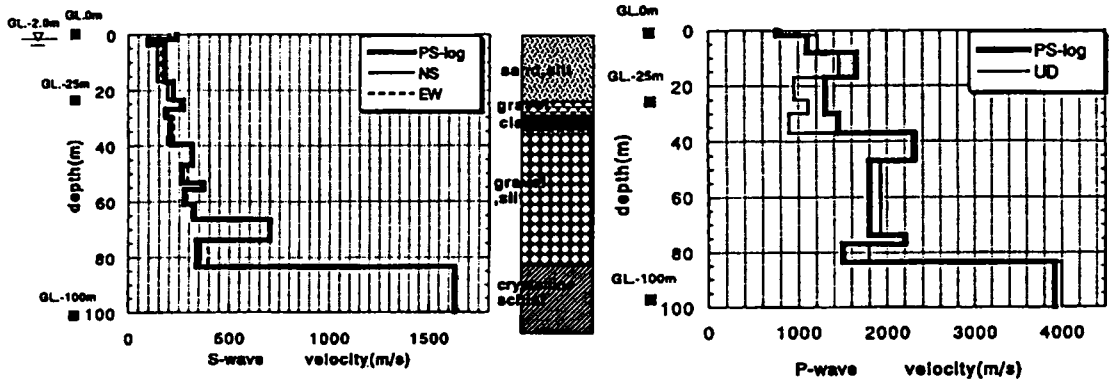

Fig.3.17 Identified soil profile of S-wave and P-wave velocities at KNK

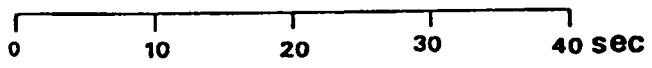

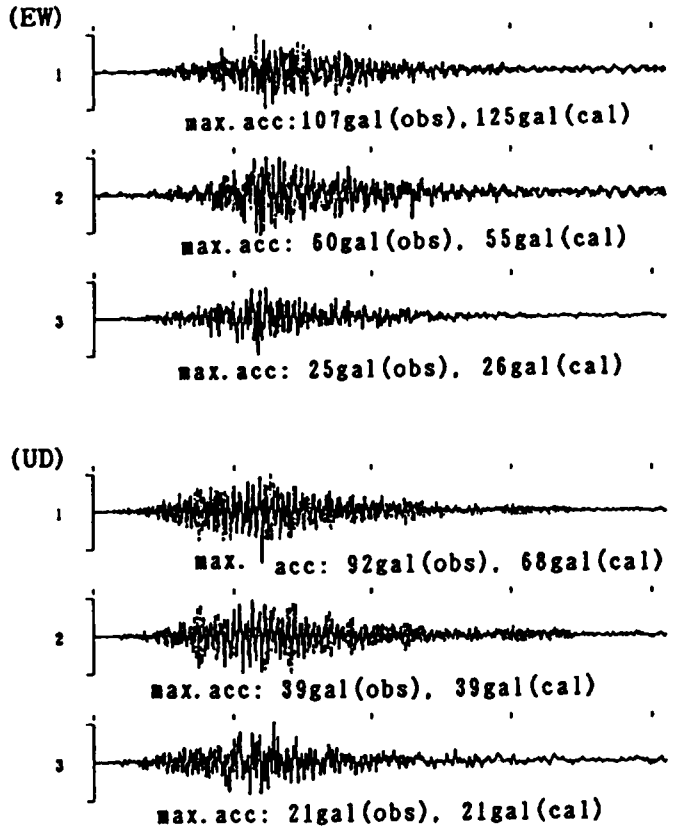

Fig.3.18 The acceleration time history of main shock at KNK

(bold line: observed motion, broken line: analyzed from 1-D identified model)

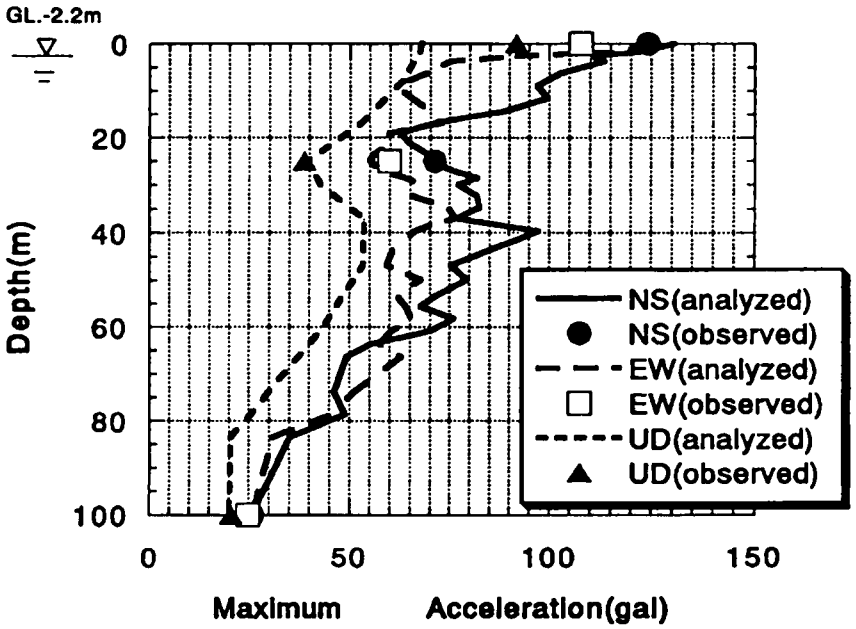

Fig.3.19 Distribution of peak ground acceleration along the depth at KNK

3.2.5 Comparison between Estimated and Observed Local Site Effects

Fig. 3.20 shows the transfer functions or spectral ratios between the records at the ground surface and base layer of the vertical array in the horizontal EW and vertical UD directions at all four sites. On the whole the spectral ratios computed using the identified 1-D model are in good agreement with the spectral ratios calculated from records during the main shock. The peaks in the spectral ratios of the EW component calculated from the recorded motions appeared at 0.7 Hz, 0.5 Hz, 0.7 Hz and 1.0 Hz at PI, SGK, TKS and KNK, respectively. The maximum values of recorded amplifications were about 3.6, 10.0, 10.0, and 19.0, at PI, SGK, TKS and KNK respectively and the corresponding maximum values are 5.0, 10.0, 8.0 and 20.0 for the transfer function computed using identified soil parameters. Fig. 3.20 clearly demonstrated that the predominant frequency recorded during the main shock moved to a lower frequency as compared to the predominant frequency estimated using PS-logging soil parameters. Such a behavior could be explained in terms of strain-dependency of Vs and h at the three sites, except for the KNK site, where the ground motion was relatively more intense. The peaks of amplifications recorded at PI were the smallest of the four sites primarily because of the extreme nonlinear behavior of the liquefied artificial sand fill.

The estimated amplifications in the UD component had the first mode peaks at 4.0 Hz in PI, 4.0 Hz in SGK, 3.0 Hz in TKS, and 5.0 Hz in KNK. The amplitude of the peaks indicated values greater than 10.0.

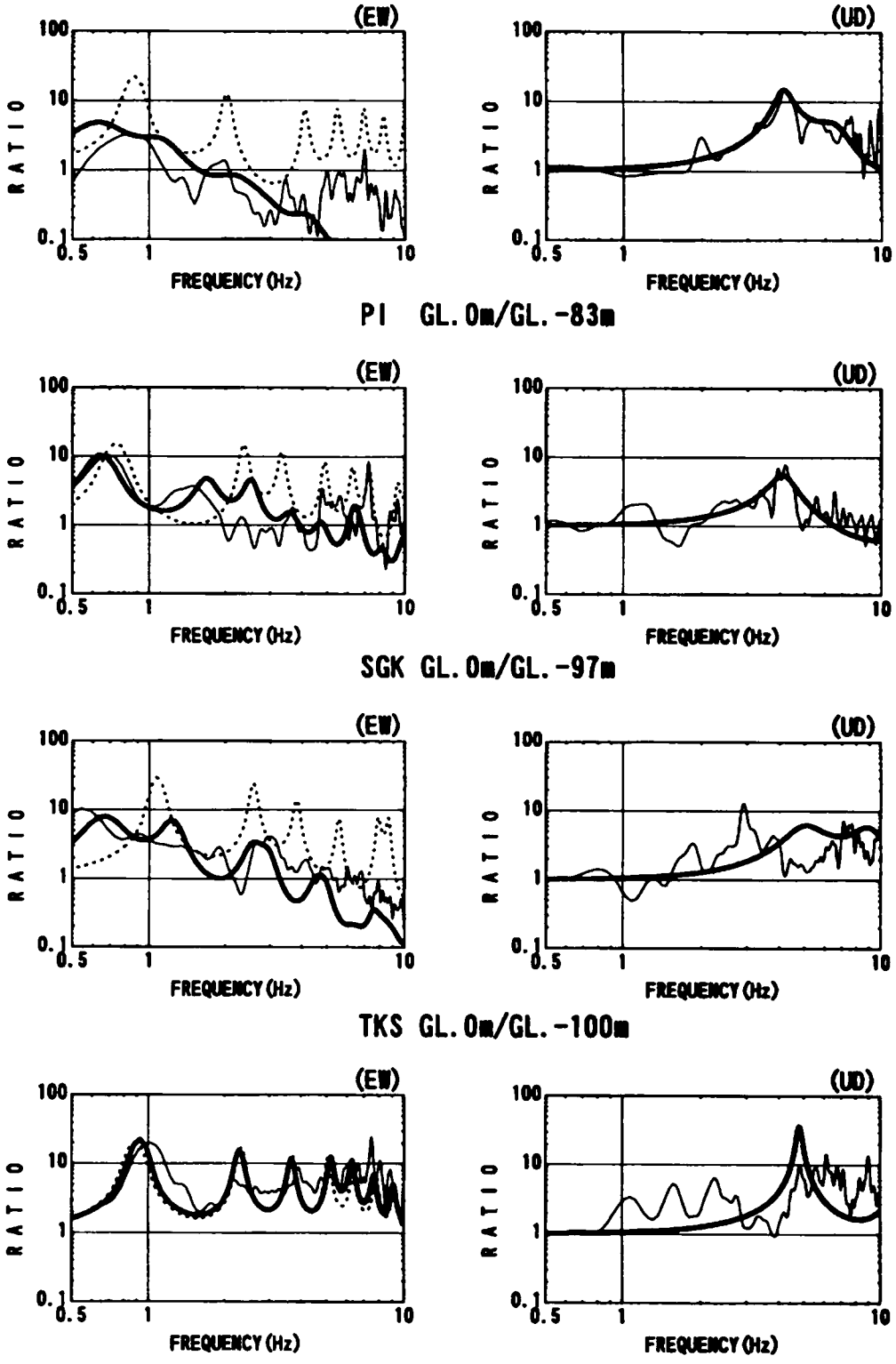

Fig.3.20 Spectral ratios at the recording sites (dashed line: PS-log, bold line: identified, thin line: observed)

3.3 Local Site Effects During Strong and Weak Motions

3.3.1 Estimation of Vertical Motion

As for the vertical motion, the arrival times of S-wave and Sp-wave could be detected in the recorded motions at the liquefied site PI. Sp-wave is a P-wave arising from the conversion of incident S-wave at the interface between the basement and the sediments of the ground. As noted earlier, at this site the vertical motion was amplified more than the horizontal motion. Vertical motion has, also, been found to be amplified at sites with steep topography[11), 12)] and Sp-waves have been detected in aftershock records from an observation site at Higashinada ward[13)-15)]. In this section, the particle motions recorded at PI in the vertical plane were analyzed at four ranges of frequency in an attempt to detect the travel time difference between S-wave and Sp-wave. In the process of estimating the S-Sp time the thickness of the deep sedimentary layer was, also, estimated.

Vertical and horizontal strong motions recorded at different depths at PI are displayed in Fig. 3.21. Also, shown are vertical and horizontal particle filtered through four frequency ranges of 0.2~0.4 Hz, 0.4~1.0 Hz, 1.0~2.5 Hz and 2.5~5.0 Hz. The arrival times of the first P-, S- and Sp-wave are indicated by arrow symbols in the trace of the acceleration time histories. The arrival times of first S-wave at the surface and bottom layers were 4 sec. In comparison, the arrival times of the first P-wave could be found at around 1 sec.

As seen clearly in the vertical motions, another phase peaked at a time in between the P- and S-wave arrivals. This distinct phase could be seen in vertical records at all depths at about 1 sec prior to the first S-wave arrival but a similar phase could not be identified in the horizontal motions. This phase found in the vertical motion has frequencies lying in the range of 2.5-5.0 Hz. Furthermore this phase was remarkably amplified near the surface liquefied layer. A similar distinct phase has been identified in a linear array along the Sumiyoshi river in the Higashinada ward in Kobe[13) 14)]. Based on observations at PI and at Higashinada ward in Kobe, this phase seen clearly in the vertical motion was interpreted as a P-wave arising from the conversion of S-wave at the interface between the deep sediments and bedrock and was denoted as a Sp-wave.

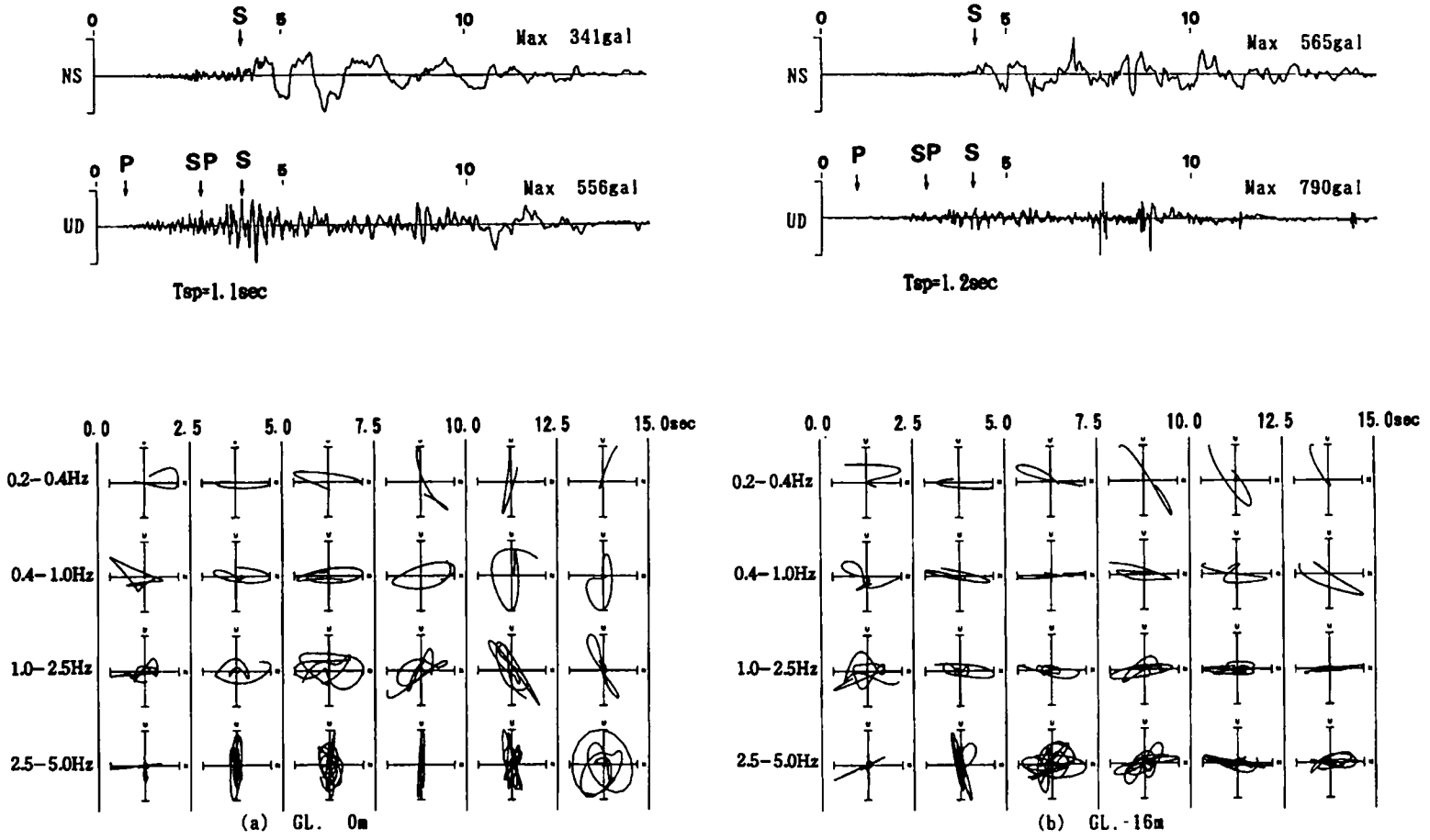

Fig.3.21 Acceleration records and the B.P.F. velocity particle motion at the vertical section

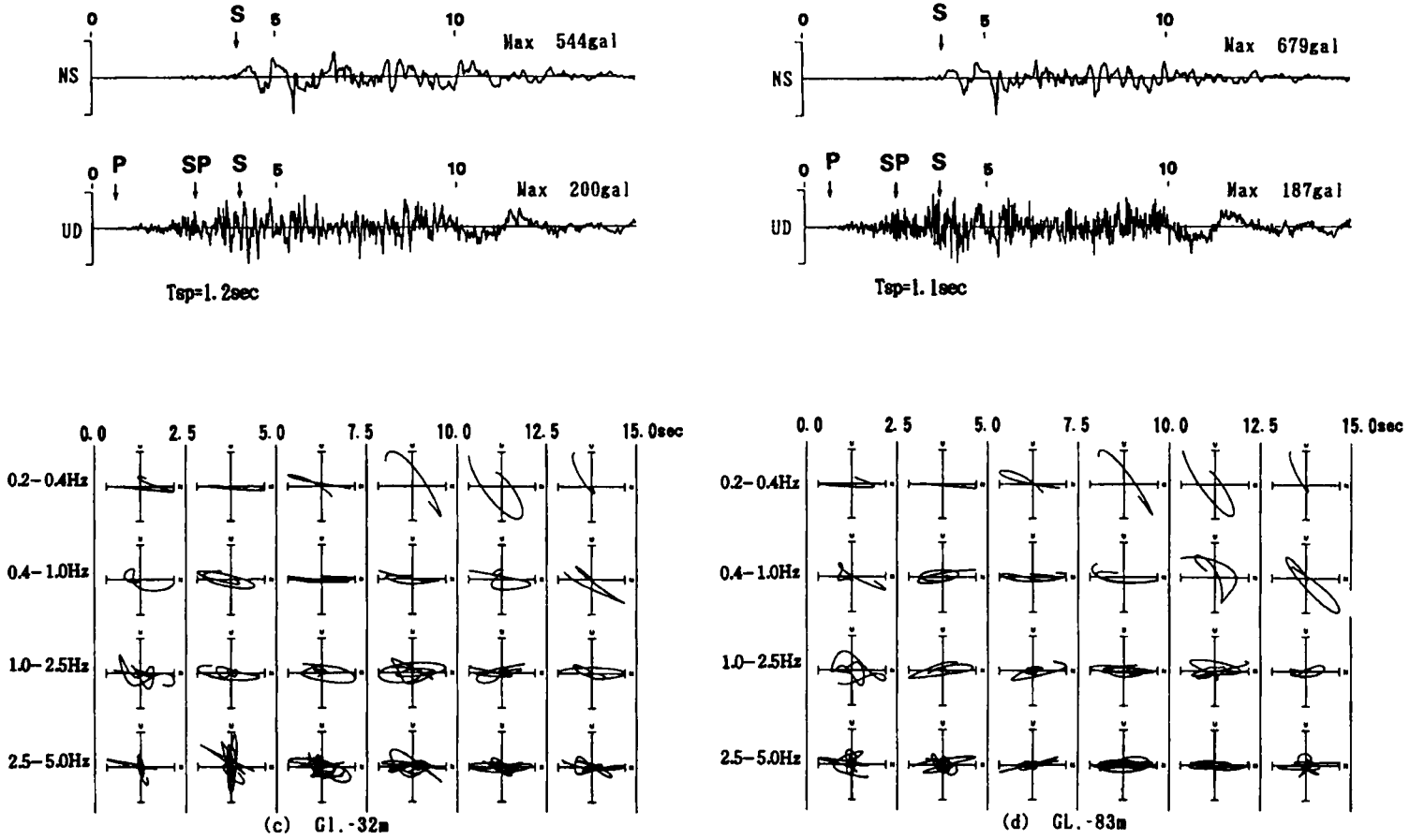

Fig.3.21 Acceleration records and the B.P.F. velocity particle motion at the vertical section (Contined)

The S-Sp time defined by the difference in arrival times of the S- and Sp-waves was about 1.1~1.20 sec at all down-hole records. Knowing the S-Sp time, the thickness of sediments Hsp was estimated using the following equation:

$$H_{sp} = \frac{T_{sp} * V_p * V_s}{V_p - V_s} \tag{3.1}$$

where Tsp is S-Sp time and Vp, Vs are the velocity for P- and S-waves of the sediments.

According to Iwata et al.[13] the mean Vp and Vs for the sediments are 2.1 and 0.8 Km/s, respectively, while Kawase et al.[14] have reported mean values of 1.9 and 0.85 Km/s. Hsp computed using the two sets of velocities is as follows:

Hsp = 1.47 Km using Iwata et al[13] values of 2.1 and 0.8 Km/s
Hsp = 1.75 Km using Kawase et al[13] values of 1.9 and 0.85 Km/s

The estimated thickness agreed with sediment thickness estimated from seismic surveys conducted after the occurrence of the main shock[12]. Therefore, the vertical motions recorded at PI were interpreted as being amplified by Sp-waves converted at the interface between deep sediments and bedrock of geological structure[16].

3.3.2 Change of Dynamic Soil Properties during Weak Motions

Some aftershocks were recorded at the down-hole sites from January 17 to February 18 following the 1995 Hyogoken-Nanbu earthquake. There were a total of 5, 6 and 7 aftershocks recorded at SGK, TKS, and KNK, respectively. In the following section the soil properties identified using these records are compared with those obtained from the main shock to investigate the variation, if any, of the soil properties during weak motions. Only at PI, we have already analyzed aftershock records[1] occurred within about two minutes after the main shock.

Figs. 3.22 and 3.23 show spectral ratios between the surface and bottom records for the weak motions. Also, shown are the average spectral ratios at each down-hole site. The average spectral ratios were taken to be indicative of the site amplification effect for weak motions. S-wave velocity profiles identified using the average spectral ratios are shown in Fig. 3.24. Also, shown are the average and the average ± standard deviation of

the S-wave velocity profiles identified using spectral ratios of individual events. The maximum values of the standard deviations of S-wave velocity profiles identified using spectral ratios during weak motions were 18.4 m/s at SGK, 31.6 m/s at TKS, and 59.0 m/s at KNK as shown in Table 3.1.

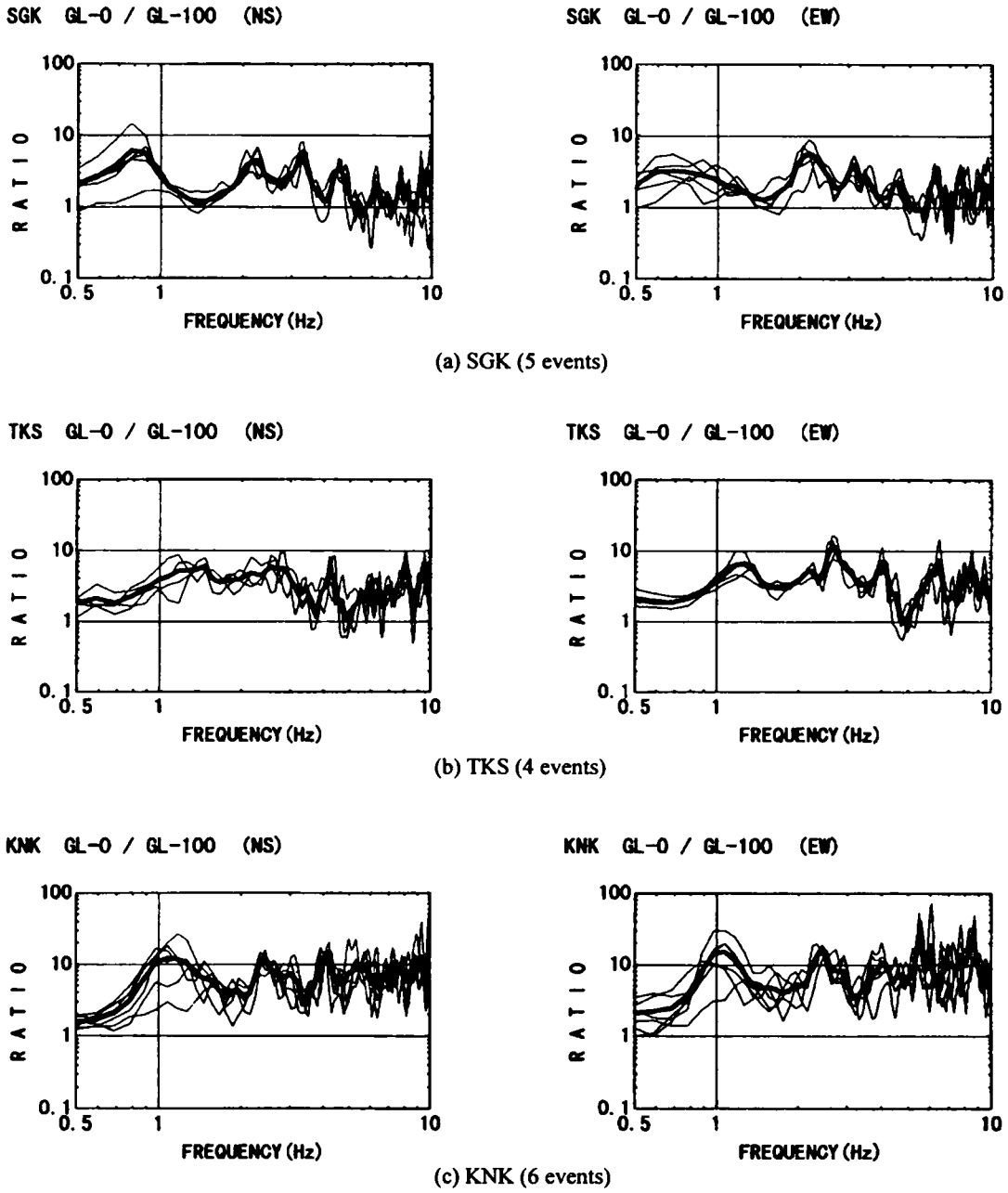

(a) SGK (5 events)

(b) TKS (4 events)

(c) KNK (6 events)

Fig.3.22 Average and all spectral ratios for the aftershocks(1/17～2/18, bold line: average , thin line: aftershocks)

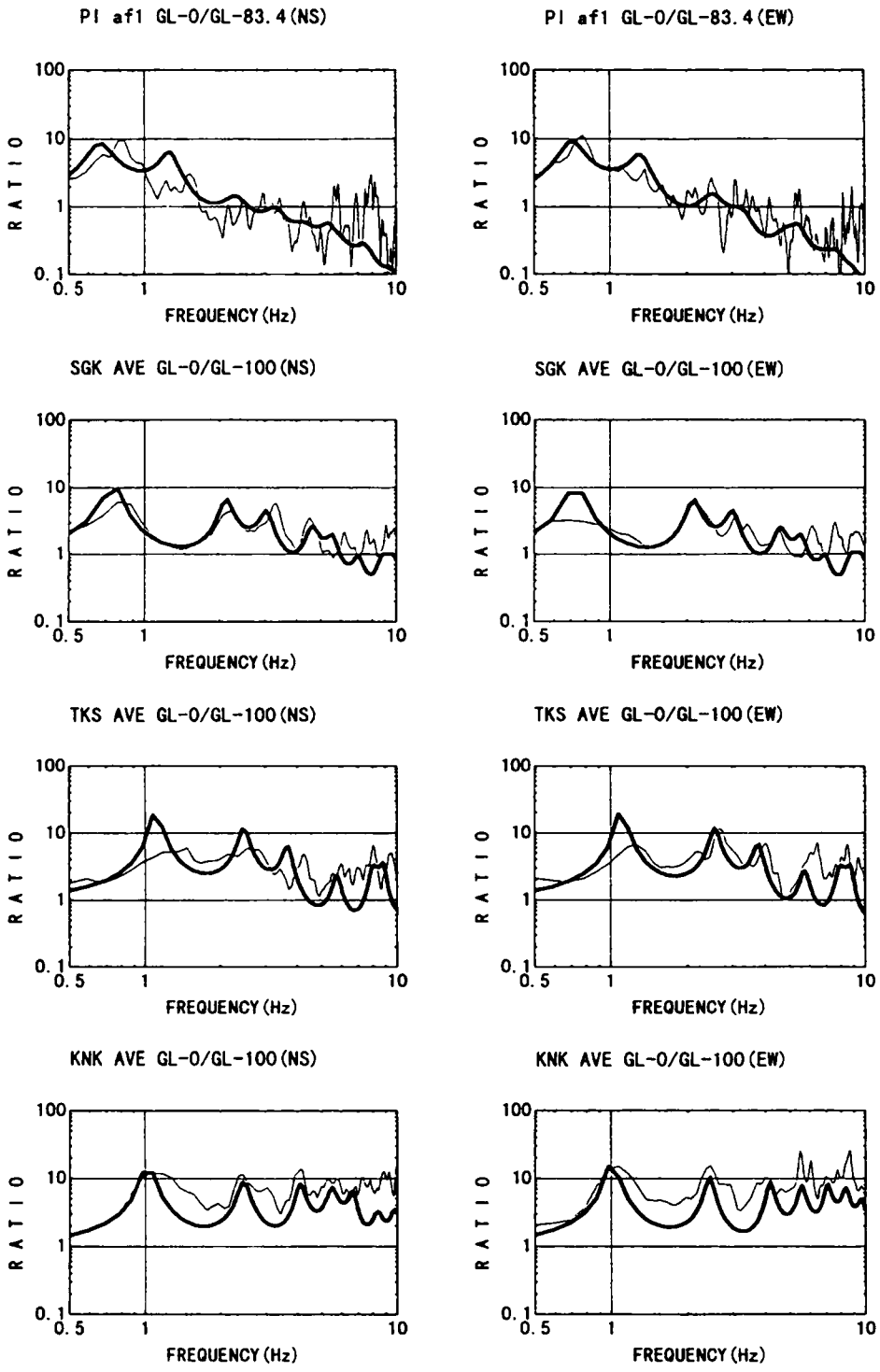

Fig.3.23 Transfer functions and averaged spectral ratios for aftershocks

(bold line: analyzed, thin line: observed)

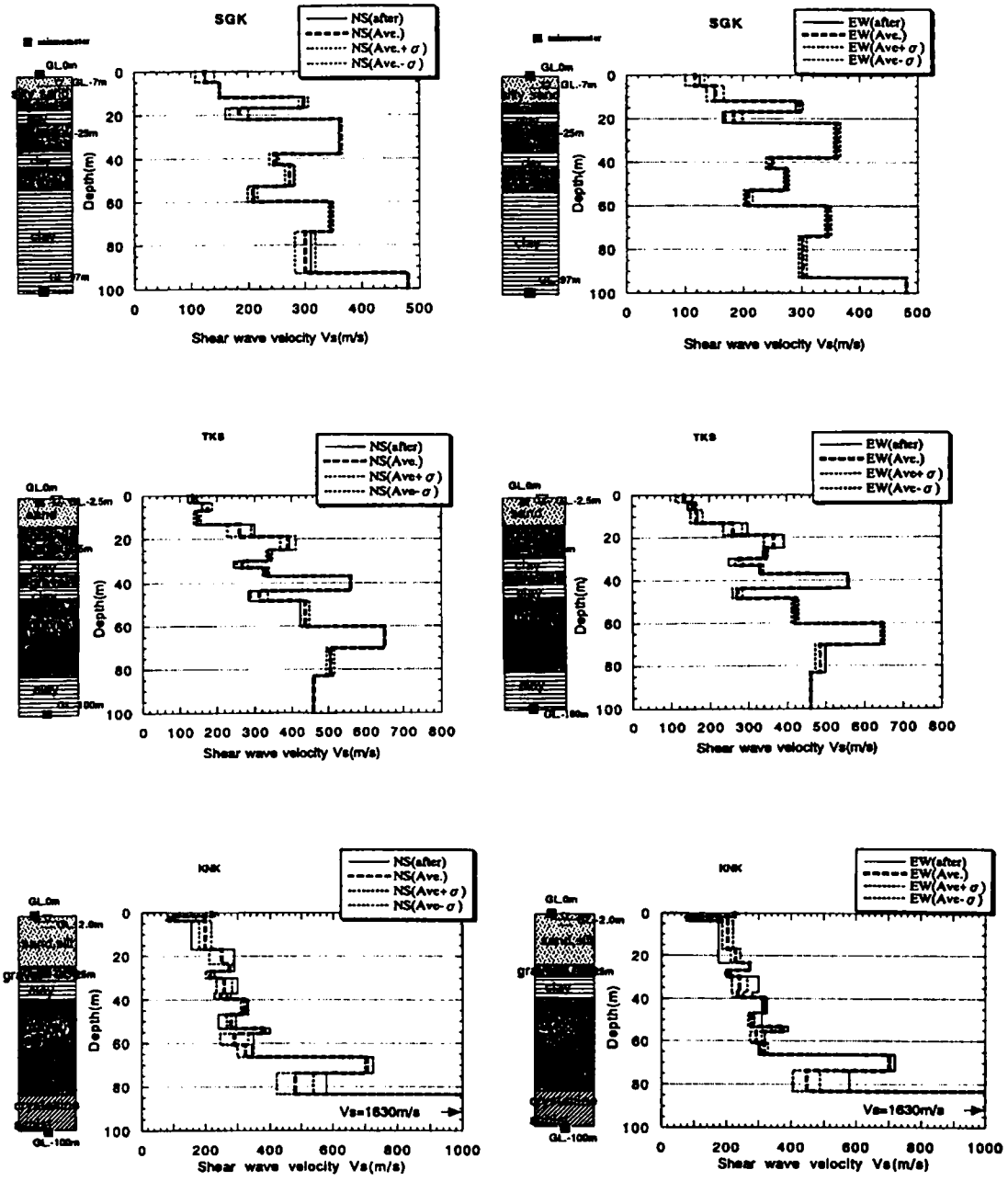

Fig.3.24 Identified average and variations of S-wave velocities for aftershocks and S wave velocity profile of the average spectral ratios
Upper: (a) SGK, Inermediate:(b) TKS, Bottom:(c) KNK

Table 3.1(a) Identified geotechnical parameters for aftershocks (SGK)

	SGK	(NS)	EQ No.						(EW)	EQ No.					
	thickness	1	2	3	4	5	Ave.	±σ	1	2	3	4	5	Ave.	±σ
layer No.	H(m)	Vs	Vs	Vs	Vs	Vs	Vs	Vs	Vs	Vs	Vs	Vs	Vs	Vs	Vs
1	5.00	100.00	125.00	120.00	130.00	145.00	124.00	16.36	90.00	120.00	120.00	120.00	135.00	117.00	16.43
2	7.00	150.00	150.00	150.00	150.00	150.00	150.00	0.00	130.00	160.00	150.00	150.00	170.00	152.00	14.83
3	5.00	310.00	290.00	300.00	300.00	290.00	298.00	8.37	305.00	290.00	300.00	295.00	290.00	296.00	6.52
4	5.00	210.00	190.00	180.00	170.00	170.00	184.00	16.73	180.00	190.00	180.00	165.00	205.00	184.00	14.75
5	16.00	360.00	360.00	365.00	365.00	365.00	363.00	2.74	355.00	360.00	365.00	360.00	370.00	362.00	5.70
6	5.00	230.00	250.00	250.00	250.00	245.00	245.00	8.66	235.00	250.00	250.00	250.00	245.00	248.00	6.52
7	10.00	260.00	275.00	275.00	285.00	270.00	273.00	9.08	270.00	275.00	275.00	280.00	270.00	274.00	4.18
8	7.00	200.00	210.00	205.00	220.00	200.00	207.00	8.37	220.00	210.00	205.00	210.00	200.00	209.00	7.42
9	14.00	350.00	345.00	345.00	350.00	340.00	346.00	4.18	355.00	345.00	345.00	345.00	340.00	346.00	5.48
10	19.00	270.00	305.00	305.00	320.00	300.00	300.00	18.37	290.00	305.00	305.00	305.00	305.00	302.00	6.71
11	4.00	480.00	480.00	480.00	480.00	480.00	480.00	0.00	480.00	480.00	480.00	480.00	480.00	480.00	0.00
12	9999.99	480.00	480.00	480.00	480.00	480.00	480.00	0.00	480.00	480.00	480.00	480.00	480.00	480.00	0.00

	SGK	(NS)	EQ No.						(EW)	EQ No.					
	thickness	1	2	3	4	5	Ave.	±σ	1	2	3	4	5	Ave.	±σ
layer No.	H(m)	Q	Q	Q	Q	Q	Q	Q	Q	Q	Q	Q	Q	Q	Q
1	5.00	5.00	20.00	20.00	10.00	15.00	14.00	6.52	5.00	20.00	20.00	10.00	20.00	15.00	7.07
2	7.00	10.00	20.00	15.00	10.00	15.00	14.00	4.18	10.00	20.00	15.00	10.00	15.00	14.00	4.18
3	5.00	10.00	10.00	10.00	10.00	10.00	10.00	0.00	10.00	10.00	10.00	10.00	10.00	10.00	0.00
4	5.00	10.00	10.00	10.00	10.00	10.00	10.00	0.00	10.00	10.00	10.00	10.00	10.00	10.00	0.00
5	16.00	10.00	10.00	10.00	10.00	10.00	10.00	0.00	10.00	10.00	10.00	10.00	10.00	10.00	0.00
6	5.00	10.00	10.00	10.00	10.00	10.00	10.00	0.00	10.00	10.00	10.00	10.00	10.00	10.00	0.00
7	10.00	10.00	10.00	10.00	10.00	10.00	10.00	0.00	10.00	10.00	10.00	10.00	10.00	10.00	0.00
8	7.00	10.00	10.00	10.00	10.00	10.00	10.00	0.00	10.00	10.00	10.00	10.00	10.00	10.00	0.00
9	14.00	10.00	10.00	10.00	10.00	10.00	10.00	0.00	10.00	10.00	10.00	10.00	10.00	10.00	0.00
10	19.00	10.00	10.00	10.00	10.00	10.00	10.00	0.00	10.00	10.00	10.00	10.00	10.00	10.00	0.00
11	4.00	10.00	10.00	10.00	10.00	10.00	10.00	0.00	10.00	10.00	10.00	10.00	10.00	10.00	0.00
12	9999.99	10.00	10.00	10.00	10.00	10.00	10.00	0.00	10.00	10.00	10.00	10.00	10.00	10.00	0.00

Table 3.1(b) Identified geotechnical parameters for aftershocks (TKS)

	TKS	(NS)	EQ No.					(EW)	EQ No.					
	thickness	1	2	3	4	Ave.	±σ	1	2	3	4	Ave.	±σ
layer No.	H(m)	Vs	Vs	Vs	Vs	Vs	Vs	Vs	Vs	Vs	Vs	Vs	Vs
1	3.40	140.00	130.00	150.00	120.00	135.00	12.91	150.00	110.00	155.00	125.00	135.00	21.21
2	3.75	170.00	190.00	160.00	180.00	175.00	12.91	170.00	150.00	160.00	160.00	160.00	8.16
3	6.25	140.00	140.00	160.00	150.00	147.50	9.57	160.00	185.00	175.00	150.00	167.50	15.55
4	5.60	270.00	230.00	300.00	240.00	260.00	31.62	240.00	280.00	240.00	285.00	261.25	24.62
5	6.00	390.00	410.00	400.00	360.00	390.00	21.60	340.00	400.00	360.00	370.00	367.50	25.00
6	5.00	350.00	340.00	340.00	330.00	340.00	8.16	350.00	350.00	350.00	340.00	347.50	5.00
7	3.00	280.00	280.00	250.00	260.00	267.50	15.00	290.00	270.00	280.00	270.00	277.50	9.57
8	4.00	340.00	330.00	320.00	330.00	330.00	8.16	340.00	330.00	335.00	340.00	336.25	4.79
9	6.70	560.00	560.00	560.00	560.00	560.00	0.00	560.00	560.00	560.00	560.00	560.00	0.00
10	4.80	340.00	320.00	290.00	300.00	312.50	22.17	290.00	260.00	270.00	270.00	272.50	12.58
11	11.80	450.00	440.00	420.00	435.00	436.25	12.50	430.00	425.00	410.00	420.00	421.25	8.54
12	10.00	650.00	650.00	650.00	650.00	650.00	0.00	650.00	650.00	640.00	650.00	647.50	5.00
13	13.00	520.00	500.00	500.00	500.00	505.00	10.00	480.00	500.00	470.00	490.00	485.00	12.91
14	16.70	460.00	460.00	460.00	460.00	460.00	0.00	460.00	460.00	460.00	460.00	460.00	0.00
15	9999.99	460.00	460.00	460.00	460.00	460.00	0.00	460.00	460.00	460.00	460.00	460.00	0.00

	TKS	(NS)	EQ No.					(EW)	EQ No.					
	thickness	1	2	3	4	Ave.	±σ	1	2	3	4	Ave.	±σ
layer No.	H(m)	Q	Q	Q	Q	Q	Q	Q	Q	Q	Q	Q	Q
1	3.40	10.00	20.00	15.00	25.00	17.50	6.45	20.00	20.00	15.00	15.00	17.50	2.89
2	3.75	10.00	15.00	15.00	25.00	16.25	6.29	20.00	20.00	15.00	15.00	17.50	2.89
3	6.25	10.00	10.00	10.00	10.00	10.00	0.00	10.00	20.00	10.00	15.00	13.75	4.79
4	5.60	10.00	10.00	10.00	10.00	10.00	0.00	10.00	20.00	10.00	15.00	13.75	4.79
5	6.00	10.00	10.00	10.00	10.00	10.00	0.00	10.00	20.00	10.00	15.00	13.75	4.79
6	5.00	10.00	10.00	10.00	10.00	10.00	0.00	10.00	10.00	10.00	10.00	10.00	0.00
7	3.00	10.00	10.00	10.00	10.00	10.00	0.00	10.00	10.00	10.00	10.00	10.00	0.00
8	4.00	10.00	10.00	10.00	10.00	10.00	0.00	10.00	10.00	10.00	10.00	10.00	0.00
9	6.70	20.00	20.00	20.00	20.00	20.00	0.00	20.00	20.00	20.00	20.00	20.00	0.00
10	4.80	20.00	20.00	20.00	20.00	20.00	0.00	20.00	20.00	20.00	20.00	20.00	0.00
11	11.80	20.00	20.00	20.00	20.00	20.00	0.00	20.00	20.00	20.00	20.00	20.00	0.00
12	10.00	20.00	20.00	20.00	20.00	20.00	0.00	20.00	20.00	20.00	20.00	20.00	0.00
13	13.00	20.00	20.00	20.00	20.00	20.00	0.00	20.00	20.00	20.00	20.00	20.00	0.00
14	16.70	20.00	20.00	20.00	20.00	20.00	0.00	20.00	20.00	20.00	20.00	20.00	0.00
15	9999.99	20.00	20.00	20.00	20.00	20.00	0.00	20.00	20.00	20.00	20.00	20.00	0.00

Table 3.1(c) Identified geotechnical parameters for aftershocks (KNK)

	KNK	(NS)	EQ No.							(EW)	EQ No.						
	thickness	1	2	3	4	5	6	Ave.	±σ	1	2	3	4	5	6	Ave.	±σ
layer No.	H(m)	Vs	Vs	Vs	Vs	Vs	Vs	Vs	Vs	Vs	Vs	Vs	Vs	Vs	Vs	Vs	Vs
1	1.80	220.00	190.00	220.00	230.00	230.00	220.00	218.33	14.72	215.00	225.00	230.00	225.00	230.00	230.00	225.83	5.85
2	2.00	90.00	100.00	80.00	80.00	80.00	100.00	88.33	9.83	90.00	95.00	80.00	75.00	70.00	80.00	81.67	9.31
3	13.20	200.00	175.00	190.00	190.00	210.00	230.00	199.17	19.08	200.00	220.00	205.00	190.00	180.00	225.00	203.33	17.22
4	6.60	250.00	205.00	320.00	240.00	230.00	280.00	250.83	38.78	210.00	215.00	225.00	250.00	230.00	240.00	228.33	15.06
5	1.40	275.00	270.00	275.00	275.00	270.00	280.00	274.17	3.76	270.00	270.00	270.00	275.00	270.00	275.00	271.67	2.58
6	2.00	275.00	270.00	275.00	275.00	270.00	280.00	274.17	3.76	270.00	270.00	270.00	275.00	270.00	275.00	271.67	2.58
7	3.00	210.00	230.00	220.00	215.00	180.00	220.00	214.17	13.57	195.00	205.00	215.00	215.00	195.00	205.00	205.00	8.94
8	7.10	240.00	270.00	290.00	275.00	225.00	255.00	259.17	23.96	270.00	220.00	240.00	270.00	225.00	220.00	240.83	23.75
9	2.60	245.00	270.00	260.00	255.00	220.00	230.00	248.67	18.89	260.00	220.00	240.00	245.00	225.00	220.00	235.00	16.12
10	7.20	320.00	310.00	335.00	335.00	315.00	310.00	320.83	11.58	320.00	315.00	330.00	320.00	320.00	320.00	320.83	4.92
11	6.50	270.00	280.00	300.00	290.00	260.00	280.00	280.00	14.14	270.00	280.00	280.00	295.00	270.00	270.00	277.50	9.87
12	2.40	380.00	390.00	380.00	380.00	370.00	375.00	379.17	6.65	380.00	370.00	375.00	380.00	370.00	370.00	374.17	4.92
13	5.20	210.00	330.00	320.00	310.00	275.00	295.00	290.00	43.70	300.00	270.00	300.00	320.00	285.00	280.00	292.50	17.82
14	5.50	320.00	280.00	350.00	350.00	325.00	320.00	324.17	25.77	310.00	300.00	320.00	330.00	330.00	320.00	318.33	11.69
15	7.40	700.00	710.00	710.00	705.00	700.00	705.00	705.00	4.47	705.00	705.00	700.00	705.00	700.00	700.00	702.50	2.74
16	9.60	480.00	580.00	480.00	450.00	400.00	490.00	480.00	58.99	500.00	465.00	440.00	470.00	380.00	425.00	446.67	41.67
17	16.50	1630.00	1630.00	1630.00	1630.00	1630.00	1630.00	1630.00	0.00	1630.00	1630.00	1630.00	1630.00	1630.00	1630.00	1630.00	0.00
18	9999.99	1630.00	1630.00	1630.00	1630.00	1630.00	1630.00	1630.00	0.00	1630.00	1630.00	1630.00	1630.00	1630.00	1630.00	1630.00	0.00

	KNK	(NS)	EQ No.							(EW)	EQ No.						
	thickness	1	2	3	4	5	6	Ave.	±σ	1	2	3	4	5	6	Ave.	±σ
layer No.	H(m)	Q	Q	Q	Q	Q	Q	Q	Q	Q	Q	Q	Q	Q	Q	Q	Q
1	1.80	5.00	10.00	5.00	5.00	5.00	5.00	5.83	2.04	10.00	5.00	5.00	5.00	5.00	5.00	5.83	2.04
2	2.00	10.00	10.00	10.00	10.00	10.00	10.00	10.00	0.00	25.00	15.00	15.00	15.00	15.00	15.00	16.67	4.08
3	13.20	10.00	10.00	10.00	10.00	10.00	10.00	10.00	0.00	25.00	15.00	15.00	15.00	15.00	15.00	16.67	4.08
4	6.60	5.00	5.00	5.00	5.00	5.00	5.00	5.00	0.00	25.00	5.00	5.00	5.00	5.00	5.00	8.33	8.16
5	1.40	5.00	5.00	5.00	5.00	5.00	5.00	5.00	0.00	10.00	5.00	5.00	5.00	5.00	5.00	5.83	2.04
6	2.00	5.00	5.00	5.00	5.00	5.00	5.00	5.00	0.00	10.00	5.00	5.00	5.00	5.00	5.00	5.83	2.04
7	3.00	10.00	10.00	10.00	10.00	10.00	10.00	10.00	0.00	20.00	15.00	15.00	15.00	10.00	10.00	14.17	3.76
8	7.10	10.00	10.00	10.00	10.00	10.00	10.00	10.00	0.00	20.00	15.00	15.00	15.00	10.00	10.00	14.17	3.76
9	2.60	10.00	10.00	10.00	10.00	10.00	10.00	10.00	0.00	20.00	15.00	15.00	15.00	10.00	10.00	14.17	3.76
10	7.20	10.00	10.00	10.00	10.00	10.00	10.00	10.00	0.00	20.00	15.00	15.00	15.00	10.00	10.00	14.17	3.76
11	6.50	10.00	10.00	10.00	10.00	10.00	10.00	10.00	0.00	20.00	15.00	15.00	15.00	10.00	10.00	14.17	3.76
12	2.40	10.00	10.00	10.00	10.00	10.00	10.00	10.00	0.00	20.00	15.00	15.00	15.00	10.00	10.00	14.17	3.76
13	5.20	10.00	10.00	10.00	10.00	10.00	10.00	10.00	0.00	20.00	15.00	15.00	15.00	10.00	10.00	14.17	3.76
14	5.50	10.00	10.00	10.00	10.00	10.00	10.00	10.00	0.00	20.00	15.00	15.00	15.00	10.00	10.00	14.17	3.76
15	7.40	10.00	10.00	10.00	10.00	10.00	10.00	10.00	0.00	20.00	15.00	15.00	15.00	10.00	10.00	14.17	3.76
16	9.60	10.00	10.00	10.00	10.00	10.00	10.00	10.00	0.00	20.00	15.00	15.00	15.00	10.00	10.00	14.17	3.76
17	16.50	10.00	10.00	10.00	10.00	10.00	10.00	10.00	0.00	20.00	15.00	15.00	15.00	10.00	10.00	14.17	3.76
18	9999.99	10.00	10.00	10.00	10.00	10.00	10.00	10.00	0.00	20.00	15.00	15.00	15.00	10.00	10.00	14.17	3.76

3.3.3 Comparison of Local Site Effects during Strong and Weak Motions

The S-wave velocity profiles identified from records of main shock and aftershocks are graphed in Fig. 3.25. The average of Vs identified from records of aftershocks was close to the PS logging value except for the sand fill at PI and the sand layer at a depth immediately below the water table at SGK and TKS. The reduction of shear rigidity as a consequence of liquefaction of sand layer at PI, SGK, and TKS was evident in this figure.

The spectral ratios at the down-hole sites computed using records of strong and weak motions are shown in Fig. 3.26. The relationships between these two sets of spectral ratios appeared to be almost like the relationships between spectral ratios from strong motion records and the transfer functions computed using PS logging soil profiles. The spectral ratios computed using strong motion records were smaller than the transfer functions based on aftershock records. This result could be interpreted to mean that the large reduction of shear rigidity was caused by liquefaction in the sand layer[17), 18), 19), 20)].

Lastly, the relationship between the intensity of input acceleration and liquefaction was investigated. As shown in Fig 3.27, the vertical distributions of the peak acceleration were de-amplified in the strong liquefied layers at PI and partly strong liquefied layer at TKS. At both sites, the distribution of maximum shear strain shown in

Fig 3.28 was above 1 % at the liquefied sand layer. It has been reported by other researchers[21), 22)] that the maximum shear strain was above 2 % to 5 % at this liquefied site. On the contrary, at non-liquefied sites such as KNK, the peak acceleration was linearly amplified from a depth of GL-20m all the way up to the surface layer. Maximum shear strain in the non-liquefied sites was about 0.6 % at SGK and about 0.06% at KNK. The intensity of input acceleration at KNK was relatively weak as it was only 50 gal at the bedrock. The peak input acceleration at SGK was much stronger, above 300 gal, but no trace of liquefaction could be found. This was most likely the case because the soil at SGK consists of a hard Holocene gravel layer with Vs greater than 300 m/s and the sand layer at the top was thin, less than 10 m. Based on observations of liquefied and non-liquefied sites, it was surmised that for extensive liquefaction to occur (i) the intensity of the input acceleration should be more than 100 gal and (ii) a water saturated porous sand layer of thickness more than 10 m should exist[23)].

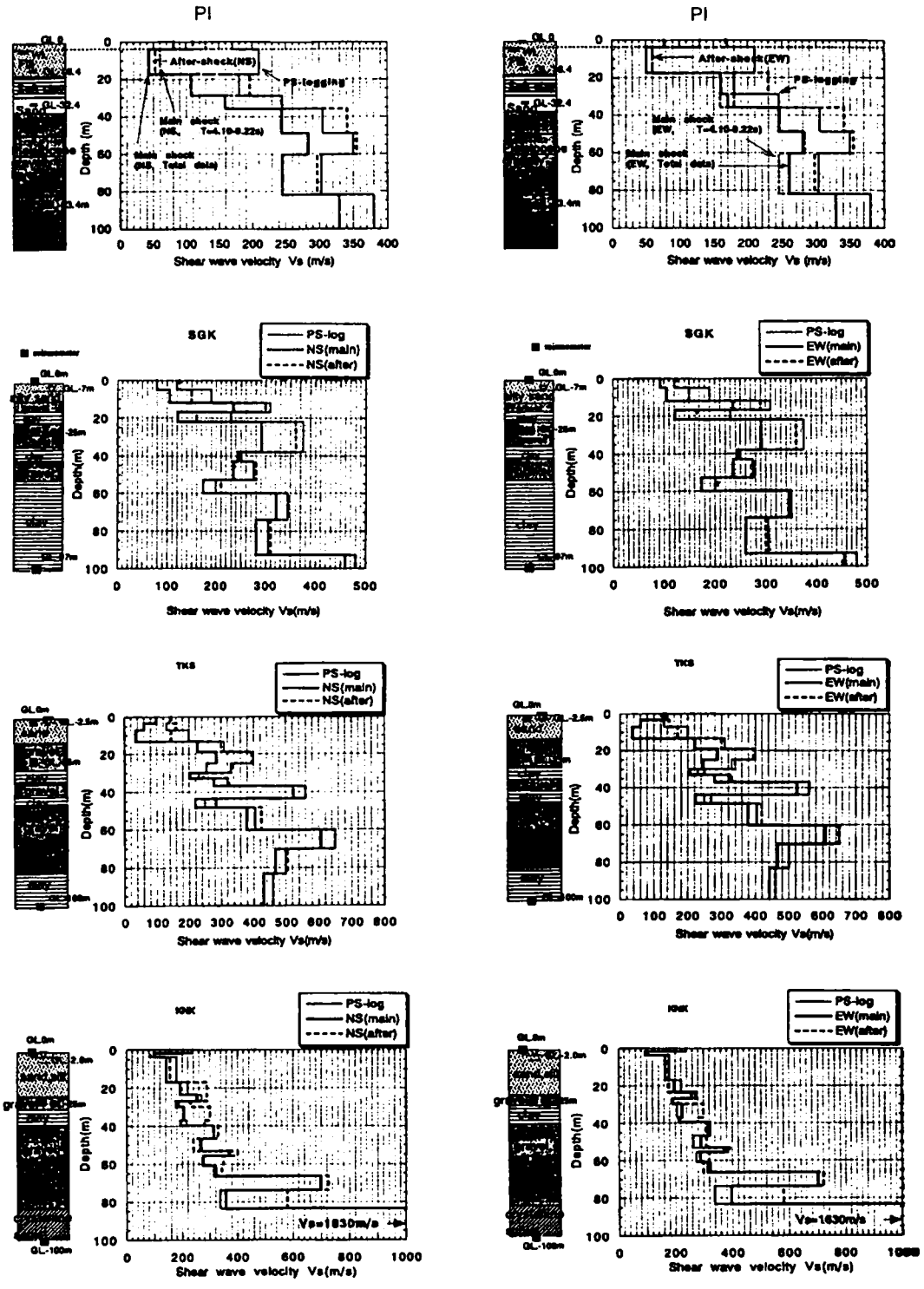

Fig.3.25 S-wave velocity profile of PS-log and identified results for the mainshock and the average aftershock

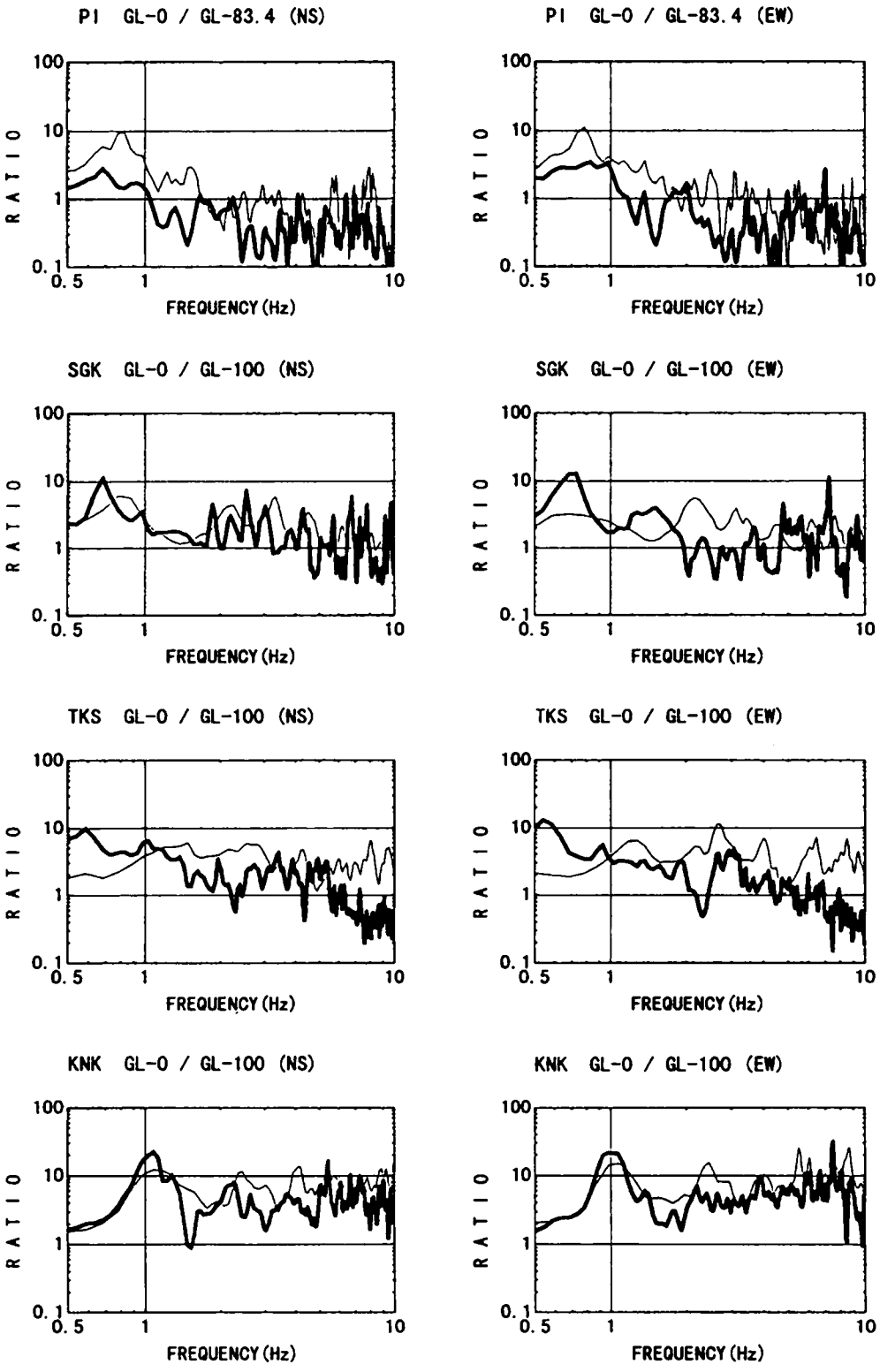

Fig.3.26 Comparison of spectral ratios for the main shock and the average aftershocks (bold line: main shock, thin line: average aftershocks)

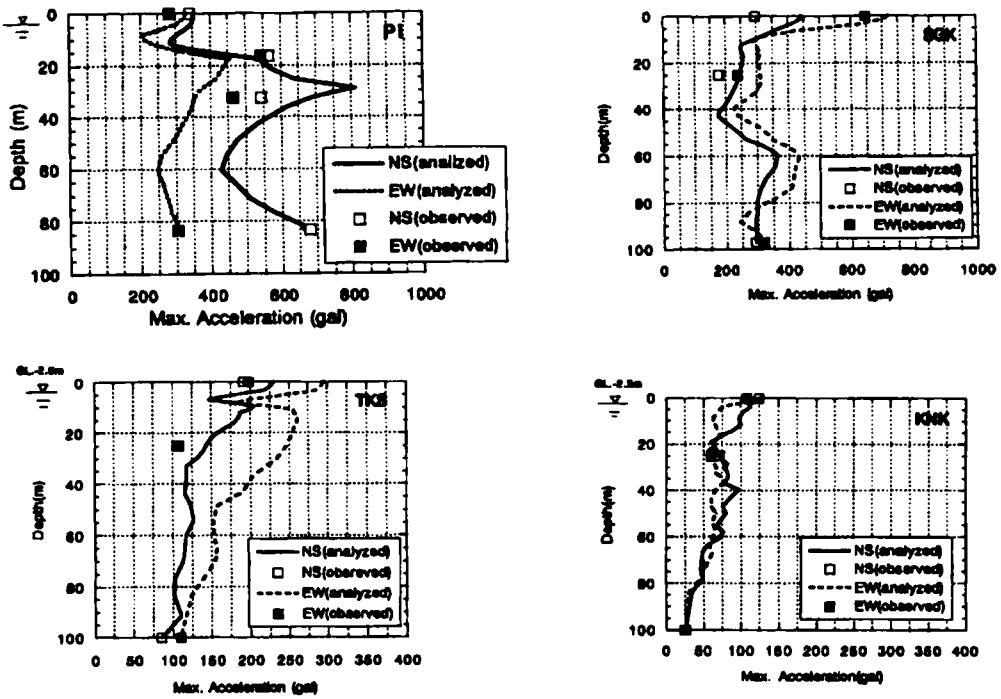

Fig.3.27 Distribution of peak ground acceleration along the depth for the mainshock analyzed from 1-D model

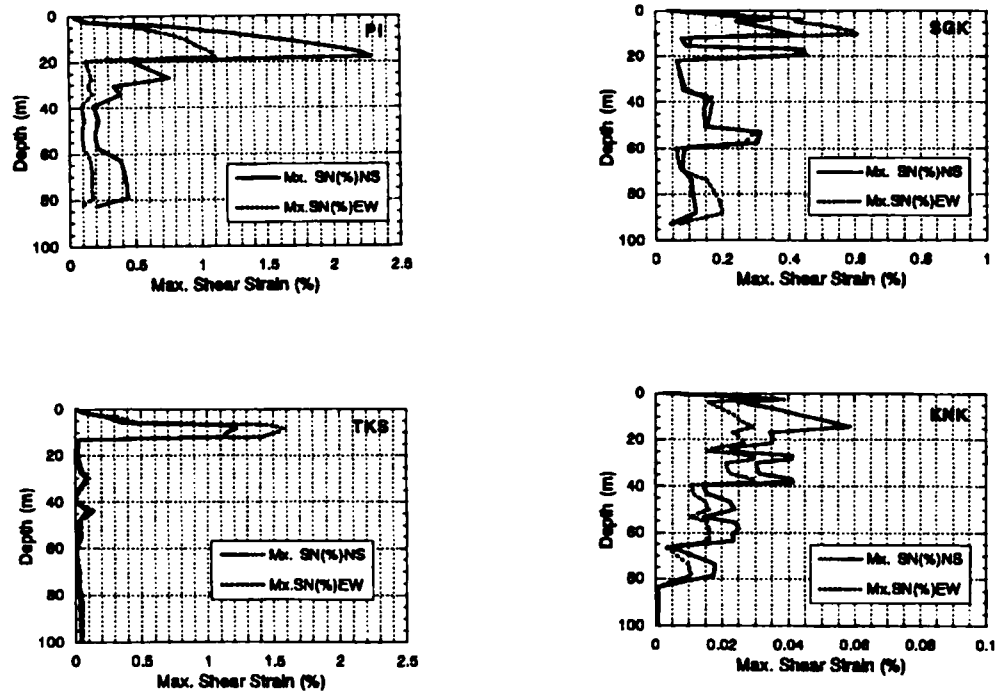

Fig.3.28 Distribution of peak shear strain along the depth for the mainshock analyzed from 1-D model

3.4 Conclusions

Strong ground motions were recorded at four vertical down-hole arrays in the Kansai area with different epicentral distances during the 1995 Hyogoken-Nanbu earthquake. These records and various others recorded during aftershocks were investigated to evaluate site amplifications. Based on the investigations reported in this chapter, the conclusions that were drawn are:

(1) Site amplification characteristics in the horizontal direction were strongly affected by the intensity of the input acceleration at the base of the vertical array. At PI, the vertical distribution of peak acceleration was essentially de-amplified because of liquefaction and the nonlinear behavior of the soil was greatly influenced by the high intensity of the input acceleration which was larger than 500 gals. At the other end of scale at KNK, the vertical distribution of peak acceleration was linearly amplified for the low level of the input acceleration of 20-30 gals.

(2) The S wave velocities (Vs) identified from the main shock records was 40-45 % and 20-25 % smaller than PS-logging values for the Holocene and Pleistocene layers at PI and SGK, respectively. At KNK, which is the most distant from the focal area, the reduction in the identified Vs was found to be only 20 % compared to the PS logging value for the Holocene soils.

(3) The P wave velocities (Vp) identified from the main shock records was almost the same as the PS-logging value at all sites. It was confirmed that the Vp was greater than 1500 m/s in the layers below the water table.

(4) The strong ground motions computed using a 1-D model with identified soil profiles had peak accelerations and acceleration timehistories that matched reasonably well with their observed counterparts at each level at most of the sites. The effect of soil liquefaction could be clearly seen in sudden changes in vertical distribution of peak acceleration at PI and TKS.

(5) With regard to transfer functions, the spectral ratios from a 1-D model agreed reasonably well with the spectral ratios calculated from the recorded motions at the surface and base layers. The peaks of transfer functions in the horizontal components of the motion during the main shock indicated a clear shift to the lower frequency region with respect to the frequencies of the peaks of the transfer function obtained from a 1-D model using PS logging soil profiles. The amplification factors from the spectral ratios of the recorded motions were, also, lower than the amplification factors of spectral ratios obtained from 1-D models using PS logging soil profiles.

(6) Using vertical components of seismograms at PI, arrivals of Sp-wave and the S-Sp

times were examined. The S-Sp time was 1.1~1.20 sec at all depths. It was surmised that Sp-wave is a P-wave arising from the conversion of the S-wave at the interface of the deep sedimentary layer and seismic bedrock.

(7) The variation of geotechnical parameters with intensity of shaking was estimated by a system identification method using aftershock records at SGK, TKS, and KNK. The average value of Vs profile identified from spectral ratios of records of individual aftershocks was in good agreement with the Vs profile identified from the average of spectral ratios. The maximum standard deviations for identified Vs profiles were 18.4 m/s at SGK, 31.6 m/s at TKS and 59.0 m/s at KNK.

(8) The average value of Vs profiles identified from aftershock records was compared with Vs profiles identified from the main shock. It was seen that most of the average values of S-wave velocity identified from aftershocks were close to PS logging values except for the sand fill at PI, and the sand layer below the water table at SGK and TKS. Layers that experienced soil liquefaction had hefty reductions in their shear rigidities.

(9) Nonlinear behavior of soil was seen at PI where the maximum shear strain was more than 0.6 % but no such non-linear behavior was seen at KNK where the shear strain was a small 0.06%. The investigations of liquefied and non-liquefied layers suggest that the conditions for strong liquefaction are (i) the intensity of input acceleration should be greater than 100 gal and (ii) a water saturated porous sand layer of thickness greater than 10 m should exist.

References

1) The Comittee of Earthquake Observation Research in the Kansai Area; Earthquake observation installed by the Comittee of Earthquake Observation Research in the Kansai Area, Abstract of 1994 No.2 autumn series of the seismological society of Japan, pp.230-231 (in Japanese), 1994.

2) Toki, K., K. Irikura and T. Kgawa; Strong motion data recorded in source area on the Hyogo-ken-nambu earthquake, January 17, 1995 Japan, Journal of Natural Disaster Science, 1995.

3) Sato,K. and T. Kokusho; Estimation of soil nonlinearlity during main-shock and after-shock of Hyogoken-Nanbu Earthquake, Proc. 50th Annual Convention of Japan Society for Civil Engineers (in Japanese), 1995.

4) Kokusho, T., K. Sato and M. Matsumoto; Nonlinear dynamic response of soil ground during 1995 Hyogo-ken nanbu earthquake, Report 2391, Soil and foundation, Vol 43, No.9, pp39-43 (in Japanese), 1995.

5) The earthquake disaster research group of CRIEPI; Preliminary report on disaster research related to the 1995 Hyogoken-nanbu earthquake, CRIEPI prompt report, U94042 (in Japanese), 1995.

6) Kameda, H.; One technique to calculate evolutionary spectrum for strong motion, JSCE Report No.235 (in Japanese), 1975.

7) Ohta, H.; Application of optimization method to earthquake engineering (Part 1)-Estimation of underground structure of SMAC observation site in Hachinohe Harbor-, Journal of Architectural Institute of Japan (in Japanese), 1975.

8) Ishida, K., K. Sato, Y. Sawada and H. Yajima; Estimation of underground structure based on earthquake observation and normalized response spectrum, CRIEPI Report No.385005 (in Japanese), 1985.

9) Kokusho, T.; In-situ dynamic soil properties and their evaluations, Proc. 8th Asian Regional Conference on soil Mechanics and Foundation Engineering, 1987.

10) Kokusho, T., J. Tohma, H. Yajima, Y. Tanaka, M. Kanatani and N. Yasuda; Seismic response of soil layer and its dynamic properties, Proc. 10th World Conference on Earthquake Engineering, 1992.

11) Kawase, H., T. Satoh and K. Fukutake; Nonlinear dynamic response simulation of soil ground based on borehole observation record at Port Island in Kobe city during Hyogoken-nanbu earthuake, ORI report, 94-05 (in Japanese), 1995.

12) Kawase, H.; Strong motion simulation in Chuo ward, Kobe, during the Hyogo-ken nambu earthquake of 1995 based on the inverted bedrock motion, Journal of

Structure Construction Engineering, Architectural Institute of Japan, pp.67-76 (in Japanese), 1996.

13) Iwata T., K. Hatayama, H. Kawase, K. Irikura and K. Matsunami; Aftershock observation at Higashinada ward, Kobe city, Journal of Natural Disaster Science (Special issue of the 1995 Hyogoken-nanbu earthquake)

14) Kawase, H., T. Satoh and S. Matsushima; Aftershock observation at Higashinada ward for the Hyogoken-nanbu earthquake and preliminary analysis by using the data, ORI report, 94-04 (in Japanese), 1995.

15) Yamanaka, H. and S. Aoi; Estimation of basement depth along the Sumiyoshi river in the Kobe city -travel time analysis of P-, and S-, and Sp-waves from an earthquake array observation-, Journal of Physics of the Earth, July 1995.

16) Sato, K.; Certification of converted SP-waves from a vertical array seismograms during the 1995 Hyogo-ken Nambu earthquake, P10, 1996 the second seismological society of Japan (in Japanese), 1996.

17) Satoh, T., H.Kawase and T. Sato; Strong motion prediction considering both non-linear behavior of soil and statistical characteristics of ground motion extracted from observed data, J. Struct. Constr., Eng., AIJ, 463, pp.27-37, (in Japanese), 1994.

18) Satoh, T., M. Horike, Y. Takeuchi, T. Uetake and H. Suzuki; Nonlinear behavior of scoria soil sediments evaluated from borehole records in eastern Shizuoka prefecture, Japan, Earthq. Eng. Struct. Dyn., vol. 26, pp.781-795, (in Japanese), 1997.

19) Satoh, T. and H. Kawase; Simulation of site amplification factors obtained from borehole records considering both two-dimensional effect and nonlinear behavior of soil sediments - Analysis of weak motion and strong motion observed at a vertical array at Kuno district in the Ashigara valley -, Struct. Constr. Eng., AIJ, No.468, pp.39-49 (in Japanese), Feb., 1995.

20) Higashi, S. and T. Sasatani; Nonlinear site response in Kushiro during the 1994 Hokkaido Toho-Oki earthquake, submitted to B.S.S.A, 1998.

21) Yoshida, N.; Earthquake response analysis at Port Island the 1995 Hyogoken-nanbu earthquake, report 2399, vol 43, No 10, pp.49-54 (in Japanese), Oct. 1995.

22) Kanatani, M., J. Tohma and H.Yajima; Study on applicability of nonlinear analysis method (NAFSS) of soil ground by earthquake records, CRIEPI Report U95027 (in Jananese), 1996.

23) Kokusho, T., M. Matsumoto and K. Sato; Strain-dependency for dynamic soil property identified from nonlinear response of soil ground, Proceeding of the second academic symposium related to Hanshin-Awaji disaster (in Japanese),

January 1997.

CHAPTER 4

ASSESSMENT OF VERTICAL DISTRIBUTION OF SEISMIC GROUND MOTION

4.1 General Remarks

In this chapter seismic wave amplifications at 11 laterally homogeneous ground sites are evaluated on the basis of weak motion records. At all 11 sites, a vertical array of strong motion seismographs[1), 2)] have been installed at various depths. The soil profiles at these sites range from hard to soft rocks and soft ground. These arrays are supported and maintained as a joint research project by a consortium of nine electric power companies in collaboration with The Japan Atomic Power Company[3)].

From the viewpoint of earthquake stability, it is very important to evaluate seismic loading on foundations and cut or filled slopes for assessing the safety of important facilities such as nuclear power plants. The purpose of this chapter is to propose a method to evaluate underground seismic coefficients taking into account dynamic response of a horizontally multi-layered ground.

At first, using a 1-D model of soil profile estimated by system identification[4)], seismic response analyses were carried out for both recorded and design input motions. The design motions for nuclear power plants were synthesized from standard design earthquakes called S2 earthquakes[5)]. The earthquake motions are synthesized from response spectra at the base layer determined from an objective evaluation of active faults and seismotectonics of oceanic inter-plate seismic sources around the site.

Two theoretical methods were used to compute the vertical distribution of underground seismic coefficients. In method 1, the seismic coefficients were computed from values of peak ground acceleration calculated at the depth of each layer. In method 2 seismic coefficients were computed from the difference of peak ground shear stress at the interface of two layers. The influence of dynamic characteristics of earthquake input motion and soil profile on the underground seismic coefficients were investigated. The

soil profile was classified into hard and soft rocks of mostly Tertiary deposits and into a soft ground of Pleistocene and Holocene deposits. The dynamic characteristics of input motion were analyzed by computing the response spectra of recorded and synthesized seismic motions on the base layer.

Both methods were used to evaluate the vertical distribution of underground seismic coefficients for rock and soft grounds. The applicability of these methods for strong motion incidence such as for those for S2 earthquakes[5] was confirmed for sites with horizontally multi-layered grounds and sloped sedimentary deposits.

4.2 Seismic Wave Amplification Based on Vertical Array Observation Sites

4.2.1 Analyzed Vertical Array Observation Sites

Table 4.1 Geologial Conditions of seismic observation site

Classification of ground	Observation site	Ground profile
Hard rock	I W K	sandstone, granite
Soft rock	T M K	mudstone, sandstone, diorite
	T T Y	loam, sandstone, mudstone
	S Z J	tuff
	H M Y	clay with gravel, mudstone
Soft ground	T K I	sand, sand and gravel, shale
	S F J	loam, scoria
	H G O	silt, sand, clay
	S I K	clay, sand with silt, sand
	J P D R	sand, sand and gravel, shale
	S D I	clay with sand, alternation of siltstone and sandstone

Weak motion records at the vertical array sites on rock[6), 7), 8)] and soft ground [9), 10), 11)] are shown in Table 4.1. At these sites strong motion seismographs have been installed on multi-levels of a vertical array[12)]. At each site geological and geotechnical data of soil profiles have been measured. Weak motion records from these sites have been collected and analyzed to study the characteristics of seismic ground motions in horizontally layered grounds.

The IWK site, which was classified as a hard rock, mainly consists of Tertiary deposits of sandstone up to a depth of GL-291 m overlying granite as shown in Fig. 4.1. Six seismographs with three components have been installed at various levels of a vertical array up to the depth of GL-330 m. The measured Vs at the rock site was 1.2

Km/s -1.5 Km/s for the sandstone and 2.8 Km/s for the granite bedrock.

The TMK site, which was classified as a soft rock, consists of Neogene sandstone. TMK has been surveyed up to a depth of GL-475 m at a down-hole site as shown in Fig.4.1. The measured Vs near the surface was 0.52 Km/s and 0.93 Km/s at lower depths. Massive sandstone and siltstone belonging to Plaeogene overlie the bedrock of Granodiorite at the depth of GL-820 m. The measured Vs was 2.1 Km/s - 2.8 Km/s for the bedrock. Six strong motion seismographs have been installed at different levels of a vertical array at this site.

The TKI site, which was classified as a soft ground, consists of surface soil, sand and gravel down to a depth of 25 m thick overlying shale as shown in Fig. 4.2. Three strong motion seismographs have been located at depths of GL-1 m, GL-7 m, and GL-28.3 m. The measured values of Vs are 120 m/s-300 m/s and 550m/s for the surface layer and shale, respectively. Fig. 4.3 shows the epicentral locations of the earthquakes recorded at TKI site during the period from April 1983 to September 1984. The figure also shows locations of the other observation sites.

All representative sites mentioned in this section are located in the Tohoku district of Japan. The results of analyses are mainly mentioned about these three sites. The other 8 sites have been referred in the report[3]. Those results were used to verify applicability of the proposed assessment method.

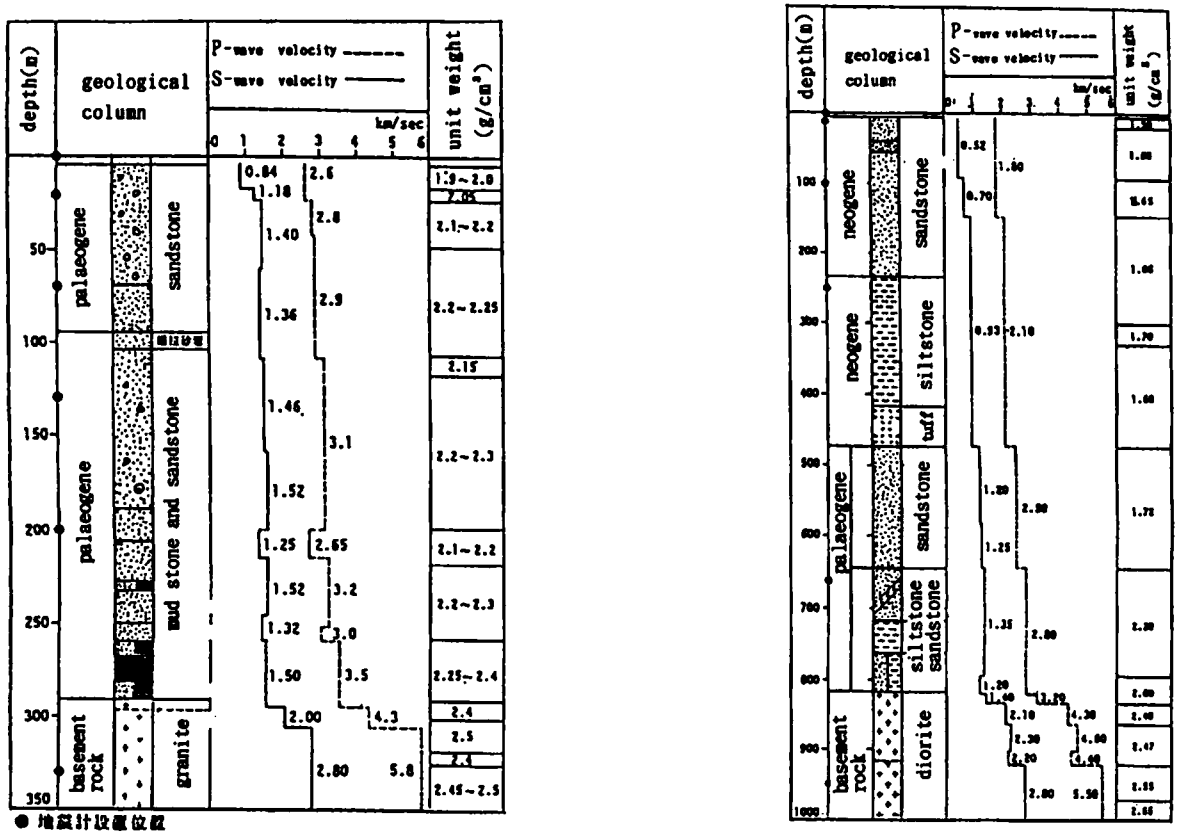

Fig.4.1 Geological and Geotechnical profile at IWK and TMK sites

(Left: IWK site, Right: TMK site)

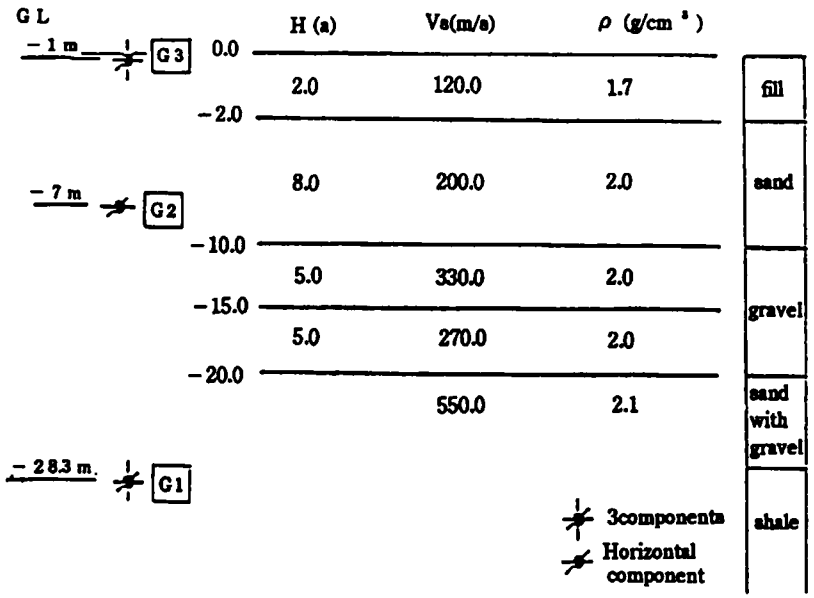

Fig.4.2 Geological and Geotechnical profile at TKI site

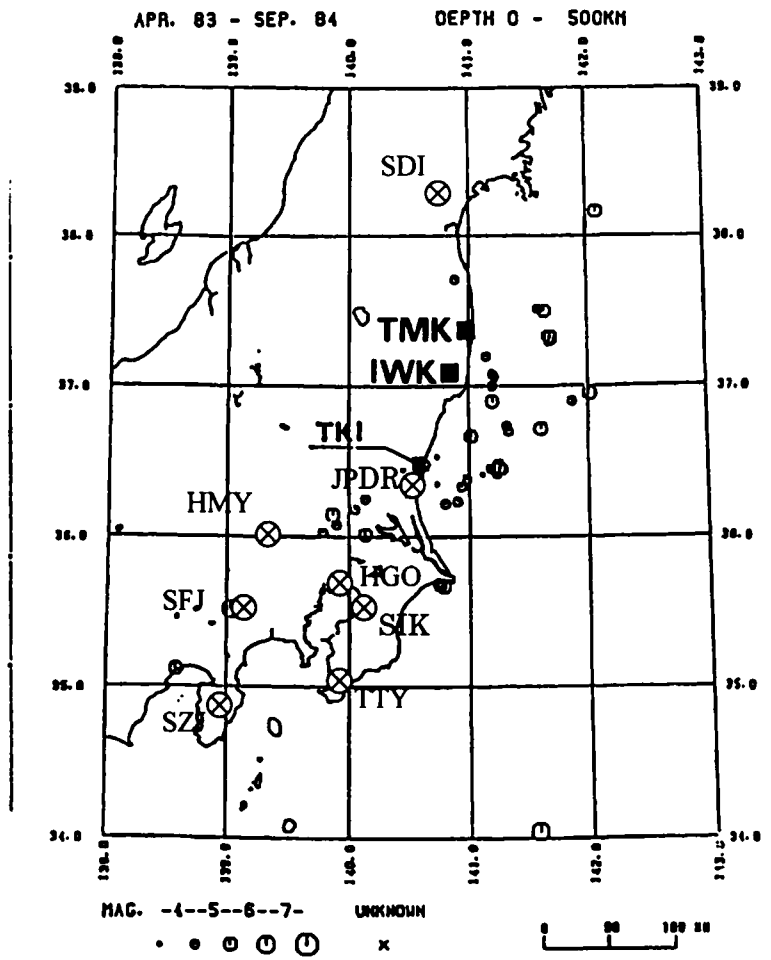

Fig.4.3 Recorded earthquake epicenter at TKI site
and the other recording sites

4.2.2 Spectral Ratios During Weak Motion

Some of earthquakes were recorded at a same time for IWK, TMK and TKI sites. The records were divided into three groups in accordance with their magnitudes. Group A consisted of events with M_j less than 5.0, B of events with M_j from 5 to 6, and C of events with M_j greater than 6. Table 4.2 lists 12 seismic records classified into the above three seismic groups. Fig. 4.4 shows the relation between magnitude of the events and epicentral distance to IWK. Spectral ratios between the surface and bottom records of each vertical array were computed and Fig. 4.5 shows the average of spectral ratios by group and across all groups at IWK.

The peak of spectral ratios at IWK (hard rock) appeared at more or less the same frequencies for all seismic groups but the amplitudes of the peaks varied by group. A similar behavior was seen at TMK (soft rock). The amplitude variations at both rock sites appeared to be quite random but at TKI (soft ground) both peak frequencies and peak amplitudes of the spectral ratios were almost the same for all three groups.

Consequently, it was recognized that peak amplitudes of spectral ratios for rock sites such as IWK and TMK could be treated as statistical variables which showed little, if any, relation to earthquake magnitudes, At the same time their peak frequencies were constant for all magnitude ranges. The variations in the amplitude were apparently determined more by seismic source and path effects and less by local site effects. On the other hand the spectral ratios for weak motions on soft ground were strongly affected by the subsurface layer and were constant across all three groups and exhibited no relation to the seismic source.

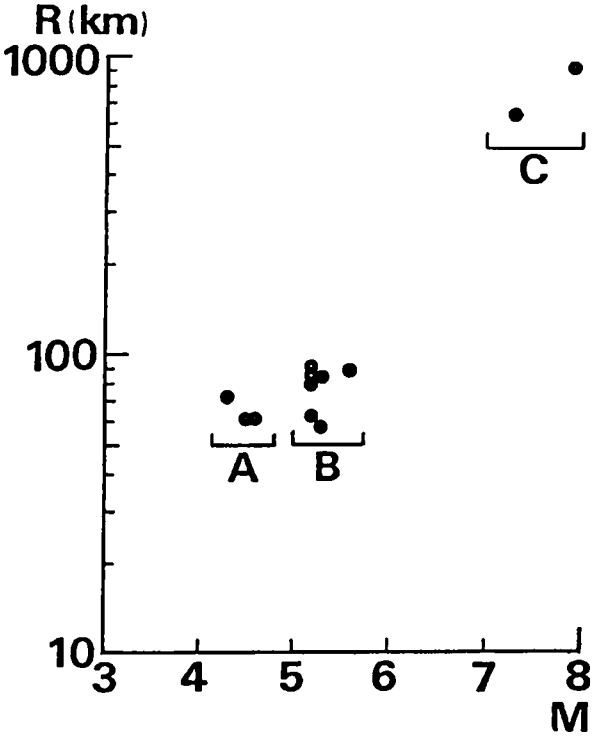

Fig.4.4 Relation between magnitude and epicentral distance for earthquake records

Table 4.2 Specification of analyzed earthquake records

Group	Origin time	Epicenter	Lat.	Long.	Depth (Km)	Mj	Epicentral (hypocentral) distance (Km)	Max.acc (gal)	EQ.No.
A	83.06.16 22:37	Off Ibaraki Pref.	36° 42'	141° 19'	45	4.3	53(73)	3.5	23
	84.02.25 13:58	Off Fukushima Pref.	37° 04'	141° 13'	54	4.6	30(62)	10.2	30
	84.02.25 16:31	Off Fukushima Pref.	37° 04'	141° 11'	55	4.5	25(62)	11.8	31
B	83.07.02 07:03	Off Fukushima Pref.	36° 54'	141° 07'	50	5.3	29(58)	23.1	21
	83.07.13 14:11	Off Fukushima Pref.	37° 19'	141° 40'	35	5.2	75(83)	6.4	22
	83.09.02 12:05	Off Ibaraki Pref.	36° 40'	141° 01'	49	5.2	48(63)	11.1	24
	83.11.16 19:44	Off Fukushima Pref.	37° 19'	141° 40'	39	5.3	75(85)	2.5	26
	84.01.17 20:13	Off Ibaraki Pref.	36° 26'	141° 14'	43	5.6	78(89)	3.3	28
	84.03.25 03:59	Off Fukushima Pref.	37° 19'	141° 40'	42	5.2	75(86)	3.3	33
	84.05.01 10:15	Off Fukushima Pref.	37° 29'	141° 38'	46	5.2	80(92)	2.0	34
C	84.01.01 16:03	SE off Izu Peninsula	33° 37'	136° 50'	333	7.3	532(653)	3.9	27
	84.03.06 11:17	Near Torishima	22° 20'	139° 12'	452	7.9	875(935)	3.0	32

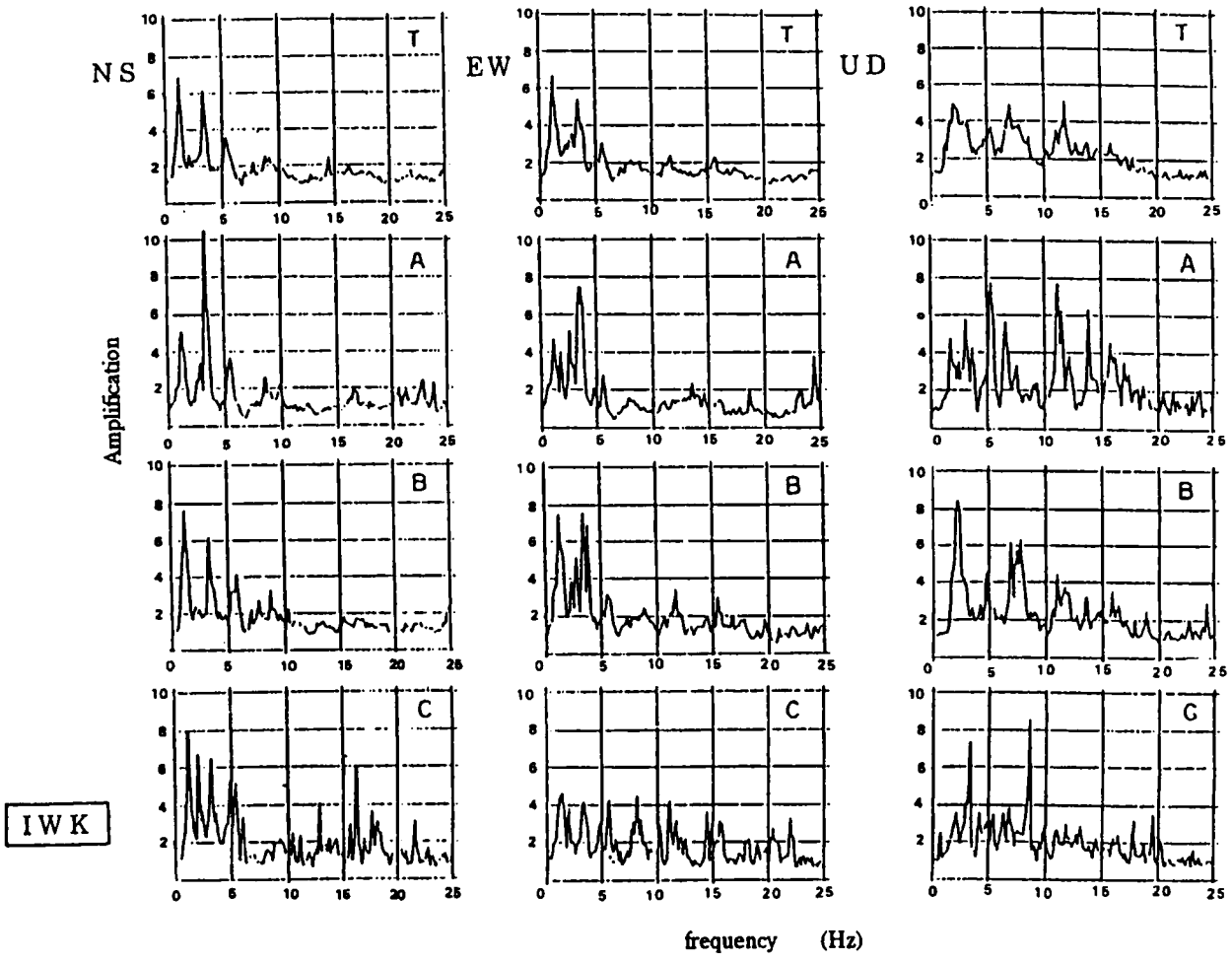

Fig.4.5 Average spectral ratios

(T:total of common earthquake records, A～C: earthquake group)

4.2.3 Identified Soil Profile of Horizontally Layered Grounds

Horizontal layered grounds have been traditionally modeled using a one-dimensional mass and damping system for each layer as shown in Fig. 4.6. Using such a model and the average of spectral ratios computed from horizontal motions recorded at each site, Vs and Q for the layered soil profile were identified using SPIN[13),14)]. The geotechnical parameters estimated from surveys at the down-hole site were used as the initial values of the parameters in SPIN. During the course of the making the runs it was observed that identified Q's were some times converging to non-physical values. In order to avoid this situation, Q was considered to have converged if Q was lying in the range from 10 to 100 and 10 to 30 for rock sites and soft sites, respectively.

Table 4.3 lists the identified geotechnical parameters of soil profile at IWK and the identified Vs and Q of the soil profile at IWK are plotted in Fig. 4.7. The identified values of Vs were quite variable but were less than about 400 m/s for the middle part of soil profile. The profile of Vs identified from the average of spectral ratios was seen to be approximately the same as the ensemble average of Vs identified from each recorded spectral ratio. Q was seen to be nearly constant but this was an artifact of the rule that was devised to limit Q to physically meaningful values.

The identified spectrum and averaged observed spectrum were in good agreement as shown in Fig. 4.8. Peaks occurred in both spectra at 1.5 Hz, 3.5 Hz and 5.5 Hz. However, the amplitudes of identified spectral ratios were somewhat reduced in the frequency region higher than 3.0 Hz, most likely because of the assumption of taking damping factor as being independent of frequency.

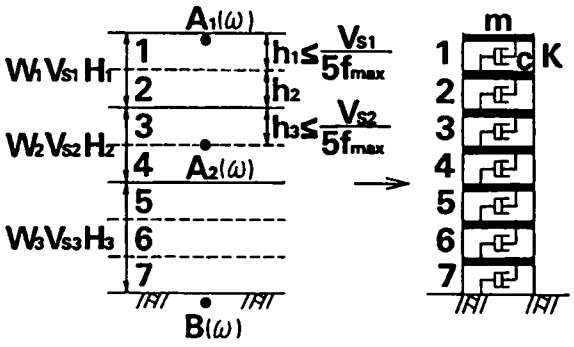

Fig.4.6 Modeling for multi-layered ground model

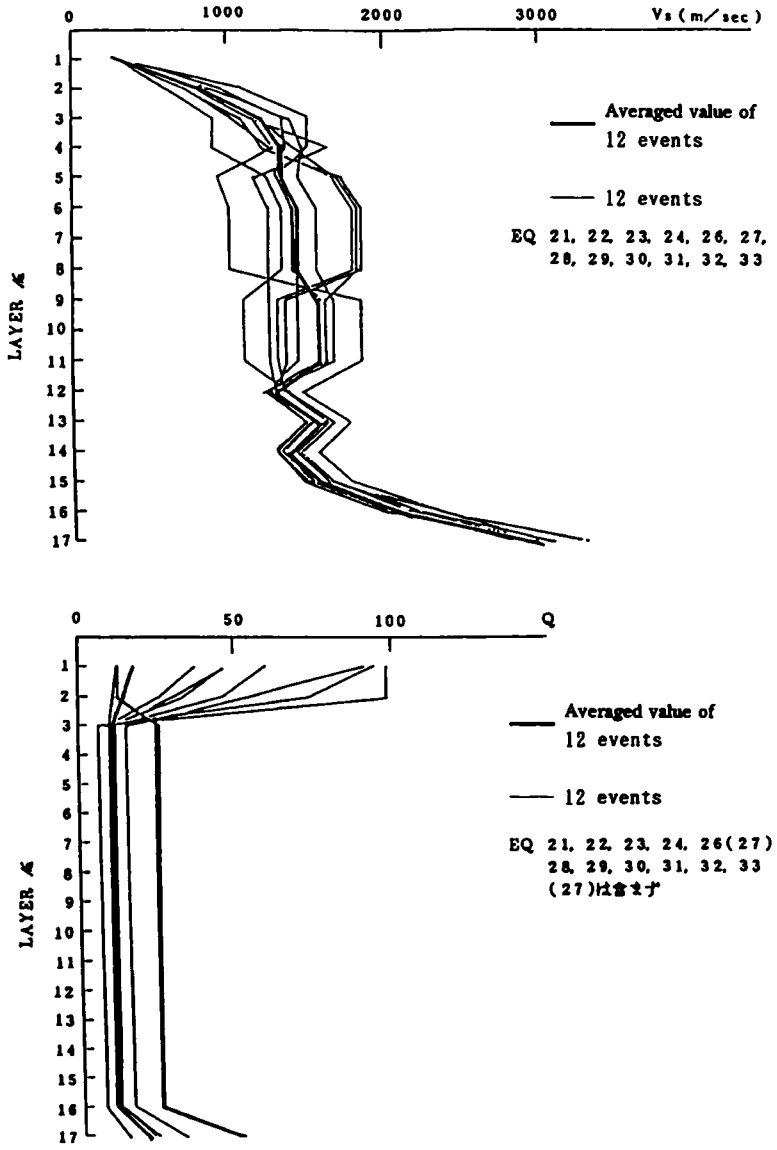

Fig.4.7 Identified soil profile at IWK site

(Upper: S-wave velocity, Lower: Q-value)

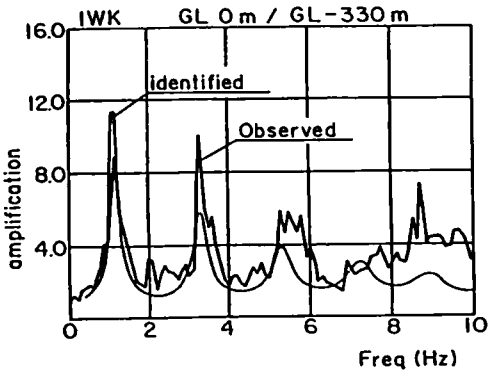

Fig.4.8 Spectral ratios at IWK site

Table 4.3 Identified soil profile

depth	Layer	Vs m/sec	Q
0.0m	1	323	16
	2	887	13
21.1 m	3	1329	11
	4	1389	11
70.7 m	5	1444	11
	6	1411	11
200.9 m	7	1516	11
	8	1323	11
	9	1588	11
	10	1497	11
	11	1587	11
	12	2116	11
330.0m	13	2420	21

4.3 Detection of Vertical Distribution of Seismic Coefficient

4.3.1 Computational Methods for Vertical Distribution of Seismic Coefficient

Using a 1-D ground model with parameter identified using SPIN, seismic ground responses were computed using 1-D multiple reflection theory.[15] The underground seismic coefficient distribution along the depth in a horizontally layered ground was then computed using methods 1 and 2 described below.

In Method 1[16], the seismic coefficient was computed from the peak ground acceleration value in each layer as:

$$K_i = A_{imax}/G \tag{4.1}$$

where i is number of the layer, K_I is seismic coefficient in i-th layer, A_{imax} is the peak ground acceleration value in i-th layer (unit; gal) and G is acceleration of gravity (unit; 9.8 m/s^2).

In method 2[17], the seismic coefficient was computed from the difference of maximum shear stress at the interface of each horizontal layer of soil profile. The seismic coefficient K was computed using the equation:

$$K_i = \left\{\tau_{i,max} - \tau_{i-1,max}\right\}/(\gamma_i * H_i) \tag{4.2}$$

where i is number of the layer, $\tau_{i,max}$ is maximum shear stress in the i-th layer (unit; tf/m^2), γ_I is unit weight gravity of the soil in the i-th layer (unit; tf/m^3), and H_I is thickness of i-th layer (unit; m). In this method, only horizontal layered ground can be applied.

Generally, the vertical distribution of seismic coefficient for layered ground, computed using method 1 showed a linear reduction from the surface to a minimum value at some depth of several tens of meters, below which the seismic coefficient fluctuated about the minimum value. The seismic coefficient computed using method 2 typically decreased rapidly and became zero at some depth. The typical vertical distributions of seismic coefficient are plotted in Fig. 4.9.

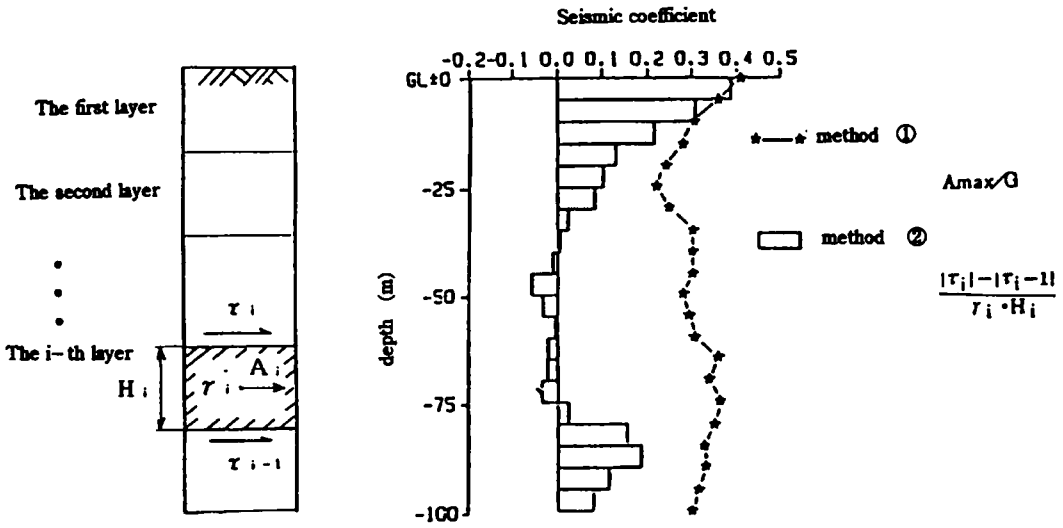

Fig.4.9 Image of calculation methods for underground seismic coefficient

4.3.2 Characteristics of the Normalized Seismic Coefficient

(1) Normalized seismic coefficient for weak motion records

The normalized underground seismic coefficients were defined by normalizing the underground seismic coefficients by the value at the ground surface. The average and standard deviation of normalized underground seismic coefficients computed using weak motion records belonging to earthquake groups B and C are shown in Fig. 4.10. Also shown are the normalized acceleration response spectra of the records at the base layer. The depths at which the minimum value of underground seismic coefficient for group C occurred was larger than the corresponding depths for other groups. The average of the normalized seismic coefficients for group B was almost the same as that for group A . The predominant periods of the normalized acceleration response spectra for group C were generally longer than those for groups A and B. From these results, it was inferred that the vertical distribution of underground seismic coefficient is dependent on the predominant period of the response spectra of the acceleration input motion at the base layer.

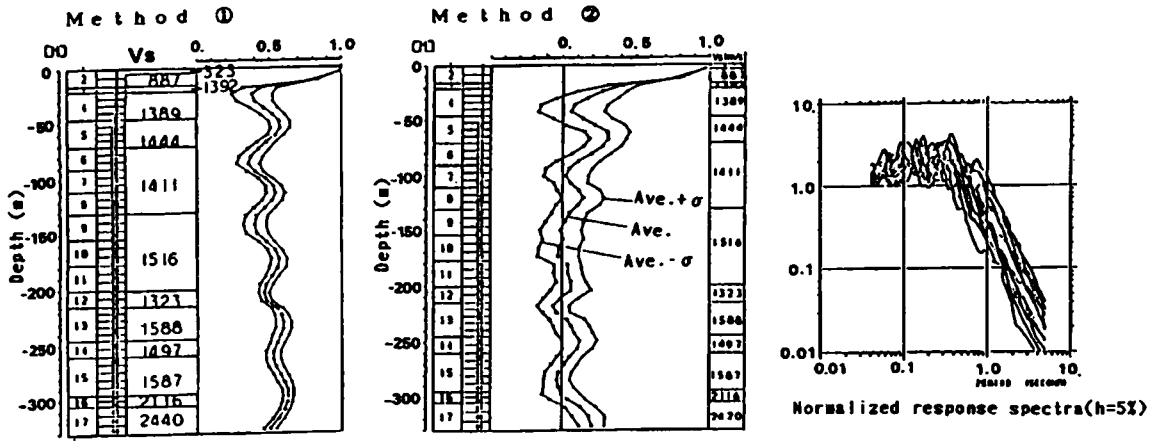

(a) B group earthquake at IWK

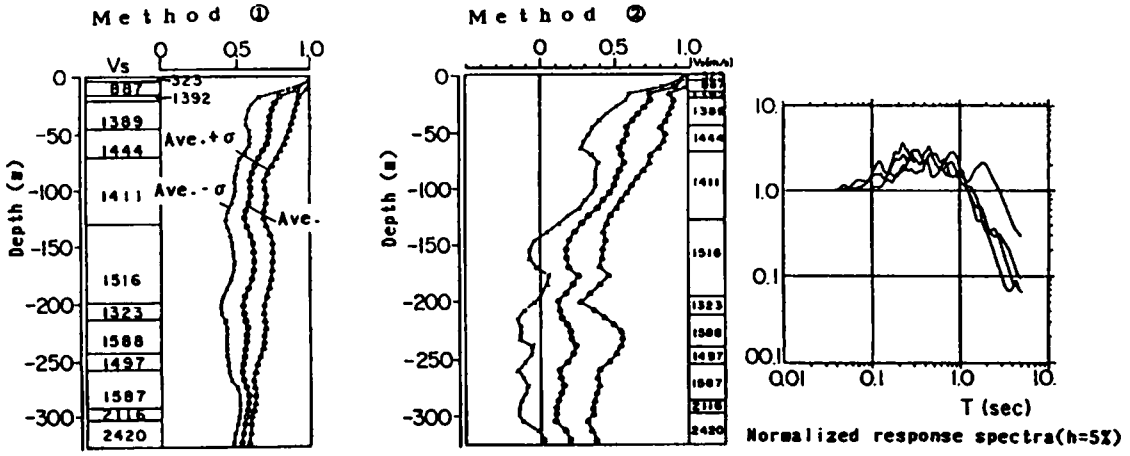

(b) C group earthquake in IWK

Fig.4.10 Normalized underground seismic coefficient at IWK

(2) Normalized seismic coefficient for strong motion records

To confirm the applicability of normalized seismic coefficients to strong motion, normalized seismic coefficients were examined using strong motion records at the base layer. Table 4.4 lists the strong motion records observed at the surface of the

rock site. The highest peak accelerations for these motions were as high as 287 gal at KNK during the 1978 Off Miyagi prefecture earthquake and 224 gal at FRF during the 1983 Nihonkai-chubu earthquake.

Table 4.4 Strong motion records

Earthquake	Site	Geology and S-wave velocity	ρ (g/cm^3)	Max.acc(gal)
Off Miyagi Pref.	OFN	rock (Vs=1.300 m/s)*	2.0*	161
('78, M7.4)	KHK	rock (Vs=1.300 m/s)	2.0*	287
	YAS	andesite (Vs=1.500 m/s)*	1.8	173
Off Izu Peninsula	NST	andesite (Vs=1.800 m/s)*	2.3	61
('80, M6.7)	MNZ	andesite (Vs=700 m/s)	2.0*	56
	NRY	tuffaceous sandstone (Vs=880 m/s)	2.0*	31
	TKY	mudstone (Vs=900 m/s)	1.8*	22
Nihon-kai-chubu	FRF	tuffaceous conglomerate (Vs=1.300m/s)	2.3	72.5
('83, M7.7)	SRN	tuffaceous conglomerate (Vs=1.500m/s)	2.3	213.5
	OCI	schist (Vs=1.300 m/s)*	2.3*	118
East Yamanashi Pref.	TSK	slate (Vs=1.300 m/s)*	2.3*	68
('83, M6.0)	HTS	basalt (Vs=1.300 m/s)*	2.0*	17
	STJ	andesite (Vs=1.300 m/s)*	2.0*	41

* estimated value

A 1-D half-space model was used to evaluate the underground seismic coefficients. The half-space ground model was taken to be 200 m deep below which Vs was more than 700 m/s for all sites. The effect of Q on underground seismic coefficient was investigated for Q in the range 10 to 30 and the results are shown in Fig. 4.11. Based on the results plotted in this figure, Q was neglected up to a depth from 150 m to 200 m in subsequent analyses. The shear wave velocities of the examined model are, 600 m/s and 1800 m/s, for the surface and base layers, respectively. In the rest of the analyses reported in this chapter, Q was taken as 10 at a rock site on the basis of the results at IWK.

The normalized underground seismic coefficients computed using strong motion records for earthquakes with magnitudes from 6.0 to 7.7 are plotted in Fig. 4.12. The vertical distribution of normalized seismic coefficients computed using method 1 appeared to have more or less the same shape for all earthquakes. The vertical distribution of normalized seismic coefficients for the Nihonkai-chubu earthquake (M_{JMA}=7.7) was a little bit smoother than the distributions of the other smaller magnitude earthquakes. The vertical distribution of normalized seismic coefficients using method 2 showed a much higher degree of variability from one earthquake to another but for earthquakes with roughly similar magnitudes the depth of the minimum value of normalized seismic coefficients seemed to be almost constant.

NME

LAYER	H	V	FOH	Q Model-1	Model-2	Model-3
1	50.0	610.0	1.80	10	20	30
2	50.0	610.0	1.80	10	20	30
3	50.0	610.0	1.80	10	20	30
4	50.0	610.0	1.80	10	20	30
5	0.0	610.0	1.80	10	20	30

NST

LAYER	H	V	FOH	Q Model-1	Model-2	Model-3
1	50.0	1800.0	2.30	10	20	30
2	50.0	1800.0	2.30	10	20	30
3	50.0	1800.0	2.30	10	20	30
4	50.0	1800.0	2.30	10	20	30
5	0.0	1800.0	2.30	10	20	30

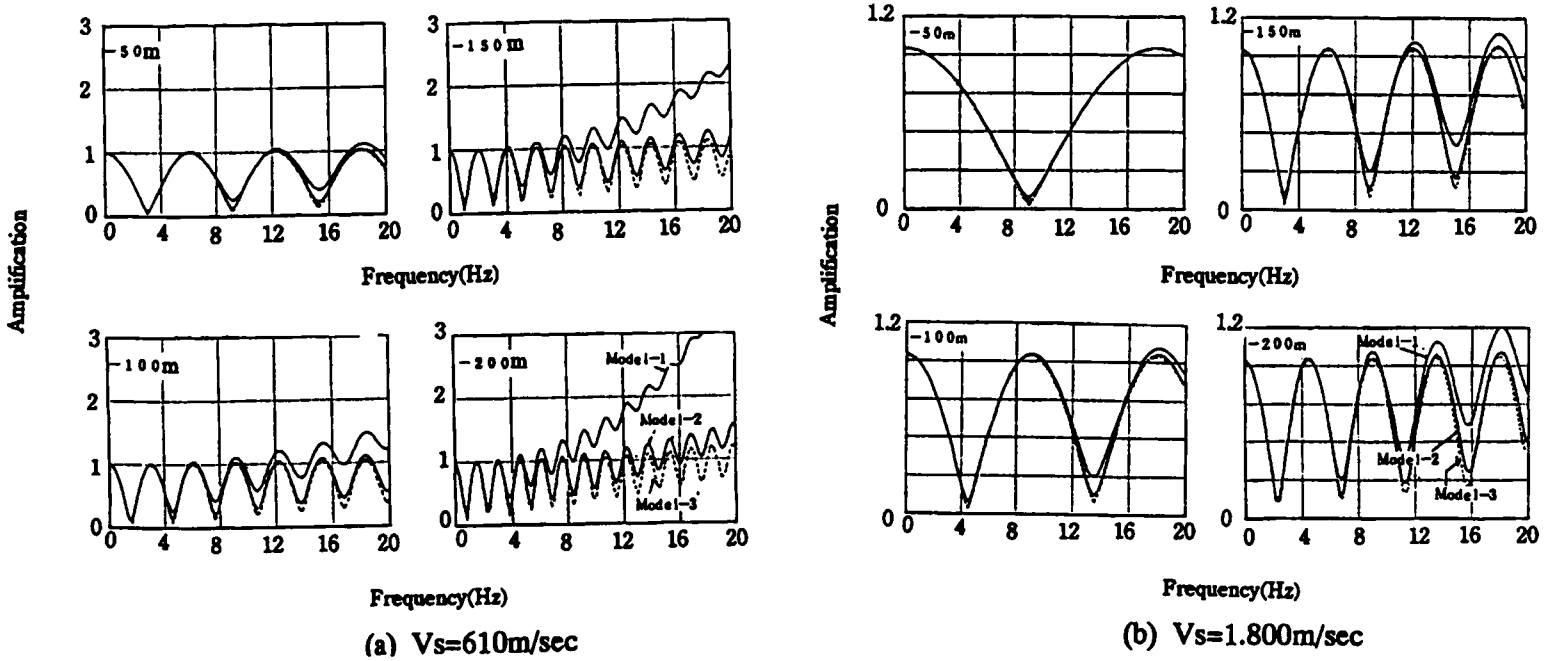

Fig.4.11 Comparison of transfer functions for different Q-values

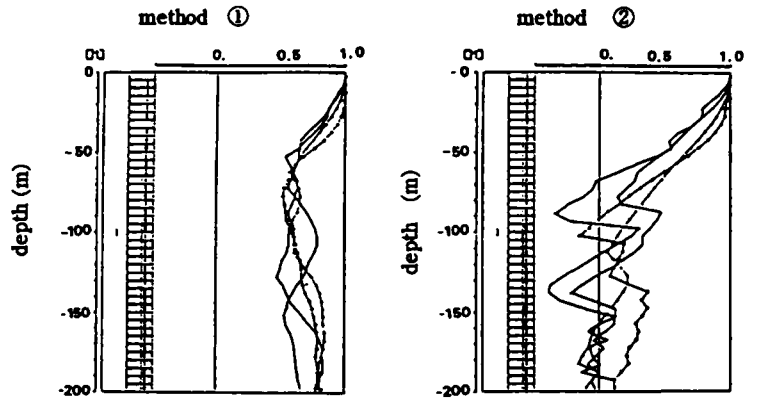

(a) Off Miyagi Pref. ('78, M7.4)

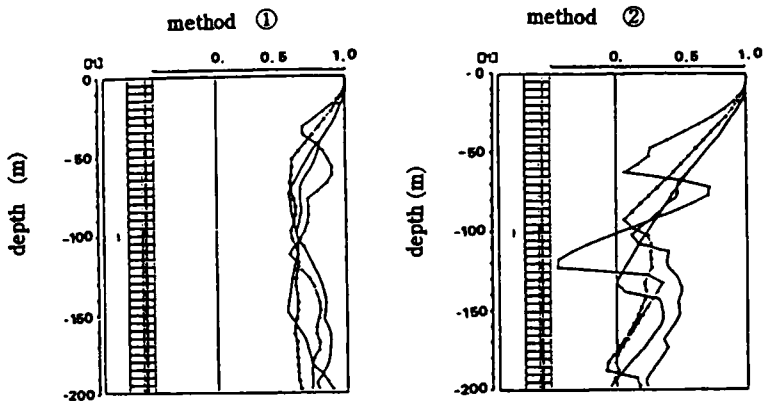

(b) Nihon-Kai-chubu ('80, M6.7)

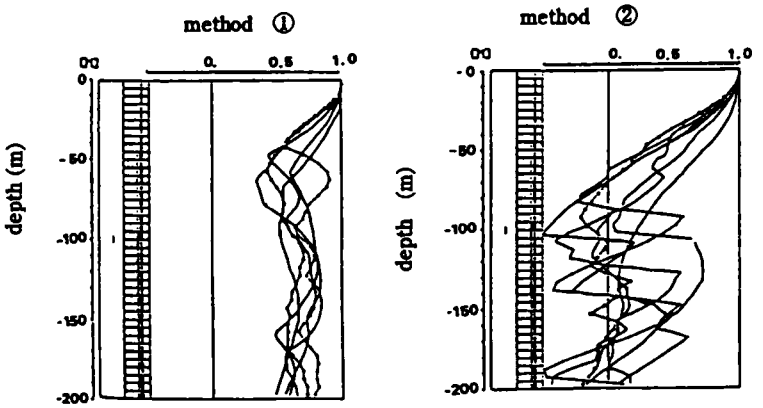

(c) East Yamanashi ('83, M6.0)

Fig.4.12 Normalized underground seismic coefficient during strong motion

(3) Normalized seismic coefficient for designed earthquake motions

Normalized underground seismic coefficients for the designed earthquake motions (S2) are examined in this section. Fig. 4.13 shows S2 earthquake motions, named No. 2, No. 7, and TAFT (EW component), which are synthesized as a near-field, a far-field and a historical destructive earthquake, respectively. The EW component of TAFT was scaled to a peak value of 600 gal. At the rock sites NST (Vs = 1800 m/s) and TKY (Vs = 900m/s), the depths of the minimum value of normalized seismic coefficient were proportional to the predominant period of the incident motion. The depth of the minimum value of normalized seismic coefficient at NST was twice as large as the depth at TKY in accordance with the ratio of Vs at the two sites.

Fig. 4.14 shows the normalized seismic coefficients computed for a layered ground such as at IWK using design earthquake motions. The seismic ground response was computed using an equivalent linear analysis[3] from considerations of strain dependency of soil rigidity and damping factor. The representative G~γ and h~γ curves are shown in Figs. 4.15(a)~(b).

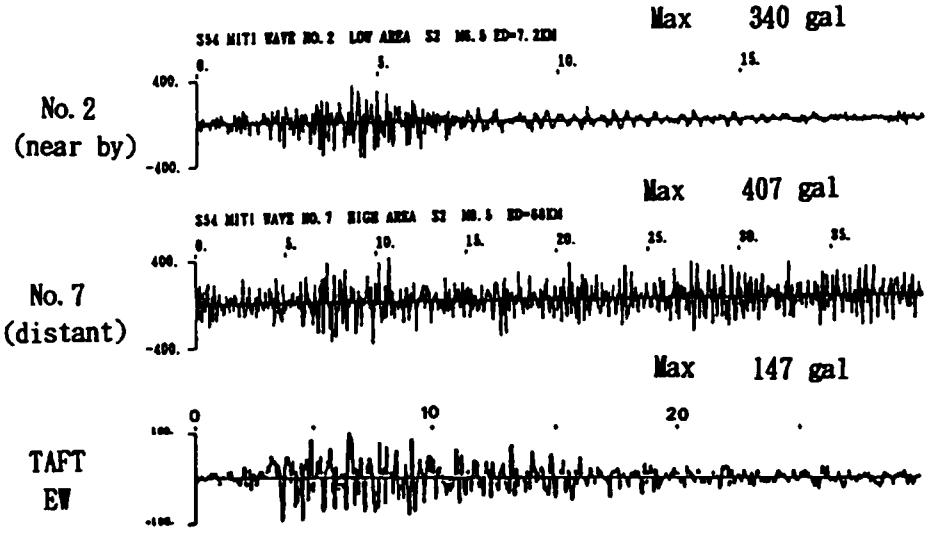

Fig.4.13 Design input motion of S2 earthquake

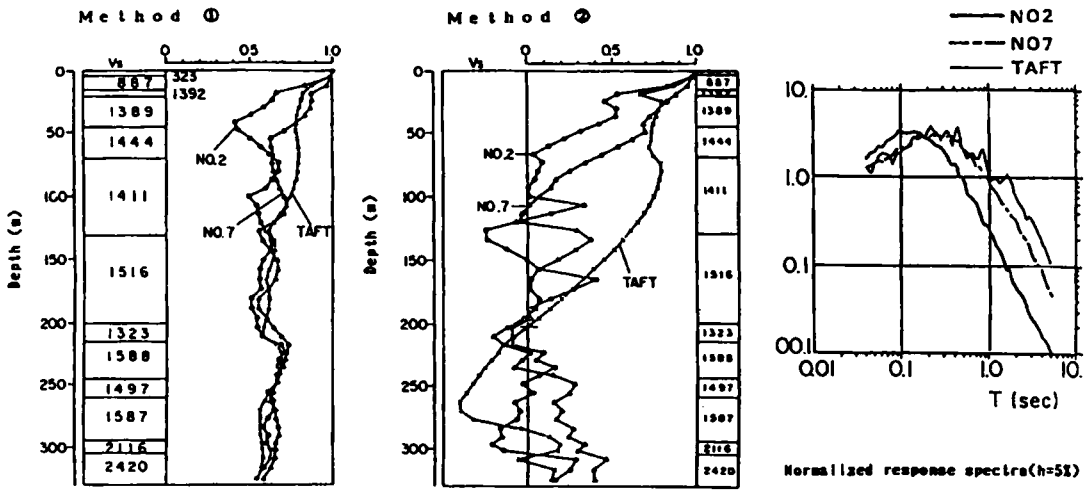

Fig.4.14 Normalized underground seismic coefficient for S2 earthquake

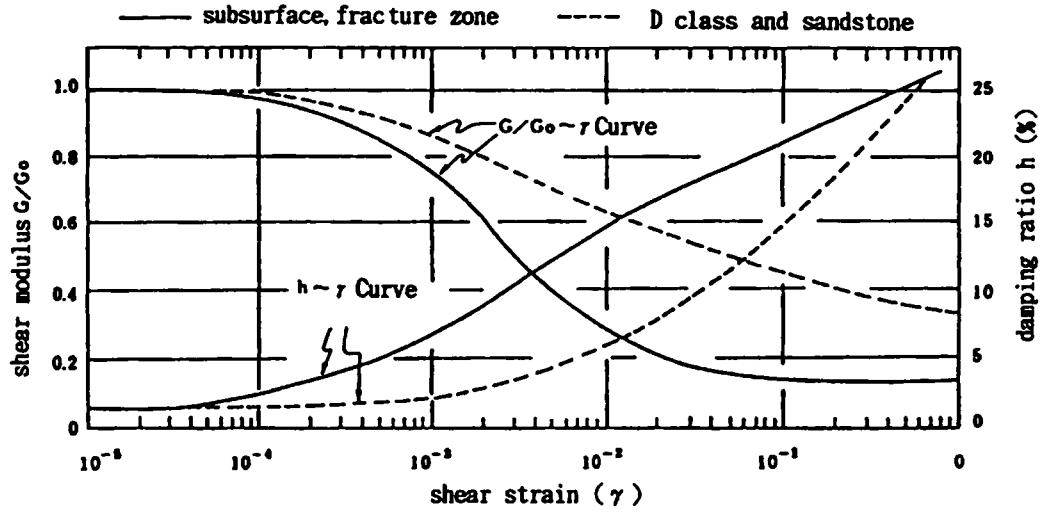

Fig.4.15(a) G/Go~ γ , h~ γ relation in soft ground and rock

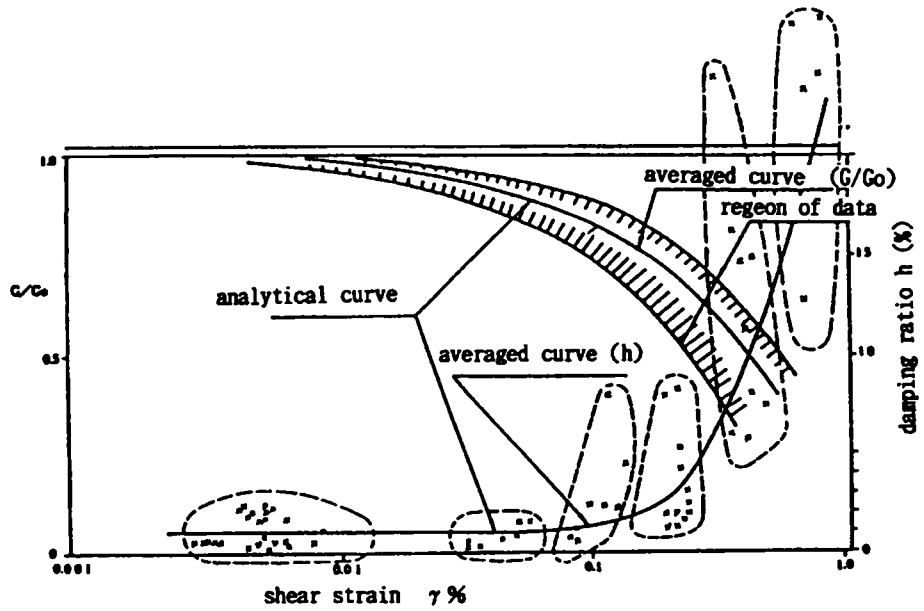

(※) analytical line is a curve which link the averaged value computed by the following equation from data (x, y) inside circled broken line indicated in above figure

$x = \Sigma xi/n$, $y = \Sigma yi/n$

Fig.4.15(b) G/Go～ γ , h～ γ relation in mudstone

As already mentioned in the previous section, the normalized seismic coefficient distributions were found to be strongly dependent on the predominant period of the response spectrum of the input acceleration. The rate of reduction of the normalized seismic coefficient with depth decreased in proportion to the values of the predominant period and Vs of the soil layers. The predominant periods of the acceleration response spectrum for No.2, No.7 and TAFT were 0.2, 0.3, and 0.4, respectively. Consequently, the depths of the minimum value of underground seismic coefficient were quite large for the S2 earthquake motions.

4.4 Evaluation of Vertical Distribution of Seismic Coefficient

4.4.1 Parameters for Evaluation of Vertical Distribution

On the basis of the computed results, the shape of the vertical distribution of the normalized underground seismic coefficient was characterized as:

1) normalized seismic coefficient is by definition equal to unity at the surface, and
2) it reduces linearly up to a depth below which it is constant.

The parameters required to quantitatively describe the assumed vertical distribution are

(i) the depth corresponding to the minimum value, and (ii) the reduction ratio which expresses the reduction in the minimum seismic coefficient as a ratio of its value to that at the surface. The depths of the minimum value for the methods 1 and 2 are denoted by H1 and H2, respectively and the reduction ratios by α_1 and α_2. The seismic coefficient for depths below H2 estimated using method 2 were seen to fluctuate and therefore α_2 was taken as the root mean square value of the normalized seismic coefficients below the depth of H2. These definitions are shown in Fig. 4.16.

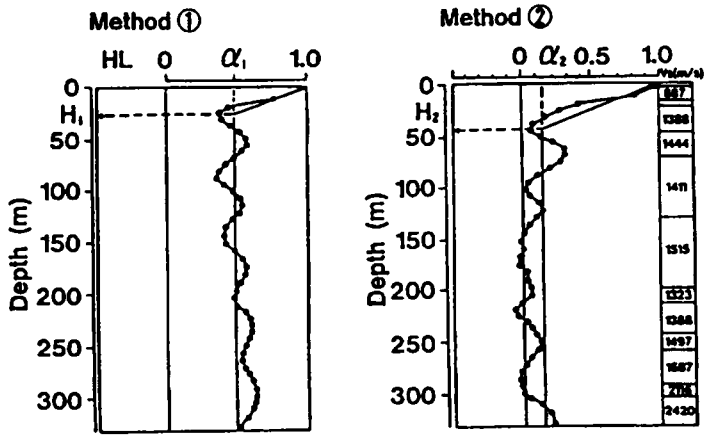

H_1=the depth ih which normalized seismic coefficient(method ①) in ground becomes minimum

α_1=the average of normalized seismic coefficient(method ①) in more deep position than H_1

H_2=the depth in which normalised seismic coefficient(mothod ②) in ground becomes zero or minimum

α_2=r.m.s of normalized seismic coefficient(method ②) in more deep position than H_2

Fig.4.16 Normalized underground seismic coefficient assessment model

The seismic coefficient computed using parameters H_1 and α_1 in method 1 is quantitatively expressed by the theoretical equation below. The equation isobtained by defining power of ground motion as a function of the root mean squared value of ground motion, as proposed by Toki et al.[18),19)]

$$\sigma(z)=\left[\frac{1}{2}\left\{\phi_s(0)+\phi_s\left(\frac{2Z}{C}\right)\right\}^{\frac{1}{2}}\right] \tag{4.3}$$

where $\sigma(z)$ is the effective value of ground motion at depth z, $\phi_s(0)$ is the autocorrelation function of ground motion at the surface, and C is the wave propagation velocity (= Vs of layered ground)

In the above equation, σ (z) becomes minimum when the autocorrelation

function $\phi_s(0)$ of ground motion Gs(t) is minimum. In this minimum point, the time lag 2Z/C of the autocorrelation function is nearly equals to one-half the value of the predominant period T of the ground motion. Thus, Z=CT/4 is solved to obtain the depth where seismic motion becomes minimum.

The parameters α_1 and α_2 are determined by assuming a functional form for the autocorrelation function $\phi_s\left(\frac{2Z}{C}\right)$ in equation (4.1). The normalized autocorrelation function $[=\phi_{SN}\left(\frac{2Z}{C}\right)]$ of ground motion is assumed to be as,

$$\phi_{SN}\left(\frac{2Z}{C}\right)=1.0-\frac{4}{T}\left(\frac{2Z}{C}\right) \text{ at } \quad \frac{2Z}{C}\le\frac{T}{4} \tag{4.4}$$

and

$$\phi_{SN}\left(\frac{2Z}{C}\right)=0 \quad \text{at} \quad \frac{2Z}{C}\ge\frac{T}{4} \tag{4.5}$$

where $\phi_{SN}(0)$ is 1.0 at ground surface (z=0), thus $\sigma(0)$ is 1.0.
Assuming a single-layered ground with shear wave velocities V_s and V_b for the surface and basement layers, respectively, the vertical distribution of seismic motion ground is estimated by using the following equation [18],

$$\sigma(Z)=\frac{1+\kappa}{2\sqrt{2}}\sqrt{\left\{1+\left(\frac{\kappa-1}{1+\kappa}\right)^2\right\}\sigma^2(0)+\phi_S\left(\frac{2Z}{C}\right)} \quad \text{at} \quad Z\ge\frac{CT}{8} \tag{4.6}$$

where κ is equal to the ratio V_s/V_b. Putting (4.4), (4.5) into (4.6), α_1 can be expressed as,

$$\alpha_1=\frac{\sigma(Z)}{\sigma(0)}=\frac{1}{2}\sqrt{1+\beta^2} \quad \text{at} \quad Z=\frac{1}{4}CT \tag{4.7}$$

α_1 is obtained by using the condition that seismic motion becomes minimum for z = CT/4.

4.4.2 Methods for Evaluation of Vertical Distribution of Single Layered Ground

A careful examination of the relationship between parameters of normalized

coefficient and seismic ground response for the design earthquake input motion, revealed that H_1 and H_2 to be closely related to the predominant period of input motion. The relationships between H_1 and H_2 and the wavelength ($\lambda = V_s \cdot T$) of the input motion are plotted in Fig. 4.17. V_s used in the soil profile was the mean value of shear velocities across the depth of the surface layer overlying the base layer. The mean value of shear wave velocity was computed using the equation $\left(V_s = (\sum_{i=1}^{n} V_{si} \cdot H_i) / \sum_{i=1}^{n} H_i, \quad i = 1 \cdots n \right)$. T is the predominant period of response spectrum of design input motion at the base layer.

On close examination of Fig. 4.18, H_1 at rock sites was seen to be distributed around the straight lines (H_1=Ho for $T \leq T_0$ and $H_1 = (\lambda / 4) H_0$ for $T > T_0$) as indicated in the figure. H_2 was, also, distributed around these straight lines but was on the average 1.5 and 1.3 times larger than H_1 for hard and soft rock sites, respectively.

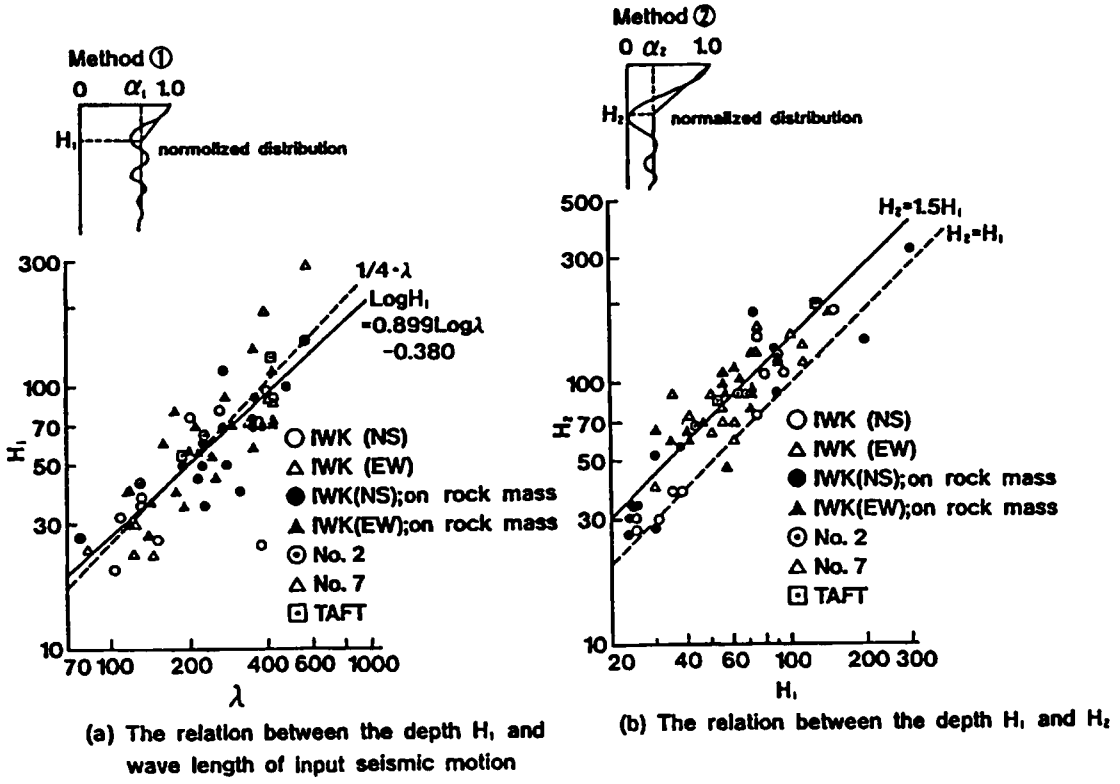

Fig.4.17 Property of H_1 and H_2 for hard rock ground

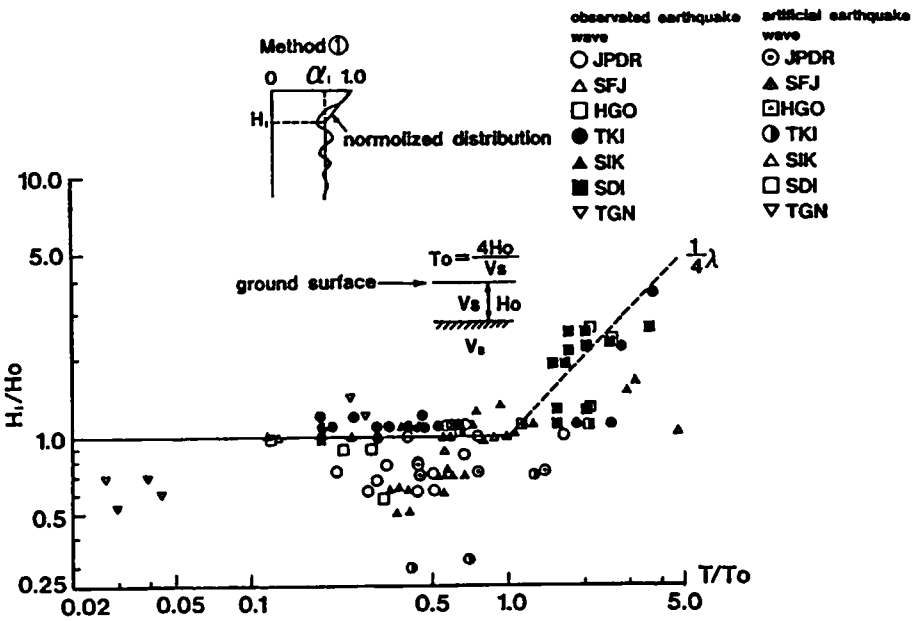

Fig.4.18 The relation between the depth H_1 and the predominant period T

For soft ground, the underground seismic coefficient was strongly dependent on the depth of the alluvial surface layer. H_1 for soft ground was almost always constant equal to the thickness H_0 but for T greater than the natural period T_0 (= $4H_0/V_s$) of the surface layer H_1 became closer to (λ / 4) H_0. Fig. 4.18 shows that H_1/H_0 was equal to 1.0 in the region of the T/T_0 less than 1.0 and distributed around the value of λ / 4 in the region of the T/T_0 greater than 1.0

The parameter α_1 obtained by equation (4.7) from method 1 was related to the ratio of shear wave velocity of the base layer to that of the surface layer for a horizontally layered ground. Fig 4.19 shows α_1 plotted against ratio of shear velocities and this figure indicated that α_1 was linearly proportional to this ratio except when there was pronounced nonlinear ground response. As shown in Fig.4.19(a), α_1 bore no relation to the predominant period T. The average $\pm$ standard variation (σ) of α_1 were distributed around the curve indicated from the relationship of the shear wave velocity ratios at all sites. Equation (4.5) gave a value of α_1 of 0.7 for a homogeneous layered ground, and 0.55 for a layered ground with a shear wave velocity ratio of 0.5. As shown in Fig 4.19(b) α_1 computed using equation (4.5) enveloped all results and was in good agreement with results for S2 earthquakes. The estimated value of α_1 agreed to nonlinear site response. Therefore, the formulation presented here was considered to be applicable in to assessing the vertical distribution of normalized seismic coefficient for strong motions in a layered ground.

The parameter α_2 was distributed around the value of zero except for soft

ground. Thus, the value of α_2 can be found to be less than 0.3 for rock sites as shown in Fig.4.20.

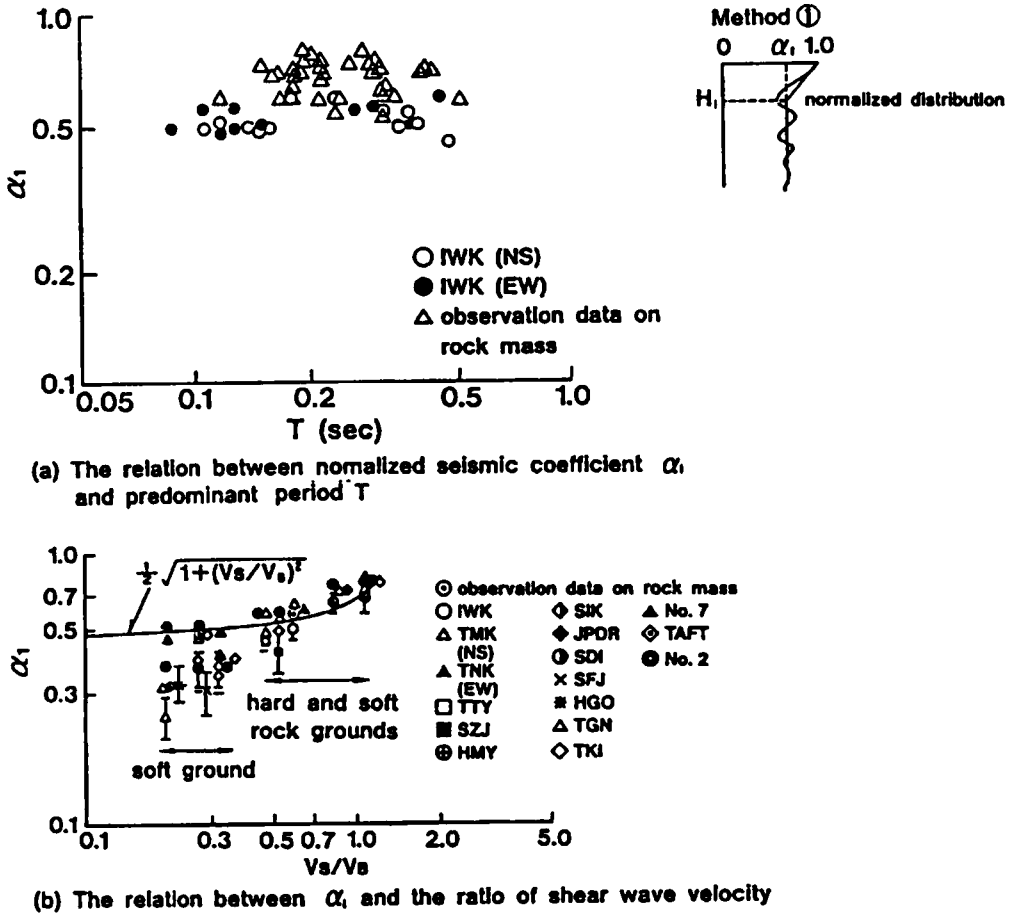

Fig.4.19 Property of normalized underground seismic coefficient for various kinds of grounds

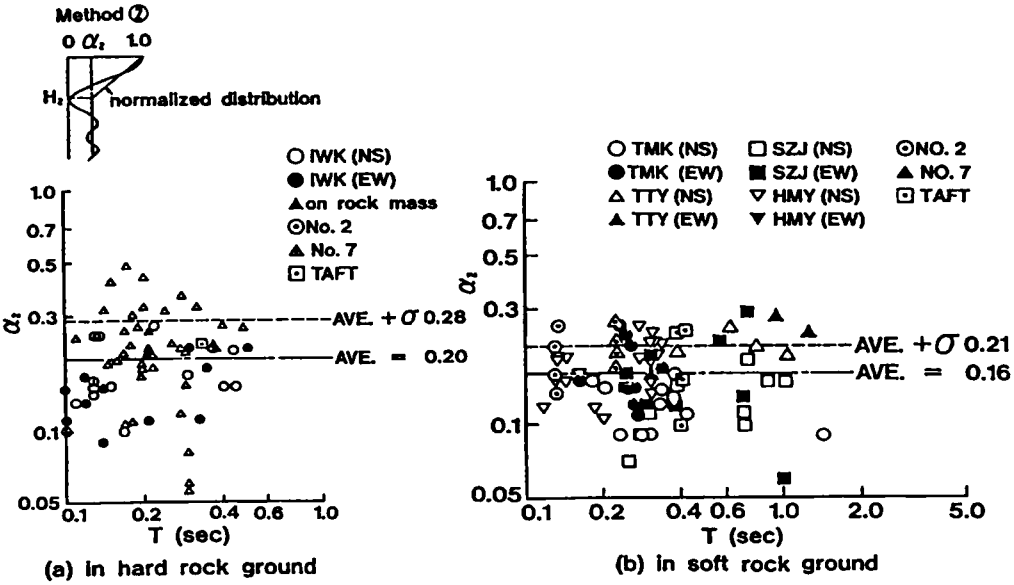

Fig.4.20 The relation between normalized seismic coefficient α_2 and predominant period T

4.5 Application of Proposed Assessment Method

4.5.1 Results of Various Types of Layered Ground

(1) Horizontal Layered ground

The proposed equations for evaluating normalized seismic coefficients are indicated in Table 4.5. Figs. 4.21(a)-(d) show the normalized seismic coefficients evaluated using methods 1 and 2. These were compared with the seismic coefficients estimated for recorded motions at rock sites IWK and TMK belonging to earthquake groups A and C. The mean value of the predominant periods for each earthquake group was used because of the similar characteristics of the acceleration response spectra on the base input motion. The seismic coefficients evaluated using method 1 for rock sites envelop the average plus the standard deviation of the observed normalized seismic coefficients. The evaluated normalized seismic coefficients for soft ground were, also, compared with the observed normalized seismic coefficient at TKI, as shown in Fig. 4.22. The evaluated values at TKI envelop observed ones except for EQ32 belonging to group C. Therefore, the value for EQ-32 was calculated using $H_1=1/4 \cdot Vs \cdot T$ in case the predominant period was longer than T_0 as was shown in Fig. 4.18.

The applicability of the assessment method has, also, been confirmed for a deep hard rock site up to a depth of 650 m using earthquake records of Kamaishi mine[20].

Table 4.5 Assessed value of normalized seismic coefficient

Calculation method of normalized seismic coefficient	Parameter	Hard and soft rock grounds	Soft rock ground
Method①	H_1	$1/4 \cdot Vs \cdot T$	$1/4 \cdot Vs \cdot T$, where $T \geqq 4 \cdot Ho/Vs$ Ho, where $T < 4 \cdot Ho/Vs$
	α_1	$1/2 \cdot \sqrt{1+(Vs/V_B)^2}$	$1/2 \sqrt{1+(Vs/V_B)^2}$
Method②	H_2	hard rock; $1.5H_1$ soft rock; $1.3H_1$	No formulation
	α_2	0.3	No formulation

(Note)

H_1 ; Depth in which normalized seismic coefficient in the ground becomes minimum.

α_1 ; Average value of normalized seismic coefficient at more deep position than H_1.

H_2 ; Depth in which normalized seismic coefficient in the ground becomes zero or minimum.

α_2 ; Root mean square value of normalized seismic coefficient at more deep position than H_2.

Vs ; Velocity of shear wave of surface layer

V_B ; Velocity of shear wave of bed rock layer

T ; Predominant period of acceleration response spectra of input seismic motion

λ ; Wave length

$4 \cdot Ho/Vs$; Natural period of surface layer

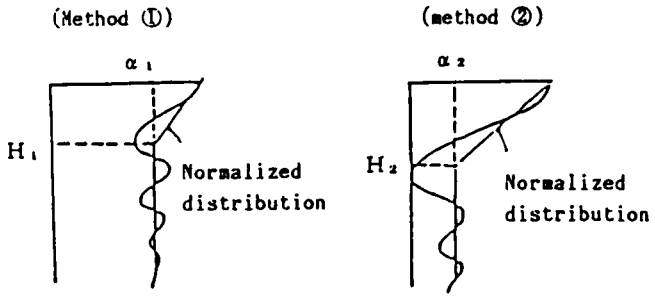

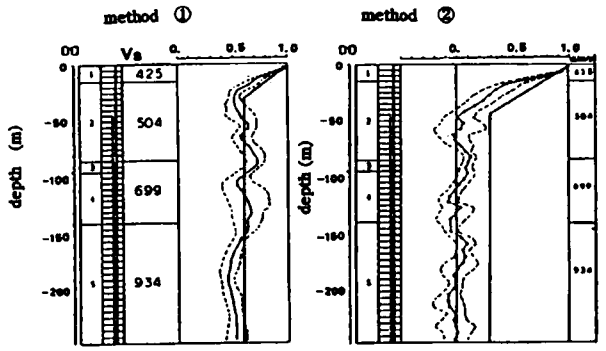

(c) TMK(NS,EW) : A group for 2 events

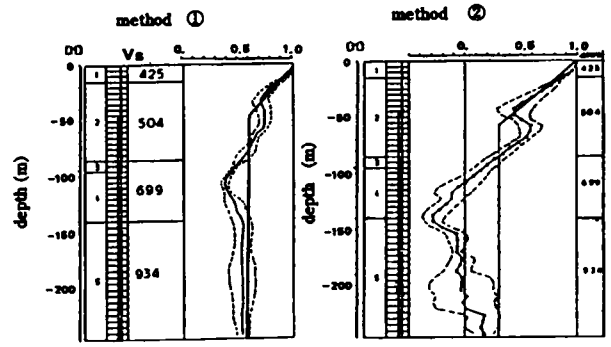

(d) TMK(NS,EW) : C group for 2 events

Fig.4.21 Average and standard deviation of normalized seismic coefficients and the assessment

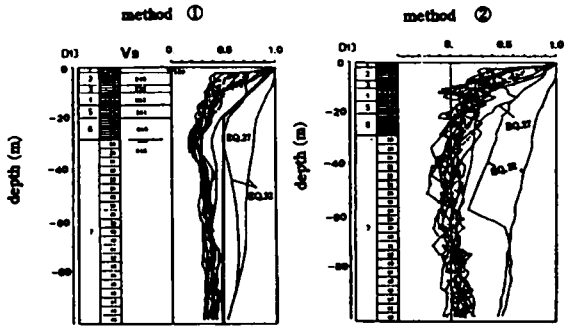

(a) TKI (NS, EW)

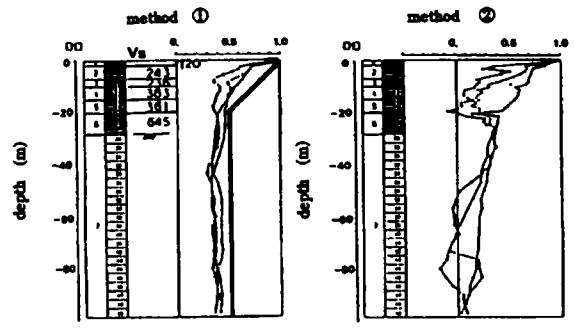

(b) TKI (NO.2, No7, TAFT)

Fig.4.22 Normalized seismic coefficient at TKI and the assessment

(2) Irregularly Layered Ground

Generally, the assessment method from method 1 can be only used for non-horizontally layered ground like as slope. The applicability of method 1 to filled slope and rock slope was investigated by applying it at two sites: one with a rock slope and the other with a filled slope. Both sites were instrumented with seismographs at the top, middle and bottom part of the slope.

The rock slope is located at ISM site on the north of Ishinomaki-shi in Miyagi prefecture. An explosive seismic survey was conducted at two measured lines along longitudinal and transverse directions of the slope. In-situ soil tests were, also, carried out about on samples picked up from the surface of the slope. Fig. 4.23 shows the identified geotechnical parameters[3)] and a 2-D finite element mesh model of the site. The boundary conditions imposed on the finite element model were a rigid boundary at the basement and transmitting boundaries at the left and right edges of the model. The S3 section at the bottom part of slope was taken as the control point for input motion for the model. Incident horizontal motions were deconvoluted for the one-dimensional layered model of the S3 section because of small effect of topography.

Fig. 4.24 shows the average of normalized seismic coefficients along the depth in each section of the slope computed using 1- and 2-D analyses. The normalized seismic coefficients computed from the earthquake records were compared with the values obtained using the proposed assessment method for the slope. The evaluated normalized seismic coefficients mostly enveloped the values computed from the recorded motion. In the section S2 at the halfway part of slope, the normalized seismic coefficients computed using 2-D analysis were larger than those computed using 1-D analysis. This was interpreted to be the effect of topography in the 2-D model. On the whole the normalized seismic coefficients computed from observed records mostly agreed with results obtained using the assessment model. Therefore, the assessment method was considered to be applicable at sites with hard rock cut slopes.

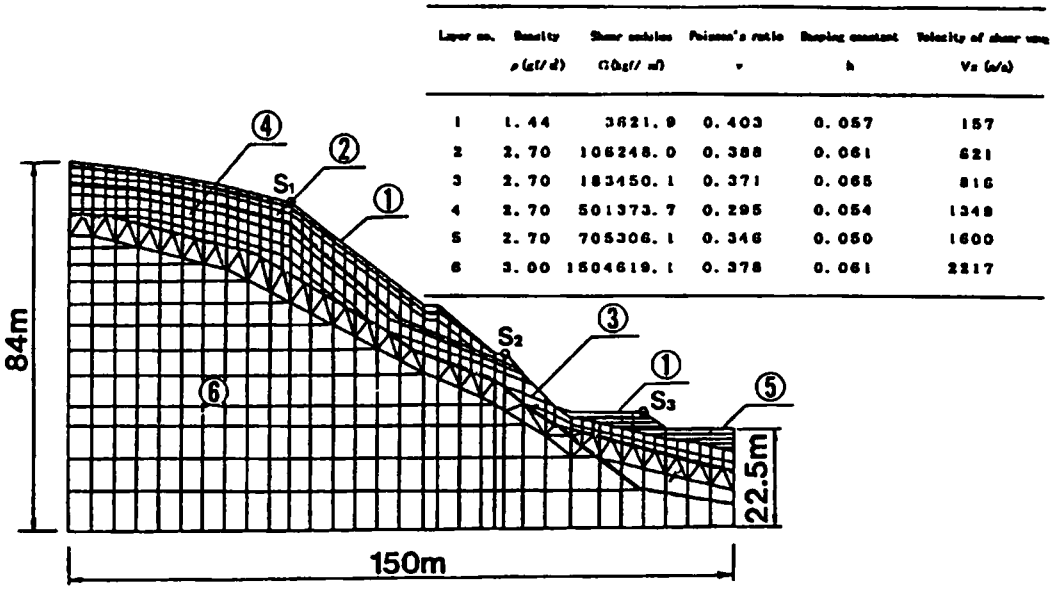

Layer no.	Density ρ (gf/cm³)	Shear modulus G (kgf/cm²)	Poisson's ratio ν	Damping constant h	Velocity of shear wave Vs (m/s)
1	1.44	3621.9	0.403	0.057	157
2	2.70	106248.0	0.388	0.061	621
3	2.70	183450.1	0.371	0.065	816
4	2.70	501373.7	0.295	0.054	1348
5	2.70	705306.1	0.346	0.050	1600
6	3.00	1504619.1	0.378	0.061	2217

Fig.4.23 The hard rock slope model at ISM

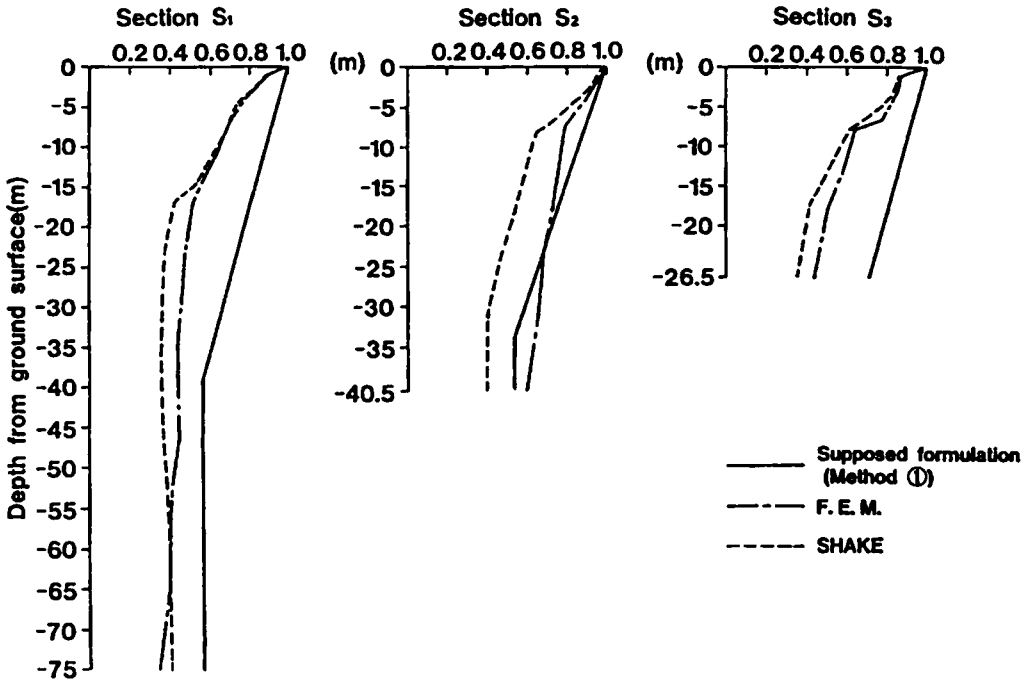

Fig.4.24 The average normalized seismic coefficient computed from 1-D and 2-D models and the assessment

Similar analyses were performed at FKS site which is located on ground that consists of mudstone filled slope. A total of five strong motion seismographs have been installed at the top, middle, bottom parts of the slope and base layer. Geotechnical parameters of slope evaluated by seismic survey and PS logging using downhole are listed in the table in Fig. 4.25. The slope is about 30 m high and 150 m long. The shear-wave velocities are about 200 m/s, 390m/s, and 520m/s for the surface, bottom of fill, and basement layers, respectively. The horizontal acceleration records at B4 on the base layer were used as input motion.

Fig. 4.26 shows the average of normalized seismic coefficients along the depth of the slope computed using 1-D and the 2-D analyses and the normalized seismic coefficient evaluated using the proposed assessment method for the slope. The assessed values almost always enveloped the average of normalized seismic coefficient computed from earthquake records.

The evaluated normalized seismic coefficient for the slope was in reasonably good agreement with the average normalized seismic coefficients computed using actual earthquake records. Therefore, the assessment method was considered to be effective for evaluating normalized seismic coefficients at sites with filled slope[21].

Layer no.	Density $\rho(gf/m^2)$	Shear modulus $G(kg/m^2)$	Poisson's ratio ν	Damping ratio h	S wave velocity Vs(m/s)
1	1.5	421.78	0.398	0.05	166
2	1.5	714.12	0.323	0.05	216
3	1.5	1509.12	0.323	0.05	314
4	1.5	1260.75	0.323	0.05	287
5	1.5	2292.38	0.420	0.05	387
6	1.5	859.73	0.465	0.05	237
7	1.6	3424.72	0.424	0.0167	458
8	1.6	4465.78	0.424	0.0167	523

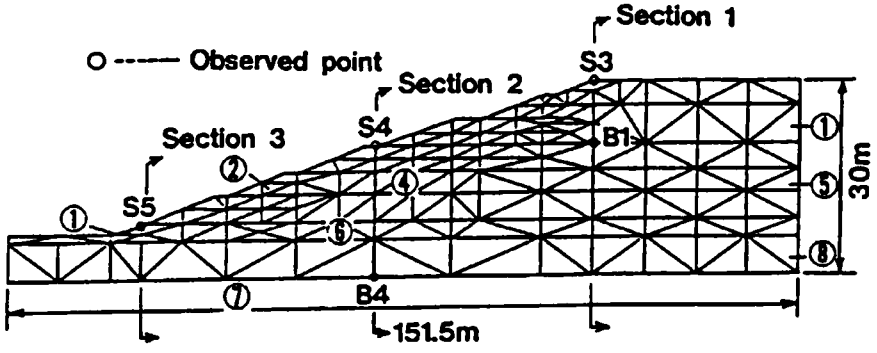

Fig.4.25 The embankment slope model at FKS

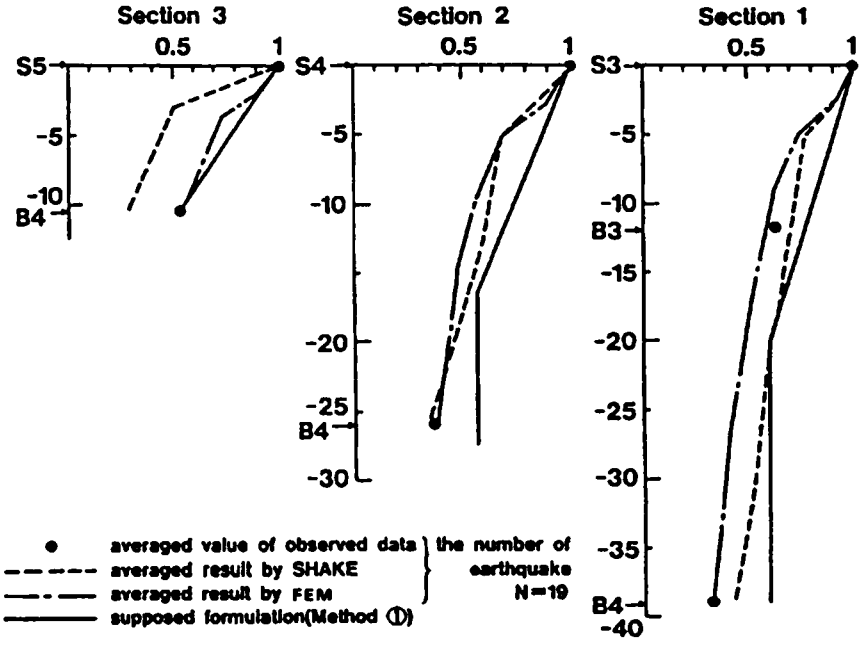

Fig.4.26 The averaged normalized seismic coefficient computed from 1-D and 2-D models and the assessment

4.5.2 Extension of Proposed Method for Horizontally Multi-layered Ground

In this section, the assessment method for the normalized seismic coefficient is extended to a horizontally multi-layered ground. When applying the assessment method to the schematic multi-layered model shown in Fig. 4.27, the assessment method for a single layer is successively applied to two adjacent layers chosen from the horizontally multi-layered model. The parameters of the assessment method can then be computed by starting from the top and proceeding below till the base layer is reached. The algorithm to do this is described below.

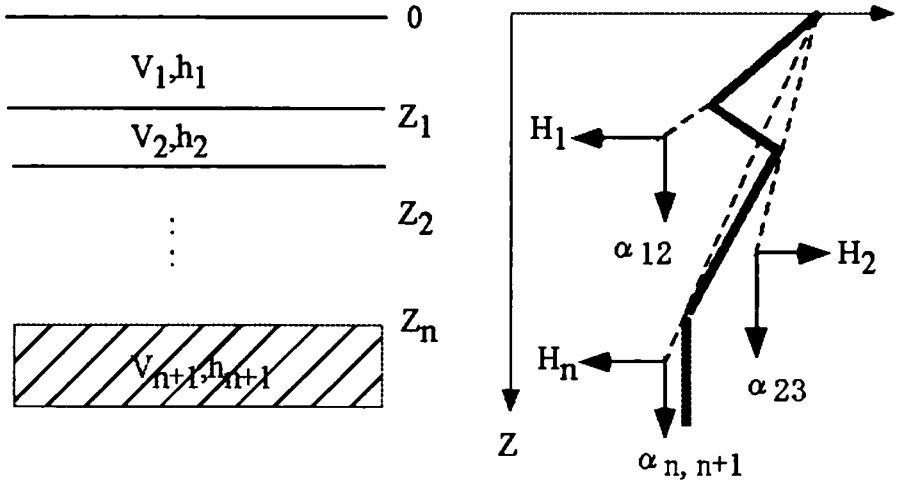

Fig 4.27 Schematic diagram of extended assessment method

At the surface Z = 0, the normalized seismic coefficient K0 = 1.0 by definition. In the first step, the assessment method is applied to the top two layers, and the parameter α_1 at the depth of $Z=Z_1=h_1$ is given as,

$$\alpha_{Z1} = \alpha_{12} + \frac{H_1 - Z}{H_1}(1 - \alpha_{12}), \text{ if } Z_1 < V_1 * T/4 = H_1. \tag{4.8}$$

where

$$\alpha_{12} = \frac{1}{2}\sqrt{1 + (V_1 / V_2)^2}\ . \tag{4.9}$$

In this case of $Z_1=H_1$ and $\alpha_{Z=Z1} = \alpha_{12}$, the assessment is applied for these top two layers. But if $Z_1 > V_1 * T/4 = H_1$, the assessment method can be applied until the depth H_1 of soil profile.

In the second step, the assessment method is applied to second and third layers at a depth of $Z=Z_2=h_1+h_2$,

$$\alpha_{Z=Z2} = \alpha_{23} + \frac{H_2 - Z}{H_2}(1 - \alpha_{23}), \text{ if } Z_2 < V_{12} * T/4 = H_2. \tag{4.10}$$

where

$$\alpha_{23} = \frac{1}{2}\sqrt{1 + (V_{12} / V_3)^2} \quad \text{and} \quad V_{12} = (V_1 h_1 + V_2 h_2)/(h_1 + h_2)$$

In this case of $Z_2=H_2$ and $\alpha_{Z=Z2} = \alpha_{23}$, the assessment is applied for these two layers. But if $Z_2 > V_{12} * T/4 = H_2$, the assessment method can be applied until the depth H_2 of soil profile.

In the ith step, applying the evaluation method is applied at the depth of $Z=Z_i=h_1+h_2\cdots+hi$,

$$\alpha_{Z=Zi} = \alpha_{i,i+1} + \frac{H_i - Z}{H_i}(1 - \alpha_{i,i+1}), \text{ if } Z_i < V_{i-1,i} * T/4 = H_i. \tag{4.11}$$

where

$$\alpha_{i,i+1} = \frac{1}{2}\sqrt{1 + (V_{i-1,i} / V_3)^2} \quad \text{and} \quad V_{i-1,i} = (V_{i-1} h_{i-1} + V_i h_i)/(h_{i-1} + h_i)$$

In the case of $Z_i \geqq H_i$, $\alpha_{Z=Zi} = \alpha_{i,i+1}$, the assessment is applied for these two layers. But if

$Z_i > V_{i-1,i}*T/4=H_i$, the assessment method can be applied until the depth H_i of soil profile. The mentioned procedure is applied repeatedly until the depth of base layer as possible as it can be.

4.5.3 Application of Assessment Method for Multi-layered Ground

(1) Single layer

The proposed assessment method was tested at sites on multi-layered ground around the city of Kobe by comparing evaluated normalized seismic coefficients with those calculated using strong motion records from the 1995 Hyogoken-Nanbu earthquake. The assessment method was applied to non-liquefied sites SGK, TKS, and KNK[22]. TKS was included in this list even though it experienced partial liquefaction however the soil deformation was not large.

Shear velocities V_s and V_b for the surface and base layers, and thickness H_0 estimated from SPT-blow counts and PS-logging surveys of down-holes are indicated in Table 4.6. The parameter α_1 computed using the assessment method is, also, shown in the same table.

Fig. 4.28 shows evaluated normalized seismic coefficients and coefficients computed using strong motion records. The evaluated values envelope the normalized seismic coefficient computed from strong motion records at all depths. The only exception is the seismic coefficient at the depth of GL-100m in the EW component recorded at SGK, which was greater than evaluated coefficient. However, it was considered to be not so much important problem because the principal direction of the horizontal strong ground motion was not in EW direction but in the NS. These results confirmed that the assessment method could be effectively applied to strong motion.

Table 4 6 Assessed parameters of normalized seismic coefficient for single layered ground

Site	H_0(m)	V_s(m/s)	V_b(m/s)	α
SGK	22	210	320	0.60
TKS	19	210	410	0.56
KNK	22	200	530	0.53

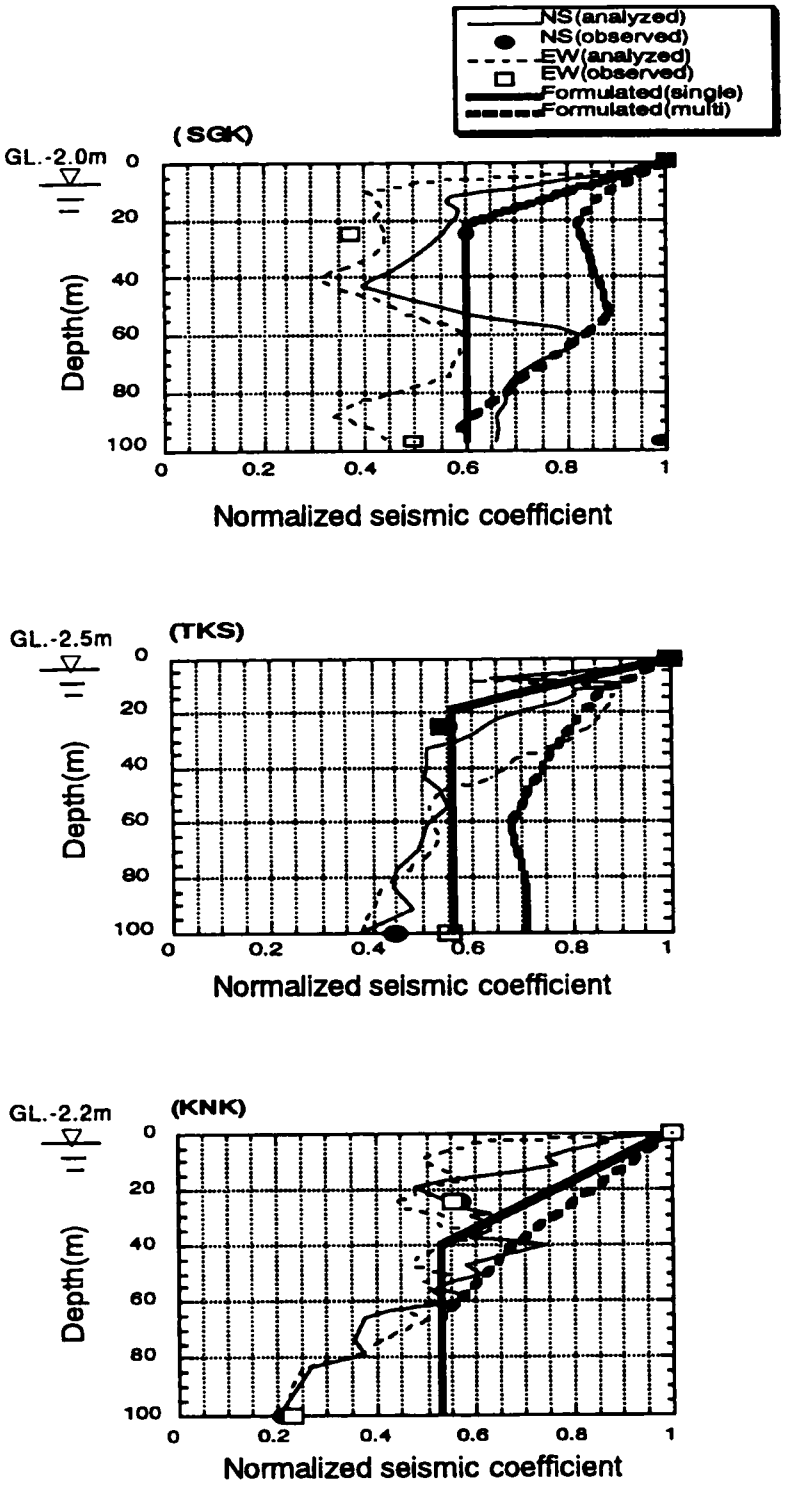

Fig.4.28 Normalized seismic coefficient for strong motions and the assessment

(2) Multi-layered ground

The extended evaluation method for multi-layered grounds was tested by applying it to a layered ground model with 4 layers of soil on top of a base layer. The soil parameters of the layers are listed in Table 4.7. The parameter α_i for the top 4 layers calculated using the extended assessment method are, also, listed in Table 4.7. The predominant period was taken as 1.0 based on the acceleration response spectra at the base layer.

The results of the assessment method are shown in Fig. 4.28. The values from the extended assessment method for a multi-layered ground were found to be over-conservative especially at shallow depths, less than about 20 m. However, for depths larger than 50 m the evaluated values were in reasonably good agreement with those calculated from recorded strong motions. Thus the assessment method was considered to be efficient for evaluating relatively deep underground seismic coefficient in a horizontally multi-layered ground larger than 50m. Application capability related to method 1 may be possible for irregularly layered ground included slope ground as can be noted in the previous section.

Table 4 7 Assessed parameters of normalized seismic coefficient for multi-layered ground

	SGK			TKS			KNK		
Layer No.	H_i(m)	V_i(m/s)	$\alpha_{i,i+1}$	H_i(m)	V_i(m/s)	$\alpha_{i,i+1}$	H_i(m)	V_i(m/s)	$\alpha_{i,i+1}$
1	12	161	0.87	13.4	165	0.859	17	177	0.862
2	10	270	0.82	23.6	329	0.756	22.7	218	0.678
3	31	323	0.89	23.3	418	0.675	23.3	301	0.675
4	40	301	0.583	23	565	0.709	23	495	0.709
Base	∞	480	*	∞	460	*	∞	1630	*

4.6 Conclusions

The conclusions that can be drawn from the results of the analyses described in this chapter are:

(1) Spectral ratios computed using records from near-field, intermediate and far-field earthquakes showed high variability at a hard rock site and a soft rock site. However, at a site on soft ground the site amplification was strongly influenced by the surface layer thus exhibiting a high dependency on the local surface geology.

(2) With regard to the application of system identification to estimate soil profiles at sites with laterally homogeneous ground using weak motion records, it was found that the

parameters identified using the average spectral ratios of recorded motions were in good agreement with the average of identified parameters obtained from all recorded spectral ratios.

(3) The vertical distribution of underground seismic coefficient for horizontal motion was found to be dependent on the predominant period of the input earthquake acceleration and the impedance ratio between the bedrock and surface layers.

(4) The vertical distribution of underground seismic coefficient was found to decrease linearly from a value of 1 at the ground surface to some depth below which it became constant. H_1 and H_2 and α_1, α_2 for the depth of the minimum value and the reduction ratios, respectively, were shown to be adequate in characterizing the normalized underground seismic coefficients using methods 1 and 2, respectively.

(5) H_1 was equal to one-fourth of the wavelength (λ /4) for hard and soft rock sites and H_2 was 1.5 times larger than H_1 at rock sites. H_1 for sites on soft ground was λ /4 when the predominant period T of the input motion was longer than the natural period T_0 (= 4Ho/Vs) of the surface layer, otherwise H_1 is equals to the thickness of surface layer H_0. α_1 was 0.7 for homogenous ground and 0.55 for grounds with Vs/Vb equal to 0.5. On the other hand, α_2 was 0.3 and showed no relation to the impedance ratio between the bedrock and surface layers. Comparison of this assessment method against values estimated from earthquake records, confirmed that the assessment method was quite effective in evaluating underground seismic coefficients.

(6) The assessment method for underground seismic coefficient was found to be effective for a filled-up slope and a hard rock cut slope. Application capability related to method 1 may be possible for irregularly layered ground included slope ground as can be noted.

(7) The assessment method was seen to be effective for strong motions, as well, except for sites that experienced strong liquefaction.

(8) The extended assessment method for multi-layered ground was found to be effective in computing underground seismic coefficients in the layers for layers at depths below 50 m.

REFERENCES

1) Sato, K., Y. Sawada, H. Kubota, H. Yajima and J. Tohma; Study of underground seismic coefficient, The 9th World Conference of Earthquake Engineering ,1984.
2) Sato, K., Y. Sawada, H. Kubota, H. Yajima and J. Tohma; Study of underground seismic coefficient, The 7th Japan Earhquake Engineering Symposium, 1986, (in Japanese with English abstract).
3) Sato, K., Y. Sawada, H. Itoh, J. Tohma, H. Yajima and M. Ogata; Reduction of underground Seismic Motion, CRIEPI Report No. U88022, 1988, (in Japanese with English abstract).
4) Ishida, K., K. Sato, H. Yajima and Y. Sawada; Estimation of soil property and characteristics of response spectra based on earthquake observations, CRIEPI Report 385005, pp55-62, August 1985.
5) Sub committee of improvement and standardization on earthquake engineering of nuclear power plant; Research report on standaridization of earthquake engineering (in Japanese), 1980.
6) Iwasaki, T. et. al; Strong motion records and its characteristics for 1978 Miyagiken-Oki earthquake, 7th Earthquake ground motion symposium, Arichtectural Institute of Japan, 1979.
7) Sawada, Y., H. Yajima, S. Sasaki and A. Sakurai; Strong earthquake motion observation on rock (Urgent report) -June 29th 1980 East Off. Izu peninsula earthquake-, CRIEPI Research report, 380009 (in Japanese), 1980
8) Komada, H. and S. Hibino; Nearby earthquake observation on Rock fill dam in Underground power station - August 8th 1983 Eastern Yamanashi pref. Earthquake, CRIEPI Research report 383036 (in Japanese), 1983.
9) Sawada, Y., H. Yajima, S. Sasaki and A. Sakurai; Sudy on earthquake resistant effect for cement mixed improved ground - Active control of vibration on improved ground based on earthquake observation part 1 -, CRIEPI Research report 380022 (in Japanese), 1980.
10) Sawada, Y. et al.; Dynamic characteristic of soil-structure system related to JPDR -Investigation of dynamic characteristic based on earthquake observation -, CRIEPI Research report 383029, 1983.
11) Hashimoto, K.; Vibration characteristics of soil and transformer in substation part 2, CRIEPI Research report, 385509, 1985.
12) Okada, T., K. Kishi and H. Ohtsuki; Evaluation of Seismic Stability of Non homogeneous Soft Bedrock, Proc. of the International Symposium on Weak Rock

'TOKYO' , Sept. 1981

13) Hanada, K.; Data Reduction Method for Forced Vibration Tests (No. 2) -system parameter identification method by Newton method-, CRIEPI Research report 383045, 1984

14) Hanada, K. and K. Andoh; System parameter identification method under dynamic load, Journal of Structural Engineering, pp.725-738 (in Japanese), March 1986.

15) Haskell, N.; Crustal reflection of plane SH waves', J.Geophys.Res., 65, pp4147-4450, 1960.

16) Sano, T.; Earthquake engineering and structural theory on a house, the first and second volume, Research report on prevention disaster (in Japanese), 1966, 1967.

17) Yamazaki, F., M. Imazu and H. Kuroda; Equivalent seismic coefficient used for seismis stability asessment of soil ground, the 18th annual symposium of geotechnical engineering, 267 (in Japanese), 1983.

18) Toki, K.; Inference of seismic ground motion from earthquake records, Journal of structural mechanics and earthquake engineering, Japan Society of Civil Engineering, No. 207, pp. 25-36, Nov. 1972

19) Toki, K.; Structural earthquake engineering analysis, New system of civil engineering 11, Japan society of civil engineering, published by Gihoudo, pp.109-115 (in Japanese), 1981.

20) Sasaki, S., K. Sato, M. Kawamura and K. Aoki; Characteristics of seismic ground motion observed at the Kamaishi Mine, The 10th Japan Earthquake Engineering Symposium, November 1998.

21) Ito, H., K. Sato and Y. Sawada; Consideration on the seismic motion and the design seismic coefficient of large cut slope under the strong earthquake, Proceedings of the 8th International congress on rock mechanics, International society for rock mechanics, pp.413-416 (in Japanese), 1995.

22) Sato, K., T. Kokusho, Y. Sawada and H. Yajima; Site amplification and seismic motion of surface geology including Pleistocene layers during Hyogoken-nanbu earthquake, Proceedings of 11th World Conference on Earthquake Engineering, No 1180, June 1996.

CHAPTER 5

EFFECTS OF RADIATION PATTERN ON LOCAL SITE EFFECTS OF SEDIMENT-FILLED VALLEYS

5.1 General Remarks

In this chapter, the effects on seismic ground motion of surface geology specifically that of laterally irregular, layered ground are investigated. Effects of such irregularities become important in the seismic design of long and large-scale structures such as electric power facilities, harbor facilities, bridges, buried lifelines, duct structures, tunnels, and pipelines. Underground geological irregularities have been recognized as contributing to local site effects by increasing both the amplitude and duration of seismic ground response. These phenomena have been reported in historical earthquakes, for instance in explaining the pronounced spatial variability of the damage observed in Mexico City during the 1985 Michoacan earthquake[1].

This kind of behavior was, also, pointed out by using the strong motion records obtained in the Pasadena area during the 1971 San Fernando earthquake. The records obtained from sites on crystalline rock and alluvium ground exhibited quite different characteristics even though they were within a distance of several hundred meters from each other. In the 1963 Skopjie, Yugoslavia earthquake the damage contribution was attributed to the lateral heterogeneity of the surface ground layer. During the 1978 off Miyagi prefecture earthquake in Japan, damage was mainly concentrated in a transitional zone between the mountains and the alluvial valley [2].

Seismic wave field at a site is related to source mechanism, path effects and local site effects. Various analytical methods[3] have been proposed to quantitatively evaluate the seismic motion at a site from considerations of all three factors. In order to fully evaluate the local site effect it is necessary to interpret the incident wave field, which is influenced by seismic source and path effects.

An array of strong motion seismographs have been installed at two sites in

Japan with irregularly layered grounds except slope sites in this dissertation. One site called AGK[4] is located in Kuno district on a small-sized diluvial and alluvial gravel ground in Ashigara valley. The other site called TKY site[5] is located on an alluvial soft clay buried valley in Takeyama district situated in the Miura peninsula. Several strong motion records have been recorded at these two sites. In this chapter, site characteristics of irregularly layered grounds are investigated using these strong motion records in conjunction with numerical analyses.

5.2 Geophysical Exploration of Sediment-Filled Valleys at Observation Sites

5.2.1 Alluvial valley

Destructive earthquakes[6] have occurred repeatedly with return periods of about 70 years in the area in the vicinity of the city of Odawara. Some seismologists[7] have predicted that an earthquake of magnitude 7.0 will occur in the near future in western Kanagawa. This is the reason why the Earthquake Research Institute at the University of Tokyo in collaboration with the electric power industry have installed spatial and vertical arrays of strong motion seismographs in this area.

The Ashigara valley, about 80 km southwest of Tokyo metropolis, lies in the Southern Kanto region, which is located near the triple junction of the Philippine Sea Plate, the Eurasian Plate and the Pacific Plate (See Fig.5.1). In particular, the Ashigara valley and its vicinities are geologically complicated and have high seismic activities as they are on the extension of the Sagami trough on the boundary of the Philippine Sea Plate and the Eurasian Plate. Underneath this region the Philippine Sea Plate collides with the Eurasian Plate. Naturally, this region has often suffered significant earthquake damage in history. As a result the topography and geology of this region have been surveyed for a long time. For example, recent studies have been conducted by Kanagawa Prefecture[8] and Yamazaki et al.[9]

As illustrated by the surface geological map in Fig. 5.2, the Ashigara Valley, surrounded by the Hakone Volcano to the west, by the Oiso Hills to the east and by the Tanzawa Mountains to the north, is about 4 Km wide and 12 Km long. It is a rectangular shaped alluvial plain developed along the lower reaches of the Sakawa River. To the east and north of this valley are the Quarternary Kozu-Matsuda fault and the Kan-nawa fault (Fig. 5.3). AGK site is located on the west of this alluvial plain, which consists of a sedimentary basin along the Kuno river. Kuno district, in which AGK is located, lies at the southwestern part of the Ashigara valley and is close to the Hakone Volcano. In this

district, an alluvial valley formed by the San-no river spreads between two 100 to 150 m tall east-west trending hills. This valley extends eastward and is about 3 Km long and about 1 Km wide.

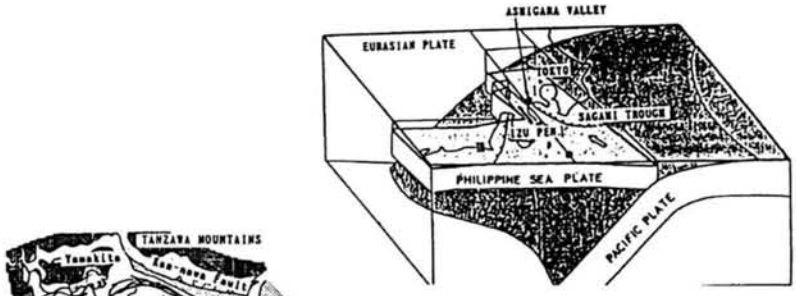

Fig.5.1 Unified plate model for interpreting the techtonics of the Kanto-Tokai area[9)]

Fig. 5.2 Subsurface geological map in and around the Ashigara Valley (by ESG[9)])

age	geology or geography	mark
Holocene	flood plain, back marsh	A
	natural levee, debris cone	N b
	Kanesoniya Terrace (Alluvial Terrace)	A t − 3
late Pleistocene	Younger loam (equivalent to Musashino, Tachikawa loam formation)	T p m
	Younger Hakone Pumice Flow (coverd by Younger loam in many cases)	H p
middle Pleistocene	Older Hakone Scoria Pyroclastic materials	O s − 2

Fig. 5.3 Subsurface geological map at AGK site
(KR1, KS1 and KS2 indicate the downhole recording test sites for ESG[10)])

The deepest formation identified in this area was formerly believed to belong to the Tertiary to Quarternary Ashigara group or the Yugashima group. As yet its depth has not been fully established. This Ashigara group or Yugashima group is covered by volcanic products (Middle Pleistocene volcanic rocks called OS-1 and OS-2), which formed the older Hakone somma. The formation of these volcanic products is hundreds of meters to more than 1,000 m thick and consists of irregular alternation of lava, volcanic ash, mudflow, pyroclastic rock, etc.

On the hills, the pyroclastic rocks of the older Hakone somma (OS-2) are covered by the younger Hakone pumice flow (HP) and the strata of volcanic ash due to a later downfall (equivalent to younger loam: Tpm) as seen in Figs. 5.3 and 5.4. At the rock site upstream of the valley, outcrops of andesite lava (OS-2) exist. These constitute the older Hakone somma. Downstream, the alluvial lowland spreads. It was formed by the sedimentation of the San-no river, and the ground consists of a sand and gravel formation overlaying pyroclastic rocks of the older Hakone somma. Presumably, this sand and gravel formation contains deposits from the inundation of the San-no river in part but most of it is constituted of deposits from a younger pumice flow (HP).

Further downstream, the alluvial silt and clay (Ac) buried the valley and the thickness of the humus soil (Ap) layer increases. On the lowest reaches of the valley, the layer approaches a thickness of approximately 20 m. Sand and gravel strata (Hpg: N value over 50 blows) are distributed at a depth of 15 m or more at the outlet of the valley.

Pyroclastic rocks of the older Hakone somma (OS-2) outcrop at rock sites. OS-2 probably exists at a depth of more than 100 m on the central part of the valley and at AGK site. Figs. 5.4(a) and 5.4(b)[10] show the strong motion observation sites and cross-sections along east to west lines measured by a reflection survey.

The velocity profile and physical properties of the subsurface ground structure at AGK and its vicinity have been geotechnically explored[10), 11)]. Fig. 5.5 shows PS logging profiles at two down-holes of AGK. P- and S-wave velocity loggings and density loggings have been carried out at five down-holes, which are designated OA, OC, OD, OE and OF at depths from 20 m to 330 m. OB is not a down-hole site but a surface ground site. The suspension method for PS logging was applied at all locations. Only at OF was the vertical seismic profiling (VSP) survey[11)], also, applied.

There are three other down-hole arrays, designated KS1, KS2 and KR1, at depths from 20 m to 100 m installed by ERI. The down-hole method of seismic survey was applied at these down-holes. From these surveys, Vs was estimated to be about 65~170 m/sec for alluvial humus soil and silt, 340~430 m/sec for loam, 620~750 m/sec for pumice flow (gravel), 400~500 m/sec for pumice flow (sand) and 700~1200 m/sec

for pyroclastic material. Vp estimated from the same surveys ranged in value from 400 to 2400 m/sec for each stratum. The density was estimated to be in between 1.4 to 2.5 g/cm$^{3)}$.

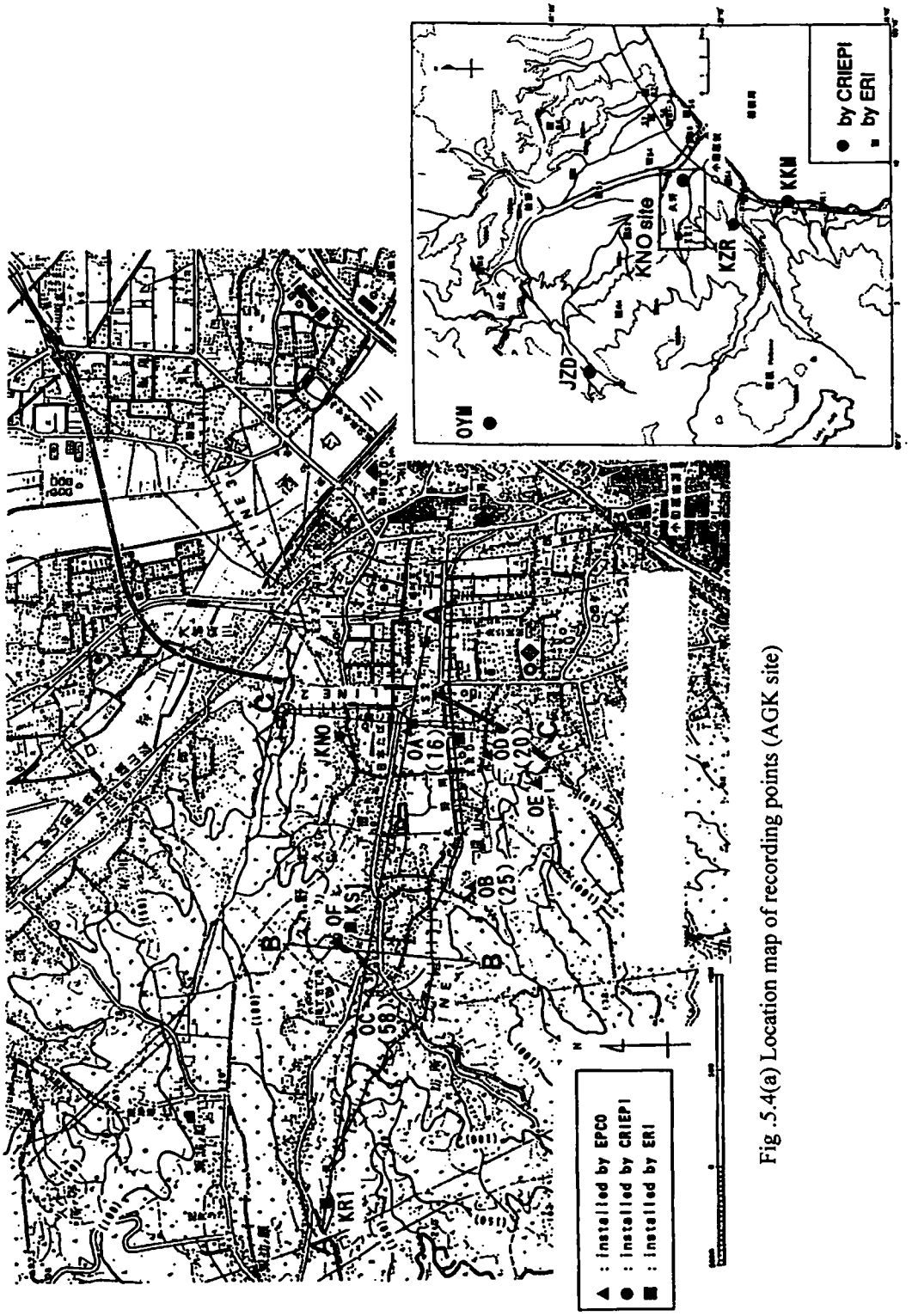

Fig .5.4(a) Location map of recording points (AGK site)

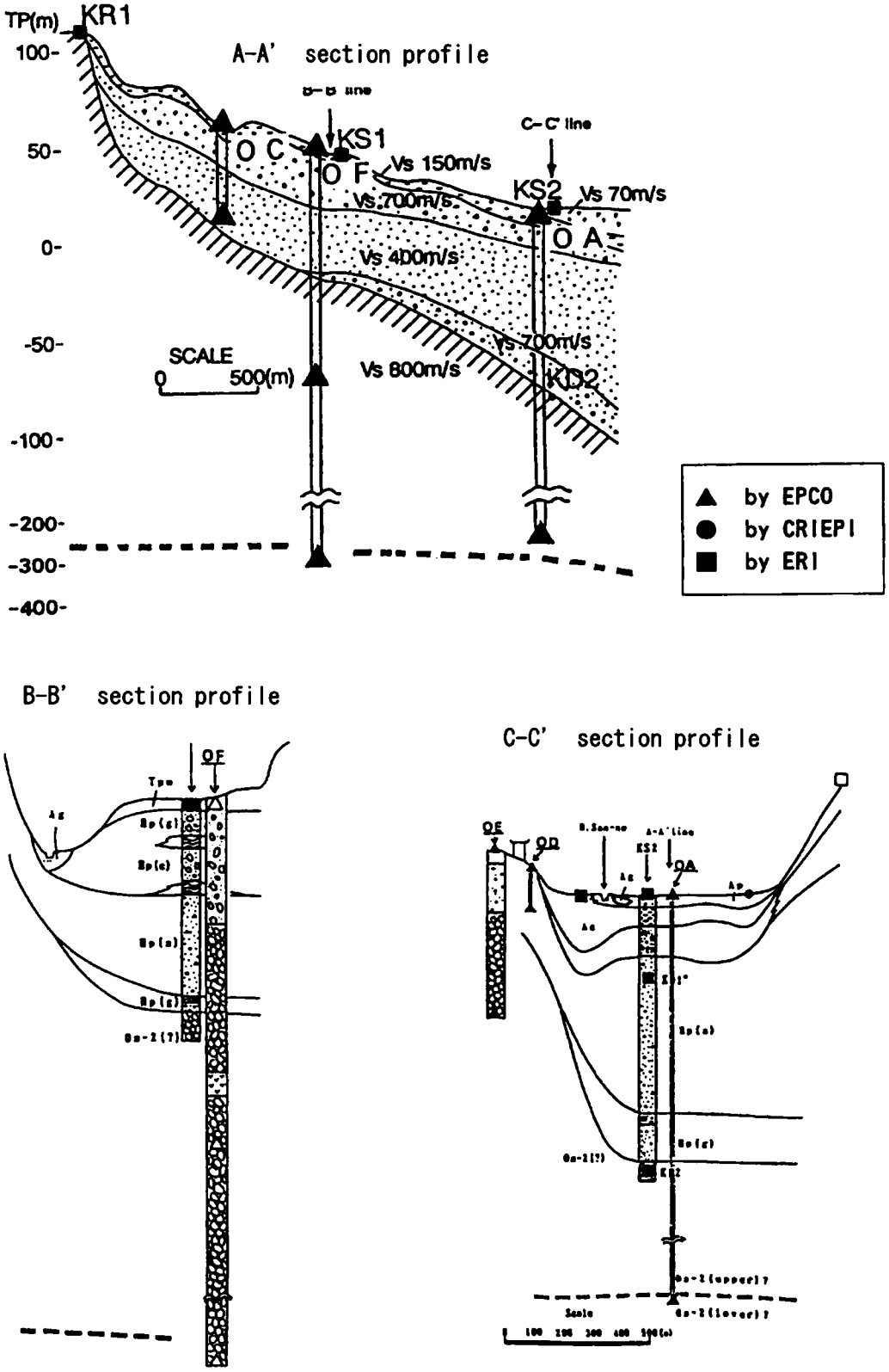

Fig. 5.4(b) Schematic cross-section at AGK site by ESG[10)]

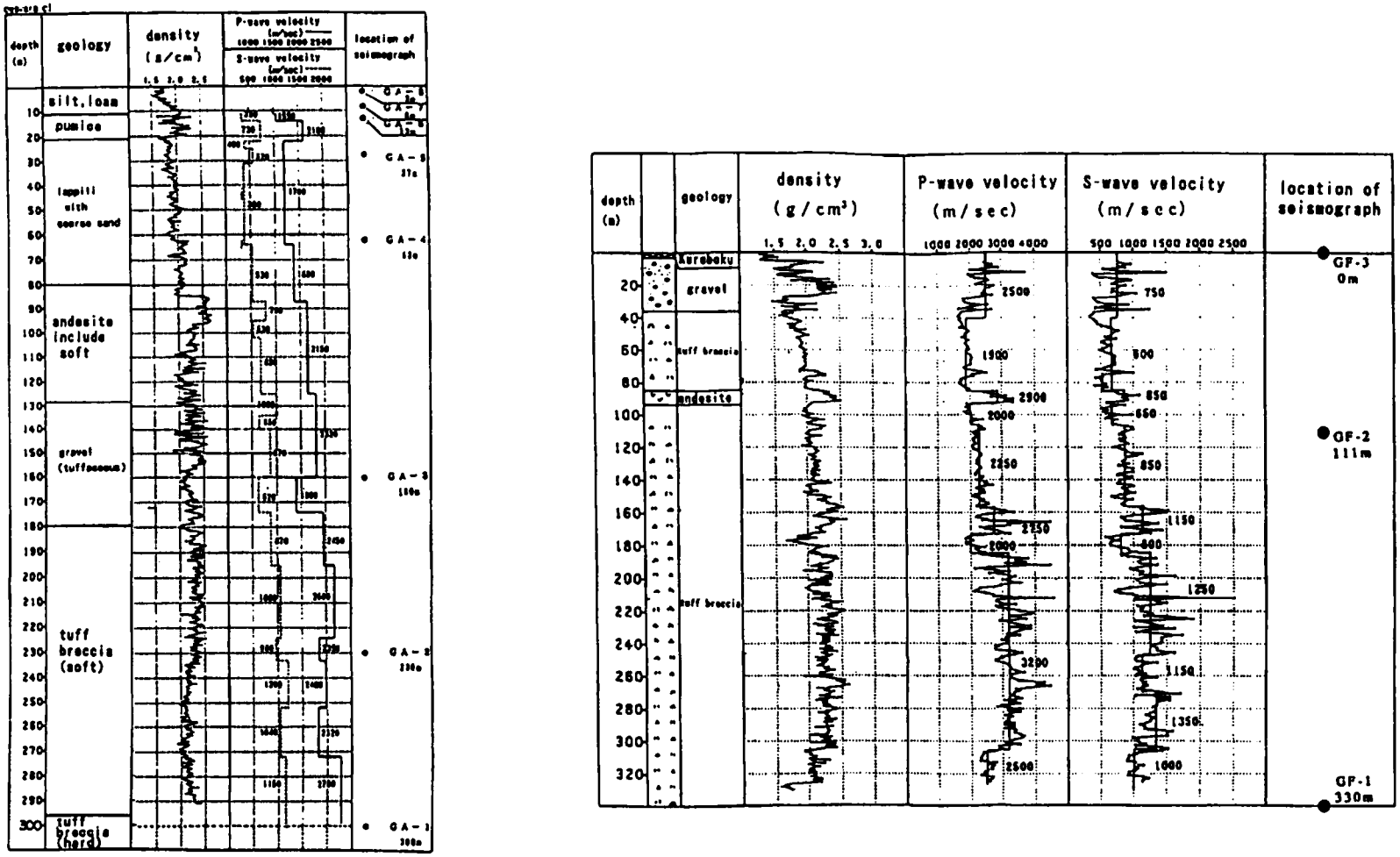

Fig.5.5 Geological profile, PS-logging and seismographs location (Left: OA, Right: OF)

5.2.2 Buried Valley

TKY site is located in Takemaya district on the mid-eastern part of Miura peninsula and lies to the east of Sagami bay. The geological formation of Miura peninsula is based on Hayama group of old Tertiary with Miura and Sagami groups distributed on top of the Hayama group. Gravel and loam layers are distributed on the terrace formation and alluvial layers are distributed over the lower land in this district. On the basis of geological surveys[5] measured at TKY, it was confirmed that the rock of Miura group outcrops on the west edge and Hayama group is distributed on the eastern side. Alluvial soft clay makes up a typical buried valley along the west to the east section.

A P-wave seismic shallow reflection survey was carried out along lines A-A', C-C', and E-E' as shown in Fig. 5.6. Fig. 5.7 shows a three-dimensional image of the geological profile viewed at three sections. This image more or less confirms that this site is a sedimentary basin of width 300 m wide and depth of 25 m. Vp was estimated to be 1.9 Km/s for the soft bedrock.

Fig. 5.8 shows the vertical distributions of Vp and Vs estimated from PS logging at SG3. Vp was estimated to be 400 to 1200 m/s for the alluvial layer and 1900 m/s for bedrock. Vs was estimated to be 90 to 180 m/s for the first clay of Ac1 layer, 150 to 180 m/s for second clay of Ac2 layer and 600 m/s for the soft bedrock of Miura group Zushi layer. These and other estimated soil parameters are listed in Table.5.1.

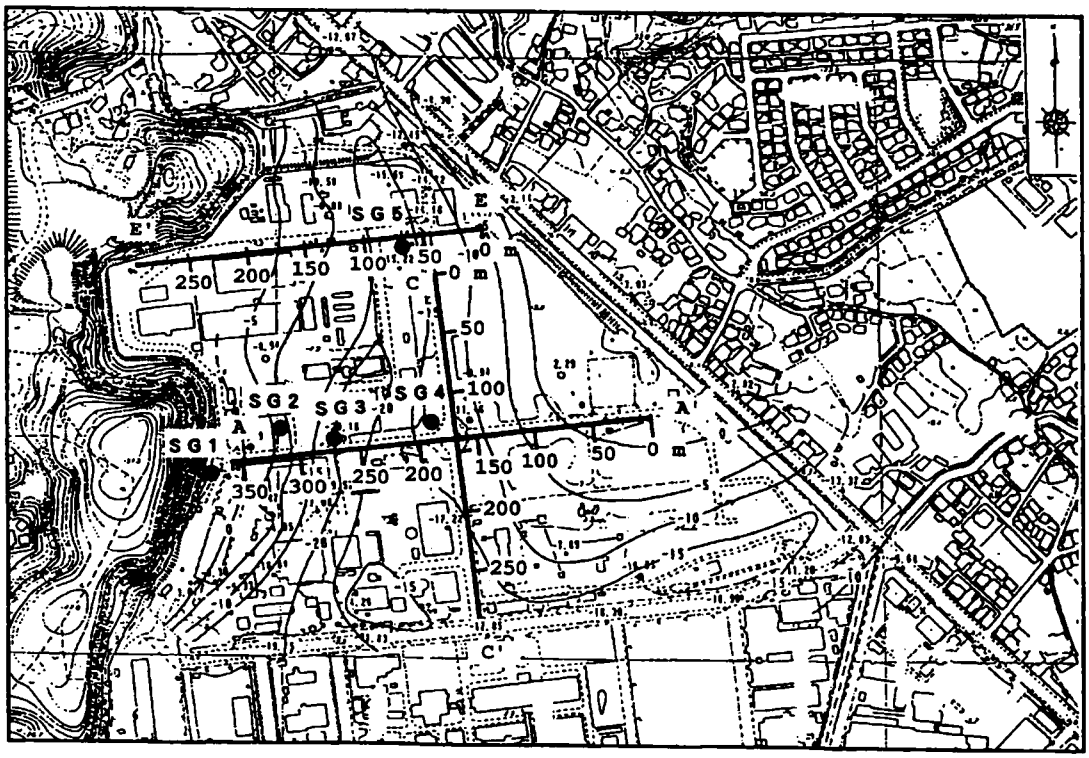

Fig.5.6 Location of seismographs and measurement lines for the seismic reflection survey at TKY site

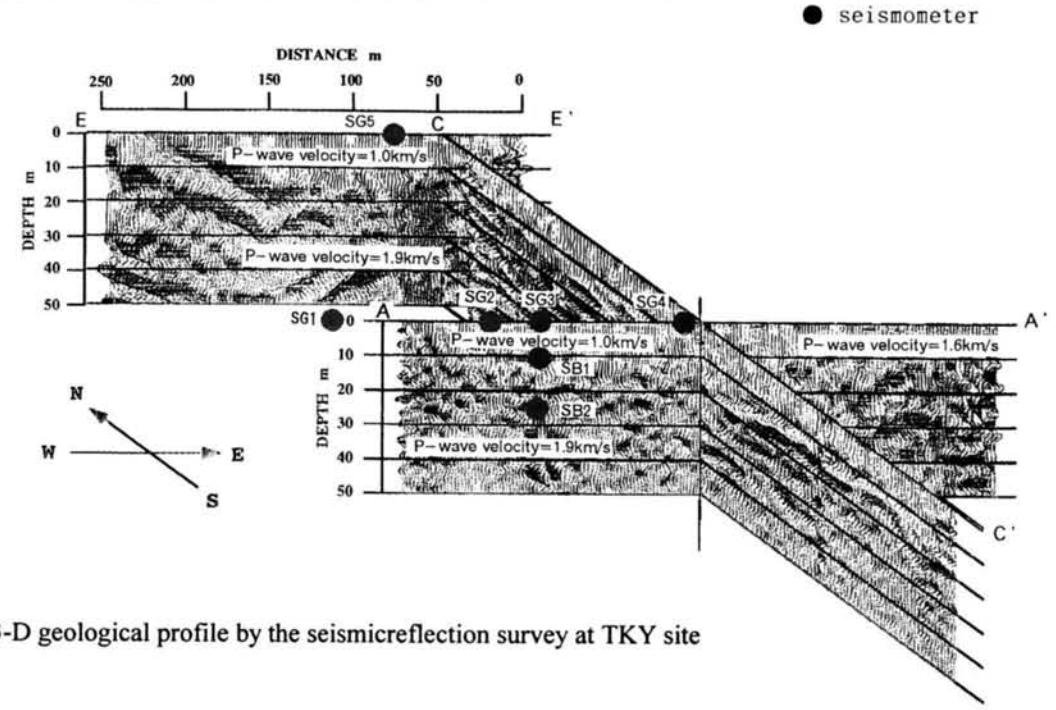

Fig.5.7 3-D geological profile by the seismicreflection survey at TKY site

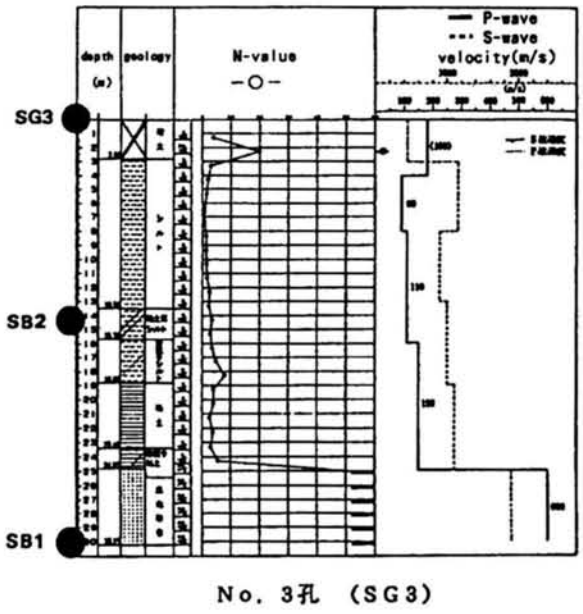

Fig.5.8 Geological profile, PS-logging and SPT blow count at TKY site

Table 5.1 Geotechnical parameters at TKY site

depth	geotechnical condition	P-wave velocity (m/s)	S-wave velocity (m/s)	density ρ (t/m**3)	Q-value
0~3	fill	400	180	1.6	25
3~4	silt	1200			
4~8			90		
8~13		900	110		
13~16		1000			
16~19	clay		150		
19~25		1200			
25~	sandstone	1900	600	1.9	50

5.3 Focal Radiation Patterns of the Recorded Earthquakes

Earthquake occurring in three source regions were recorded at the same time at both sites. In addition there were records from other earthquakes recorded at only one of the two sites. Table 5.2 lists the events and the sites where the records were available and Fig. 5.9 shows the epicenters of these events and the locations of the observation sites on a map. In this section, the focal radiation pattern and seismic path effect of the seismic source events listed in Table 5.2 are investigated.

Table 5.2 Earthquake records at TKY and AGK sites

EQ No.	Name of Earthquake	Date	Origin time	Latitude	Longitude	Depth (km)	Magnitude Mj	Epicentral distance from AGK (km)	Epicentral distance from TKY (km)
1	Suruga bay	1995/4/18	20:26	35° 03′	138° 35′	24	4.5	57.0	—
2	Sagami bay	1995/7/3	8:53	35° 09′	139° 34′	122	5.2	40.0	8.2
3a	E. Yamanashi	1996/3/6	23:12	35° 30′	138° 54′	16	4.3	34.5	—
3b	E. Yamanashi	1996/3/6	23:35	35° 30′	138° 54′	17	5.3	34.5	—
4	E. Off.Chiba	1996/9/11	11:37	35° 38′	141° 12′	53	6.2	190.4	153.9
5a	E. Yamanashi	1996/10/25	12:25	35° 27′	139° 00′	23	4.5	24.6	61.7
5b	E. Yamanashi	1996/10/25	21:06	35° 28′	138° 59′	18	4.1	26.9	—
6	E. Off. Izu Penin.	1997/3/4	12:51	34° 10′	139° 10′	2	5.7	35.2	49.5
7	S. Ibaraki	1997/3/23	20:36	35° 58′	140° 06′	72	5.0	—	103.6
8	W. Kanagawa	1997/11/4	10:31	35° 12′	139° 06′	20	3.9	9.1	—

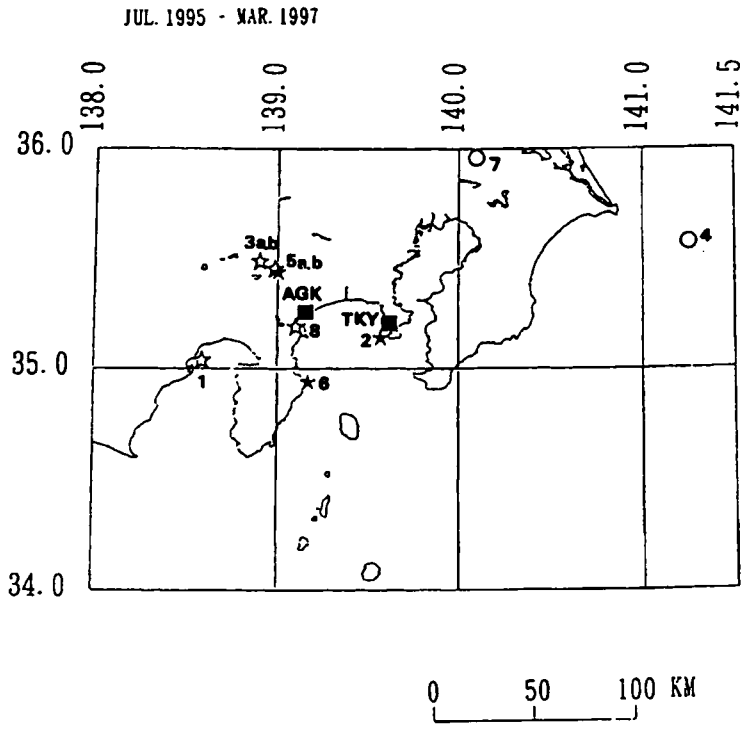

Fig.5.9 Location map of strong motion observatories at TKY(■) and AGK(■) and recorded earthquake epicenter
(☆:AGK records, O:TKY records, ★:both records, ■:observatories)

5.3.1 Effects of Focal Radiation on Alluvial Valley

As seen in Table 5.2 earthquakes in 5 different source regions were recorded in the period from April 1995 to November 1997. The Western Kanagawa earthquake (EQ.8) is at an epicentral distance of 9.1 Km. The other events such as the East Yamanashi (EQ.3a, 3b, 5a, 5b), East off Izu peninsula (EQ.6), Suruga bay (EQ.1) and Sagami bay (EQ.2) occurred in the region at epicentral distances from 20 to 60 Km. The magnitude of these events range from 3.9 to 5.7. Most of the recorded events occurred at focal depths of less than about 70 Km except the Sagami bay earthquake which occurred at a depth of 122 Km. The lengths of the ruptured faults estimated using the empirical equation devised by Matsuda[12] for even the relatively larger earthquakes, such as the E. Yamanashi (EQ.3b) and E. off Izu peninsula (EQ.6) earthquakes, were much smaller than the epicentral distances. Therefore, these events could be adequately modeled as a point source with respect to the observations at AGK.

First, the focal S-wave radiation patterns of these earthquakes were evaluated by moment tensor solution Mpq of a point source[13] in a homogenous medium. Source parameters, such as strike angle ϕ, dip angle δ and slip angle λ for the source fault mechanism estimated by the National Institute for Earth Science and Disaster Prevention (NIED) are listed in Table.5.3. The S-wave focal radiation patterns were given by moment tensor solutions for SH and SV waves and these solutions were expressed in terms of the source parameters. The moment tensor solutions are given by equations (5.1) and (5.2), expressed in dimensionless form, and they represent Green's functions for calculating the far-field displacement for a point source in a homogeneous medium.

Table 5.3 List of CMT solutions for the seismic source (by http://www.bosai.go.jp)

EQ. No	strike ϕ s (deg)	dip δ (deg)	slip λ (deg)	Magnitude Mj	depth h (km)
1	162.0	56.7	166	4.5	24
2	252.0	83.8	114	5.2	122
3b	24.3	50.0	102	5.3	20
4	132.0	63	-50	5.0	53
5a	207.0	35.0	90	4.5	23
6	69.8	58.2	-154	5.7	2
7	118.8	59.5	64.3	5.0	72
8	232.0	80.0	158	3.9	15

calaloged by NIED

$$\mathfrak{I}^{SV} = V_p \gamma_q M_{pq}$$
$$= \sin\theta\cos\theta(\cos^2\phi M_{xx} + \sin 2\phi M_{xy} + \sin^2\phi M_{yy} - M_{zz}) + \cos 2\theta(\cos\phi M_{xz} + \sin\phi M_{yz}) \tag{5.1}$$

$$\mathfrak{I}^{SH} = H_p \gamma_q M_{pq}$$
$$= \sin\theta[\sin\phi\cos\phi(M_{yy} - M_{xx}) + \cos 2\phi M_{xy}] + \cos\theta[\cos\phi M_{yz} - \sin\phi M_{xz}] \tag{5.2}$$

where Mpq is moment tensor, $V_p\gamma_q$ is a unit vector in the SV direction and $H_p\gamma_q$ is a unit vector in the SH direction as shown in Fig. 5.10. The focal radiation patterns for SH and SV waves were calculated at every 10^o interval of the azimuth and take-off angles. Next the vectors were mapped using an equal area projection of the lower hemisphere of the focal sphere as shown in Fig. 5.11. The amplitude of the vector is represented by the length of the vector computed at ten steps of 0.1 from 0.1 to 1.0. Tables 5.4(a) and (b) list the estimated azimuth and take-off angles of every event recorded at OA at AGK and SG1 at TKY using a model of the earth's crustal structure[14] evaluated by an artificial explosive seismic survey in Izu district. Table 5.5 lists the properties of the model of the earth's crust.

Table 5.4(a) Estimated azimuth and take-off angles for OA

unit(degree)

EQ.No.	OA	
	azimuth Φ	take-off θ
1	66	60
2	290	161
3b	139	118
5a	146	120
6	356	58
8	32	148

Table 5.4(b) Estimated azimuth, take-off and incident angles for TKY

unit(degree)

EQ.No.	SG1		
	azimuth Φ	take-off θ	incident θ i
2	212	6	1.6
4	72	78	15.5
5a	295	85	17.9
6	234	58	22
7	28	59	13.6

Table 5.5 Earth's crust structure in Izu district

Layer No.	Thickness (km)	Vp (km/s)	Vs (km/s)	ρ (t/m**3)
1	1.0	3.0	1.2	2.2
2	3.0	5.0	2.7	2.8
3	15.0	5.9	3.7	2.8
4	11.0	6.8	3.9	3.0
5	∞	7.7	4.4	3.3

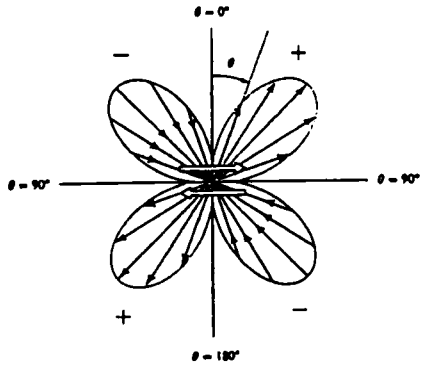

P wave's radiation pattern

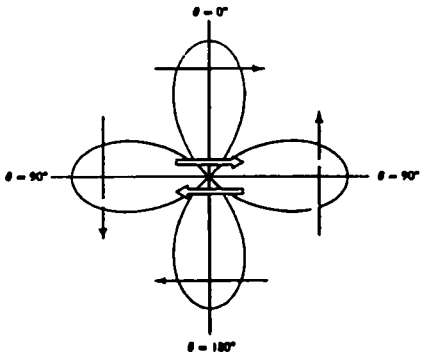

S wave's radiation pattern

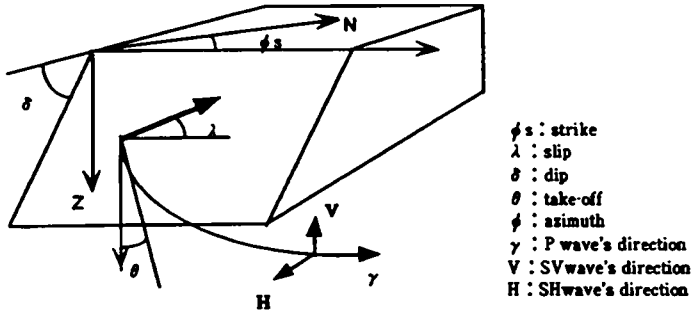

Fig.5.10 Diagrams for relationship between source parameters and S wave radiation patterns

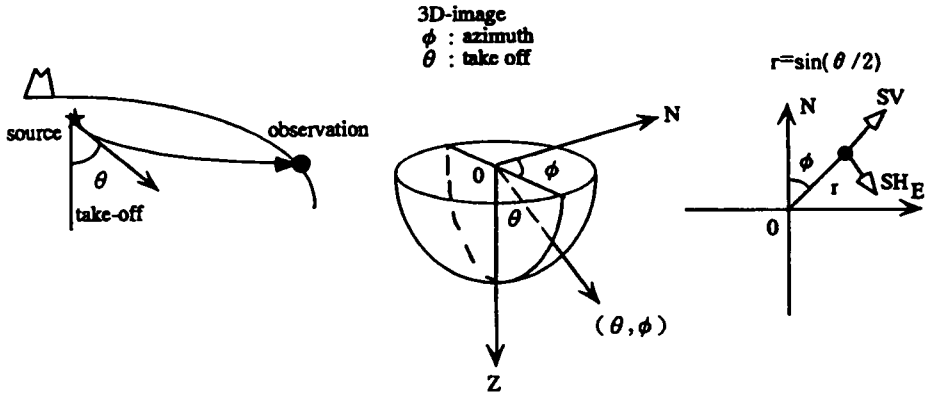

Fig.5.11 Diagram for an equalarea projection of the focal sphere map

With regard to the E.Yamanashi (EQ.3b) earthquake, the SV wave radiation pattern is relatively larger than the SH wave radiation pattern at OA as seen in Fig. 5.12. In the figure, these patterns were realized with reference to the S-wave principal shocks of the integrated velocity seismograms at the surface of OC, OF, and OA. Those records were filtered out using a Chebyshev bandpass filter with a pass band of 0.4 to 1.0 Hz. The velocity timehistories at the bottom of the down-hole and at the outcrop rock point at AGK are shown in Fig. 5.13. From this figure, it was recognized that the first S wave motions in the EW component appeared in phase in all the velocity timeshistories. To investigate this performance, the principal axis was evaluated with reference to radial and transverse components of the horizontal motions by using the complex polarization filter[15]. As seen in Fig. 5.14, the principal axis of the first S wave motion was found to be inclined along the EW direction as a result of the propagation in the geological structure of Ashigara valley[15]. It was, also, found that the secondary surface waves were still present inside the AGK basin after the principal S-wave motion recorded at the outcropped rock site stopped. This kind of behavior is typical of ground motions in sedimentary basins. Moreover, it was seen that the input ground motion recorded at the bedrock was influenced by the source radiation pattern.

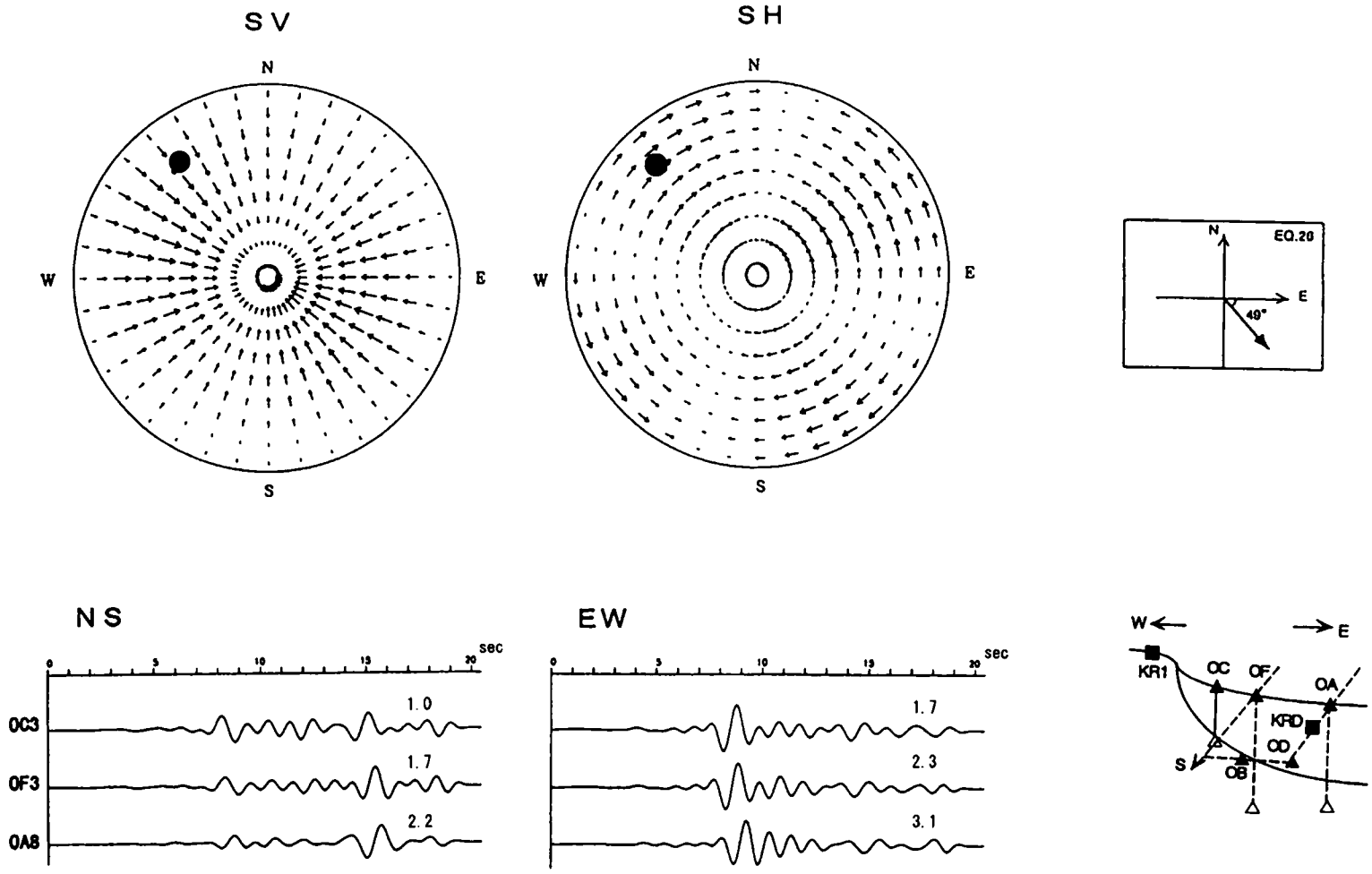

Fig.5.12 Upper:Focal radiation patterns for S waves at OA point, Lower: Velocity filtered in the frequency of 0.4～1.0Hz (EQ.3b:E.Yamanashi, unit:kine)

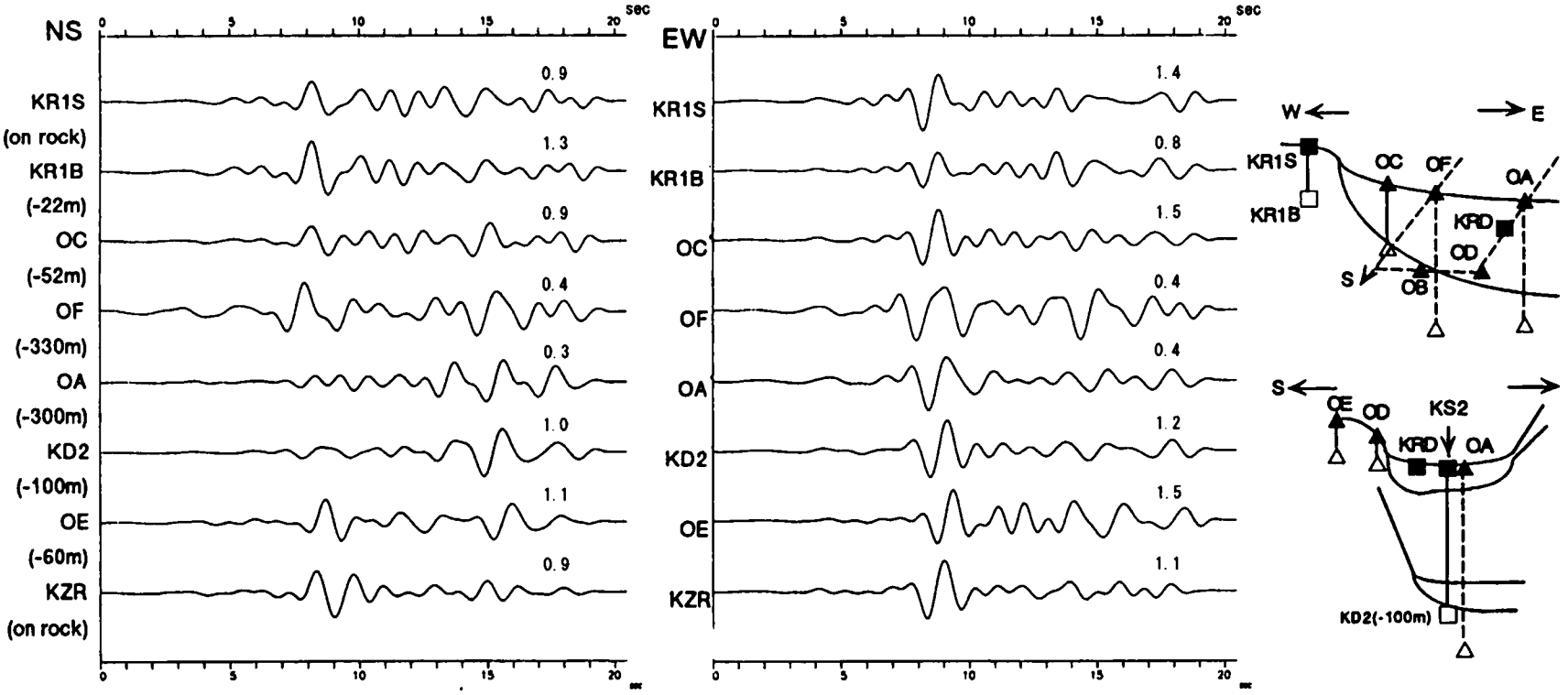

Fig.5.13 Velocity records filtered in the frequency of 0.4～1.0Hz

at the base of downhole and on rock sites (EQ.3b:E.Yamanashi, unit:kine)

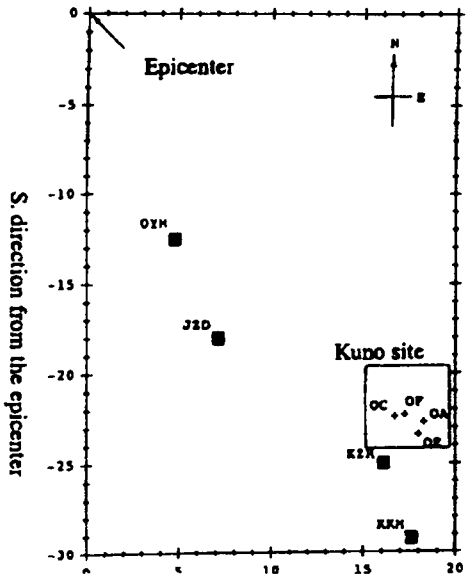

E dirction from the epicenter (unit:km)

(a) location of observation on rock

(■:on rock, ＋:at the base of downhole)

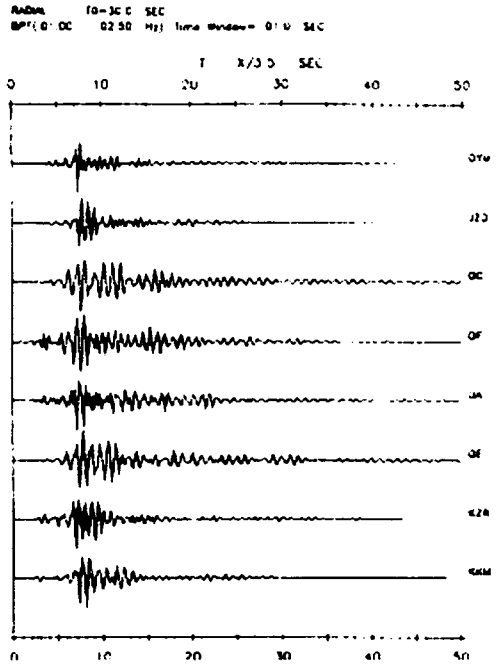

First S wave: part A (t=6.0-8.0sec)

Later S wave: part B (t=20-22sec)

(b) Radial velocity records filtered in the frequency of 1.0～2.5Hz

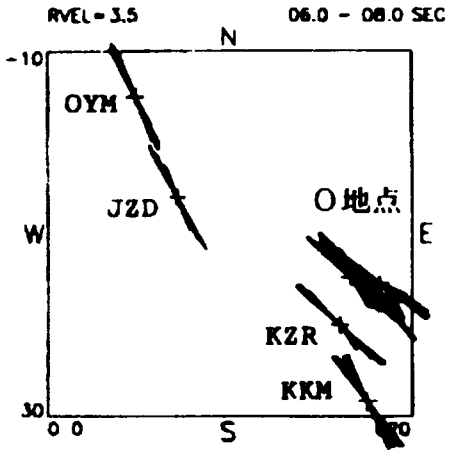

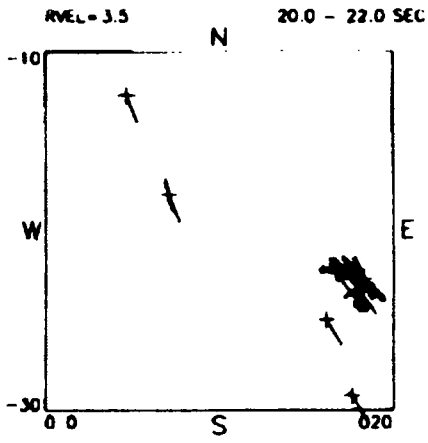

(c) First and Later S wave's pricipal axis in the horizontal particle motion (6~8sec, 20~22sec)

Fig.5.14 Velocity records at rock and base of AGK sites

and the S wave's pricipal axis in the horizontal particle motions (EQ.3b:E.Yamanashi)

With respect to the E. Off Izu peninsula (EQ.6) earthquake, the SH-wave radiation pattern is larger than the SV-wave radiation pattern as seen in Fig. 5.15. In the same figure, the principal S-wave shocks can be found with reference to the velocity time histories recorded at the surface of the sedimentary deposits at OC, OF, and OA. The first S-wave motions were apparently predominant in the EW component and were much larger than in the NS component and therefore, the S-wave motions, also, coincided with the focal radiation pattern for this event. Furthermore, the SH wave radiation pattern was much larger than the SV wave radiation pattern for the Sagami bay (EQ.2) and Suruga bay (EQ.1) earthquakes. Thus the first S-waves were predominant in the NS component and were much larger than the first S-waves in the EW component, as shown in Fig. 5.16. Therefore, in these events the principal axis of the S-wave motion was in agreement with the estimated focal radiation pattern.

With respect to the W. Kanagawa (EQ.8), the SV-wave radiation pattern was much larger than the SH wave radiation pattern. The azimuth angle of this event measured at OA was 32° which indicated that the first S-wave motions were predominant in both NS and EW components.

At the down-hole sites OA, OC, OD, OE, and OF, the spectral ratios between the surface and bottom records were computed for the horizontal components of the principal S wave shock. The earthquake records were divided into two groups: one with the principal axis of the S-wave motion predominant in the NS direction and the other predominant in the EW direction. The spectral ratios were compared for records of both groups. Records from the Suruga bay (EQ.1) and Sagami bay (EQ.2) earthquakes belong to the NS predominant group while those from the E. Yamanashi (EQ.3b and 5a) and E. Off Izu peninsula (EQ.6) earthquakes belong to the EW predominant group. Only records from W. Kanagawa (EQ.8) earthquake belong to both groups because the principal axis of the S-wave was predominant in both NS and EW components.

As seen in Fig. 5.17(a), the spectral ratios were constant for frequencies lower than 2.5 Hz in the NS component for the NS predominant group. On the other hand, as seen in Fig.5.17 (b), the spectral ratios were highly variable around 1 Hz in the NS component for the EW predominant group.

The spectral ratios were found to be more or less constant in the lower frequency regions for S-wave motions and the principal axis of the S-wave is in good agreement with the focal radiation pattern. Thus the local site characteristics at AGK could be evaluated by considering the incident wave field related to a given source radiation pattern.

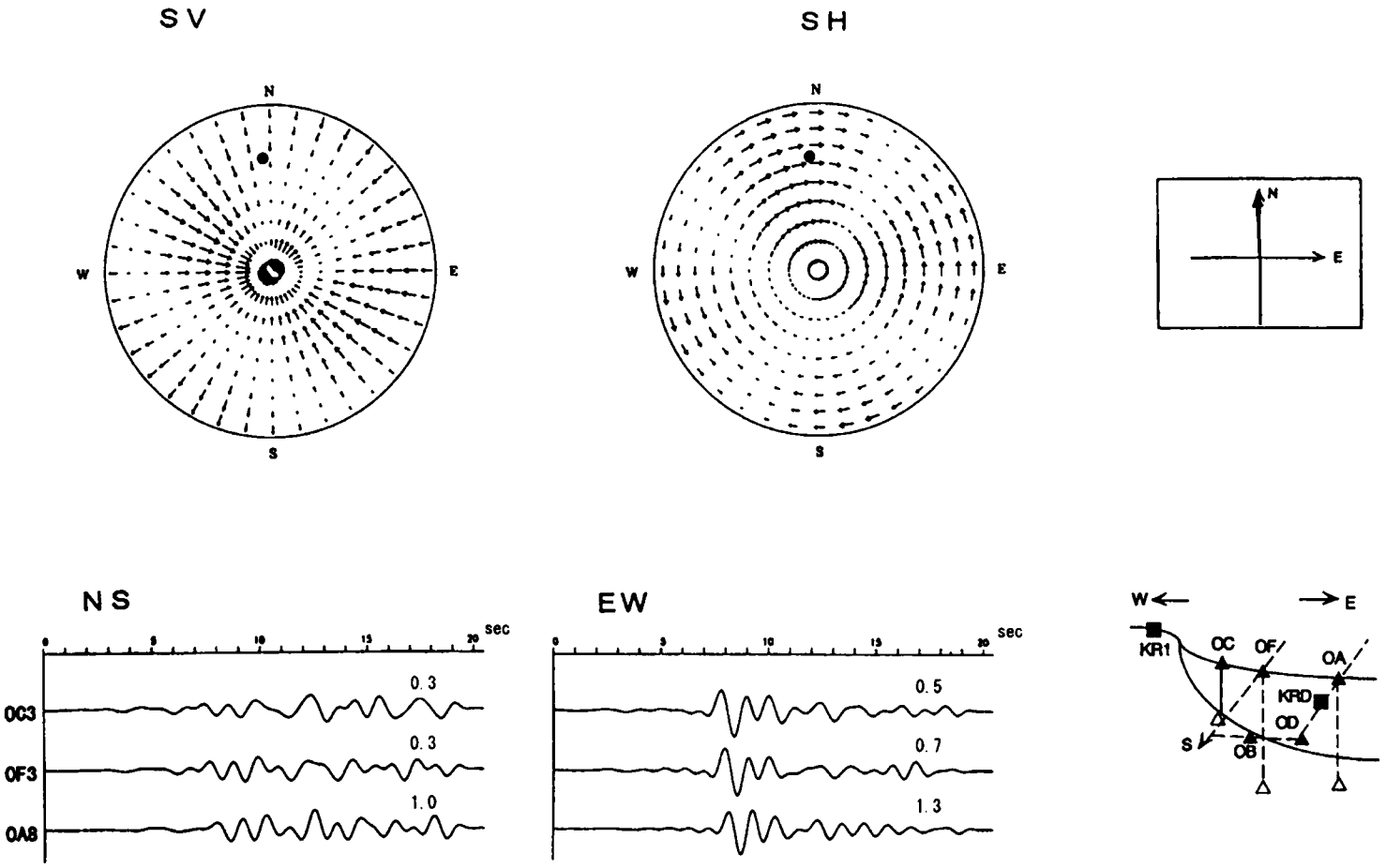

Fig.5.15 Upper: Focal radiation pattern for S waves at OA, Lower: Velocity records filtered in the frequency of 0.4～1.0Hz (No.6:E.Off Izu.EQ-34)

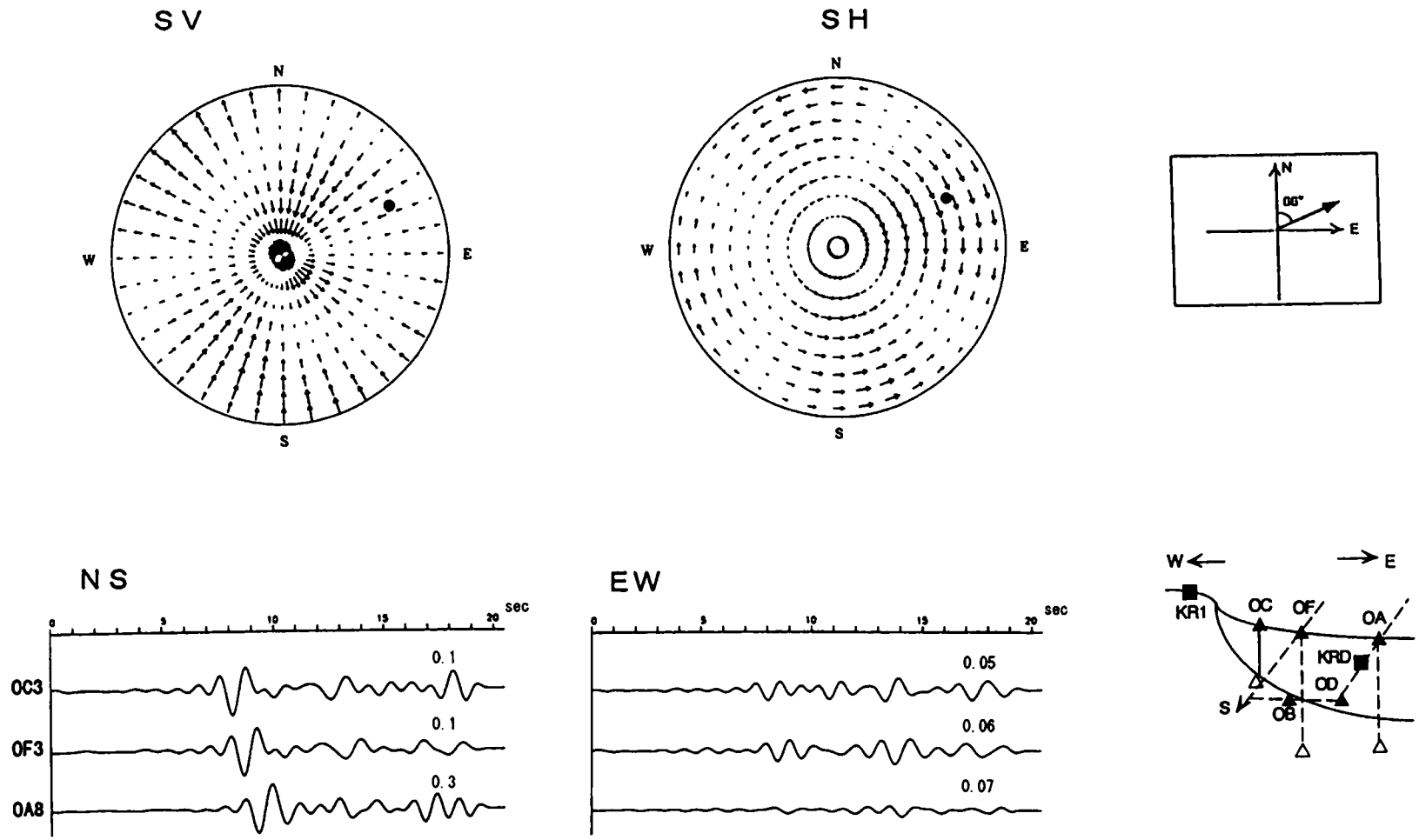

Fig.5.16 Upper: Focal radiation pattern for S waves at OA, Lower: Velocity records at AGK filtered in the frequency of 0.4～1.0Hz (No.1:Suruga bay.EQ-21, unit:kine)

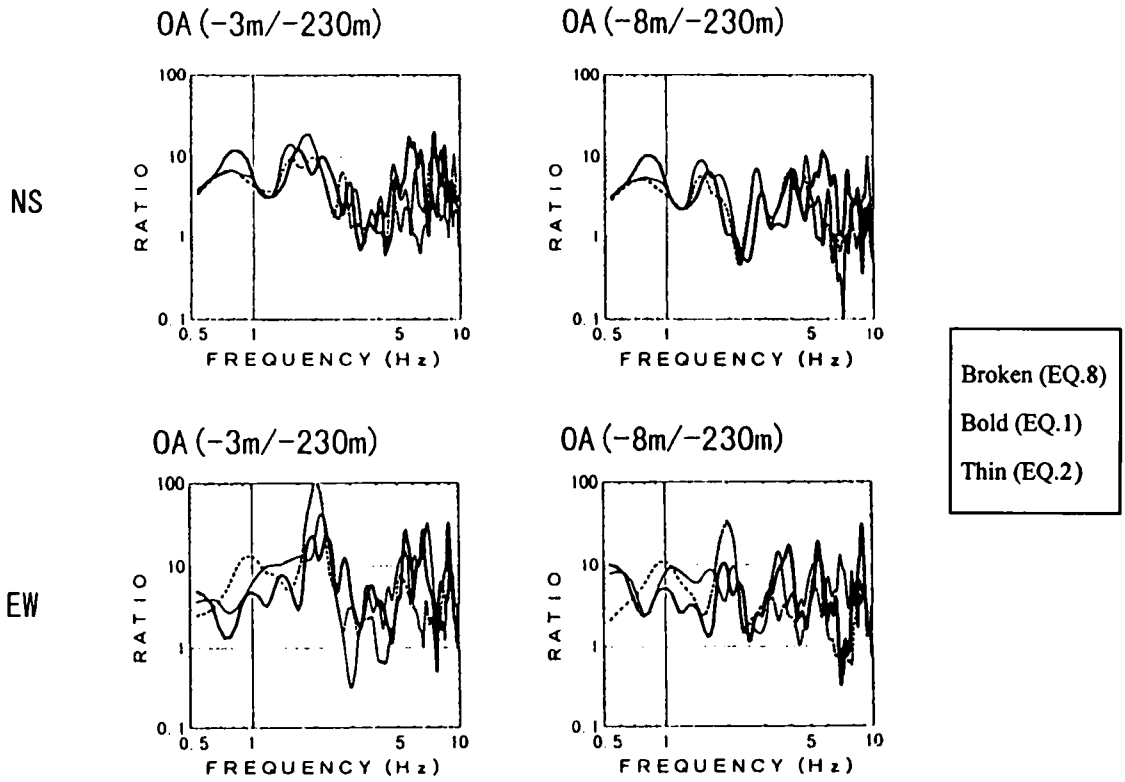

Fig.5.17 (a) Spectral ratios of downhole records
(NS predominant records of EQ.8,1,2)

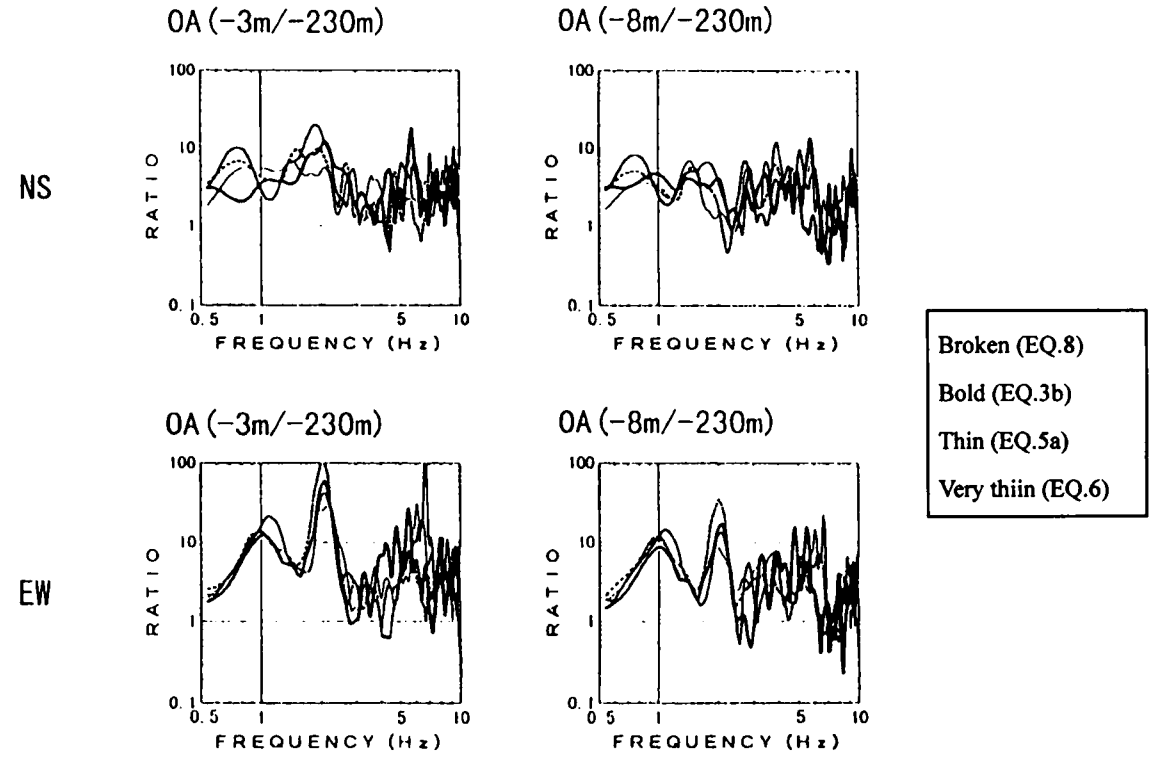

Fig.5.17 (b) Spectral ratios of downhole records
(EW predominant records of EQ.8,3b, 5a, 6)

5.3.2 Effects of Focal Radiation on Buried Valley

The Sagami bay (EQ.1), E. Yamanashi prefecture (EQ.5a) and E. Off Izu peninsula (EQ.6) earthquakes were, also, recorded at TKY. E. The Yamanashi prefecture (EQ.5a) and E. Off Izu peninsula (EQ.6) earthquakes occurred at epicentral distances of 50 to 60 Km. The Sagami bay Earthquake occurred at a depth of 122 Km in the intra-plate of the Pacific plate. The South Ibaraki prefecture (EQ.7) and E. Off Chiba prefecture (EQ.4) earthquakes with magnitudes of Mj = 5.0 and Mj = 6.2, respectively, occurred at epicentral distances of 104 Km and 154 Km, respectively. The focal radiation patterns of those events modeled as a point source and the site effects at TKY were investigated in a manner similar to the investigation at AGK.

The radiation patterns of SH- and SV-waves from the records of the E. Off Izu peninsula earthquake are shown in Fig. 5.18. The azimuth and take-off angles of those events at TKY were, also, evaluated using the earth crustal structure estimated at Izu district. The estimated points were plotted on closed circle symbol in the same figures. The SH-wave radiation pattern was found to be predominant and much larger than the radiation pattern for the SV-wave.

The velocity time histories obtained by integrating the accelerograms recorded at rock and sediments points are traced in Fig. 5.18. With respect to SG1 located on rock, the principal axis of the S-wave was predominant in the NS component and much larger than the S-wave in the EW component. This was in conformity with the focal radiation pattern, similar to the observation at AGK. However with regard to ground motions recorded at the sediments at SG3, SG4 and SG5, the S wave motions were amplified not only in the predominant NS component but also in the EW component. The principal axis of the principal S-wave shocks in the 4 seconds duration from 2 to 6 second of the time was evaluated by applying the complex polarization filter[15]. The principal motions of the S-wave were filtered out using a band-pass filter with a band-pass range of 1.0 to 2.5 Hz. The principal axes in the higher frequency regions at SG1 and SG2 were inclined a little along the EW direction of the buried valley. SG1 and SG2 are located at outcrop of rock and the edge of sedimentary basin, respectively. The principal axes in the lower frequency regions at SG1 and SG2 were in accordance with the focal radiation pattern. The principal axis of the S-wave at SG3 located on the central part of the basin was inclined along the NS direction

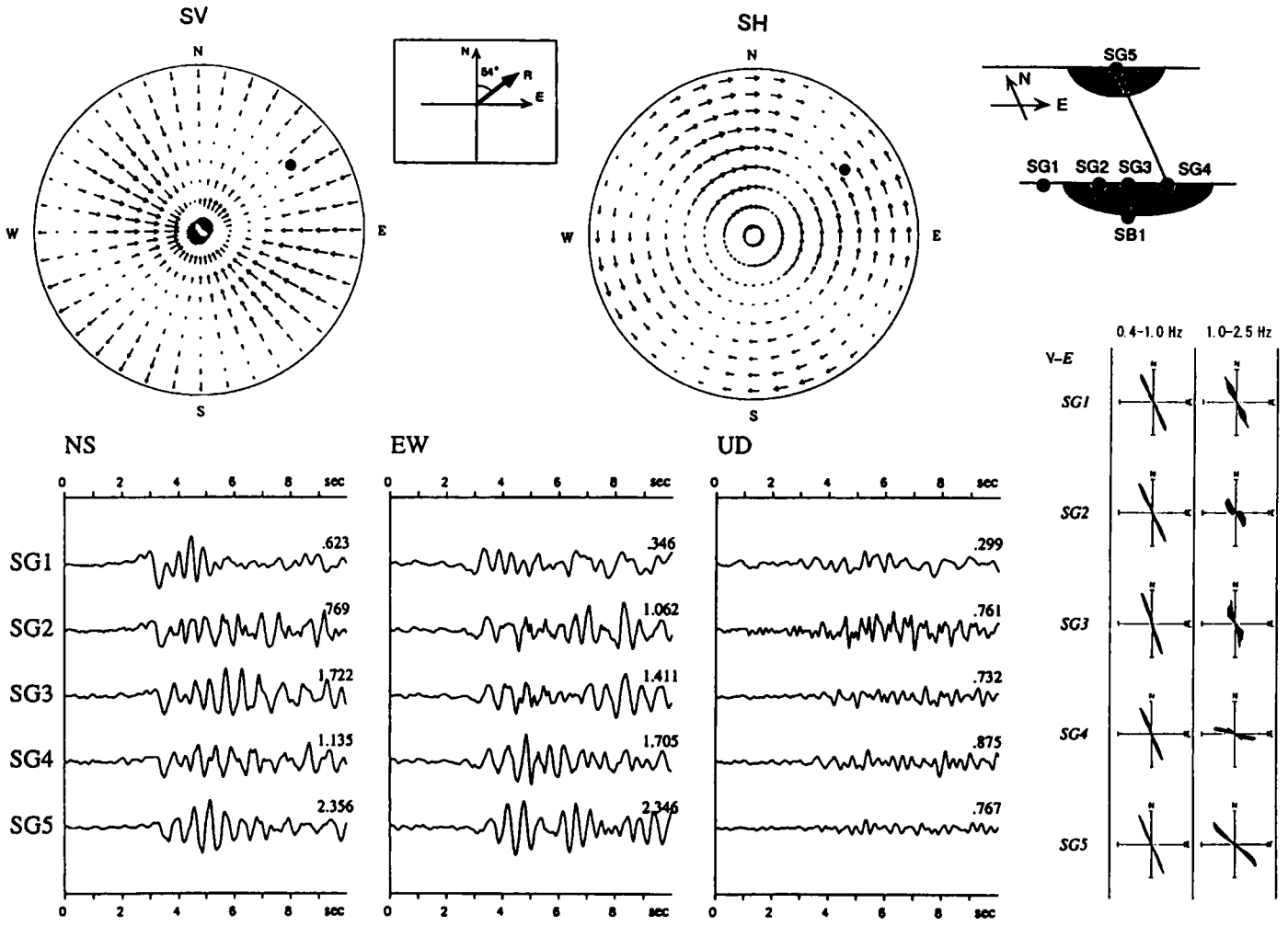

Fig.5.18 Upper: Focal radiation pattern for S waves (●:SG1 point),

Lower: Velocity records at TKY (EQ.6: E.Off Izu, unit:kine)

Right: Principal axis for horizontal particle motion (t=2.0-6.0sec, BPF: 0.4-1.0Hz, 1.0-2.5Hz)

A similar trend in the principal axis of S-wave motion was found in the records of the E. off Chiba prefecture, Sagami bay and S. Ibaraki prefecture earthquakes. As seen in Figs. 5.19-20, the S wave motions were especially amplified at SG3, SG4 and SG5 located in the central part of the buried valley. Those waves were strongly traced at the latter part of the principal S wave motion in the NS component, which is in the direction along the anti-plane of the profile of the buried valley. The spectral ratios between the surface and bottom records for the only horizontal components of the down-hole at SG3 were very much alike, as indicated in Fig. 5.21, and bore no relation to the focal radiation pattern. This result indicated that the local site effect at TKY was mostly dependent on the lateral irregularity of the buried valley. At this site the contrast between the alluvial clay and the sandstone was high with an impedance ratio less than 0.2 and therefore, the local site effect was influenced by the subsurface structure. Furthermore it was recognized that the vertical motion was amplified much more at SG2 on a steep dipping base layer larger than at sites on gently dipping base layers.

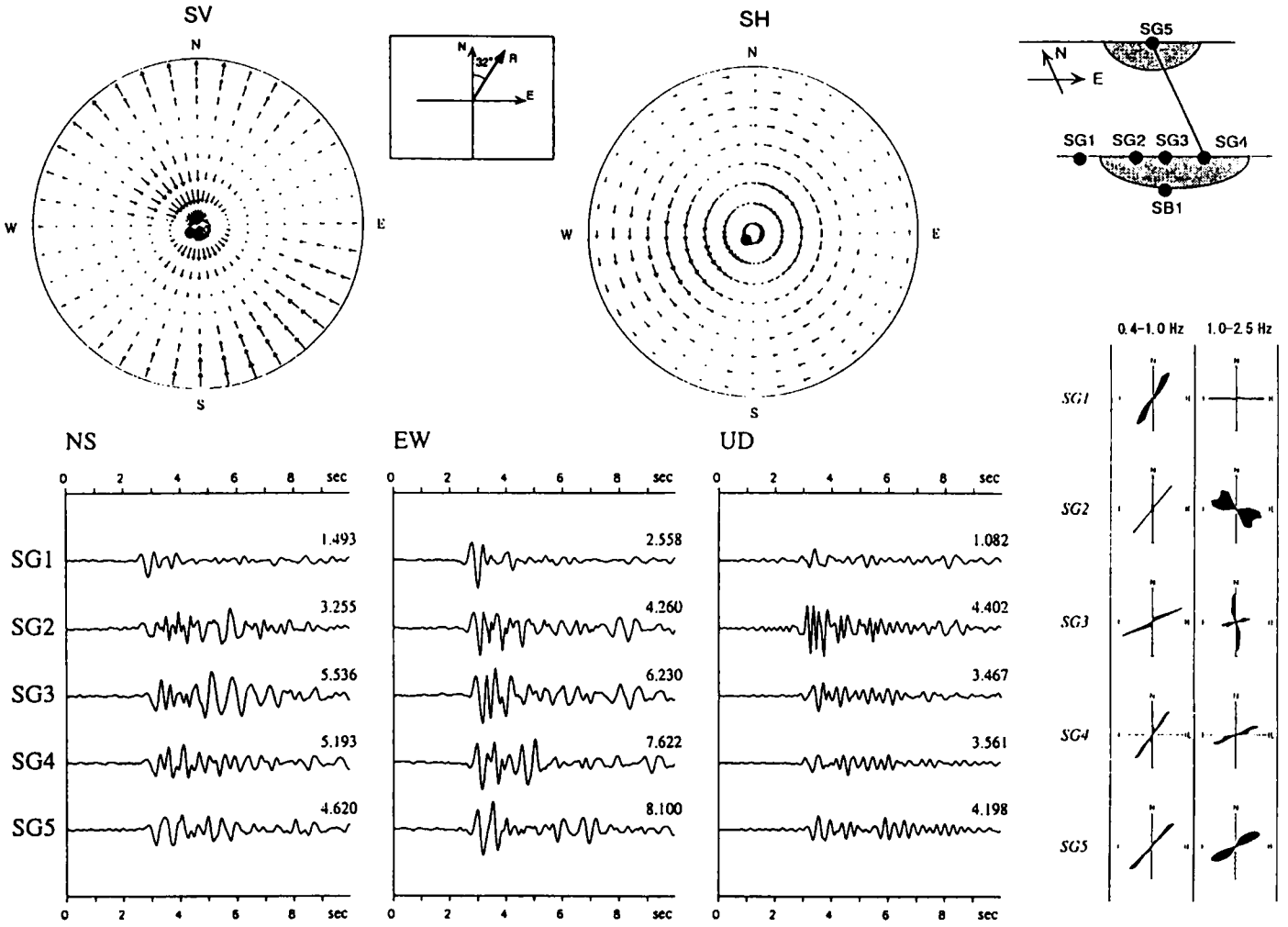

Fig.5.19 Upper: Focal radiation pattern for S waves (●:SG1 point)

Lower: Velocity records at TKY (EQ.2: Sagami bay, unit:kine)

Right: Principal axis for horizontal motion (t=2.0-6.0sec, BPF: 0.4-1.0Hz, 1.0-2.5Hz)

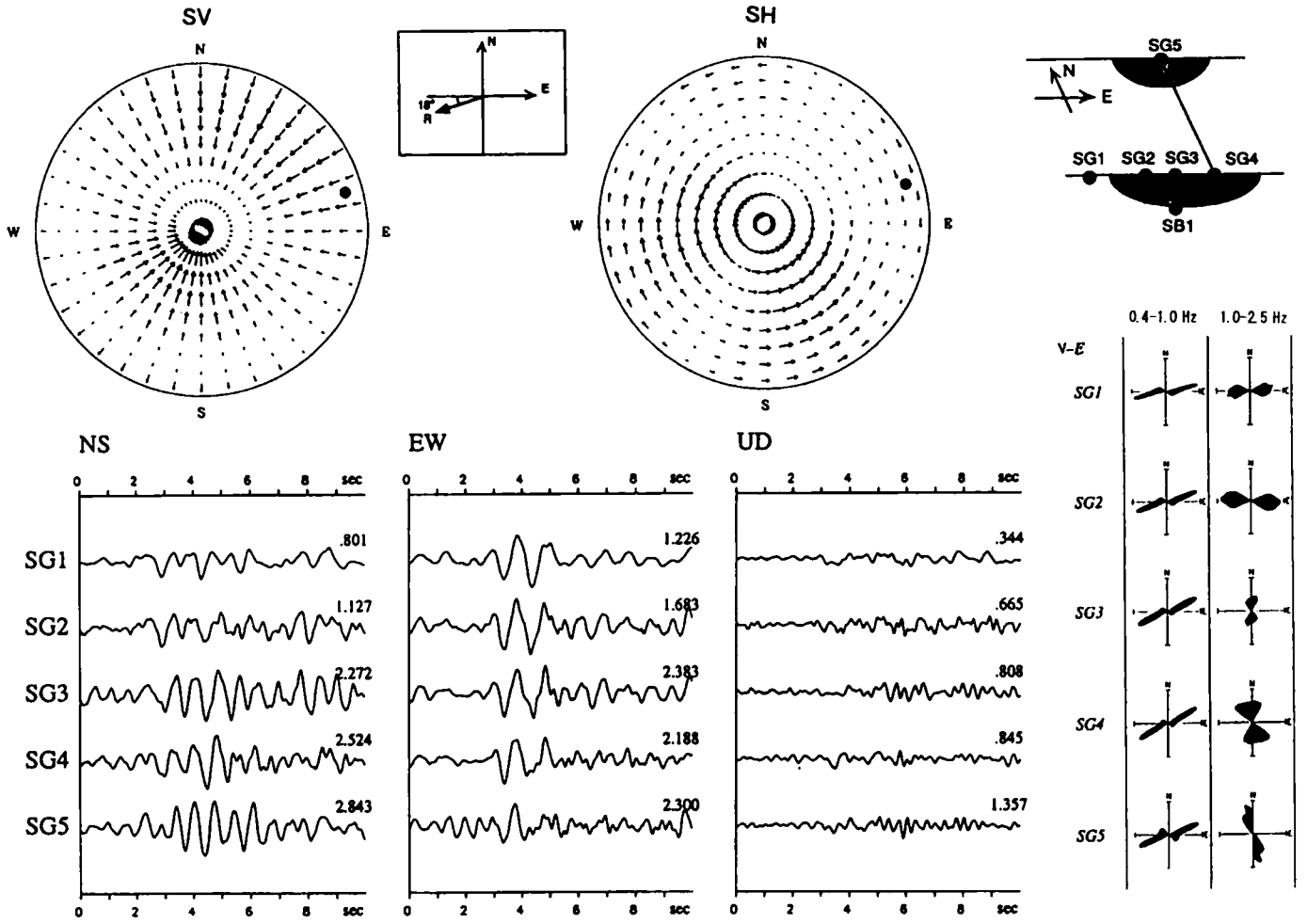

Fig.5.20 Upper: Focal radiation pattern for S waves (●:SG1 point)

Lower: Velocity records at TKY (EQ.4: E.Off Chiba, unit:kine)

Right: Principal axis for horizontal particle motion (t=2.0-6.0sec, BPF: 0.4-1.0Hz, 1.0-2.5Hz)

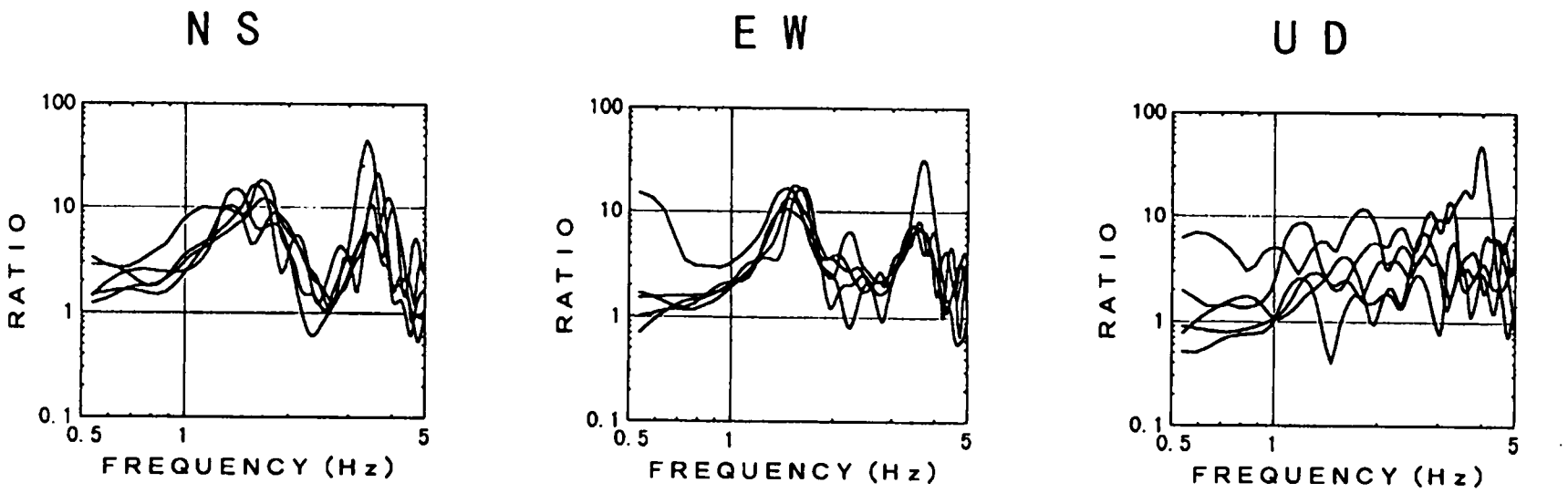

Fig.5.21 Spectral ratios of down-hole records (EQ.2, 4, 5, 6 and 7)

5.4 Modeling of Irregularly Layered Ground

5.4.1 Local Site Effects of Alluvial Valley

Fig. 5.22 shows an E-W cross-section of the ground at AGK. The ground here consists of 150 m deep sediments on bedrock. The geotechnical parameters identified by spectral inverse analysis[16),17)], PS logging, VSP survey[11)], and seismic reflection survey[11)] are shown in Fig. 5.23. Two-dimensional (2D) response analysis was carried out using a ground model consisting of sediment layers for Hakone volcanic gravel (Hp(g)), sand (Hp(s)) and basement rock for old Pleistocene layer(Os). The top alluvial layer, which is soft and thin was removed from the model, since it posed computational problems at high frequencies. The geotechnical parameters used in the 2-D model are listed in Table 5.6.

Table 5.6 Geotechnical parameters for ground model at AGK

Geology	Age	Vs(km/s)	Vp(km/s)	Q	ρ(t/m**3)
Hp(g)	late Pleistocene	0.7	2.0	50	1.9
Hp(s)	late Pleistocene	0.4	2.0	50	1.8
Hp(g)	late Pleistocene	0.75	2.5	50	2.0
Os2	middle Pleistocene	1.2	3.0	50	2.2

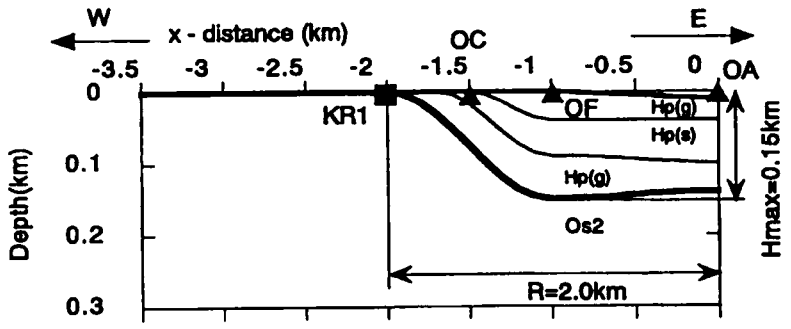

Fig.5.22 Two-dimensional ground model at AGK

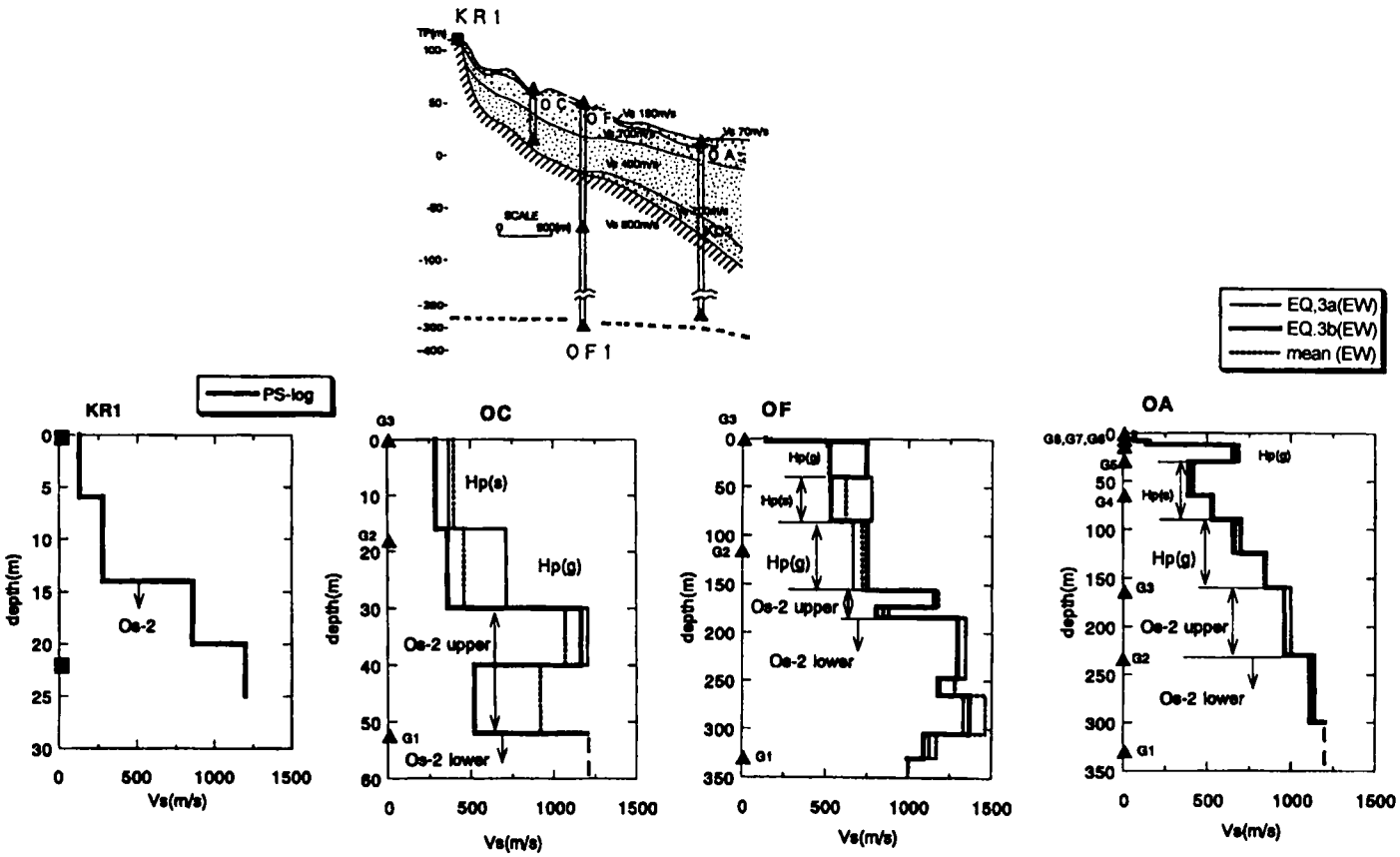

Fig.5.23 Identified S- wave velocity profile at KR1, OC, OF, and OA

Two-dimensional response analyses[18), 19), 20), 21)] due to both anti-plane SH-wave and in-plane SV-wave incidences were computed using the AL. The incident wave field was considered as described later in section 5.3. Ground response was, also, calculated using a 1-D layered model with geotechnical parameters the same as those used in the 2-D model. A Ricker wave[19)] with a natural frequency of 1.0 Hz was used as the incident wave. The 1-D and 2-D spectral ratios between the surface and basement seismograms were compared with the observed spectral rations.

Fig. 5.24(a) shows the 1-D and 2-D transfer functions for SH-wave incidence and the spectral ratios calculated from the NS predominant group of records. The anti-plane direction of the 2-D model is along the NS direction. As seen in Fig. 5.24 both 1-D and 2-D spectral ratios computed at OC, OF and OA almost coincided with the observed spectral ratios. The 2-D amplification factors agreed better with observed factors in the low frequency range around 0.8 Hz at OF and around the spectral peak frequency of 1.5 Hz at OA than 1-D amplification factors.

Fig. 5.24(b) shows 1-D and 2-D transfer functions for SV-wave incidence for the EW predominant group of records. As in the case of the NS predominant group the computed spectra agreed with the observed spectral ratios at OC, OF and OA. Comparing the spectral ratios plotted in Figs. 5.24(a)-(b) the spectra in the two horizontal components were very nearly the same. The 2-D transfer function was found to be closer to the observed spectra at frequencies around 1.0 Hz at OF and 1.5 Hz at OA. These results indicate that 2D analysis of SH- and SV-wave incidence is quite adequate in evaluating the ground response of irregular layered media if due consideration is given to the incident wave fields during strong motion.

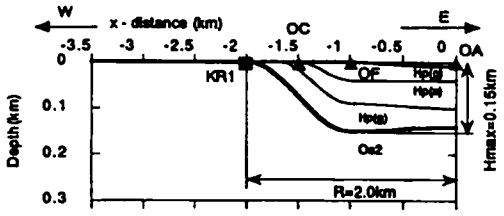

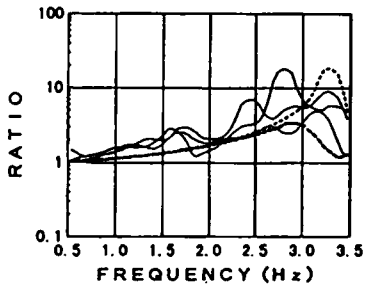

OC (0m/-52m)

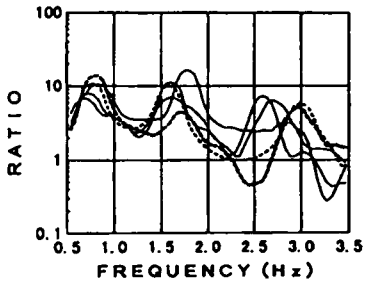

OF (0m/-330m)

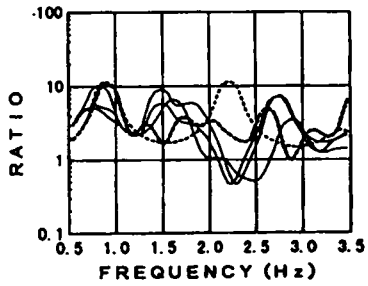

OA (-8m/-230m)

Fig.5.24 (a) Spectral ratios at downhole sites

(Thin line: NS predominant records of EQ.8, 1, 2

Broken line: identified 1-D model, Bold line: ALSH (2-D))

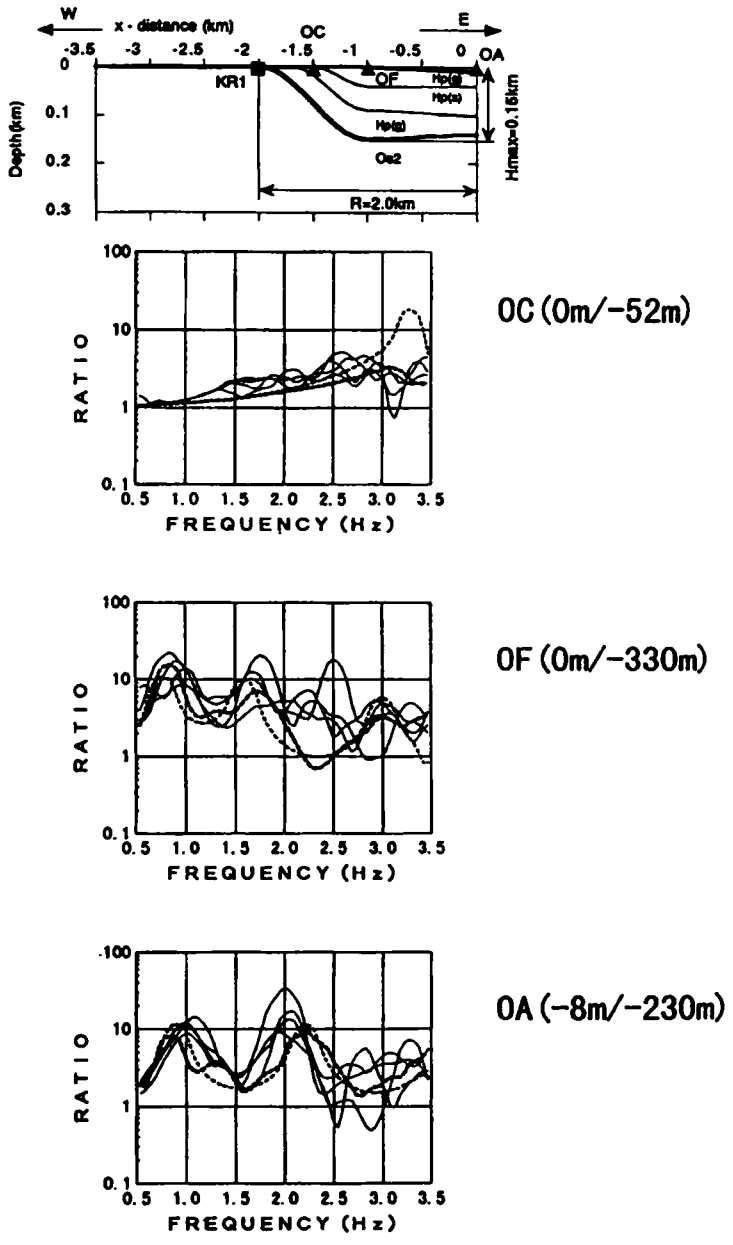

Fig.5.24 (b) Spectral ratios at downhole sites

(Thin line: EW predominant records of EQ.8, 3b, 5a, 6

Broken line: identified 1-D, Bold line: ALSV (2-D))

5.4.2 Local Site Effects of Buried Valley

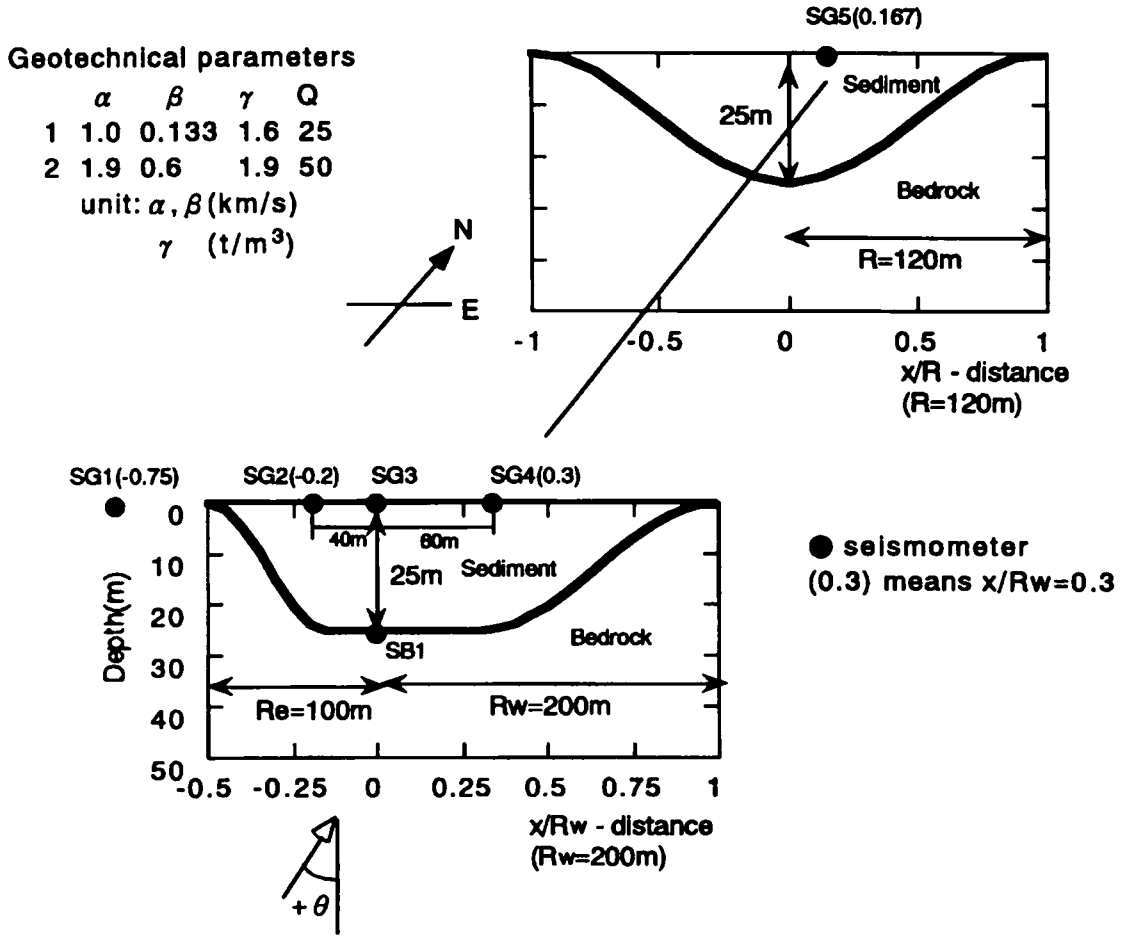

Fig.5.25 Two-dimensional ground model at TKY

2-D layered models at TKY based on ground profiles obtained from shallow reflection surveys and PS loggings along two cross-sections in the EW direction are shown in Fig. 5.25. SG2 through SG5 are located on the sediments while SG1 is located at the outcrop of bedrock at the west edge of the basin. The geotechnical parameters listed in Fig. 5.25 are for the sedimentary layer and bedrock. The 2-D models depict two buried valleys, one of which is non-symmetrical and 300 m long, and the other is symmetrical and 240 m long. In both models the depth of the sediment at the center of the valley was 25 m. As well as at AGK, 2-D analyses were carried out using the AL method[18), 19), 20), 21)].

The Vs for the alluvial layer was taken as 133 m/s and 600 m/s for the soft bedrock. Vs measured by elastic wave velocity exploration was 900 m/s at the surface of

the outcrop and this value, also, represented Vs of the bedrock at TKY. A Ricker wave with natural frequency of 1.3 Hz corresponding to a 1-D ground model of a 25 m thick sedimentary layer was used as input to the model.

The S-wave spectral ratios of the surface records with respect to the record at SG1 at the outcrop and the record at SB1 at the bottom of a down-hole were compared with the computed 1-D and 2-D transfer functions. The earthquake records were divided into two groups. One consists of records from the Sagami bay, E. off Izu peninsula and E. Yamanashi earthquakes, for which motions are traveling from the west of TKY. The other consists of records from the S. Ibaraki and E. Off Chiba earthquakes, for which motions are traveling from the east side of TKY. Incidence angles for all records were estimated by ray theory using the model of the earth's crust structure measured at Izu district[14] to account for the traveling phase difference[22), 23)] in the incident wave field. The Vs of 900 m/s in the soft bedrock at TKY was included in the model of the earth's crust structure. 2-D analyses due to both anti-plane SH-waves and in-plane SV-waves at the estimated incidence angles were computed. Table 5.4 lists the incident angles that were estimated for the earthquakes recorded at TKY.

As indicated by Fig. 5.26, the horizontal spectral ratios computed with reference to the record at SB1 agreed with the observed spectral rations. These spectral ratios did not show any relation to the seismic groupings. The computed vertical component spectral ratios due to vertical and oblique SV- wave incidence are very similar characteristics.

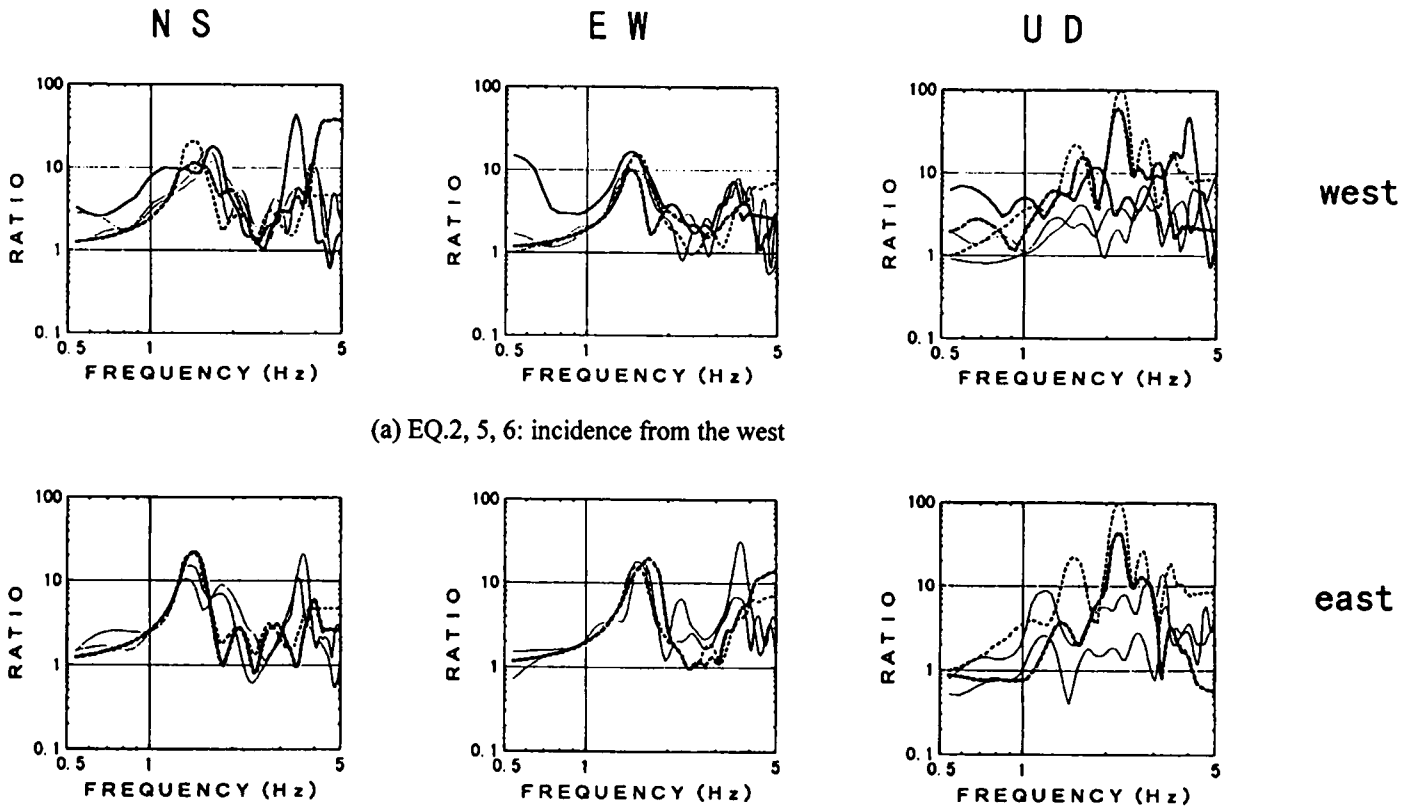

(a) EQ.2, 5, 6: incidence from the west

(b) EQ.4, 7: incidence from the east

Fig.5.26 Spectral ratios of downhole records

Thin line: Observed (EQ.4, 7)

Broken line: 2-D for vertical SV incidence

Bold line: 2-D for 15 degrees oblique SV incidence

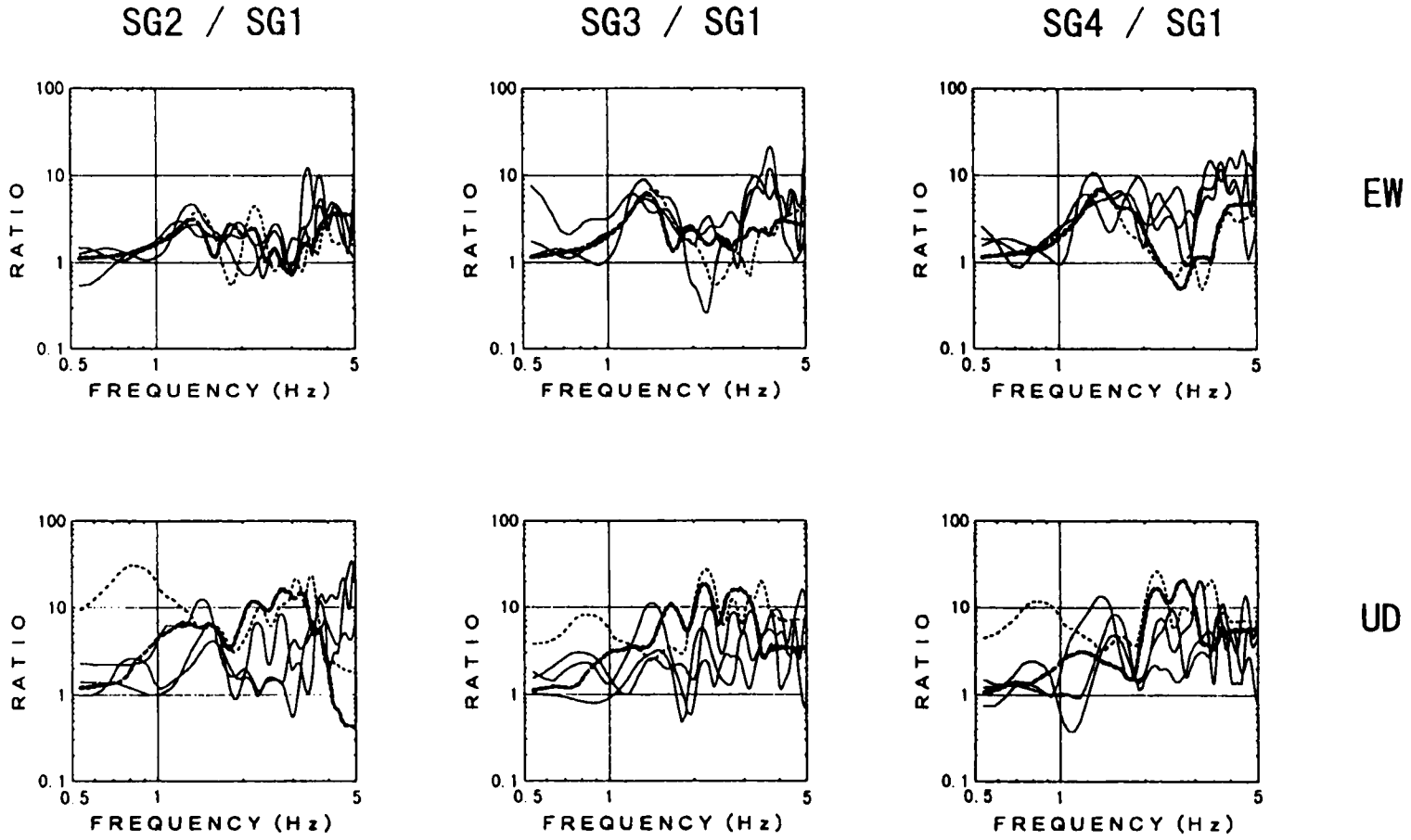

Fig.5.27(a) Site amplifications at SG2～SG4

Thin line: Observed (EQ.2, 5, 6)

Broken line: 2-D for vertical SV incidence

Bold line: 2-D for 15 degrees oblique SV incidence

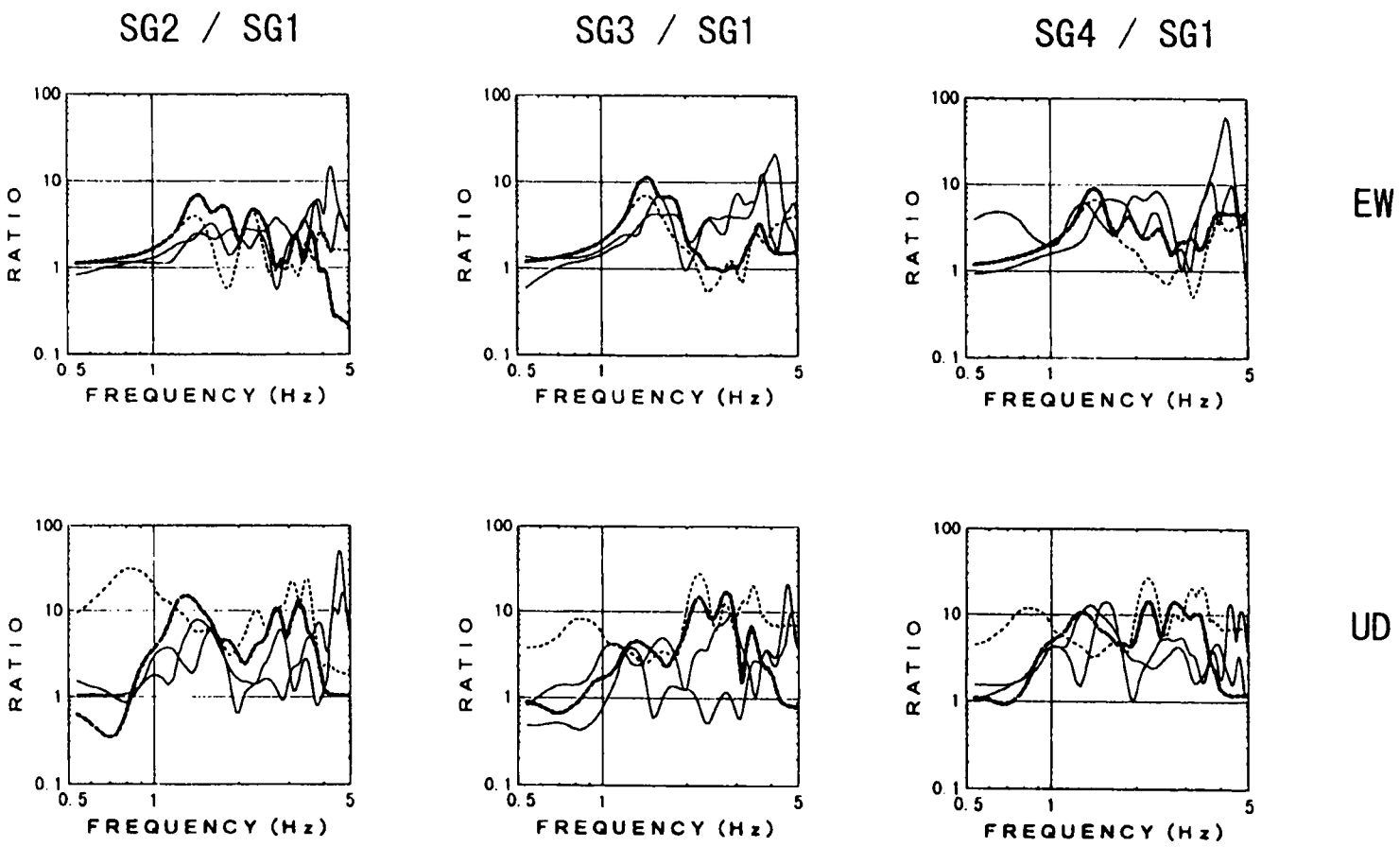

Fig.5.27(b) Site amplifications at SG2～SG4

Thin line: Observed (EQ.2, 5, 6)

Broken line: 2-D for vertical SV incidence

Bold line: 2-D for 15 degrees oblique SV incidence

Fig. 5.27 shows the spectral ratios computed with reference to the record at SG1. The computed spectra for oblique SV-wave incidence agreed much better with the observed spectra in both horizontal EW and vertical UD components than the computed spectra for vertical incidence. In the case of 2-D analysis for a 15° oblique SV-wave incidence from the east side, the computed spectral ratios were quite different from the spectral ratios computed for vertical incidence. Similar differences were, also, found in the computed spectral ratios for 15° oblique SV-wave incidence from the west.

The local site effect at TKY was more or less constant in both EW and NW components and appeared not to be influenced by the incident wave field. This was interpreted to be the result of the high impedance ratio between the sediments and the bedrock. However, when site effects are evaluated using spectral ratios referenced to records from points at outcrop of bedrock, it is necessary to consider the effects of the incoming direction of the incident wave and its incident angle at the reference point. Thus 2-D response analyses which took into account the incident angle were shown to be effective in evaluating both horizontal and vertical site effects in buried valleys with high impedance between the sediments and the base layer. For the case when records at outcrop of rock were used as the reference, it was necessary to consider the incident wave field such as the incident angle and the incoming direction. This meant that the spectral ratios calculated using record at rock outcrops and base of down-hole arrays could be quite different even if the spatial distance between the two reference points is less than 100 m.

5.5 Conclusions

On the basis of the analyses of the records on gravel deposits of alluvial valley at AGK, the following can be concluded:

(1) The predominant directions of S-waves in the sedimentary layer corresponded to the focal radiation pattern of a point source.
(2) The spectral ratios between the records at the surface and base layer for the principal S-wave, was constant for frequencies lower than 2.5 Hz. The principal axis of the S-wave showed the influences of both the focal radiation pattern and seismic path. Consequently, local site effect was found to be dependent on not only the geological structure at the site but, also, the incident wave field related to the source and path effects.

On the basis of the analyses of the records on soft clay of buried valley at TKY, the following can be concluded:

(3) The spectral ratios calculated with reference to the record from the base of down-hole array were more or less the same in the EW and NS directions and did not show any influence of the source effects. However, spectral ratios calculated with reference to records from a point at the outcrop of bedrock were quite different and showed the influence of the incident wave field even though the spatial separation was less than 100 m. This meant that it was necessary to consider the incident wave field such as the incident angle and the incoming direction when the spectral ratios were referenced with respect to records at the outcrop of bedrock even if the reference point was as close as 100 m.

(4) 2-D response analysis for in-plane SV-wave incidence was found to be effective and adequate for evaluating the site amplifications at sites on a sediment-filled valley with a high impedance ratio between the bedrock and sedimentary deposit.

Lastly, the following general conclusion was made:

(5) Local site effects of small- and medium-sized sediment-filled valleys were seen to be different and revealed the influences of both the incident wave field and geological structure at the site. The results described in this chapter clearly indicated that 2-D response analyses for SH- and SV-wave incidence were useful in modeling the incident wave field to evaluate local site amplification characteristics.

References

1) Campillo, M., F.J. Sanchez-Sesma and K. Aki; Influence of small Lateral variations of a soft surficial Layer on seismic ground motion, Soil Dynamics and Earthquake Engineering, Volume 9, Number 6, November 1990.
2) Kawase, H. and K. Aki; A Study on The Response of a Soft Basin for Incident S, P, and Rayleigh Waves with Special Reference to The Long Duration Observed in MEXICO City", Bulletin of the Seismological Society of America, Vol.79, N0.5, pp.1361-1382, October 1989.
3) Kawase, H.; Amplification of seismic waves by sedimentary layers and its simulation; Zishin Vol.46, No.2, pp171-190, 1993 (in Japanese).
4) Sato, K., S. Higashi, Y. Shiba, H. Yajima and S. Sasaki; Site amplification and incident wave field at Kuno in Odawara city during 1996 East Yamanashi earthquake, CRIEPI Report U98061,1998 (in Japanese).
5) Sato, K., S. Higashi, Y. Shiba and S. Sasaki; Seismic amplification of irregular subsurface layer-Various geological survey and modeling for subsurface layer and seismic amplification characteristics based on earthquake observation-, CRIEPI Report U95061, 1996 (in Japanese).
6) Ishibashi, K.; Possibility of a large earthquake near Odawara, central Japan, preceding the Tokai earthquake, Earthq. Predic. Res., vol.3, pp319~344, 1985.
7) Ishibashi, K.; East Kanagawa earthquake and earthquake prediction I and II, the Science, vol.58, pp.537~547, 771~780, 1988 (in Japanese).
8) Kanagawa prefecture; Report of earthquake countermeasures in Kanagawa prefecture, pp.1-450, 1980 (in Japanese).
9) Yamazaki et al.; Seismo-techtpnics at the north margin of the Philippine Sea Plate, Special Rep. of Sci. and Tech. Agency, pp.368-392, 1982.
10) IASPEI/IAEE Joint WG and Japanese National WG: Proceedings of the International Symposium on the Effect of Surface Geology on Seismic Motion, ESG 1992 Vol. II, March 1992.
11) Higashi, S., K. Sato, H. Yajima, S. Sasaki and H. Ishikawa; Underground structure of Kuno-site on the basis of reflection seismic survey, Academic association of earth and planet, p142, B42-P12, 1997 (in Japanese).
12) Matsuda, T.; Magnitude and return period of earthquake occurred from active fault, vol.128, pp.269-283, 1974 (in Japanese).
13) Kennet, B.L.N.; Radiation from a Moment-Tensor Source, Seismological Algorithms, pp.427-441,1988.

14) Yoshii, T., S. Asano, S. Kubota, Y. Sasaki, H. Okada, T. Masuda, H. Murakami, S. Suzuki, T. Moriya, N. Nishide and H. Inatani; Detailed Crustal Structure in the Izu Peninsula as Revealed by Explosion Seismic Experiments, J. Phys. Earth, 34, Suppl., S241-S248, 1986.
15) Higashi, S., K. Sato, H. Yajima, S. Sasaki and H. Ishikawa; Analysis of incident wave field on Kuno site, The 10th JEES, October 1998.
16) Ishida, K., K. Sato, Y. Sawada and H. Yajima; Estimation of soil profiles and characteristics of normalized response spectrum on based on earthquake observation, Research report of CRIEPI 385005, pp55-62, August 1985.
17) Ishida, K., Y. Sawada, K. Sato and H. Yajima; Concerning a damping of soil - Estimation of Q-value by applying spectral inverse method - The proceeding of the seismological society of Japan, Autumn meeting 1984
18) Aki, K. and K. Larner; Surface motion of a layered medium having an irregular interface due to incident plane SH waves, Journal of Geophysical Research, Vol.75, No.5, February 1970.
19) Ohori, M.; Seismic response analysis of sedimentary basin by using two-dimensional AL method, Journal of Zishin, vol,165, 1990 (in Japanese).
20) Bard, Pierre-Yves and Michel Bouchon; The Seismic Response of Sediment-Filled Valleys Part1. (The Case of Incident SH Waves), Bulletin of the Seismological Society of America, Vol.70, No.4, pp.1263-1286, August 1980a
21) Bard, Pierre-Yves and Michel Bouchon; The Seismic Response of Sediment-Filled Valleys Part 2. (The Case of Incident P and SV Waves), Bulletin of the Seismological Society of America, Vol.70, No.4, pp.1263-1286, August 1980b
22) Yamahara, H.; Input loss of ground motion and seismic wave (the first report), The journal of the Architectural Institute of Japan, 1969 (in Japanese).
23) Sato, K., Y. Sawada, H. Yajima and T. Iwadate; Passive control effect of the foundation by the phase difference of seismic wave, Research report of CRIEPI 87062 May 1988 (in Japanese).

CHAPTER 6

CONCLUDING REMARKS

Research on historical earthquake disasters related to the local site effects has clearly indicated that the seismic ground response is strongly affected by sedimentary deposits during strong motion. In this dissertation local site characteristics of sedimentary deposits were investigated from seismic observations considering incident wave field and soil profile.

In chapter 1, general remarks were made on past disastrous earthquakes in which site effects played a significant role. In previous research on historical disastrous earthquakes, it has been pointed out that damage in these earthquakes was strongly correlated to the geological and geotechnical structure of the ground. It has been noted from reconnaissance reports of past disastrous earthquakes that damage to buildings and other structures was locally concentrated on filled lands, unconsolidated sedimentary deposits, transitional zones between soft and hard grounds, edges of topography like a cliff and irregularly layered ground at the interface of sedimentary deposits and base layers.

Ground motions are influenced by various factors, but generally a deep geological structure contributes to long- period motions and shallow geological structures to short-period motions. Therefore geological and geotechnical information of the soil structure at a site are required to assess the design input ground motion for important structures.

In chapter 2, analytical methods related to numerical simulation of seismic wave propagation were investigated and evaluated using earthquake records and models of layered soil. All investigated methods were found to be useful to simulate seismic wave amplification based on a consideration of the incident wave field related to source and path effects. The feasibility of various analytical methods, the importance of a proper delineation of geological structure and the use of seismic observation records are examined.

In chapter 3, characteristics of nonlinear seismic amplifications were investigated based on strong motion records from down-hole vertical arrays during the 1995 Hyogoken-Nanbu (M_{JMA} = 7.3,

corrected). A few of the records demonstrated peculiar nonlinear behavior of seismic amplification in reclaimed land areas with Holocene and Pleistocene deposits.

The identified S wave velocities (Vs) became about 20 % to 45 % smaller at sites located on such deposits but the identified P wave velocities (Vp) almost coincided with the PS-logging value at all sites. Comparing S-wave profiles estimated from weak and strong motions to PS-logging values it was seen that S-wave profiles estimated from the weak motion records were closer to the PS-logging values except at liquefied sites.

Sp-wave arrivals were detected in the vertical motions and S-Sp time ranged from 1.1 to 1.2 sec for all depths of the vertical array. These results were indicative of the inversion of Sp-waves at the interface of deep sedimentary and base layers.

Nonlinear behavior of soil during strong motion was found at a site where the strain was more than 0.6 % of at PI but no such behavior was found at a site with a maximum shear strain of 0.06%. It was concluded that the conditions for strong liquefaction are (i) intensity of the input acceleration should be more than 100 gal, and (ii) the existence of a water saturated porous sand layer more than 10 m thick.

In chapter 4, seismic wave amplification at 11 sites located on laterally layered ground ranging from hard rock to relative soft ground were analyzed using weak motion earthquake records from multi depths of vertical arrays. The vertical distribution of the normalized underground seismic coefficient of the respective grounds for horizontal motion was calculated using these records. Based on these results a method for assessing was developed. The vertical distribution of underground seismic coefficient for horizontal motion was found to be dependent on the predominant period of the input earthquake acceleration and the impedance ratio between the bedrock and surface layers. The vertical distribution of underground seismic coefficient was found to decrease linearly from a value of 1 at the ground surface to some depth below which it became constant.

The assessment method for underground seismic coefficient was found to be effective for a filled-up slope and a hard rock cut slope. Application capability related to method 1 may be possible for irregularly layered ground included slope ground as can be noted. Subsequently, this assessment method was extended for a multiple layered ground and irregularly layered ground. Moreover the assessment method was seen to be effective for strong motions, as well, except for sites that experienced strong liquefaction. This extended assessment method was found to be quite efficient in assessing normalized underground seismic coefficient at layers deeper than 50 m except at layers that liquefied significantly.

In chapter 5, the seismic ground response of laterally irregularly layered grounds was investigated. Understanding these effects is important in earthquake resistant design of long and large-scaled civil structures such as buried lifelines, duct structures, tunnels, and pipelines. Records

obtained from vertical arrays of strong motion seismographs at two sites fronting the Sagami bay are analyzed. One observation site is located at Kuno on the Ashigara plane and the ground at the site consists of diluvial and alluvial gravel deposits of sediment-filled valley. The second site is located at Takeyama in Miura peninsula on soft clay of alluvial buried valley. Records from these two sites are extensively analyzed to evaluate the influences of incident wave field related to the source and path effects on local site effects.

The site amplification characteristics of gravel deposits of alluvial valley were apparently constant in the frequency region lower than 2.5 Hz in the direction along the principal axis of the S-wave. The principal axis of the S-wave corresponded very well with the focal radiation pattern and seismic path effects at a site located on a gravel soil of sedimentary basin. The local site effect at this site was clearly influenced by both geological structure at the site and the incident wave field related to the source and path effects.

Using records at another site located on soft clay of buried valley it was shown that a 2-D response analysis taking into account the incident angle could be effectively used to evaluate site amplifications in both horizontal and vertical directions. It was shown that when evaluating spectral ratios of the surface records with reference to records on outcrops it is necessary to consider the incident angle and incoming direction of the incident wave field even for records obtained from outcrop sites that are no farther than 100 m.

Local site effects of sediment-filled valleys were found to be quite variable depending on the incident wave field. 2-D response analyses for SH- and SV-wave incidences were found to be useful in evaluating site amplification characteristics if considerations of incident wave field were made.

The remaining problem is to quantitatively evaluate the spatial variation of local site effects and the incident wave fields during strong motion on the basis of available information on deep and shallow geological structures. In the future, a concerted effort is required to develop analytical methods for investigating local site effects using data from a variety of sources such as dense array seismographs, geological surveys, micro tremors, weak and strong motions.